UNIVERSITY OF FLORENCE

International Doctorate in Structural Biology

- Cycle XXIII (2008-2010) -

Structural and functional properties of proteins involved in metal transfer and redox reactions

---

Ph. D. thesis of

Tatiana Kozyreva

Tutor	Coordinator
Prof. Lucia Banci	**Prof. Ivano Bertini**

This thesis has been approved by the University of Florence,
the University of Frankfurt and the Utrecht University

Contents

Acknowledgements

To acknowledge all those people that have contributed to the work described in the thesis is absolutely not an easy task. I'd say this is an impossible task, given the many people that have helped to design, implement, apply, criticize, sponsor the full 3 years doctorate work. I am going to try anyway, and if your name is not listed, rest assured that my gratitude is not less than for those listed below.

I would like to express my thanks to the people who have been very helpful to me during the time it took me to prepare this thesis. It would not have been possible to write this doctoral thesis without my supervisor, Prof. L. Banci and director of CERM Prof. I. Bertini that gave me the opportunity to join CERM's research team for these 3 years and for their invaluable suggestions during my work here.

During my time as a PhD-student, I have been lucky enough to have been surrounded by wonderful collegues. I am very grateful to Simone. Besides providing useful comments/criticisms and contributing his all important signatures to my thesis, his wide knowledge and logical way of thinking have been of great value for me along the way. I owe my deepest gratitude to Francesca for guiding me through the writing of the thesis, and for all the corrections and revisions made to text that is about to be read. For her understanding, encouraging and personal guidance along the last two years, that we were working together.

I'd like to thank Mirko and Shenlin, without they help we would never arrive to the publication of the "endless" Sco-Cyt project.

Biotech group of CERM, especially Leonardo for his suggestions and Valentina for 24h willingness to help.

Furthermore I am deeply indebted to my friends and colleagues at Chemistry Department: Maciej, Chiara, Mirella, Doros, Miguella all with their own inimitable and unique personalities, helped eliminate drudgery from work and life in general. Our tea/coffee meetings followed by "profound" discussions, that have provided the environment for sharing the experiences about the problem issues as well as in developing solutions to the identified problems. Thanks to computer "genious" Joao that had a patience to solved all my continious problems in the word of computer technologies. I have been fortunate to come across many funny & good friends, without whom life would be bleak. Special thanks go to Niko for his ever-present support and help and for making me laugh in the difficult moments.

I would like to thank the laboratory of Gene Technology from Tallinn University of Technology, especially Professor Peep Palumaa and my friend and co-author Kairit for their extremely valuable experiences, help and insights in the mass experiments performing and data analysis.

Lastly, I would like to express my thankfulness to my family for all their love**,** patience and encouragement. To my parents who raised me with a love for science and supported me in all my pursuits. And I'd like to dedicate these thesis to my father, who always was the main reference for me. Last of all my gratitude must fall upon my most patient sweetheart, who has shared most of the ups and downs of this thesis. His belief in what I have been doing has on many occasions been stronger than my own.

List of figures

1. INTRODUCTION

1.1 THE ROLE OF COPPER IN BIOLOGICAL SYSTEMS

Transition metal ions, such as copper, iron, molybdenum and cobalt, play central roles in biology, largely because they are able to exist in multiple oxidation states *in vivo*.[1,2,3] Copper ions undergo unique chemistry due to their ability to adopt distinct redox states, either oxidized as Cu (II) or in the reduced state Cu(I).[4,5] Cells use copper as a structural element in regulatory proteins and harness the chemistry of this element in single-electron-transfer reactions.

Copper clearly is required for the immune system, the nervous system, the cardiovascular system, skeletal health, for iron metabolism, and for formation of red blood cells. However, the roles of copper in other functions such as the regulation of cholesterol, glucose, and blood clotting are not well understood. Some disorders of the vascular and nervous systems induced by copper deficiency during prenatal development in animals cannot be reversed by copper supplementation after birth. Thus, copper must be provided during pregnancy. Copper's role in cardiovascular and skeletal health also has important implications for major public health problems seen in industrialized nations, namely heart disease and osteoporosis. [6]

The bioavailability of copper is decreased by high intakes of several nutrients, including zinc, iron, molybdenum, ascorbic acid, sucrose, and fructose. It is well documented that high intakes of zinc interfere with copper absorption in humans and animals.[6] The mechanism appears to involve the induction by zinc of metallothionein synthesis in the intestine and copper becomes 'trapped' in this protein and is not available for transport into the circulation. Zinc probably has little influence on copper content when the zinc to copper ratio is 15:1 or less.[6]

Copper plays a vital role as a co-factor for a number of metalloenzymes including Cu/Zn superoxide dismutase (antioxidant defense), cytochrome c oxidase (mitochondrial respiration), lysyl oxidase (development of connective tissue), tryrosinase (melanin biosynthesis), ceruloplasmin (iron homeostasis), hephaestin (intestinal iron efflux), dopamine β-hydroxylase (catecholamine production), and peptidylglycine α-amidating mono-oxygenase (peptide hormone processing).[7]

1.1.1 Copper enzymes

Copper enzymes have been classified into three types having distinctive geometries and ligand environments surrounding the metal center.[8] The Cu sites observed in proteins are classified into three types based on their structural and spectroscopic properties. Type I, Type II, and Type III (Tab.1). Blue, or type I, copper proteins are spectroscopically characterized by their intense absorption at 600 nm, resulting from a sulfur to copper ligand to metal charge transfer. [9] Typically, type I copper sites exhibit a trigonal planar coordination geometry with the sulfur of one cysteine residue and two nitrogens from histidine residues. Often, there are one or two weakly bound ligands in the axial positions. Type I sites are usually electron transfer sites. They are found in small electron transfer proteins like cupredoxins that ferry electrons between larger enzymes such as components of the denitrification pathway and photosynthesis. Also, they are found in the larger enzymes nitrite reductase and multicopper oxidase and function in intramolecular electron transfer to copper active sites. Within some of the large enzymes, a CuA site functions as an electron entry point. This site is an expansion of the type-1 site by a second Cu to form a metal-metal bond. Both type-1 and CuA sites are rigid and characterized by low reorganization energies to facilitate electron transfer.[1011] Type II sites are, generally, four or five coordinate structures of distorted tetrahedral or tetragonal geometry, respectively, and have strictly nitrogen or oxygen donors as ligands. Also, type II sites generally have very weak optical spectra but do have a very characteristic EPR spectrum. Type II copper sites are catalytically active sites, carrying out oxygen activation. In addition, they are able to perform the dismutation of superoxide and reduce nitrite to nitric oxide. A Type III or coupled dinuclear site, contains two antiferromagnetically coupled copper atoms bridged by molecular oxigen or hydroxyl, generally involved in oxygen binding or oxygen activation.[12]

Table 1. Classification of copper proteins by Cu centre type

COPPER CENTRE	PROTEIN CLASS / FAMILY
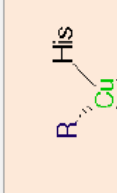 $Cu(N^{\delta}_{His})_2S^{\gamma}_{Cys}R$ R = S^{δ}_{Met} (azurin, plastocyanin, laccase) R = O^{ε}_{Glu} (phytocyanins) R = H_2O (ceruloplasmin)	➢ **Type I (blue copper proteins)** ✓ Small blue proteins – Auracyanin – Azurin – Phytocyanin family – Plastocyanin family – Rusticyanin ✓ Blue oxidases – Ascorbate oxidase – Ceruloplasmin – Laccase ✓ Nitrite reductase
 $Cu(N^{\delta}_{His})_m R_n$ L = N, O or S ligands; R = O or S ligands m = 1 to 4; n = 0 to 3; m+n = 4 or 5	➢ **Type II** ✓ Cu,Zn superoxide dismutase ✓ Dioxygenases ✓ Monooxygenases – Dopamine β-hydroxylase – Methane monooxygenase – Peptidylglycine α-hydroxylating monooxygenase – Phenylalanine hydroxylase ✓ Nitrite reductase ✓ Nonblue oxidases – Amine oxidase – Diamine oxidase – Galactose oxidase – Lysyl oxidase
 $\mu O_2[Cu(N^{\varepsilon}_{His})_3]_2$	➢ **Type III** ✓ Catechol oxidase ✓ Haemocyanins ✓ Tyrosinase
 $Cu(N^{\varepsilon}_{His})_2OH{-}\mu OH[Cu(N^{\varepsilon}_{His})_3]_2$	➢ **Trinuclear centre (type II + type III)** ✓ Blue oxidases – Ascorbate oxidase – Ceruloplasmin – Laccase
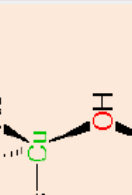 $Cu_2(N^{\delta}_{His})_2O^{\varepsilon}_{Glu}S^{\delta}_{Met}(\mu S^{\gamma}_{Cys})_2$	➢ **Cu_A** ✓ Cytochrome c oxidase ✓ N2O reductase
 $CuN^{\delta}_{His}(N^{\varepsilon}_{His})_2L$ L = bridging ligand between Cu_B and Fe of haem a_3	➢ **Cu_B** ✓ Cytochrome c oxidase ✓ Ubiquinone oxidase

1.2 COPPER TOXICITY AND DISEASES

However, the redox property that makes copper an essential element of biological systems also contributes to its inherent toxicity. Redox cycling between Cu^{2+} and Cu^{1+} can catalyse the production of highly toxic hydroxyl radicals, with subsequent damage to lipids, proteins, DNA and other biomolecules.[13] It appears to be responsible to fort the intracellular generation of superoxide. [14] High levels of copper can be fatal. Toxic effects of copper can be seen after ingestion of one gram. The fatal dose for an adult is estimated at more than 10 grams of copper.[15] Acute copper poisoning has the symptoms of diarrhea, circulatory collapse, and haemolysis. Chronic copper poisoning can lead to hepatic failure.[16] Disruptions to normal copper homeostasis are evident in three human genetic disorders: Menkes disease (MD), occipital horn syndrome (OHS) and Wilson's disease (WD). Each disease results from the absence or dysfunction of homologous copper - transporting ATPases.

Wilson's disease is a genetic disorder caused by a mutation of the protein that transports copper out of the liver, the Wilson's disease protein (ATP7B) (Figure 1.1). As a result, copper accumulates in the body, as it cannot be excreted into the bile. The symptoms of Wilson's disease include mental retardation and fulminant hepatic failure.[17] Treatment of WD consists on orally administered chelator agents or zinc salts to remove excess copper from the body with no toxic side effects. [18]

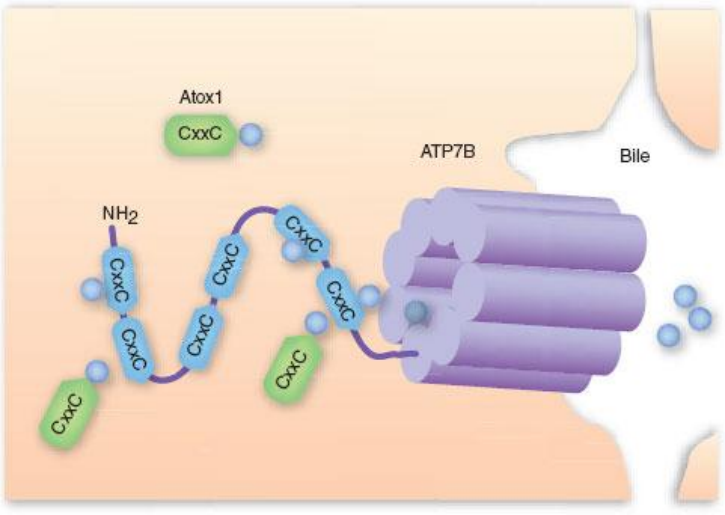

Figure 1.1. Cu^{1+} delivery pathway to P-type ATPases that mediate Cu excretion in the bile and Cu passage into the lumen of the secretory apparatus

Cytosolic Cu^{1+} is bound by the Atox1 Cu chaperone on an exposed surface. A series of ligand exchange reactions between Atox1 and the metal binding motifs of ATP7B (CxxC) results in the movement of Cu^{1+} from Atox1 to ATP7B, followed by transport across the hepatocyte membrane into the bile. [Reprinted from B.-E. Kim et al. Nat.Chem.Biol. 2008]

MD, also called the kinky hair disease or Menkes kinky hair syndrome is a fatal X-linked disorder caused by diverse mutations in a copper-transporter gene, ATP7A. Symptoms of the disease are mostly associated with the lack of activity of copper dependent enzymes leading to various clinical features such as weak muscle tone, seizures, mental retardation, developmental delay, and premature death.[19] MD can be diagnosed by genetic screening to ascertain mutations in the ATP7A gene. Historically, the treatment of MD required subcutaneous or intravenous administration of copper salts. The knowledge gained from the studies of its chemistry and physiological significance led to treatment of MD by copper–histidine formulations.[18]

Among others, there is now increasing evidence that, altered copper homeostasis may be involved in the progression of neurodegenerative diseases.[20,21] Protein-metal interactions appear to play a critical role in protein aggregation and are therefore likely to provide a link between the accumulation of aggregated proteins, oxidative damage of the brain, and neuronal cell loss in an age-dependent manner.[22] Actually, copper is also implicated in Creutzfeldt Jakob (prion) disease,[23] Disturbed copper homeostasis has been implicated in diseases such as Alzheimer disease, cystic fibrosis and Parkinson disease.[24]

Alzheimer's disease (AD) is a progressive neurodegeneration disease characterized by extra cellular deposition of Aβ peptides in senile plaques and intracellular accumulation of hyperphosphorylated τ protein in neuronal cells as neurofibrillary tangles. Potentially toxic Aβ peptides are generated from the copper-binding APP which is actively involved in balancing copper concentration in cells.[25]

Parkinson's disease (PD), the second most common neurodegenerative disorder, is associated with the degeneration of dopaminergic neurons in the substantia nigra pars compacta. Occupational exposure to transition metals, especially Fe and Cu, has been proposed as risk factor for the development of PD.[24]

Copper toxicity also results from the high affinity that Cu(I) and Cu(II) exhibit for a range of protein sites, with cysteine, methionine and histidine side chains as potential ligands, resulting in the displacement of native metal ions from their active sites, as well as in the misfolding of proteins.[26]

The remarkable metabolic changes that have long been known to occur in cancer cells have been associated, among other factors, with copper handling and copper utilizing proteins.[27] Mixtures constituted by the combination of copper(II) salts and specific copper

chelators have been shown to suppress proliferation and clonogenicity of different types of human cancer cells.[28]

In addition, the reduction of Cu(II) to Cu(I) under anaerobic conditions lead to the increase of the copper toxicity. [29]

1.3 COPPER HOMEOSTASIS

Due to the copper toxicity the copper uptake, distribution, utilization and excretion must be tightly regulated, and copper ions must be bound to proteins or low molecular weight ligands.[30,31] The distribution of copper among the various proteins and ligands in the cell is therefore dictated by thermodynamics if copper is exchangeable, and by kinetics, that ensures thermodynamic process with subsequent block of copper.[32] Several highly sophisticated systems of cellular copper transport have been discovered in both prokaryotic and eukaryotic cells. [33]

Keeping the importance of cupric Cu in biological function, an elaborate mechanism is set by Nature for maintaining Cu homeostasis, which includes a wide array of proteins namely (i) family of Cu bearing proteins (metallothioneins, prion proteins), (ii) cuproenzymes, (iii) Cu transporters (high-affinity transporter CTR1, low-affinity transporter CTR2 and the copper efflux transporters ATP7A and ATP7B) and (iv) Cu chaperone proteins (CCS, Atox1, Cox17, Sco1 and Sco2).[34] In recent years, it has also become apparent that, in addition to membrane transporters, cells contain a complex network of soluble regulator molecules that allow for the fine tuning of copper homeostasis and precise temporal and spatial allocation of copper in a cell.[34] Interactions with dynactin, ADP-ribosylation factor (Arf)1 GTPase, phosphatidylinosytol-binding protein (COMMD1), ubiquitinating machinery and other proteins have been reported, illustrating the potential dependence of normal copper distribution on many cellular factors that have not been traditionally linked to copper metabolism. [35,36,37]

The family of Cu bearing proteins plays a significant role in metal detoxification and keeps the Cu in non ionic curpric state. They are metallothioneins, prion protein, albumin, transcuperin, CP, phycocyanins of blue green algae and haemocyanins of blue blooded organisms.[38]

1.3.1 Copper uptake into the cell

Dietary copper, absorbed in the stomach and upper intestinal tract, reaches liver as a complex with serum proteins, albumin or transcuperin or the amino acid histidine.[38] Studies of Nose provide the evidence that Ctr1 in enterocytes is required for a complex process of transfering dietary copper from the lumen of the intestine into the blood.[39] (Figure 1.2)

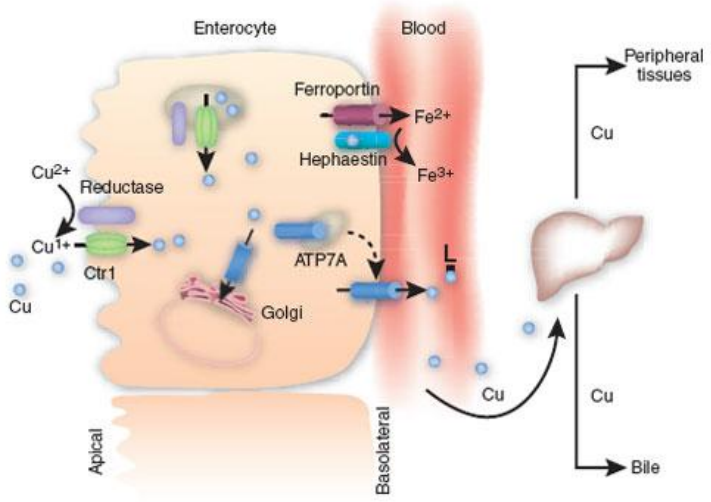

Figure 1.2. **Model for intestinal Cu absorption and peripheral distribution.**
[Reprinted from B.-E. Kim et al. Nat.Chem.Biol. 2008]

The permeating form of copper is Cu(I). Metalloreductases (Fre1 and Fre2 are needed to keep copper in the Cu(I) state, but how this oxidation state may be stabilized in the presence of oxygen is not clear yet.[40,41] In addition, when competitive studies have been performed using other metal ions, there is no inhibition of copper transport by added divalent cations, such as Zn, Mn, Cd, etc, but Ag causes inhibition. [42] It has been assumed that Ag(I) would also be transported, although this has not been demonstrated. The similarity in size of Cu(I) and Ag(I) cations has been taken as good evidence that Cu(I) is the permeant species. Genetic experiments with baker's yeast resulted in the identification of the plasma membrane-associated high-affinity copper transport protein Ctr1.[43] Zhou et al. isolated the human high-affinity copper transporter 1 (hCtr1), and it was determined to be 29% identical to Ctr1 of *S. cerevisiae.*[44] All members of the Ctr family of copper transporters possess a significant sequence homology and remarkable functional conservation. Ctr1 mRNA is ubiquitously expressed, with the highest levels found in the liver and lower levels detected in the brain and spleen. Northern blot analysis using human tissues revealed that hCtr1 has two major transcripts of approximately 2 and 5.5 kb in size and a less abundant transcript of 8.5 kb.[44]

Ctr1 has three transmembrane domains, a hydrophilic amino terminus typically rich in methionine residues outside of the membrane and a number of Cys/His conserved residues at the C-terminus in he cytoplasm. It exists as a homotrimer, and has been shown to be extensively glycosylated.[42,45] Ctr oligomer has a symmetrical channel-like structure. The protein has a visible pore surrounded by monomers, where copper is likely to enter the transporter. The conserved Met residue of the MxxxM motif in transmembrane helix 2 may provide binding sites for copper and facilitate copper entry into the pore.[46] (Figure 1.3)

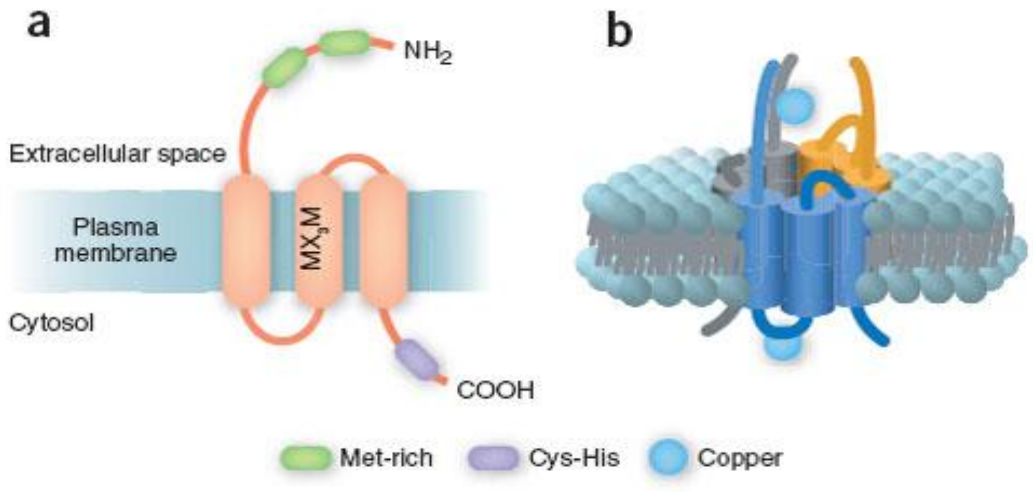

Figure 1.3. Structural model for the Ctr1 Cu1+ channel

a) A human Ctr1 monomer of 190 amino acid residues has two methionine-rich domains (MX_2M, shown in green) that function to enhance Cu^{1+} uptake and Ctr1 endocytosis at low Cu^{1+} concentrations. Three membrane-spanning domains are shown (orange), with the MX_3M motif in domain II having an essential function in Cu^{1+} import that may involve direct binding to Cu^{1+}. A cysteine-histidine motif (purple), typical of this protein family but with unknown function, is present at the C terminus of Ctr1. (**b**) A model for Ctr1 in a phospholipid bilayer. Each monomer is shown as a unique color, with the N termini projecting outside the cell or into the lumen of an endosomal vesicle. Cu is represented by blue spheres, and the phospholipid bilayer is modeled in blue and gray. [Reprinted from B.-E. Kim et al. Nat.Chem.Biol. 2008]

In the suggested model for the function of the Ctr protein family Cu(I) first coordinates to the methionine-rich (Mets) motifs in the Ctr extracellular N-terminus. Then it involves in a chain of copper exchange reactions between defined Cu(I)-binding sites, involving well-defined conformational changes. This way copper ions move through Ctr from N-terminal extracellular binding sites, furnished by the Met conserved residues, to Cys/His conserved residues in the cytoplasmic C - terminus, which in turn serve as intracellular donors for Cu(I) and its mobilization to the copper chaperones. Although it is currently unclear whether the copper chaperones directly dock to the Ctr1 homotrimer to engage in cargo transfer or whether there are other intermediates in the delivery system.[47]

It is not yet clear how hCTR1 abundance, localization, or transport activity changes in response to the extracellular copper concentration. Also unknown is whether copper levels inside the cell might modulate the activity, trafficking, or localization of hCTR1.[48] It seems reasonable to suppose that the transport activity, or the abundance of hCTR1 in the plasma membrane, or both might also change in response to copper deficit or excess. The absorption of copper by intestinal epithelial cells might also be regulated by hCTR1 abundance or transport activity.

In contrast to eukaryotes, bacteria may not have a general requirement for cytoplasmic copper. Copper proteins are localized to the cytoplasmic membrane or the periplasm, and copper loading of these proteins could take place in these compartments. For example, *E. coli* has copper-requiring proteins only in the periplasm and embedded in the plasma membrane.[5] Similarly no cytoplasmic protein requiring copper to function have been found in gram-positive bacteria.[49] Thus, many bacteria do not appear to have a requirement for intracellular copper, and the copper homeostatic machinery in these organisms may have the sole purpose of eliminating adventitious copper ions. This concept is supported by the complete absence of copper chaperones in many bacteria[50], whereas in eukaryotes, copper chaperones are essential for delivering copper to enzymes such as cytochrome *c* oxidase and superoxide dismutase. Nevertheless, specific copper importers that are expressed under copper-limiting conditions or in metal-sensitive *E. coli* strains have been described in the gram-positive *E. hirae*[51] and *B. subtilis* and in the gram-negative *Ps. aeruginosa* Q9I147 [52], but the functional meaning of the copper import process in the cytoplasm remains to be tested.

1.3.2 Copper trafficking pathways

Despite of the copper abundance, the concentration of free o labile form of copper ion in the cytoplasm of eukaryotic cell is less, than 10^{-18} M, which represents many orders of magnitude less than one atom of free copper per cell. [31] So free copper is a thermodynamic term, which corresponds to aquo (hydrated) Cu(I) or Cu(II) complexes not coordinated by tight binding ligands such as amino acids or biopolymers. A similar conclusion regarding the scarcity of free intracellular copper ions can also be derived in kinetic terms; less than 0.01% of the total cellular copper becomes free in the cytoplasm during the lifetime of the cell. [30] Part of this pool is bound to general metal binding proteins called metallothioneins. Recently have been identified another elements for the management of cellular copper is the copper chaperone. [30,53,54,55] Copper chaperones can acquire the metal under conditions where the

metalloenzymes can not. They perform a dual role of both binding free copper, to inhibit any possible toxic reactions, and they also sequester copper for delivery to proteins that utilize copper. In essence, these molecules act to escort copper ions and protect them from copper-scavenging detoxification mechanisms.[54] Once it has been transferred across the cell membrane, copper is delivered to intracelullar destinations through pathways of protein-protein interactions. Thus far, three copper trafficking pathways have been identified that require the action of copper chaperones. These include: (i) copper delivery to the secretory pathway for activation of enzymes destined for the cell surface or extracellular milieu; (ii) copper delivery to Cu/Zn superoxide dismutase (SOD1) in the cytoplasm; and (iii) delivery of copper in the mitochondria for activation of cytochrome oxidase.[54] (Figure 1.4) In the following sections I will describe in details the above pathways.

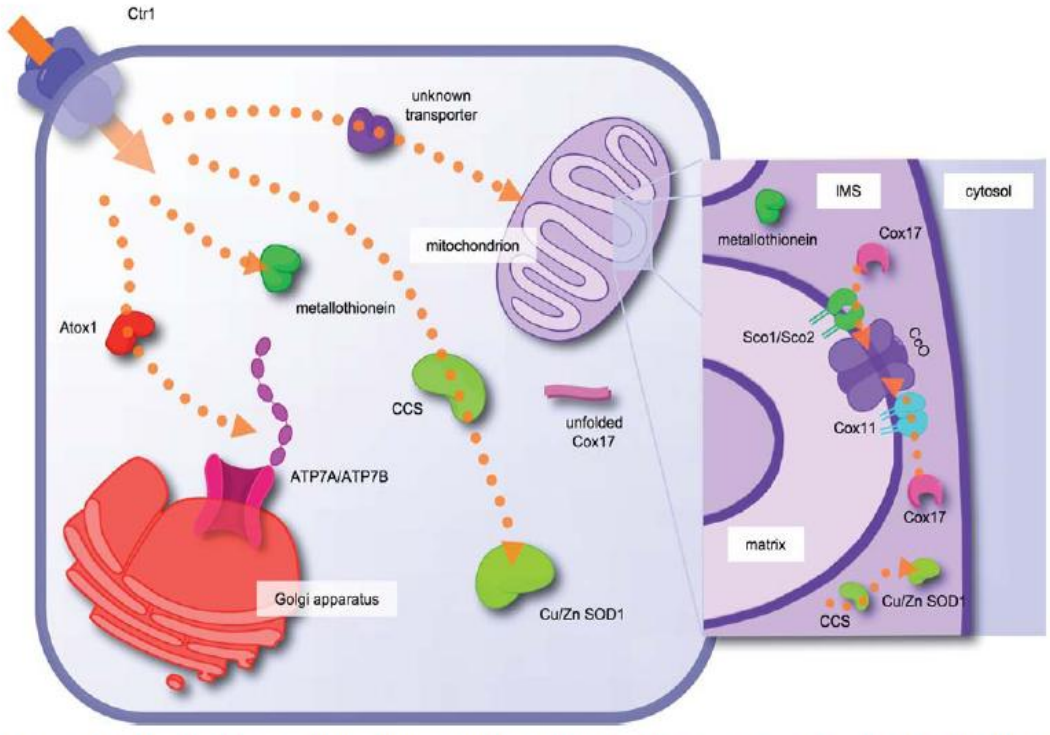

Figure 1.4. Copper pathways in a human cell.

Cu(I) is imported through the high-affinity Ctr1 copper transporter and delivered through an unknown mechanism to copper chaperones: (i) Atox1 for delivery to the P-type ATPases ATP7A and ATP7B in the Golgi apparatus; (ii) CCS, the copper chaperone for copper/zinc superoxide dismutase 1 (SOD1), for transfer to SOD1; (iii) the mitochondrion, through an unknown transporter, for insertion into cytochrome c oxidase (CcO) and SOD1. Metallothioneins also bind copper ions in the cytoplasm and in the IMS and may serve as copper reservoirs during times of deficiency. In the mitochondrial intermembrane space (IMS), Cox17 delivers Cu(I) to either Sco1/Sco2 for transfer to subunit II of CcO or Cox11 for delivery to subunit I. [Reprinted from L.Banci et al. Nat.Prod.Rep. 2010]

1.3.2.1 Copper delivery to the trans-Golgi network

The best understood metallochaperone protein, Atx1, was originally isolated as an antioxidant protein in *Saccharomyces cerevisiae*.[56] Atx1 delivers Cu(I) to Ccc2, the yeast P-type ATPase, in the trans-Golgi network, where it can then be incorporated into enzymes such as the multicopper ferroxidase Fet3. Atx1's human homolog, known as Hah1 or Atox1, delivers copper to the Menkes and Wilson's disease P-type ATPases (ATP7A and ATP7B, respectively), which in turn are able to pump the copper ions in the Golgi organelle for subsequent incorporation into copper enzymes.[57] The Atx1-like proteins and their target ATPases are characterized by conserved MT/HCXXC motif. In the structure the CXXC motif housed on a solvent-exposed loop. (Figure 1.5) The important elements of this sequence are the two ligating cysteines, which change conformation as a function of copper transfer and release.[58] This type of metal binding site was first structurally characterized with metal ions other than copper due to the instability of Cu(I) in aqueous solution.[53]

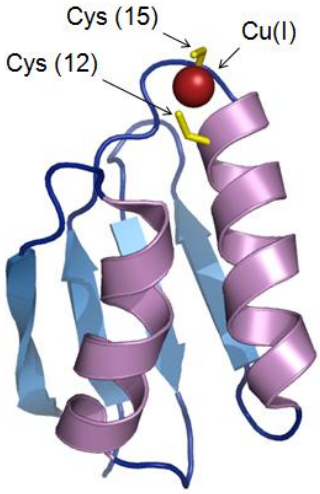

Figure 1.5. The Cu(I) form of Hah1 protein. (PDB 1TL4)

The overall structure of Atx1-like copper chaperones comprises a βαββαβ fold. This fold has been shown to provide a tight Cu(I)-binding site and protects the metal center from both oxidants and from capture by excess competing thiols such as glutathione.

The target ATPases is the class of ion transporters, that use energy from the hydrolysis of ATP and undergo a structural change upon phosphorylation that leads to Cu(I) ion pumping across cell membranes.[59] They are 160–170-kDa membrane proteins with eight TM segments and several cytosolic domains: A-domain and ATP-binding domain. The transmembrane helices define the ion chanel. The highly conserved CPC sequence in the sixth helix is one of the specific characteristic. Another particular feature of these proteins is the presence of a

long N-terminal tail, which contains variable independently folded domains,[50] (Figure 1.6) each of them contains copper binding sites formed by GMxCxxC motif and possesses a βαββαβ ferredoxin fold, similar to that dicribed for the Atx-like proteins. The ATP-binding domain consists of two parts, the N- and P-domains, and is involved in ATP binding and hydrolysis. The solution structure of A-domain is characterized by seven antiparallel β-strands arranged in two sheets packed against each other and forming a distorted double-stranded beta-helix fold (Figure 1.6).

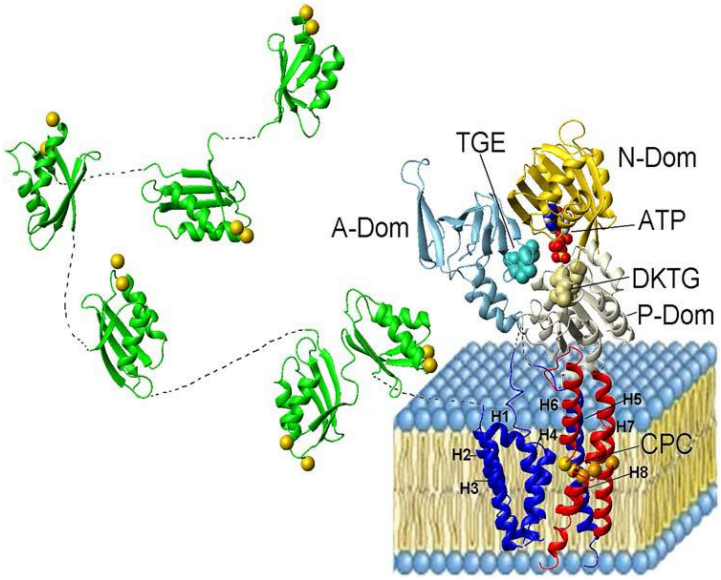

Figure 1.6. Schematic representation of the topology of copper(I)-transporting ATP7A and ATP7B in analogy with SERCA.

The topological scheme includes the A-domain (PDB 2KIJ), the ATP-bound N-domain (PDB code 2KMV) and each NMBDs (domain1 PDB code 1KVJ; domain2 PDB code 1S6U; domains 3–4 PDB code 2ROP; and domains 5–6 PDB code 2EW9) structures. The structure of the P-domain was modeled using as template the structure of corresponding domain in the homologous protein from A. fulgidus (PDB code 2B8E). The structural arrangement of the eight transmembrane helices is obtained from the cryoelectron microscopy model of CopA from A. fulgidus (PDB code 2VOY). The copper(I)-binding cysteines in both N-terminal domains and transmembrane CPC region are shown as yellow spheres. The predicted position of the residues constituting site II in the transmembrane region are shown as orange spheres. [Reprinted from L.Banci et al. Cell.Mol.Life Sci. 2010]

The A-domain interacts with the ATP-binding domain and is required for conformational changes during ATP hydrolysis.[34] The characteristic mechanistic feature of this family of P-type ATPases is the formation of a transient phosphorylated intermediate during ATP hydrolysis.[59] Under basal conditions, these transporters are located in the TGN, where they receive copper from Hah1. Hah1 transfers copper to one of the metal-binding sites in the N-terminal domain of Cu-ATPase.[60] Initial copper binding results in a conformational change that allows Hah1 transfer copper to other sites in the N-terminal domain or between sites[61], or

even donate copper to the TM-sites, as suggested by studies in the archeal CopA[62]. The last one can be considered as a plausible alternative for the copper transfer to the ATPases. Copper is required for the formation of a weak, reversible interaction between the partners, indication that the intermolecular complexes are metal-mediated.[63] Similar to the mechanism observed by coupling mutagenesis and advanced NMR experiments, for the interactions between Atx1 and the N-terminal metal binding domains of Ccc2.[64] The mechanism of copper transfer from Atx1 to the Ccc2 copper transporter is shown in Figure 1.7.

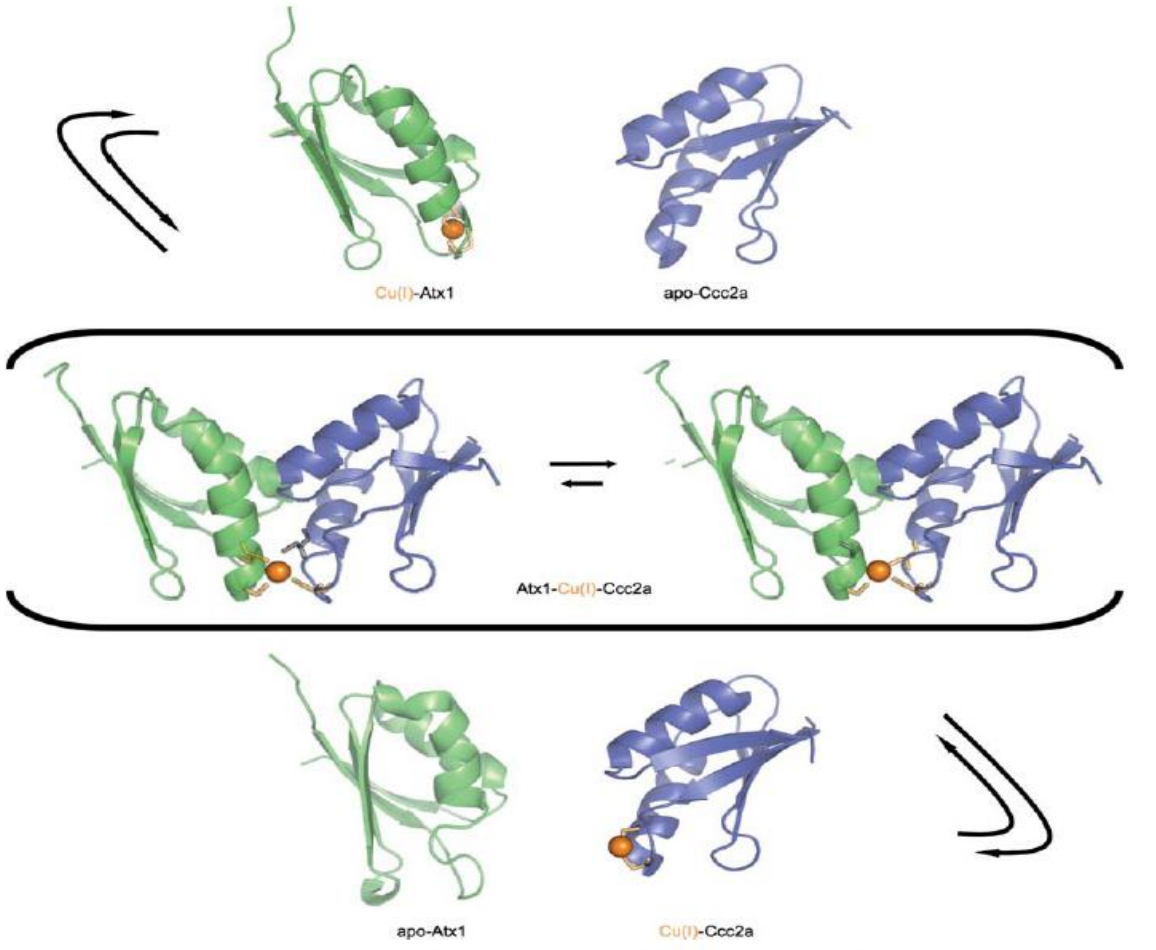

Figure 1.7. The mechanism for the transfer of Cu(I) between Atx1 and Ccc2a.

The interaction between these two proteins is metal-mediated. The top structures show Cu(I) bound to Cys15 and Cys18 of Atx1, and Ccc2a in its apo state. In the center structures, copper is additionally bound by Cys16 and Cys13 of Ccc2a, while Cys18 of Atx1 detaches from the metal ion.62 The lower structures show the completed copper transfer, with Atx1 in its apo state and copper bound to Cys13 and Cys16 of Ccc2a. [Reprinted from L.Banci et al. Nat.Prod.Rep. 2010]

Copper transfer to the TM domain is accompanied by ATP hydrolysis and phosphorylation of the catalytic Asp. This in turn induces the change in protein conformation exposing copper to the lumen of the TGN vesicles. The low pH within the TGN may facilitate

copper release, leading to Cu-ATPase dephosphorylation and return in the original state. When Cu is elevated, all sites within the N-terminal domain are saturated with copper; this results in weakening interactions between the N-terminus and the ATP-binding domain and an increased rate of catalytic phosphorylation[65]. Thus, copper is not only a transported ion but also a modulator of its own transporter activity. Both of these proteins exhibit copper-induced trafficking and redistribution in response to changes in copper abundance.[66]

1.3.3.2 Copper delivery to superoxide dismutase in cytosol

One of the cellular defense systems from oxidative stress is the antioxidant enzyme Cu,Zn-superoxide dismutase (SOD1). SOD1 is a copper-zinc enzyme, catalyzing the disproportionation of superoxide anion to oxygen and hydrogen peroxide.[67] In eukaryotes, it is mainly localized in cytosol with a smaller fraction in the mitochondrial intermembrane space (IMS).[68] It has also been reported in nuclei, lysosomes and peroxisomes.[69] Both the primary sequence and the three-dimensional structure of SOD1 are highly conserved from prokaryotes to eukaryotes.[70] SOD1 forms a tight non-covalent homodimer with a dissociation constant of $1.0 * 10^{-10}$ M^{-1} for the human enzyme[71], and each subunit has an immunoglobulin-like β-sandwich fold with an intrasubunit disulfide bond. SOD1 has to undergo several post-translational modifications before reaching its mature form. The protein requires insertion of zinc and copper atoms, followed by the formation of a disulfide bond between Cys-57 and Cys-146, which makes the protein fully active.[72] One copper and one zinc ion are bound per monomer subunit (Figure 1.8).

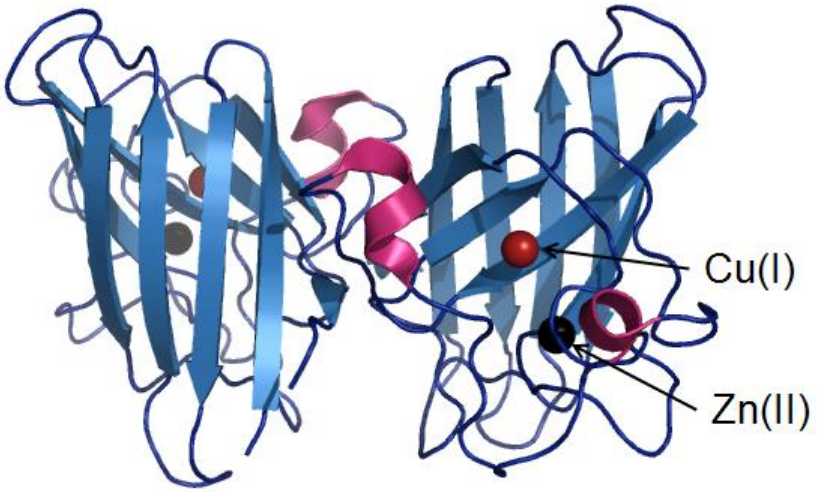

Figure 1.8. Human CuZnSOD1 (PDB 1L3N)

The Cu(II) ion is coordinated by four histidine residues (His46, 48, 63 and 120), forming a distorted square plane, and interacts with a water molecule. His 63, is also a ligand of the Zn(II) ion, which completes its coordination sphere with three other amino acid residues (His71, His80 and Asp83) in a distorted tetrahedral arrangement. Binding of the Zn(II) ion is not essential for the dismutation reaction, but stabilizes SOD1 structure.[73] An intramolecular disulfide bond is highly conserved in the SOD1 proteins from all known species. It confers stability to the protein fold and plays a structural role through the formation of a hydrogen bond with Arg 143 for the uptake of the superoxide anion.[73]

Although SOD1 binds copper with high affinity *in vivo* and *in vitro*, copper insertion requires a copper chaperone protein, the copper chaperone for superoxide dismutase (CCS).[31,74] CCS, which is found in both yeast (yCCS) and humans (hCCS), belongs to an emerging family of metallochaperone proteins that function specifically in the intracellular delivery of metal ions.[55]

These 26–30-kDa proteins possess an Atx1-like sequence at the N terminus, complete with the MXCXXC metal- binding motif, which is fused to a sequence homologous to its SOD1 target (Figure 1.9).

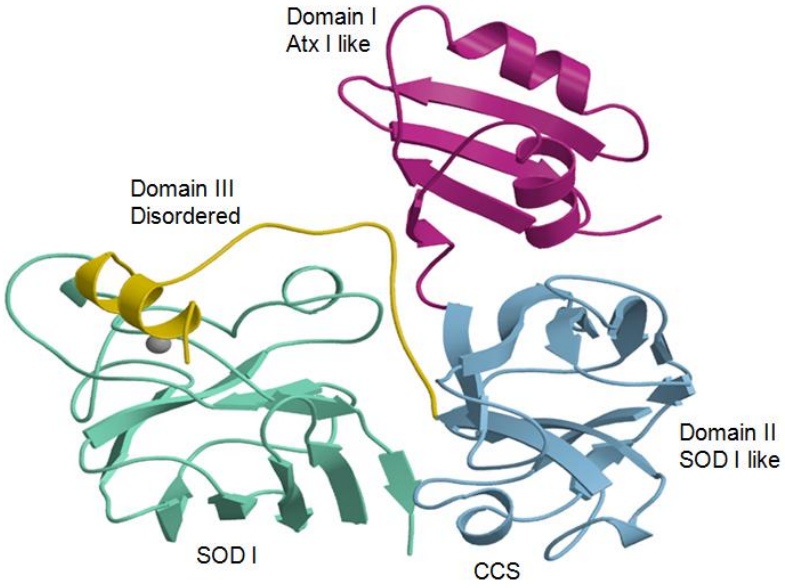

Figure 1.9. Structual model of copper chaperone for superoxide dismutase.

The C-terminal region of CCS has high sequence homology with CCS proteins from other species, and also contains two highly conserved cysteine residues.[75] The three regions correspond to domain 1 (Atx1-like), domain 2 (SOD1-like), and domain 3, representing a unique CCS sequence (Figure 1.10). The domain 1 (~8 kDa) has a structure similar to Atx1

copper chaperone and can bind one copper ion when the domain is expressed as isolated, but is not essential to SOD1 activation in cells under normal conditions.[76] Recent crystallographic structures for yeast and human CCS show that domain 2 from yeast and human adopts a "Greek key" β-barrel fold that is quite similar to its target enzyme SOD1.[77,78] The dimeric domain 2 of hCCS contains a Zn(II) site similar to SOD1 but lacks the ligand set for Cu coordination: three of the four histidine residues present in the SOD1 copper-binding site are also conserved in domain 2 of hCCS, with the fourth histidine replaced by an aspartate. The copper ion is not bound at this site, Copper binding to domain 2 would thus not be required for copper incorporation into SOD1. In contrast, yCCS domain 2 lacks both the Zn and Cu centers. Domain 2 is important for docking with SOD1 during the activation reaction.[79] Domain 3 of CCS is a short polypeptide (30–40 amino acids) without any tendency to form secondary structures, but is essential to CCS function. It exhibits a low homology with a portion of prolyl cis-trans isomerase and features a CXC motif, which is highly conserved among all species. The domain 3 polypeptide alone is sufficient to bind a Cu(I). [76]

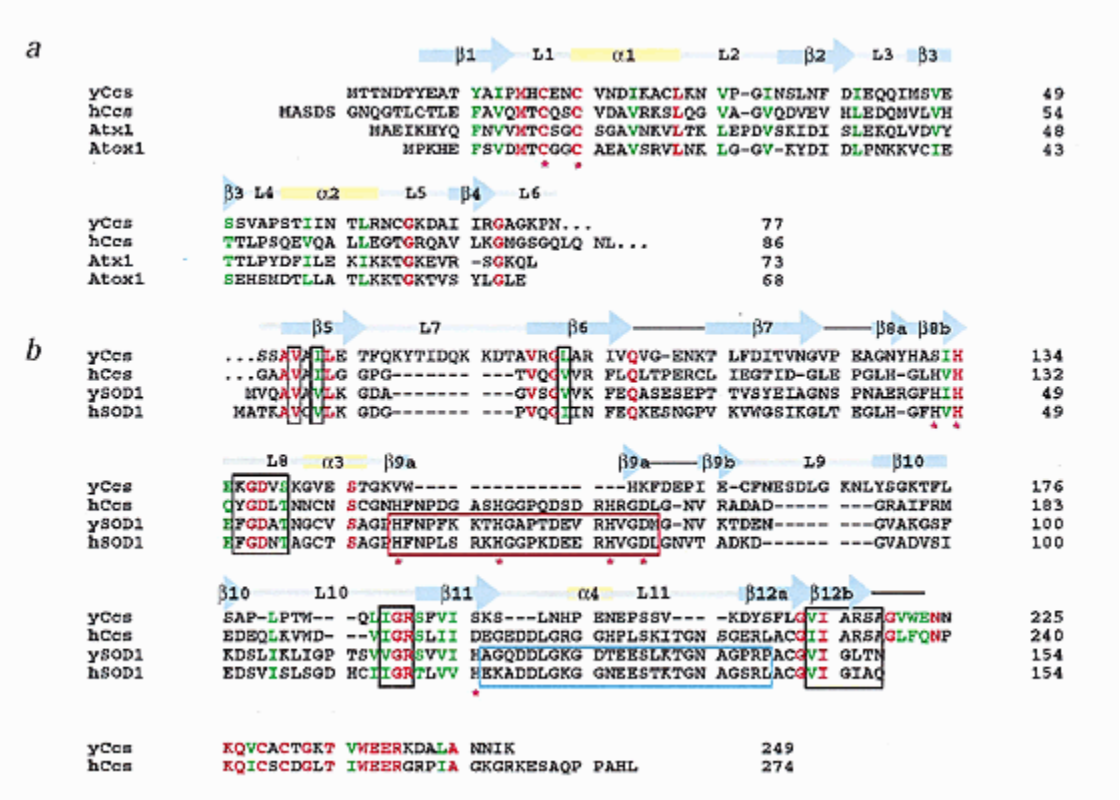

Figure 1.10. Structure-based alignments comparing the amino acid sequences of CCS to Atx1 and to SOD1

a, The sequences of yCCS (Domain I) and hCCS are aligned with yeast Atx1 and its human homolog Atox1. ***b***, The sequences yCCS (Domain II) and hCCS are aligned with yeast and human SOD1. The positions of the yCCS secondary structure elements determined from the crystal structure are shown above the yCCS sequence. β-strands are shown as blue arrows, α-helices are shown as thick yellow lines, and loop regions are shown as thin gray lines. Residues that are identical in all four sequences are shown in red. Similar residues are shown in

green. Residues involved in metal ion coordination are denoted by magenta asterisks. The SOD1 zinc subloop is enclosed in a red box, the SOD1 electrostatic channel binding loop is enclosed in a blue box, and residues involved in dimerization in CCS and SOD1 are enclosed in black boxes. Dimerization residues are defined as residues whose accessible surface area decreases by >1 $Å^2$ upon dimer formation. The most conserved regions in CCS and SOD1 clearly correspond to the dimer interface. [Reprinted from A.Lamb et al. Nat.Struct.Bio. 1999]

Copper coordination in full-length CCS is still quite controversial as, variable amounts of bound copper ions have been observed in both yeast and human CCS proteins. Extensive EXAFS experiments gave rise to the possibility of the formation in hCCS of two distinct clusters with different stoichiometry: a polynuclear Cu_4S_6 cluster involving extra Cys residues from domain 2 and a dinuclear Cu_2S_4 cluster when these extra Cys residues are unavailable. The functional significance of this complex copper(I) coordination in CCS is still not clear.[80,81]

Several laboratories have suggested that the most likely mode of copper delivery from yCCS or hCCS to SOD1 occurs via a mechanism where a monomer of the CCS forms a domain 2-mediated heterodimer with a monomer of SOD.[82] The heterodimer interfaces are similar to both the SOD and CCS homodimeric interfaces. However, the metal binding region in the Atx1-like domain is approximately 40 Å from the copper binding site in SOD.[83] Therefore, for direct copper transfer to occur via this domain, there must be substantial motion to donate the copper to SOD. One of the theoretical modeling study based on a monomer of the hCCS forming a heterodimer with human SOD suggested that the flexible CXC motif in domain 3 can coordinate copper held in the domain 1 and then move to deposit copper into the SOD copper binding site. But also this mode of copper delivery would require a very large movement.[84] However, the metal binding studies performed for the tomato CCS showed, that domain 1 and 3 may bridge via a dinuclear copper cluster in the fully metallated protein, suggesting a mechanism for a transfer of a single metal ion from the sequestring site to the translocation site.[85,86] SOD1 is a very tight homodimer and exists in many-fold excess relative to the copper chaperone in vivo.[75] Full-length yCCS (hCCS) is also dimeric.[77] These facts, coupled with the problems inherent in the heterodimer model described above, led scientists to search for an alternative mechanism of copper delivery to SOD that can involve dimer of dimers CCS and SOD interactions. This model possesses some advantages over the heterodimer one. There is no need to disrupt the very stable SOD homodimer and the movement by either domain 1 or the CXC motif of domain 3 to the copper binding site of SOD, would be much shorter, minimizing the possibility of copper loss.[82] However, the crystal structure of the y SOD1-yCCS complex supports the monomer-monomer interaction model.[87,88] The formation of the intermolecular disulfide between SOD1

and CCS in the crystal structure suggests the involvement of CCS in SOD1 disulfide formation. It has recently been shown that the copper-bound yCCS can activate the disulfide-reduced apo-ySOD1 monomeric form in the presence of oxygen.[89,73] The model, proposed by O'Halloran group suggests (Figure 1.11) that Cu-charged CCS interacts with newly synthesized SOD1 polypeptides prior to completion of its native fold with the formation of noncovalent heterodimeric complex. Zn(II) binding to SOD1 can occur either prior to CCS complex formation or concomitantly. The subsequent reaction of the docked heterodimer with dissolved O_2, leads to formation of a disulfide-linked heterodimer of CCS and SOD1. After the oxidation step, the intermolecular disulfide is envisioned to undergo exchange to give an intramolecular disulfide in SOD1 thus releasing active enzyme.[73] Thus CCS plays a functional role in the SOD activation not only in copper insertion, but also in the disulfide bond formation.

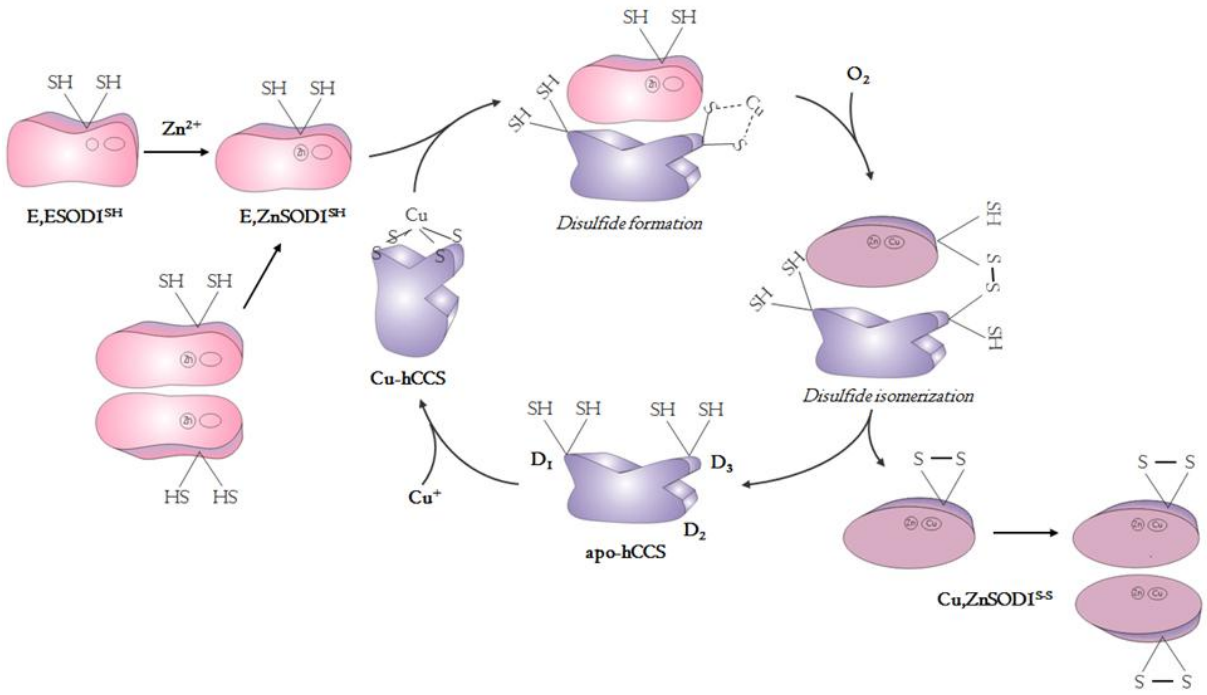

Figure 1.11. Proposed mechanism of the O_2-dependent post-translational modification of SOD1 by Cu-hCCS.

However, it was discovered that CCS is not the only way to activate SOD1.[90] Some experiments with CCS-knockout mice cells showed that a certain degree of SOD1 activity remain in the absence of the copper chaperone.[91] It was found that the reduced glutathione is needed for activating SOD1 with Cu in the cells null for CCS. [90] Although, in all organisms tested until now, maximal SOD1 activity is obtained with CCS, suggesting that CCS may represent the preferred route of enzyme activation, while the CCS-independent pathway acts

as a backup under conditions in which CCS is limited. [91] The dual pathway for SOD1 activation can be interpreted by dual role of SOD1 in oxidative stress protection and cell signaling in higher organisms: ander aerobic conditions the maximal activity can be achieved through oxygen-regulated CCS and inder hypoxic the reactant oxygen species products and reactants of SOD can effect cell signaling processes.[91]

Posttranslational activation of SOD1 including Cu/Zn binding and disulfide formation should be well coordinated. If defects are present in the posttranslational activation pathway, the SOD1 could be toxic to the cell. In particular, SOD1 protein aggregates have been found in the motor neurons of SOD1-related amyotrophic lateral sclerosis (ALS) patients and transgenic mouse models, and have therefore been proposed to be related to the familial form of amyotrophic lateral sclerosis.[92] ALS mutantions in SOD have been demonstrated to increase the propensity of the protein to for insoluble aggregates by decreasing both disulfide stability and metal affinity[93]

1.3.3.3 Copper trafficking to the mitochondrion and assembly of mitochondrial copper enzymes

The mitochondrial pathway appears to be the most complex of the three currently known copper chaperone pathways. The essential need for copper in mitochondria derives from its role in the cytochrome c oxidase (CcO) enzyme, which is required for cellular utilization of oxygen. Copper is also needed in the mitochondrion for the protection against oxidative stress. Indeed, cellular energy production occurring in mitochondria is obviously beneficial for the cell, but also bears the risk of producing oxygen radicals that have a high redox potential, damaging important mitochondrial components. In order to avoid superoxide accumulation, which determines serious cellular oxidative damage, eukaryotic cells exploit mitochondrial superoxide dismutase (SOD) enzymes both in the intermembrane space (IMS)[68], as Cu,Zn-SOD1, and in matrix, as MnSOD2[94]. Mitochondrial SOD1 is imported in the IMS in the apo-form, so its metallation must likewise occur within the IMS. Moreover, since the copper-binding subunits of CcO are encoded by the mitochondrial genome, its copper metallation must also occur within the organelle. The presence of two copper metalloenzymes that are metallated within the mitochondrion needs a specific copper transport pathway to this organelle for the correct functioning of CcO and SOD1 enzymes. However, how copper is trafficked from the cytoplasm to mitochondrion is still an open question. A labile copper pool was found in mitochondria of yeast and human cells, and it was

proposed to be the source of copper used in the metalation of CcO and of SOD1 within the IMS[95]. The labile copper pool is formed by a low mass ligand complex that resides within the matrix and stably binds Cu(I) in an anionic complex (CuL), but its nature has yet to be elucidated. The suggested model predicts that Cu(I) binding to the ligand within the cytosol triggers the translocation of the anionic CuL complex to the mitochondrion[95]. Once copper ions reach the IMS, complex protein machinery operates in the case of CcO to correctly insert them in the nascent CcO enzyme (Figure 1.12).

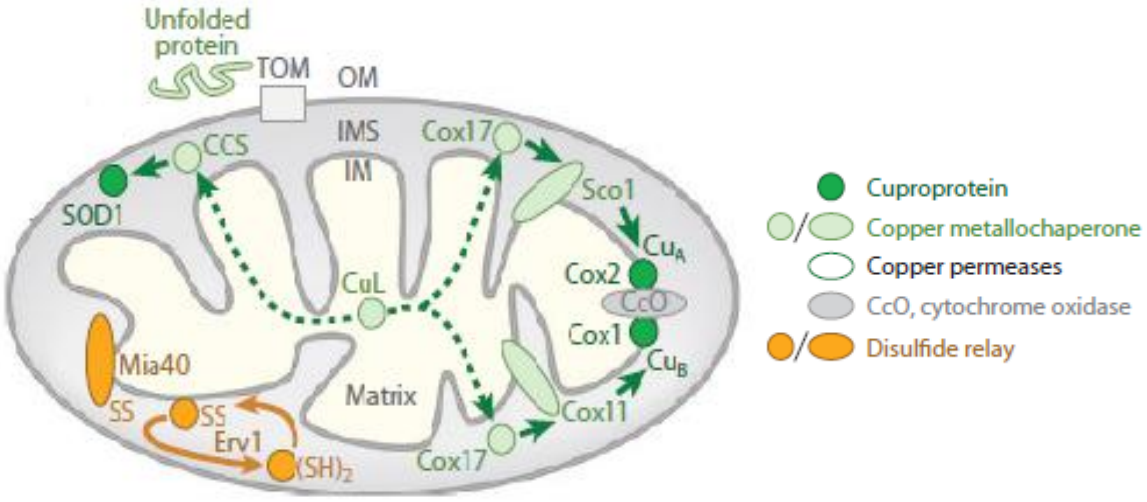

Figure 1.12. Cuproproteome of mitochondrion

Cytochrome c oxidase - (common abbreviations: CO, CcO, COX, or complex IV) is the terminal enzyme of electron transport chains in eukaryotes and some prokaryotes. It belongs to the superfamily of terminal oxidases known as the heme-copper oxidases. Members of this superfamily are redox driven proton pumps that couple the reduction of molecular oxygen to vectorial translocation of protons across the membrane.[96] Cytochrome c oxidase (CcO) is an oligomeric complex localized within the mitochondrial inner membrane (Figure 1.13).

Eukaryotic COX is a 200kDa complex enzyme, which consists of 11–13 subunits depending on the organism.[97] Prokaryotic homologues usually have a less complex organization. The core of the eukaryotic enzyme is formed by three subunits, which are encoded by mitochondrial DNA and translated on mitochondrial ribosomes. The three core subunits are highly conserved between different organisms. Their prokaryotic homologues constitute the functional enzyme. They contain a couple of redox-active metal centers which play a key role in the assembly steps and function of the enzyme.

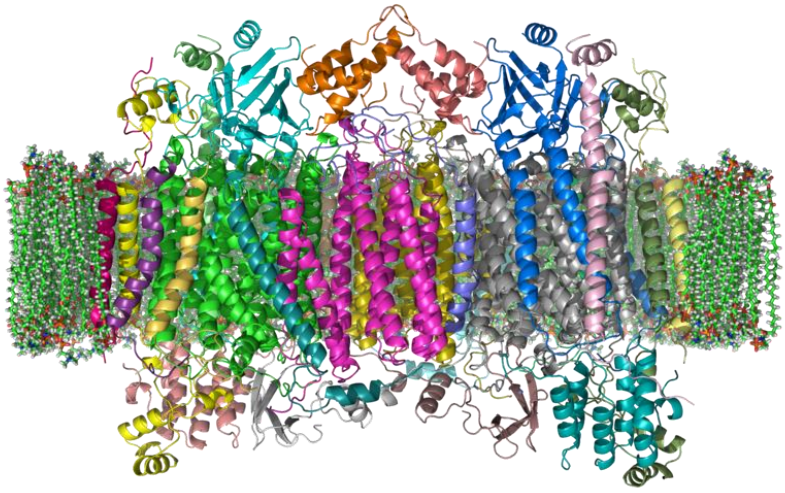

Figure 1.13. Structure of Bovine Heart Cytochrome c Oxidase (PDB 1OCC)

The low-spin heme *a* and a bimetallic site composed of high-spin heme a_3 and a copper ion (Cu_B) reside in subunit Cox1p. The binuclear Cu_A center is coordinated by subunit Cox2p and—together with heme *a*—constitutes the entry site for electrons which are channelled through the respiratory chain to COX. The other subunits are encoded by the nuclear genome, that complicates the assembly of the enzyme. The subunits synthesized in two compartments must be coordinately recruited to assembly sites. Besides the above mentioned metal centers, COX contains magnesium, sodium and zinc ions. Only few data are available on the role of these metals for COX function.[98]

Based on a large body of spectroscopic and kinetic data[99] it is generally accepted that internal electron transfer in oxidase proceeds, in four repetitive steps, from the CuA center located in subunit II to the three redox sites in subunit I, heme a and the binuclear center composed of heme a_3 and CuB where dioxygen reduction to water is catalyzed:

$$4\text{cyt c}^{\text{red}} + 8H^+_{(in)} + O_2 \rightarrow 4\ \text{cyt c}^{\text{ox}} + 2H_2O + 4\ H^+_{(out)}$$

Electrons enter the oxidase complex exclusively via its CuA center. Subunit II has been described as the main docking site for cytochrome c. Its interaction with oxidase is based on long-range electrostatic preorientation between the highly basic mitochondrial cytochrome c and an extended lobe of acidic residues on the surface of subunit II close to the CuA site.[100]

Assembly of a functional cytochrome c oxidase apparently is an ordered multistep process in humans and other eukaryotes, while the sequence of assembly events is less strict in prokaryotic organisms. In this process about thirty accessory proteins have been identified

necessary for the complex assembly. The putative process of the cytochrome oxidase assembly could be devided in four steps.[101] (Figure 1.14)

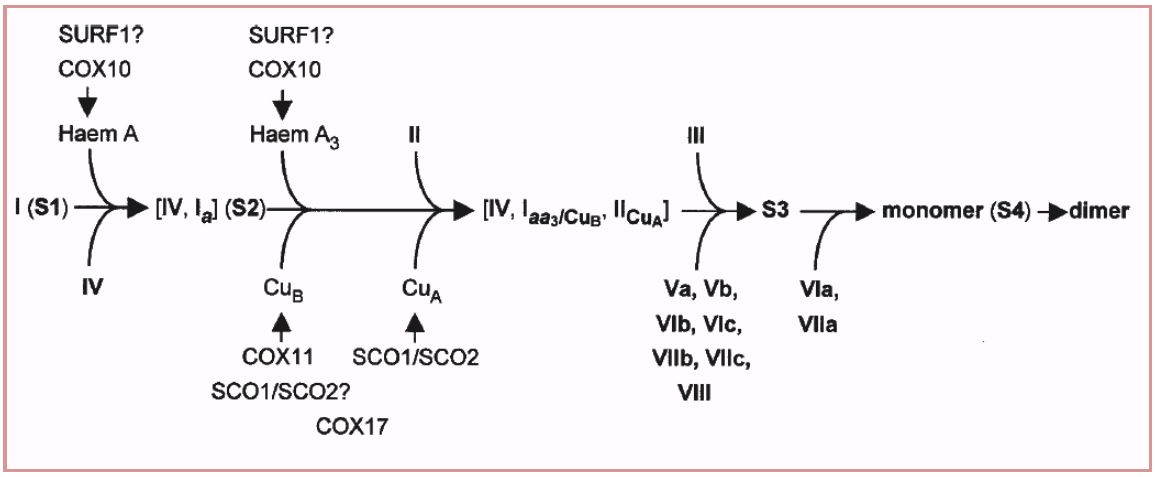

Figure 1.14. Model of the assembly pathway of human CcO.

I: Cox1, II: Cox2, III: Cox3, IV: Cox4, V: Cox5, VI: Cox6, VII: Cox7, VIII: Cox8, SURF1: Surf1, COX10: Cox10, Heam A: heme *a*, Heme A_3: heme a_3, SCO:Sco. [Reprinted from J.-Taanman et al., Biochem Soc. Trans 2001]

At the first step, the Cox1 is folded into the inner membrane and that concurrently the heme a moiety is buried inside the protein by the interaction with Cox10/Cox15. The inner-membrane protein Surf1 is possibly involved in heme *a* insertion or in the folding of Cox1. The first subcomplex comprises Cox1 and Cox4 subunits. In the next step, the CuB-haem a_3 centre of Cox1 is formed and, simultaneously, Cox2 associates with Cox1 to stabilize the active site. The CuA centre of Cox2 is also created at this phase. Possibly that the CuB centre of Cox1 is generated at a later stage. A number of proteins are involved in the copper insertion at two copper sites of the CcO, including Cox11, Cox17, Sco1 and Sco2, that will be described subsequently. In the final steps of the assembly, Cox3, Cox5a, Cox5b, Cox6b, Cox6c, Cox7c and Cox8 subunits become part of the subcomplex Cox1/Cox4/Cox2. The monomeric enzyme is formed when Cox6a and Cox7a subunits associate to Cox3 subunit. The assembly is completed with the holoenzyme dimerization. [102]

Cox17 - It has been demonstrated that Cox17, a copper chaperone that was originally a candidate for the transport of cytosolic copper to the mitochondrial IMS, functions in the delivery of copper to CcO within the IMS.[103] Unlike Atx1 and CCS that donate Cu(I) directly to the target molecule, Cox17-mediated Cu(I) donation to cytochrome c oxidase subunits involves two accessory proteins Cox11 and Sco1, which function in the metallation of the

CuB site in CcO subunit Cox1 and CuA site in Cox2 subunit respectively.[104] Cox17 is a small hydrophilic protein of 63 residues in humans. Prokaryotic homologs of Cox17 have not been identified.[105] The mammalian Cox17 contains six conserved cys residues and can exist in three redox states corresponding to the fully reduced $Cox17_{0S-S}$, the partially oxidized $Cox17_{2S-S}$, and the fully oxidized $Cox17_{3S-S}$ protein.[106] Redox reactions are important for targeting of Cox17 into IMS, where $Cox17_{0S-S}$ is oxidized to $Cox17_{2S-S}$ through a mechanism mediated by Mia40 proteins.[107] The oxidation leads to the formation of an active protein with coiled coil helix–coiled coil helix structural motif (CHCH), where two short helixes are connected with two interhelical disulfide bonds and oxidative folding is crucial for retention of this protein in IMS. $Cox17_{2S-S}$ is also a functional form of Cox17, it is responsible for the metallation of Sco1 chaperone.[108] Cox17 binds Cu(I) in one monomer conformer consisting of a simple helical hairpin structure stabilized by two disulfides. Although Cu(I)Cox17 can adopt multiple oligomeric states forming polycopper clusters.[108] (Figure 1.15) Recent data indicate that metal transfer between Cox17 and Sco1 might be coupled to electron transfer and highlighting the importance of redox reactions in functioning of Cox17.[109]

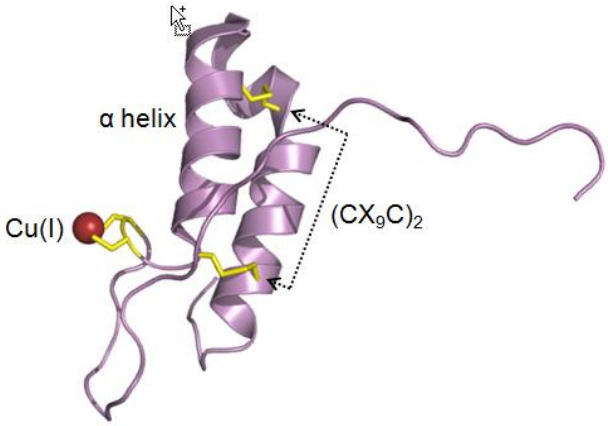

Figure 1.15. Copper metallochaperone Cox17.

Disulfide bonds between two pairs of cysteine residues (*yellow*) on antiparallel α-helices (violet*)* create a helical hairpin of Cox17 (PDB 2RNB)

Sco1 and Sco2 - Both human Sco1 and Sco2 proteins are required for CcO biogenesis and have nonoverlapping functions.[110] Sco1 and Sco2 are highly similar proteins with C-terminal region protruding the IMS and tethered to the IM by a single transmembrane helix at the N-terminus. The function of Sco1 is dependent on its single transmembrane helix since targeting of Sco1 to IMS as a soluble protein yields a nonfunctional protein.[111] Cells lacking yeast Sco1 are respiratory deficient and are devoid of CcO activity, while yeast sco2Δ cells

lack a obvious phenotype associated with respiration[69]. Cu(I) is trigonally coordinated by two cysteinyl residues within a CPDVC sequence motif plus a histidine imidazole.[112] (Figure 1.16) Mutation of the Cys or His residues abrogates Cu(I) binding, resulting in a nonfunctional CcO[112]. These proteins have thioredoxin folds, raising questions about whether Sco proteins may function in redox reactions. Thus it was found, that *Thermus* Sco1 functions as an oxidoreductase, rather than a Cu(I) donor, to form the CuA center in CcO. The direct Cu(I) transfer from Cu-PCuAC to subunit II may involve ligand-exchange steps with the two Cys residues in the CuA center.[113]

Direct Cu(I) transfer from Cox17 to Sco1 has been shown *in vitro* and *in vivo*. This likely occurs through a highly transient interaction of the two molecules[108]. The Cu(I) ions transferred from Cox17 to Sco1 appear to be donated subsequently to Cox2 as an intermediate step in CcO assembly. The Sco1-mediated metallation of Cox2 likely occurs after extrusion of the Cox2- soluble domain into the IMS by the Cox18 translocase. Information on the Sco1-mediated metallation of Cox2 in eukaryotes is limited, although a group of conserved residues on the dynamic protruding loop in Sco1 was shown to be important for function with Cox2.[114] Sco1 proteins transfer both a Cu(I) and Cu(II) ion to form the mixed valent CuA site. This molecular mechanism has been recently investigated in a bacterial organism showing that, even if the proteins involved in the bacterial CuA assembly are partially different with respect to the eukaryotic ones, a sequential insertion of two Cu(I) ions occurs yielding a reduced CuA site that can be converted to the oxidized, mixed valence site through electron transfer after the complex assembly.[113]

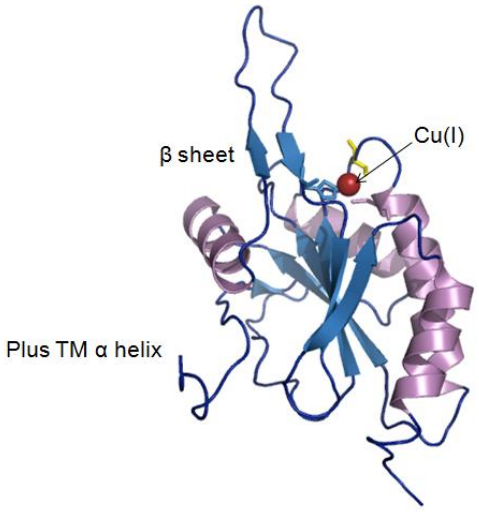

Figure 1.16. Copper metallochaperone Sco1.

Sco1 is tethered to the inner membrane (IM) (hydrophobic α-helix not shown) with a thioredoxin fold (β-strand, *blue*; histidine, *cyan*) in the intermembrane space (PDB 2GQM)

Cox11 - Formation of the CuB site is also dependent on accessory proteins for both the insertion of copper and heme groups. A copper-binding protein of the IM space, Cox11, is implicated in the formation of the CuB site of CcO. *S. cerevisiae* lacking Cox11 has impaired CcO activity and lower levels of Cox1.[115] Cox11 has a single transmembrane helix just downstream the N-terminal mitochondrial targeting sequence and a C-terminal domain protruding into the IMS which binds a single Cu(I) ion.[116] Three conserved Cys residues were candidate ligands for the Cu(I) ion. The structure of the globular domain of a Cox11 homolog from *Sinorhizobium meliloti* adopts an immunoglobulin-like β fold.[117] Two of the conserved cysteines are located on one side of the β-barrel structure, while the third is located far from the others in the unstructured N-terminal region only five/four residues from the IM. (Figure 1.17) Cox11 dimerizes upon Cu(I) binding to form a binuclear Cu(I) thiolate cluster at the dimer interface.[116] If Cox11 directly transfers the metal to Cox1 subunit, the copper transfer could occur in a heterodimeric Cox1-Cox11 complex at the membrane interface. Therefore, it might be possible that the dimeric state of Cox11 may stabilize copper binding, protecting the copper ion until transfer to Cox1 occurs. Thus, Cox11 may disrupt the dimer to form a heterodimer with Cox1 to insert co-translationally the copper ion in the CuB site.[118] CuB site formation occurs in Cox1 prior to addition of the Cox2 or Cox3 subunits. The CuB-heme a_3 binuclear site forms in an early assembly intermediate of Cox1 that is stabilized by the Shy1 assembly factor. Cox11 forms a transient interaction with Shy1, which may be important to coordinate CuB site formation.[104]

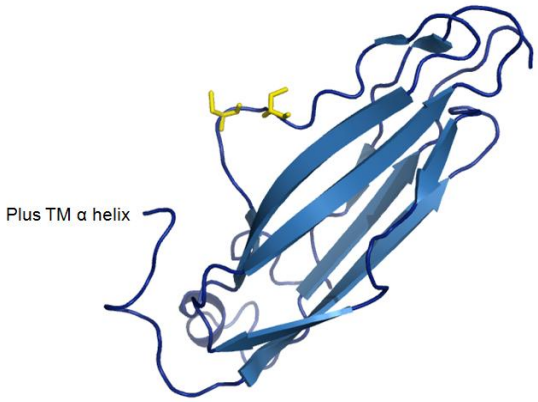

Figure 1.17. Copper metallochaperone Cox11.

Cox11 is tethered to the IM (hydrophobic α-helix not shown) with an immunoglobulin-like β-barrel in the IMS (PDB 1SPO)

As it was already mentioned also the mitochondrial fraction of the SOD1 undergoes the assembly process whithin the IMS of the mitochondria. The SOD1 cross the OM only in its non-metallated and disulfide reduced state. Once inside the IMS, SOD1 maturation is

facilitated by mitochondrially-localized CCS, through the same modifications described for the cytosolic SOD1.[119] Moreover, it was proposed, that the SOD1 import indirectly depends on Mia40/Erv1 disylfide relay system and respiratory chain function, via the interaction with mitochondrial CCS.[120] According to this mechanism, apoCCS enters the IMS, where it forms a disulfide intermediate with Mia40. This interaction results in the formation of the intramolecular disulfide bond in CCS, which trap it in IMS. In turn, mature CCS interacts with incoming apoSOD1 and promotes its folding and metallation, trapping SOD1 in IMS.[120] It has been shown that the high levels of CCS in IMS promote the import of SOD1 protecting the cells against oxidative damaged. The CCS control of mitochondrial uptake of SOD1 could have important implications with regard to SOD1-linked ALS. In one hypothesis for the disease, the mitochondrial pool of mutant SOD1 causes damage to mitochondrial function and structure. Mitochondrial uptake of ALS mutant SOD1 is increased upon CCS overexpression, resulting in mitochondrial respiratory defects and anacceleration in SOD1-linked motor neuron disease.[121]

1.3.3 GSH and metallothioneins

For mantaining cellular copper homeostasis in addition to proteins involved in described trafficking machinery the Cu(I) ions are coordinated to low molecular weight ligands such as reduced glutathione (GSH), which is the most abundant intracellular low molecular weight copper ligand found in living cells[122]. It is present at high concentration in a number of tissues, and has been shown to bind Cu(I) and to play a role in biliary excretion of copper.[123] In addition, GSH can transfer copper to cuproproteins including metallothioneins.[124]

Metallothioneins (MTs) are a class of low molecular weight proteins that have one of the highest affinity for copper(I), and may play special roles in the regulation of cellular copper distribution; however, for kinetic reasons they cannot demetallate copper enzymes.[32] Found in all eukaryotes and some prokaryotes, metallothioneins are thought to be involved in the detoxification of metals including nonessential and excess essential metals, storage of essential metals, sequestration of reactive oxygen and nitrogen species and electrophiles, and intracellular trafficking of zinc.[125,126] MTs are generally devoid of histidines and aromatic amino acids, but their amino acid content is up to one-third cysteine. These proteins typically have a one- or two-domain structure, and these structures and the nature of their metal binding reveal extensive evolutionary diversification.[127] In its fully metallated form, mammalian MT adopts a conformation with distinct metal–thiolate clusters located within two domains with

stoichiometries of $M_3(S_{cys})_9$ and $M_4(S_{cys})_{11}$ for divalent metal ions.[128] The folding of the protein chain around the clusters is entirely driven by the coordination of the metal ions. The exact mechanism of metal ion chelation: the order of metal binding, the eventual cooperativity of the process, the rate of binding of each metal ion is not well clarified so far, but this information is probably the key to reveal the role of MTs in the cell.The two main copper thioneins in eukaryotes are Cup1 and Crs5.[129]

1.4 AIMS AND TOPICS OF THE RESEARCH

My research during the three years of the doctorate was focused on the study of the mechanisms that ensure the copper homeostasis in both eukaryotes and prokaryotes. In particular, I studied metalloproteins belong to two different copper trafficking pathways: i.e. copper delivery to the cytochrome c oxidase and to superoxide dismutase.

The first project contributes to the understanding of the molecular function of the Sco proteins. The implication of Sco proteins in the copper delivery to cytochrome c oxidase was proposed more than ten years ago. But the futher structural and biochemical studies strongly suggested that Sco proteins may exhibit more than one function that include copper transfer. In our work, we analyzed the genome of Pseudomonas putida KT2440, which contains six Sco-like sequences in different genomic contexts. The protein named pp3183, containing a Sco-like sequence fused with a Cyt c-like sequence has been chosen as a target to investigate the electron transfer properties of Sco protein family and they possible role as a redox proteins. To address this question, the solution structures of both cyt c and Sco domains, separately expressed, were determined and the electron transfer reaction between them was investigated in accordance to their here measured redox potentials. Copper binding and thioredoxin properties of the Sco domain were also investigated to characterize this class of the proteins in order to understand the evolution link between thioredoxins and copper chaperones.

The second project dealt with human coper chaperone for superoxide dismutase. This metallochaperone activates the target enzyme through the insertion of the copper cofactor by unknown mechanism. Knowledge of the mechanism by which copper is transferred from CCS to SOD could provide the opportunity to interfere with copper incorporation and to plan a strategy for reducing or preventing degeneration in ALS. Newly synthesized SOD1 polypeptide undergoes several post-translational modifications prior the formation of an

active enzyme, that involve copper and zinc binding, disulfide formation, and dimerization. The structural interplay of conserved disulfide bond and metal-site occupancy in human Cu,Zn-SOD1 is of increasing interest as these post-translational modifications are known to dramatically alter the catalytic chemistry, the subcellular localization, and the susceptibility of the protein to aggregation. The general aim of this project is to study protein-protein interactions between hCCS and it's physiological partner protein SOD1 in order to understand recognition details, mechanism of the copper transfer process and disulfide linkage formation. For this purpose the hCCS full length protein as far as the constructs of the separate domains of this protein have been cloned and expressed for subsequent biochemical and biophysical studies and interactions of these proteins with different forms of SOD1 proteins have been performed by solution NMR and ESI - mass spectrometry.

1.5 REFERENCES

1. Bertini, I. *Biological inorganic chemistry: structure and reactivity*. (University Science Books: 2007).
2. Harrison, M., Jones, C., Solioz, M. & Dameron, C. Intracellular copper routing: the role of copper chaperones. *Trends in Biochemical Sciences* **25**, 29-32 (2000).
3. Silva, J.J.R.F.D. & Williams, R.J.P. *The biological chemistry of the elements: the inorganic chemistry of life*. (Clarendon Press: 1991).
4. Linder, M.C. & Goode, C.A. *Biochemistry of copper*. (Plenum Press: 1991).
5. Rensing, C. & Grass, G. Escherichia coli mechanisms of copper homeostasis in a changing environment. *FEMS Microbiology Reviews* **27**, 197-213 (2003).
6. Johnson, M.A. *Encyclopedia of Food Sciences and Nutrition*. (Elsevier: 2003).
7. Bertinato, J. & L'Abbé, M.R. Maintaining copper homeostasis: regulation of copper-trafficking proteins in response to copper deficiency or overload. *J. Nutr. Biochem* **15**, 316-322 (2004).
8. Messerschmidt, A. *Multi-copper oxidases*. (World Scientific: 1997).
9. Nersissian, A.M. & Shipp, E.L. Blue copper-binding domains. *Adv. Protein Chem* **60**, 271-340 (2002).
10. Wijma, H.J. et al. Effect of the methionine ligand on the reorganization energy of the type-1 copper site of nitrite reductase. *J. Am. Chem. Soc* **129**, 519-525 (2007).
11. Farver, O., Hwang, H.J., Lu, Y. & Pecht, I. Reorganization energy of the CuA center in purple azurin: impact of the mixed valence-to-trapped valence state transition. *J Phys Chem B* **111**, 6690-6694 (2007).
12. MacPherson, I.S. & Murphy, M.E.P. Type-2 copper-containing enzymes. *Cell. Mol. Life Sci* **64**, 2887-2899 (2007).
13. Halliwell, B. & Gutteridge, J.M.C. The importance of free radicals and catalytic metal ions in human diseases. *Molecular Aspects of Medicine* **8**, 89-193 (1985).
14. Kimura, T. & Nishioka, H. Intracellular generation of superoxide by copper sulphate in Escherichia coli. *Mutat. Res* **389**, 237-242 (1997).
15. Haywood, S., Trafford, J. & Loughran, M. Copper toxicosis and tolerance in the rat: IV. Renal tubular excretion of copper. *Br J Exp Pathol* **66**, 699-707 (1985).
16. Sandstead, H.H. Requirements and toxicity of essential trace elements, illustrated by zinc and copper. *Am. J. Clin. Nutr* **61**, 621S-624S (1995).

17. Walshe, J.M. Monitoring copper in Wilson's disease. *Adv Clin Chem* **50**, 151-163 (2010).

18. Tisato, F., Marzano, C., Porchia, M., Pellei, M. & Santini, C. Copper in diseases and treatments, and copper-based anticancer strategies. *Med Res Rev* **30**, 708-749 (2010).

19. Tümer, Z. & Møller, L.B. Menkes disease. *Eur. J. Hum. Genet* **18**, 511-518 (2010).

20. Bush, A.I. Metals and neuroscience. *Curr Opin Chem Biol* **4**, 184-191 (2000).

21. Gaeta, A. & Hider, R.C. The crucial role of metal ions in neurodegeneration: the basis for a promising therapeutic strategy. *Br. J. Pharmacol* **146**, 1041-1059 (2005).

22. Uversky, V.N., Li, J. & Fink, A.L. Metal-triggered structural transformations, aggregation, and fibrillation of human alpha-synuclein. A possible molecular NK between Parkinson's disease and heavy metal exposure. *J. Biol. Chem* **276**, 44284-44296 (2001).

23. Gaggelli, E. et al. Interaction of the human prion PrP(106-126) sequence with copper(II), manganese(II), and zinc(II): NMR and EPR studies. *J. Am. Chem. Soc* **127**, 996-1006 (2005).

24. Rivera-Mancía, S. et al. The transition metals copper and iron in neurodegenerative diseases. *Chemico-Biological Interactions* **186**, 184-199 (2010).

25. Bayer, T.A. et al. Key factors in Alzheimer's disease: beta-amyloid precursor protein processing, metabolism and intraneuronal transport. *Brain Pathol* **11**, 1-11 (2001).

26. Halliwell, B. & Gutteridge, J.M. Role of free radicals and catalytic metal ions in human disease: an overview. *Meth. Enzymol* **186**, 1-85 (1990).

27. Gupte, A. & Mumper, R.J. Elevated copper and oxidative stress in cancer cells as a target for cancer treatment. *Cancer Treat. Rev* **35**, 32-46 (2009).

28. Ruiz-Azuara, L. & Bravo-Gómez, M.E. Copper Compounds in Cancer Chemotherapy. *Curr Med Chem* (2010).

29. Beswick, P. Copper toxicity: Evidence for the conversion of cupric to cuprous copper in vivo under anaerobic conditions. *Chemico-Biological Interactions* **14**, 347-356 (1976).

30. O'Halloran, T.V. & Culotta, V.C. Metallochaperones, an Intracellular Shuttle Service for Metal Ions. *Journal of Biological Chemistry* **275**, 25057 -25060 (2000).

31. Rae, T.D., Schmidt, P.J., Pufahl, R.A., Culotta, V.C. & V. O'Halloran, T. Undetectable Intracellular Free Copper: The Requirement of a Copper Chaperone for Superoxide Dismutase. *Science* **284**, 805-808 (1999).

32. Banci, L. et al. Affinity gradients drive copper to cellular destinations. *Nature* **465**, 645-648 (2010).

33. Kim, B., Nevitt, T. & Thiele, D.J. Mechanisms for copper acquisition, distribution and regulation. *Nat Chem Biol* **4**, 176-185 (2008).

34. Gupta, A. & Lutsenko, S. Human copper transporters: mechanism, role in human diseases and therapeutic potential. *Future Med Chem* **1**, 1125-1142 (2009).

35. Burkhead, J.L., Morgan, C.T., Shinde, U., Haddock, G. & Lutsenko, S. COMMD1 forms oligomeric complexes targeted to the endocytic membranes via specific interactions with phosphatidylinositol 4,5-bisphosphate. *J. Biol. Chem* **284**, 696-707 (2009).

36. Holloway, Z.G. et al. Activation of ADP-ribosylation factor regulates biogenesis of the ATP7A-containing trans-Golgi network compartment and its Cu-induced trafficking. *Am. J. Physiol., Cell Physiol* **293**, C1753-1767 (2007).

37. Lim, C.M., Cater, M.A., Mercer, J.F.B. & La Fontaine, S. Copper-dependent interaction of dynactin subunit p62 with the N terminus of ATP7B but not ATP7A. *J. Biol. Chem* **281**, 14006-14014 (2006).

38. Krupanidhi, S., Sreekumar, A. & Sanjeevi, C.B. Copper & biological health. *Indian J. Med. Res* **128**, 448-461 (2008).

39. Nose, Y., Kim, B. & Thiele, D.J. Ctr1 drives intestinal copper absorption and is essential for growth, iron metabolism, and neonatal cardiac function. *Cell Metab* **4**, 235-244 (2006).

40. Hassett, R. & Kosman, D.J. Evidence for Cu(II) reduction as a component of copper uptake by Saccharomyces cerevisiae. *J. Biol. Chem* **270**, 128-134 (1995).

41. Martins, L.J. et al. Metalloregulation of FRE1 and FRE2 homologs in Saccharomyces cerevisiae. *J. Biol. Chem* **273**, 23716-23721 (1998).

42. Lee, J., Peña, M.M.O., Nose, Y. & Thiele, D.J. Biochemical Characterization of the Human Copper Transporter Ctr1. *Journal of Biological Chemistry* **277**, 4380 -4387 (2002).

43. Dancis, A., Haile, D., Yuan, D.S. & Klausner, R.D. The Saccharomyces cerevisiae copper transport protein (Ctr1p). Biochemical characterization, regulation by copper, and physiologic role in copper uptake. *J. Biol. Chem* **269**, 25660-25667 (1994).

44. Zhou, B. & Gitschier, J. hCTR1: A human gene for copper uptake identified by complementation in yeast. *Proceedings of the National Academy of Sciences of the United States of America* **94**, 7481 -7486 (1997).

45. Klomp, A.E.M., Tops, B.B.J., Van Denberg, I.E.T., Berger, R. & Klomp, L.W.J. Biochemical characterization and subcellular localization of human copper transporter 1 (hCTR1). *Biochem. J* **364**, 497-505 (2002).

46. De Feo, C.J., Aller, S.G., Siluvai, G.S., Blackburn, N.J. & Unger, V.M. Three-dimensional structure of the human copper transporter hCTR1. *Proc. Natl. Acad. Sci. U.S.A* **106**, 4237-4242 (2009).

47. Eisses, J.F. & Kaplan, J.H. The mechanism of copper uptake mediated by human CTR1: a mutational analysis. *J. Biol. Chem* **280**, 37159-37168 (2005).

48. Maryon, E.B., Molloy, S.A., Zimnicka, A.M. & Kaplan, J.H. Copper entry into human cells: progress and unanswered questions. *Biometals* **20**, 355-364 (2007).

49. Solioz, M., Abicht, H.K., Mermod, M. & Mancini, S. Response of gram-positive bacteria to copper stress. *J. Biol. Inorg. Chem* **15**, 3-14 (2010).

50. Arnesano, F. et al. Metallochaperones and metal-transporting ATPases: a comparative analysis of sequences and structures. *Genome Res* **12**, 255-271 (2002).

51. Solioz, M. & Stoyanov, J.V. Copper homeostasis in Enterococcus hirae. *FEMS Microbiol. Rev* **27**, 183-195 (2003).

52. Lewinson, O., Lee, A.T. & Rees, D.C. A P-type ATPase importer that discriminates between essential and toxic transition metals. *Proc. Natl. Acad. Sci. U.S.A* **106**, 4677-4682 (2009).

53. Rosenzweig, A.C. Copper Delivery by Metallochaperone Proteins. *Accounts of Chemical Research* **34**, 119-128 (2001).

54. Field, L.S., Luk, E. & Culotta, V.C. Copper chaperones: personal escorts for metal ions. *J. Bioenerg. Biomembr* **34**, 373-379 (2002).

55. Pufahl, R.A. et al. Metal ion chaperone function of the soluble Cu(I) receptor Atx1. *Science* **278**, 853-856 (1997).

56. Lin, S.J., Pufahl, R.A., Dancis, A., O'Halloran, T.V. & Culotta, V.C. A role for the Saccharomyces cerevisiae ATX1 gene in copper trafficking and iron transport. *J. Biol. Chem* **272**, 9215-9220 (1997).

57. Petris, M.J. et al. Ligand-regulated transport of the Menkes copper P-type ATPase efflux pump from the Golgi apparatus to the plasma membrane: a novel mechanism of regulated trafficking. *EMBO J* **15**, 6084-6095 (1996).

58. Huffman, D.L. & O'Halloran, T.V. Function, structure, and mechanism of intracellular copper trafficking proteins. *Annu. Rev. Biochem* **70**, 677-701 (2001).

59. Kühlbrandt, W. Biology, structure and mechanism of P-type ATPases. *Nat. Rev. Mol. Cell Biol* **5**, 282-295 (2004).

60. Walker, J.M. et al. The N-terminal metal-binding site 2 of the Wilson's Disease Protein plays a key role in the transfer of copper from Atox1. *J. Biol. Chem* **279**, 15376-15384 (2004).

61. Achila, D. et al. Structure of human Wilson protein domains 5 and 6 and their interplay with domain 4 and the copper chaperone HAH1 in copper uptake. *Proc. Natl. Acad. Sci. U.S.A* **103**, 5729-5734 (2006).

62. González-Guerrero, M. & Argüello, J.M. Mechanism of Cu+-transporting ATPases: soluble Cu+ chaperones directly transfer Cu+ to transmembrane transport sites. *Proc. Natl. Acad. Sci. U.S.A* **105**, 5992-5997 (2008).

63. Banci, L. et al. An NMR study of the interaction of the N-terminal cytoplasmic tail of the Wilson disease protein with copper(I)-HAH1. *J. Biol. Chem* **284**, 9354-9360 (2009).

64. Banci, L. et al. The Atx1-Ccc2 complex is a metal-mediated protein-protein interaction. *Nat. Chem. Biol* **2**, 367-368 (2006).

65. Huster, D. & Lutsenko, S. The distinct roles of the N-terminal copper-binding sites in regulation of catalytic activity of the Wilson's disease protein. *J. Biol. Chem* **278**, 32212-32218 (2003).

66. Lutsenko, S. Human copper homeostasis: a network of interconnected pathways. *Current Opinion in Chemical Biology* **14**, 211-217 (2010).

67. McCord, J.M. & Fridovich, I. Superoxide dismutase. An enzymic function for erythrocuprein (hemocuprein). *J. Biol. Chem* **244**, 6049-6055 (1969).

68. Sturtz, L.A., Diekert, K., Jensen, L.T., Lill, R. & Culotta, V.C. A fraction of yeast Cu,Zn-superoxide dismutase and its metallochaperone, CCS, localize to the intermembrane space of mitochondria. A physiological role for SOD1 in guarding against mitochondrial oxidative damage. *J. Biol. Chem* **276**, 38084-38089 (2001).

69. Banci, L., Bertini, I., Cantini, F. & Ciofi-Baffoni, S. Cellular copper distribution: a mechanistic systems biology approach. *Cell. Mol. Life Sci.* **67**, 2563-2589 (2010).

70. Bordo, D., Djinović, K. & Bolognesi, M. Conserved patterns in the Cu,Zn superoxide dismutase family. *J. Mol. Biol* **238**, 366-386 (1994).

71. Khare, S.D., Caplow, M. & Dokholyan, N.V. The rate and equilibrium constants for a multistep reaction sequence for the aggregation of superoxide dismutase in amyotrophic lateral sclerosis. *Proc. Natl. Acad. Sci. U.S.A* **101**, 15094-15099 (2004).

72. Banci, L., Bertini, I., Cantini, F., D'Amelio, N. & Gaggelli, E. Human SOD1 before harboring the catalytic metal: solution structure of copper-depleted, disulfide-reduced form. *J. Biol. Chem* **281**, 2333-2337 (2006).

73. Furukawa, Y., Torres, A.S. & O'Halloran, T.V. Oxygen-induced maturation of SOD1: a key role for disulfide formation by the copper chaperone CCS. *EMBO J* **23**, 2872-2881 (2004).

74. Culotta, V.C. et al. The Copper Chaperone for Superoxide Dismutase. *Journal of Biological Chemistry* **272**, 23469 -23472 (1997).

75. Rae, T.D., Torres, A.S., Pufahl, R.A. & O'Halloran, T.V. Mechanism of Cu,Zn-superoxide dismutase activation by the human metallochaperone hCCS. *J. Biol. Chem* **276**, 5166-5176 (2001).

76. Schmidt, P.J. et al. Multiple protein domains contribute to the action of the copper chaperone for superoxide dismutase. *J. Biol. Chem* **274**, 23719-23725 (1999).

77. Lamb, A.L. et al. Crystal structure of the copper chaperone for superoxide dismutase. *Nat. Struct. Biol* **6**, 724-729 (1999).

78. Lamb, A.L., Wernimont, A.K., Pufahl, R.A., O'Halloran, T.V. & Rosenzweig, A.C. Crystal structure of the second domain of the human copper chaperone for superoxide dismutase. *Biochemistry* **39**, 1589-1595 (2000).

79. Schmidt, P.J., Kunst, C. & Culotta, V.C. Copper activation of superoxide dismutase 1 (SOD1) in vivo. Role for protein-protein interactions with the copper chaperone for SOD1. *J. Biol. Chem* **275**, 33771-33776 (2000).

80. Stasser, J.P., Siluvai, G.S., Barry, A.N. & Blackburn, N.J. A multinuclear copper(I) cluster forms the dimerization interface in copper-loaded human copper chaperone for superoxide dismutase. *Biochemistry* **46**, 11845-11856 (2007).

81. Barry, A.N., Clark, K.M., Otoikhian, A., van der Donk, W.A. & Blackburn, N.J. Selenocysteine positional variants reveal contributions to copper binding from cysteine residues in domains 2 and 3 of human copper chaperone for superoxide dismutase. *Biochemistry* **47**, 13074-13083 (2008).

82. Hall, L.T. et al. X-ray crystallographic and analytical ultracentrifugation analyses of truncated and full-length yeast copper chaperones for SOD (LYS7): a dimer-dimer model of LYS7-SOD association and copper delivery. *Biochemistry* **39**, 3611-3623 (2000).

83. Poulos, T.L. Helping copper find a home. *Nat Struct Mol Biol* **6**, 709-711 (1999).

84. Falconi, M., Iovino, M. & Desideri, A. A model for the incorporation of metal from the copper chaperone CCS into Cu,Zn superoxide dismutase. *Structure* **7**, 903-908 (1999).

85. Eisses, J.F., Stasser, J.P., Ralle, M., Kaplan, J.H. & Blackburn, N.J. Domains I and III of the human copper chaperone for superoxide dismutase interact via a cysteine-bridged Dicopper(I) cluster. *Biochemistry* **39**, 7337-7342 (2000).

86. Zhu, H. et al. Cobalt(2+) binding to human and tomato copper chaperone for superoxide dismutase: implications for the metal ion transfer mechanism. *Biochemistry* **39**, 5413-5421 (2000).

87. Lamb, A.L., Torres, A.S., O'Halloran, T.V. & Rosenzweig, A.C. Heterodimer formation between superoxide dismutase and its copper chaperone. *Biochemistry* **39**, 14720-14727 (2000).

88. Lamb, A.L., Torres, A.S., O'Halloran, T.V. & Rosenzweig, A.C. Heterodimeric structure of superoxide dismutase in complex with its metallochaperone. *Nat. Struct. Biol* **8**, 751-755 (2001).

89. Brown, N.M., Torres, A.S., Doan, P.E. & O'Halloran, T.V. Oxygen and the copper chaperone CCS regulate posttranslational activation of Cu,Zn superoxide dismutase. *Proc. Natl. Acad. Sci. U.S.A* **101**, 5518-5523 (2004).

90. Carroll, M.C. et al. Mechanisms for activating Cu- and Zn-containing superoxide dismutase in the absence of the CCS Cu chaperone. *Proc. Natl. Acad. Sci. U.S.A* **101**, 5964-5969 (2004).

91. Leitch, J.M., Yick, P.J. & Culotta, V.C. The right to choose: multiple pathways for activating copper,zinc superoxide dismutase. *J. Biol. Chem* **284**, 24679-24683 (2009).

92. Chattopadhyay, M. & Valentine, J.S. Aggregation of Copper–Zinc Superoxide Dismutase in Familial and Sporadic ALS. *Antioxid Redox Signal* **11**, 1603-1614 (2009).

93. Prudencio, M., Hart, P.J., Borchelt, D.R. & Andersen, P.M. Variation in aggregation propensities among ALS-associated variants of SOD1: correlation to human disease. *Hum. Mol. Genet* **18**, 3217-3226 (2009).

94. Weisiger, R.A. & Fridovich, I. Mitochondrial superoxide simutase. Site of synthesis and intramitochondrial localization. *J. Biol. Chem* **248**, 4793-4796 (1973).

95. Cobine, P.A., Pierrel, F., Bestwick, M.L. & Winge, D.R. Mitochondrial matrix copper complex used in metallation of cytochrome oxidase and superoxide dismutase. *J. Biol. Chem* **281**, 36552-36559 (2006).

96. Abramson, J., Svensson-Ek, M., Byrne, B. & Iwata, S. Structure of cytochrome c oxidase: a comparison of the bacterial and mitochondrial enzymes. *Biochim. Biophys. Acta* **1544**, 1-9 (2001).

97. Carr, H.S. & Winge, D.R. Assembly of cytochrome c oxidase within the mitochondrion. *Acc. Chem. Res* **36**, 309-316 (2003).

98. Khalimonchuk, O. & Rödel, G. Biogenesis of cytochrome c oxidase. *Mitochondrion* **5**, 363-388 (2005).

99. Schultz, B.E. & Chan, S.I. Structures and proton-pumping strategies of mitochondrial respiratory enzymes. *Annu Rev Biophys Biomol Struct* **30**, 23-65 (2001).

100. Richter, O.H. & Ludwig, B. Cytochrome c oxidase--structure, function, and physiology of a redox-driven molecular machine. *Rev. Physiol. Biochem. Pharmacol* **147**, 47-74 (2003).

101. Nijtmans, L.G., Taanman, J.W., Muijsers, A.O., Speijer, D. & Van den Bogert, C. Assembly of cytochrome-c oxidase in cultured human cells. *Eur. J. Biochem* **254**, 389-394 (1998).

102. Taanman, J.W. & Williams, S.L. Assembly of cytochrome c oxidase: what can we learn from patients with cytochrome c oxidase deficiency? *Biochem. Soc. Trans* **29**, 446-451 (2001).

103. Banci, L., Bertini, I., McGreevy, K.S. & Rosato, A. Molecular recognition in copper trafficking. *Nat Prod Rep* **27**, 695-710 (2010).

104. Robinson, N.J. & Winge, D.R. Copper metallochaperones. *Annu. Rev. Biochem* **79**, 537-562 (2010).

105. Arnesano, F., Banci, L., Bertini, I. & Martinelli, M. Ortholog search of proteins involved in copper delivery to cytochrome C oxidase and functional analysis of paralogs and gene neighbors by genomic context. *J. Proteome Res* **4**, 63-70 (2005).

106. Zovo, K. & Palumaa, P. Modulation of redox switches of copper chaperone Cox17 by Zn(II) ions determined by new ESI MS-based approach. *Antioxid. Redox Signal* **11**, 985-995 (2009).

107. Chacinska, A. et al. Essential role of Mia40 in import and assembly of mitochondrial intermembrane space

proteins. *EMBO J* **23**, 3735-3746 (2004).

108. Banci, L. et al. Human Sco1 functional studies and pathological implications of the P174L mutant. *Proc. Natl. Acad. Sci. U.S.A* **104**, 15-20 (2007).
109. Banci, L. et al. Mitochondrial copper(I) transfer from Cox17 to Sco1 is coupled to electron transfer. *Proc. Natl. Acad. Sci. U.S.A* **105**, 6803-6808 (2008).
110. Leary, S.C. et al. Human SCO1 and SCO2 have independent, cooperative functions in copper delivery to cytochrome c oxidase. *Hum. Mol. Genet* **13**, 1839-1848 (2004).
111. Beers, J., Glerum, D.M. & Tzagoloff, A. Purification and characterization of yeast Sco1p, a mitochondrial copper protein. *J. Biol. Chem* **277**, 22185-22190 (2002).
112. Nittis, T., George, G.N. & Winge, D.R. Yeast Sco1, a protein essential for cytochrome c oxidase function is a Cu(I)-binding protein. *J. Biol. Chem* **276**, 42520-42526 (2001).
113. Abriata, L.A. et al. Mechanism of Cu(A) assembly. *Nat. Chem. Biol* **4**, 599-601 (2008).
114. Rigby, K., Cobine, P.A., Khalimonchuk, O. & Winge, D.R. Mapping the functional interaction of Sco1 and Cox2 in cytochrome oxidase biogenesis. *J. Biol. Chem* **283**, 15015-15022 (2008).
115. Tzagoloff, A., Capitanio, N., Nobrega, M.P. & Gatti, D. Cytochrome oxidase assembly in yeast requires the product of COX11, a homolog of the P. denitrificans protein encoded by ORF3. *EMBO J* **9**, 2759-2764 (1990).
116. Carr, H.S., George, G.N. & Winge, D.R. Yeast Cox11, a protein essential for cytochrome c oxidase assembly, is a Cu(I)-binding protein. *J. Biol. Chem* **277**, 31237-31242 (2002).
117. Banci, L. et al. Solution structure of Cox11, a novel type of beta-immunoglobulin-like fold involved in CuB site formation of cytochrome c oxidase. *J. Biol. Chem* **279**, 34833-34839 (2004).
118. Carr, H.S., Maxfield, A.B., Horng, Y. & Winge, D.R. Functional analysis of the domains in Cox11. *J. Biol. Chem* **280**, 22664-22669 (2005).
119. Kawamata, H. & Manfredi, G. Import, maturation, and function of SOD1 and its copper chaperone CCS in the mitochondrial intermembrane space. *Antioxid. Redox Signal* **13**, 1375-1384 (2010).
120. Reddehase, S., Grumbt, B., Neupert, W. & Hell, K. The disulfide relay system of mitochondria is required for the biogenesis of mitochondrial Ccs1 and Sod1. *J. Mol. Biol* **385**, 331-338 (2009).
121. Son, M., Fu, Q., Puttaparthi, K., Matthews, C.M. & Elliott, J.L. Redox susceptibility of SOD1 mutants is associated with the differential response to CCS over-expression in vivo. *Neurobiol. Dis* **34**, 155-162 (2009).
122. Deneke, S.M. & Fanburg, B.L. Regulation of cellular glutathione. *Am. J. Physiol* **257**, L163-173 (1989).
123. Houwen, R. et al. Two pathways for biliary copper excretion in the rat. The role of glutathione. *Biochem. Pharmacol* **39**, 1039-1044 (1990).
124. Ferreira, A.M., Ciriolo, M.R., Marcocci, L. & Rotilio, G. Copper(I) transfer into metallothionein mediated by glutathione. *Biochem. J* **292 (Pt 3)**, 673-676 (1993).
125. Feng, W. et al. Metallothionein transfers zinc to mitochondrial aconitase through a direct interaction in mouse hearts. *Biochem. Biophys. Res. Commun* **332**, 853-858 (2005).
126. Yoshida, M., Saegusa, Y., Fukuda, A., Akama, Y. & Owada, S. Measurement of radical-scavenging ability in hepatic metallothionein of rat using in vivo electron spin resonance spectroscopy. *Toxicology* **213**, 74-80 (2005).
127. Vasák, M. et al. Investigation of the structure of metallothioneins by proton nuclear magnetic resonance spectroscopy. *Biochemistry* **19**, 416-425 (1980).
128. Robbins, A.H. et al. Refined crystal structure of Cd, Zn metallothionein at 2.0 A resolution. *J. Mol. Biol* **221**, 1269-1293 (1991).
129. Culotta, V.C., Howard, W.R. & Liu, X.F. CRS5 encodes a metallothionein-like protein in Saccharomyces cerevisiae. *J. Biol. Chem* **269**, 25295-25302 (1994).

2. MATERIALS AND METHODS

2.1 GENOME BROWSING

Over the past few decades rapid developments in genomic and other molecular research technologies and developments in information technologies have combined to produce an incredible amount of information related to molecular biology. Genome sequencing projects have made available, the complete genome of more than 60 species in addition to the thousands of viruses and primary sequence of an enormous number of new genes. This sudden increase in the amount of genomic information, has provided a new starting point for understanding our basic genetic machinary. This wealth of genomic data can be fully exploited only through elucidation of the three-dimensional structures of the corresponding proteins. Structural genomics requires a large number of process steps to convert sequence information into a 3D structure, which includes: choosing proper expression constructs, setting up of right growth conditions and efficient purifying strategy. And different scientific fields like bioinformatics, biochemistry and molecular biology have to cooperate in order to proceed in the target selection, protein expression, and finally structural and functional characterization.

Bioinformatics has an essential role in understanding genomic and proteomic data, and in organizing experimental data. It is an interdisciplinary research area at the interface between the biological and computational science.

A number of data banks are available and provide the scientific community with tools for searching gene banks, for the analysis of protein sequences, for the prediction of a variety of protein properties. Databases contain information and annotations of DNA and protein sequences, protein structures and protein expression profiles. The most used databases and genome browsing softwares are:

- ✓ **NCBI**: is a web site which integrates information from several databases (Swissprot, EMBL and all geneBank). [www.ncbi.nlm.nih.gov/Entrez/],
- ✓ **PDB:** A 3-D biological macromolecular structure database. [www.rcsb.org/pdb],
- ✓ **PFAM**: is a collection of different protein families organized in terms of different domains as obtained from multiple alignment. [http://pfam.wustl.edu],
- ✓ **PROSITE**: SCANPROSITE allows to scan a protein sequence, provided by the user, for the occurrence of patterns and profiles stored in the PROSITE database, or to search in protein databases all sequences with a user entered pattern [www.expasy.org/prosite/],

- ✓ **STRING**: is a database of predicted functional associations among genes/proteins. Genes of similar function tend to be maintained in close neighbourhood and tend to be present or absent together [www.dag.embl-heidelberg.de].
- ✓ **BLAST** (The Basic Local Alignment Search Tool): is a set of similarity search programs designed to explore all of the available sequence databases regardless of whether the query is protein or DNA. PHIBLAST is designed to search for proteins that contain a pattern specified by the user, and simultaneously are similar to the query sequence. [www.ncbi.nlm.nih.gov/BLAST/].
- ✓ **CLUSTALW**: is a general purpose multiple sequence alignment program for DNA or proteins. It produces biologically meaningful multiple sequence alignments of divergent sequences. It calculates the best match for the selected sequences, and lines them up so that the identities, similarities and differences can be seen. Evolutionary relationships can be seen via viewing Cladograms or Phylograms [www.ebi.ac.uk/clustalw/]

Once selected a protein target of particular interest is subjected to further bioinformatics investigations. In case where the target will be used for recombinant protein expression the following characteristic of the protein can predicted and be used for defining constructs:

a) **Post-translational modification prediction**: signal peptides, glycosylation, phosphorylation and cleavage sites: TargetP, SIGNALP.[1]

b) **Topology prediction of transmembrane (TM) regions**: prediction of membrane-spanning regions and their orientation: TMHMM[2], TMpred[3], HMMTOP.[4]

c) **Secondary structure prediction**: of the regions with tendency to form helices, beta-sheet, coil or turns. Combining these predictions with homologue proteins alignment, can be used to select the exact residues that define a construct minimizing the possibility of destroying a region with certain secondary structure. NPS@. [5]

d) **Prediction of intrinsically unstructured /disordered regions**: recognition of such regions from the amino acid sequence based on the estimated pairwise energy content. The underlying assumption is that globular proteins are composed of amino acids which have the potential to form a large number of favorable interactions, whereas intrinsically unstructured proteins adopt no stable structure because their amino acid composition does not allow sufficient favorable interactions to form. IUPred.[6]

e) **Rare codon calculation**: Over-expression of recombinant protein in *E. coli* may be severely diminished (to the point of being undetectable) if the ORF that codes for the

protein uses "rare" codons that are infrequently used by *E. coli*. In particular, codons for arginine (AGG, AGA, CGA), leucine (CTA), isoleucine (ATA), and proline (CCC) may be a problem.[7]

2.2 CLONING TECHNIQUES

2.2.1 Gene cloning

The terms "recombinant DNA technology," "DNA cloning," "molecular cloning," and "gene cloning" all refer to the same process: the transfer of a DNA fragment of interest from one organism to a self-replicating genetic element such as a bacterial plasmid. The DNA of interest can then be propagated in a foreign host cell. This technology has been around since the 1970s, and it has become a common practice in molecular biology labs today.

The strategy for cloning the target protein has to be carefully designed since it will influence the behaviour of the protein, e.g. yield, solubility, folding, etc. Standard procedure when setting out to express a recombinant protein is to screen a series of constructs to identify the most appropriate vehicle for the generation of sufficient soluble protein for downstream purposes.

The first step of the cloning process consists in the amplification of target gene from cDNA (synthetic or extracted from the organism of interest) or plasmids via PCR (Polymerase Chain Reaction) using specific primers. After purification, the amplified product is inserted into a specific expression vector using one of the methods described below. The protein can be cloned in different vectors in order to obtain a native protein or a protein fused with different tag. The tag has a known size and biological function and can enhance, for example, solubility or affinity for some specific purification systems or can permit the transport of protein in the periplasmic compartment. Later on, these tags can be removed by a proteolytic cleavage with an enzyme such as factor XA or TEV.[8,9,10]

The classic method to insert a gene in a vector is using restriction enzymes that cleave DNA at specific recognition sites. Both DNA and a cloning vector have to be treated with two restriction enzymes that create compatible ends. The next step is the ligation of the insert into the open vector. This involves the formation of phosphodiester bonds between adjacent 5'-phosphate and 3'-hydroxyl residues, a reaction catalyzed by the bacteriophage T4 DNA ligase. Finally an aliquot of this reaction is transformed in DH5α *E. coli* competent cells and positives clones are screened both by PCR and DNA sequencing. The yield of this procedure

depends on the efficiency of the ligation step which is affected by the DNA concentration, the vector/DNA insert ratio and the transformation efficiency of the cells. Moreover the parallelization of this approach is not so easy because not all the host vectors and the target genes can be cleaved by the same restriction enzymes.[11]

The other cloning strategy exploits ligation-independent cloning (LIC), such as Gateway (Invitrogen, The Netherlands), is useful for simultaneous preparation of plasmids for different expression systems. (Figure 2.1) It's a universal cloning method that takes advantage of the site-specific recombination properties of bacteriophage lambda.[12] Mainly it consists in the creation of a common entry vector that can be recombined in several compatible vectors without the use of any restriction enzyme. The entry vector can be obtained via a ligation reaction of the entry vector with DNA construct amplified; the reaction is catalyzed by the topoisomerase I. After isolation of the entry vector, the second step is to generate an expression vector by performing a recombination reaction between the entry clone and a Gateway destination vector of choice.

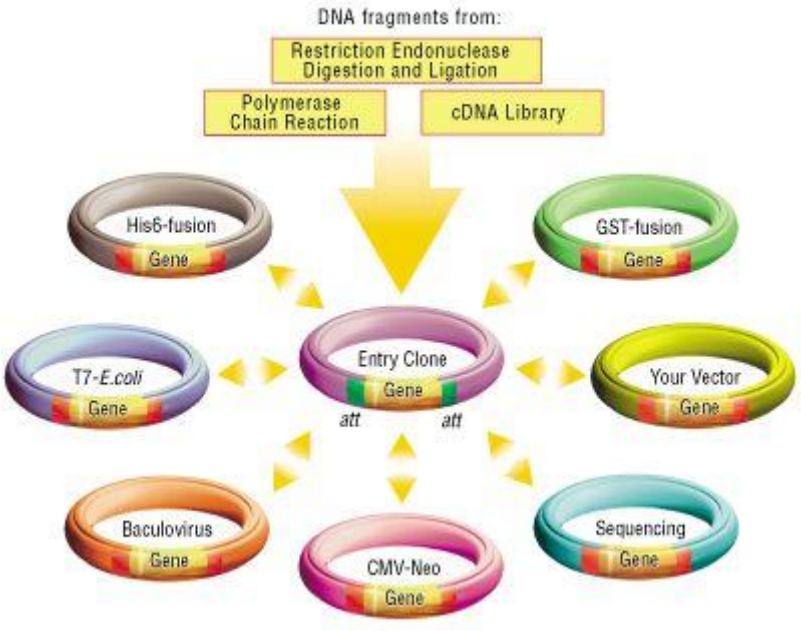

Figure 2.1. The flexibility of the Gateway Technology.

After cloning the gene of interest into the Entry vector, you can transfer the gene of interest simultaneously into multiple destination vectors. [Reprinted from Gateway Technology handbook]

In the present thesis as cloning system was used mainly the Gateway Cloning System, pENTR/TEV/D-TOPO version. As expression vectors the following vectors have been used: pDEST-17/O (His), pETG-20A (His-Trx), pETG-30A (His-GST), pDEST-His-MBP, pDEST-His-MBPperi, and pTH34 (His-GB1).

2.2.2 Site directed mutagenesis

Site-directed mutagenesis is a technique for carrying out vector modification and characterizing the dynamic, complex relationships between protein structure and function. The basic procedure (Figure 2.2) utilizes a supercoiled double-stranded DNA vector with insert the gene of interest and two synthetic oligonucleotide primers, both containing the desired mutation. The primers, each complementary to opposite strands of the vector, are extended during PCR reaction by a high fidelity DNA polymerase (PfuUltra, Stratagene). Extension of the oligonucleotide primers generates a mutated plasmid. After PCR reaction the product is treated with an endonuclease specific for methylated and hemimethylated DNA, DpnI. This enzyme is used to digest the parental DNA template and thus select only the mutation-containing synthesized DNA; this happens because DNA isolated from almost all *E. coli* strains is dam methylated and therefore susceptible to endonuclease digestion. The vector containing the desired mutations is then transformed into XL1-Blue supercompetent cells and subsequently subjected to sequencing analysis.

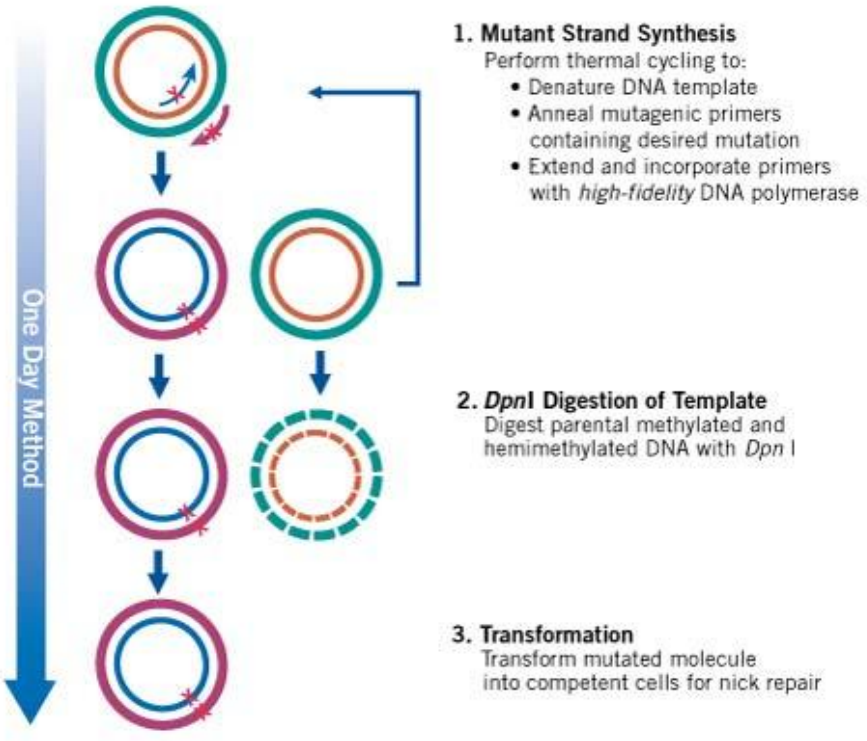

Figure 2.2. Overview of the QuikChange II Site-directed Mutagenesis Method.

2.3 PROTEIN EXPRESSION

2.3.1 Expression systems

Several host systems are available for protein production, including bacteria, yeast, plants, fungi, insect and mammalian cells.[13] The choice of an expression system for the high-level production of recombinant proteins depends on many factors. These include cell growth characteristics, expression levels, intracellular and extracellular expression, posttranslational modifications, and biological activity of the protein of interest, as well as regulatory issues in the production of therapeutic proteins. In addition, the selection of a particular expression system requires a cost breakdown in terms of process, design, and other economic considerations.[14] The many advantages of *E. coli* have ensured that it remains a valuable organism for the high-level production of recombinant proteins, since it is the easiest, quickest and cheapest expression system. There are many commercial and non-commercial expression vectors available with different N- and C-terminal tags and many different bacterial strains which are optimized for special applications. Moreover one of the major advantages of *E. coli* is that the production of isotope labelled protein for NMR, is less complex compared to other systems. However, in spite of the extensive knowledge on the genetics and molecular biology of *E. coli*, not every gene can be expressed efficiently in this organism. This may be due to the unique and subtle structural features of the gene sequence, the stability and translational efficiency of mRNA, the ease of protein folding, degradation of the protein by host cell proteases, major differences in codon usage between the foreign gene and native *E. coli*, and the potential toxicity of the protein to the host. The major drawbacks of *E. coli* as an expression system include the inability to perform many of the posttranslational modifications found in eukaryotic proteins, the lack of a secretion mechanism for the efficient release of protein into the culture medium, and the limited ability to facilitate extensive disulfide bond formation. Many eukaryotic proteins can be produced in *E. coli* but sometimes they are produced as non-functional inclusion bodies protein.[14,15] Therefore, researchers have recently turned to eukaryotic yeast and insect cell expression systems for protein production.

2.3.2 Recombinant proteins production in *E.coli*.

Similarly to gene cloning, also for protein production the best strategy is the use of a parallel expression strategy; depending on the number of targets the possible choices are: (i)

to express more genes in the same bacterial strain, (ii) to express a single gene in different strains or (iii) to express more genes in different strains.[16]

A preliminary expression test is performed in a small-volume scale. Since *E. coli* is a simple organism, it is highly amenable for growth in 96–24-deep-well block format (1–10 mL) using standard shaking incubators. This utility allows many hundreds of parameters to be analysed simultaneously in very small volumes which therefore allows the rapid identification of clones, constructs, fusion tags, induction conditions, which provide optimal conditions for the generation of large quantities of a soluble recombinant protein.[17] Usualy we perform these tests using three groups of strains (e.g.: Bl21(DE3)pLysS a protease deficient strain, Rosetta(DE3) for rare codons containing genes and Origami(DE3) for disulphide containing proteins), three expression temperatures (37-25-17°C), three inducer (isopropyl-beta-D-thiogalactopyranoside) concentrations, different expression time (3h, 5h and overnight) and three culture media of different composition. Expression results are checked on SDS polyacrylamide gel (SDS-PAGE).

In case of negative or partially positive results some or all variables can be modified, in particular the more influencing ones like the choice of bacterial strain, the induction times, the kind of vectors and expression promoters used. If the main fraction of the protein is produced in the insoluble fraction, refolding trials can be performed. The last choices are to redesign the expressed domains or to use another expression system.

Dependence of the expression purposes, protein expression is performed in differently composed media. In fact, when large amounts of proteins must be isolated for techniques that do not require isotopic labelling, the culture is usually performed in a so-called rich or complex medium. Rich media contain water soluble extracts of plant or animal tissue (e.g., enzymatically digested animal proteins such as peptone and tryptone), and for this reason are rich in nutrients and minerals, assuring a fast bacterial growth and a high expression level. Their exact composition is unknown and this can impair the reproducibility of cultures. Chemically defined (or minimal) media are composed of pure ingredients in measured concentrations, dissolved in purified water; this way the exact chemical composition of the medium is known, allowing high reproducibility of protein yields. Typically, this class of media is composed of a buffering agent to maintain culture pH around physiological values, a carbon source like sugar (glucose) or glycerol, and an inorganic nitrogen source, usually an ammonium inorganic salt. Depending on the bacterial strain and the expressed proteins various mineral salts can be added and, if necessary, growth factors such as purified amino

acids, vitamins, purines and pyrimidines. Chemically defined media are easier to isotopically enrich, simply by using ^{15}N and ^{13}C enriched nitrogen and carbon sources.

2.4 PROTEIN PURIFICATION

The strategy of purification depends mainly upon the localization of the produced protein within the host; for example the protein can be excreted into the growth media, transported in the periplasmic space or produced like a soluble or insoluble (inclusion bodies) protein within the cytoplasm and finally directed to the cell membranes. In each of the cases the isolation has to be performed in different ways.[18,19]

Cell lysis is the first step in protein purification and the technique chosen for the disruption of cells must be compatible with the amount of material to be processed and the intended downstream applications. Many techniques are available, spanning from physical to detergent-based methods. The most frequently used method for cell disruption in our loboratory is sonication, which comprises pulsed, high frequency sound waves to agitate and lyse cells. Gentler ways of disrupting cells are freeze-thaw lysis, detergent lysis, enzymatic lysis and osmotic lysis. The latter method is well suited when the protein is expressed in the periplasm of the cell and it was used fort the purification of ppCyt c and SOD AS proteins. The big advantage of this technique is that all the interferents coming from the cytoplasmic region are eliminated, since the inner membrane is not broken, preventing also genomic DNA and proteases release.

The following step of purification procedure is composed of normally two or more rounds of chromatography, based on the different physical chemical and biological characteristics of the protein. A powerful chromatographic technique is Ion exchange chromatography (IEX) that separates the proteins on the basis of a reversible interaction between the polypeptide chain and a specific, charged ligand attached to a chromatographic matrix (Figure 2.3). The sample is applied in conditions that favour specific binding, e.g. low ionic strength of the solution and carefully calibrated pH, in order to enhance interaction with the target of interest. The unbound material is washed away and the bound protein is recovered by changing conditions to those favouring desorption. This can be achieved by changing pH or ionic strength of the eluent. The most used resin is the anionic one, since the majority of proteins carry an overall net negative charge at physiological conditions.

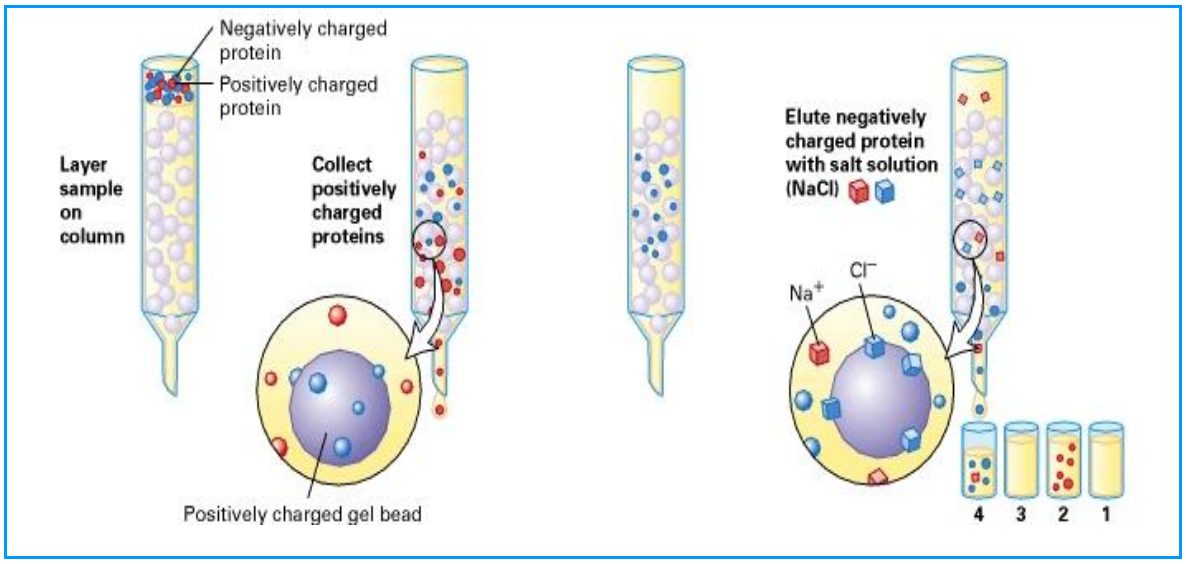

Figure 2.3. Scheme of the ion exchange chromatography.

Size-exclusion chromatography (SEC) is the simplest and mildest of all the chromatographic techniques; the support for gel filtration chromatography is composed of beads which contain holes, called "pores," of given sizes. Larger molecules, which can't penetrate the pores, move around the beads and migrate through the spaces which separate the beads faster than the smaller molecules, which may penetrate the pores (Figure 2.4). In this technique the buffer composition does not play any role in the resolution. SEC can be performed on a "rough" level, separating the components of a sample in major groups to remove for example high or low molecular weight contaminants or to exchange buffers, while high resolution fractionation of biomolecules allows to isolate one or more components of a protein mixture, to separate monomers from aggregates, to determine molecular weights or to perform a molecular weight distribution analysis, provided that suitable standards are available.

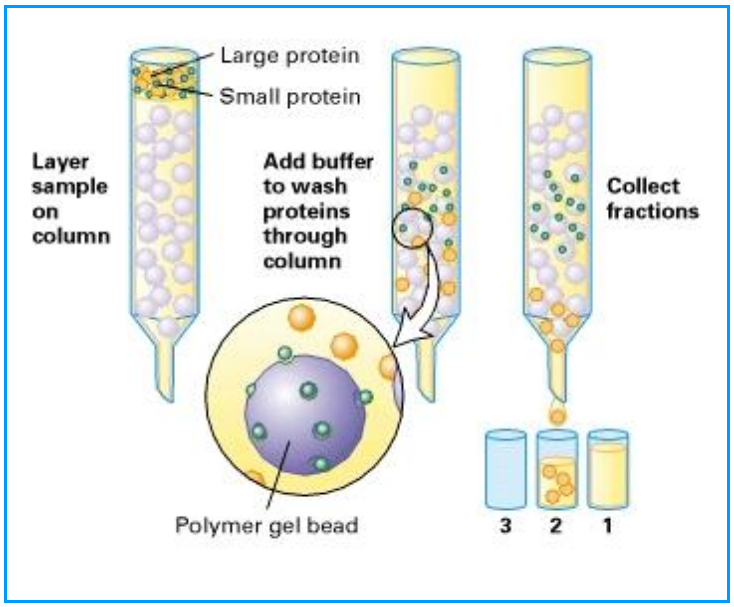

Figure 2.4. Scheme of the size exclusion chromatography.

In case of peptide fusion tags, a variety of affinity purification methods are available. Immobilized metal ion affinity chromatography (IMAC) is currently the most used affinity technique, it exploits the interaction between chelated transition metal ions (generally Zn^{2+} or $Ni^{2+)}$ and side-chains of specific amino acids (mainly histidine) on the protein. In IMAC chromatography, the target protein is usually washed from the impurities and then eluted using increasing concentration of imidazole, which acts like a competitive agent.

Enzymatic digestion using a specific protease is then necessary to remove the fusion partner from the target protein and a second IMAC purification is generally performed in order to separate the two proteins. TEV, Fatt.Xa, Thrombin, Prescission Protease, recombinant Enterokinase are some example of proteases that are normally used for the cleavage of fusion proteins. The protease specific recognition site is selected and cloned in the vector codifying for the protein sequence at the cloning step. For each protease/fusion protein pilot experiments should be done to find out suitable conditions.

2.5 SAMPLE PREPARATION

Copper and zinc metalloproteins, which in many cases bind metal atoms through Cys residues are not easy to handle. Disulfide reduction prior to metallation have to be performed. Protein reduction and metallation were carried out under nitrogen atmosphere in an anaerobic

chamber to prevent oxidation of the cysteine residues. Dithiothreitol (DTT) was added to the protein in a 0,5 - 5mM concentration to reduce the cysteine residues in the metal binding motif prior to metal reconstitution. The excess of DTT was removed after using PD-10 desalting column or dialysis. In order to obtain Cu(I)-, Cu(II)-metallated protein, progressive titration, monitored by UV-Visible spectroscopy or ^{1}H-^{15}N-HSQC experiment were performed, using the metals respectively in the $[Cu(I)(CH_3CN)_4]PF_6$ and Cu_2SO_4 forms. The titration was performed using a maximum protein concentration of 0.2 mM avoiding aggregation of the protein. The excess of metals was removed by PD-10 desalting column or dialysis. All the NMR samples were prepared in phosphate buffer at pH 6-7.5.

2.6 BIOCHEMICAL AND BIOPHYSICAL CHARACTERIZATION

2.6.1 Circular dichroism spectroscopy

Circular dichroism (CD) is a spectroscopy based on the differential absorption of left- and right-handed circularly polarized light. CD is an excellent tool for rapid determination of the secondary structure and folding properties (i.e.arrangement of peptide bonds in secondary protein structure elements like helices and strands) of proteins that have been obtained using recombinant techniques. One of most widely used application of CD in protein studies is to determine whether a purified protein is folded and how a mutation or conditions of sample (denaturant) affects its conformation or stability.

In proteins the major optically active groups are the amide bonds of the peptide backbone (peptide bond: absorption below 240 nm, aromatic aminoacid side chains: absorption in the range 260 to 320 nm and disulphide bonds: weak broad absorption bands centred around 260 nm), typically disposed in highly ordered arrays such as α-helices or β-pleated sheets. The different types of regular secondary structure found in proteins give rise to characteristic CD spectra in the far UV (Figure 2.5).[20]

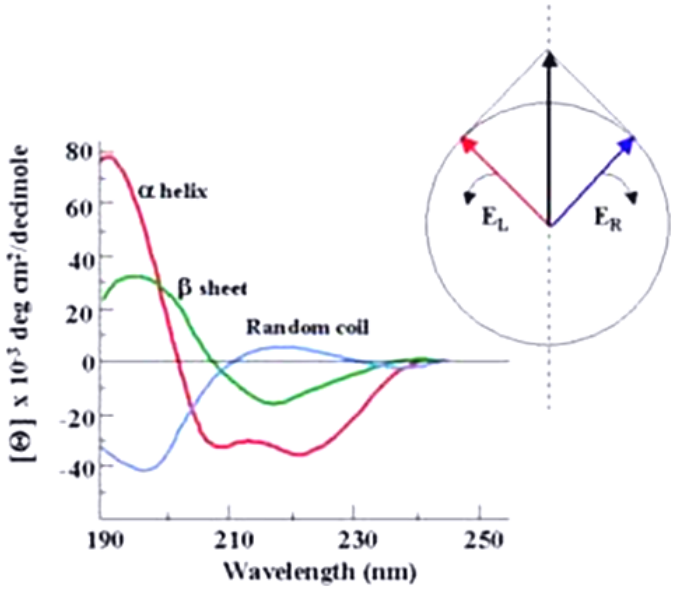

Figure 2.5. CD spectra of poly-lysine in three conformations.

The CD investigations were carried out in a Jasco J-715 spectropolarimeter using a 0.1-cm pathlength cell with cooling jacket connected to a water thermostatic device at 25°C. Spectra were recorded from 190-250nm at a scan speed of 20 nm/min and resulted from averaging 4 scans. The final spectra were baseline-corrected by subtracting the corresponding buffer obtained under identical conditions. Results were expressed as the mean residue ellipticity [θ] at a given wavelength. The data were fitted with the secondary structure estimation program DicroProt [21]

2.6.2 Dynamic light scattering

Dynamic light scattering (DLS), also known as Photon correlation spectroscopy or Quasi-elastic light scattering is a technique which can be used to determine the size distribution profile of small particles in solution like proteins. In the present thesis DLS was applied in chromatography mode for the investigation of the aggregation state of the proteins. 0.1–1 mM protein samples were injected on a Superdex75 HR-10/30 size-exclusion column on an AKTAFPLC system (Amersham Pharmacia Biosciences) connected with a multiangle light scattering (DAWN-EOS, Wyatt Technologies, Santa Barbara, CA) coupled with quasielastic light scattering detectors (Figure 2.6). Data analysis and average MW were automatically calculated by the Wyatt's Astra software.

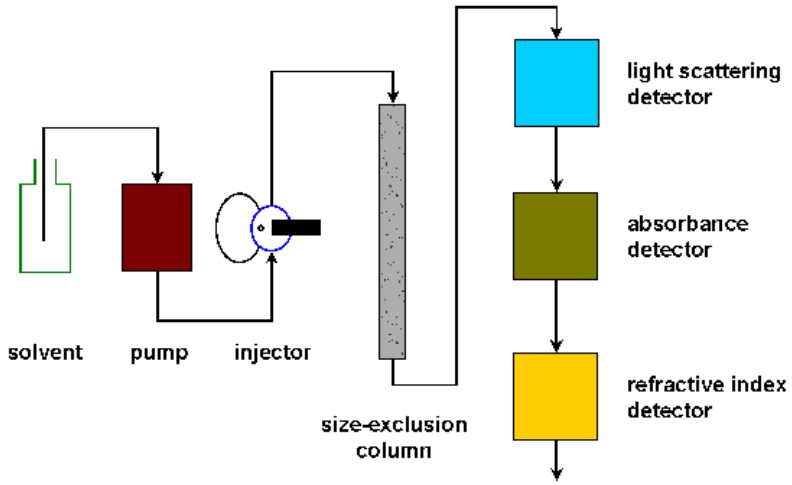

Figure 2.6. Diagram of light scattering in the chromatography mode.

The protein sample is injected (injector), separated in the size-exclusion column. After elution the different properties of the protein are measured by the detectors. [Reprinted from Alliance protein laboratories home page]

2.6.3 UV-visible spectroscopy

UV-visible spectroscopy involves the spectroscopy of photons in the UV-visible region. It uses light in the visible and adjacent near ultraviolet (UV) and near infrared (NIR) ranges. In this region of the electromagnetic spectrum, molecules undergo electronic transitions. UV-visible spectroscopy is routinely used in the quantitative determination of protein and DNA solution. Protein concentration can be determined by the absorption at 280 nm (mainly due to Tyr and Trp residues) using the protein extinction coefficient, estimated by Protparam [www. expasy.org/tools/protparam/], or by any colorimetric assay e.g. Bradford. The molar extinction coefficient (or molar absorptivity) is defined via the Beer-Lambert law:

$$\varepsilon = \frac{\mathrm{A}}{c \times l}$$

where A absorbance, c the sample concentration (M) and l the length of light path through the sample in cm.

DNA quantification is based on the absorption purines and pyrmidines which show absorption maxima around 260nm (alternatively DNA can be quantified on agarose gel by ladder markers).

2.6.4 Metals content determination by ICP

Inductively Coupled Plasma (ICP) is an analytical technique used for the detection of trace metals and allows multi-elemental, simultaneous analysis of most elements in the

periodic table, with excellent sensitivity (ng/L or ppt) and high sample throughput. The analytical principle used is optical emission spectroscopy, triggered by plasma ionization. The liquid sample is introduced in the prechamber, usually by mean of a peristaltic pump, then nebulized and entrained in the flow of plasma support gas, which is typically Argon. The analytes are excited into a state of radiated light emission by the plasma vapour and the emitted radiation is converted to an electrical signal that can be measured quantitatively by resolving the light into its component radiation (almost always by means of a diffraction grating). The light intensity is measured, at the specific wavelength for each element line, with a CCD (*charge coupled device*, basically an array of tiny, light-sensitive diodes) which converts it to electrical signals. The electron signal intensity is then compared to previously measured intensities of standard solutions of the target elements, and a concentration is computed. This spectroscopic technique is very suitable for the proteins metal content determination, since it requires very small amounts of sample, and is not perturbed by the polypeptidic matrix.

The samples were diluted 50 times with HNO_3 at pH 1,5 and analized with ICP-AES Varian 720-ES supplied with supersonic pulverizer CETAC 5000AT+.

2.6.5 Mass Spectrometry

Mass spectrometry is an important emerging method for the characterization of proteins. The two primary methods for ionization of whole proteins are electrospray ionization (ESI) and matrix-assisted laser desorption/ionization (MALDI).[22] They are strategies that can be used to retrieve information regarding protein–metal and protein–ligand noncovalent complexes. Indeed, when using carefully controlled conditions in the atmospheric pressure–vacuum interface of the mass spectrometer, and when sample preparation is optimized, it is possible to preserve large specific multiprotein–metal–ligand noncovalent complexes during MS analysis.[23]

For molecular mass definition the samples were preparing, using micro C18 ZipTips. The proteins were eluted from the ZipTips with a 20µl elution solution of 50% acetonitrile and 0.1% TFA in water. Alpha-cyano-4-hydroxycinnamic acid was used as matrix. Mass spectra were recorded in positive reflectron mode of a MALDI-TOF mass spectrometer (Bruker Daltomics Ultraflex TOF/TOF). The measured protein mass profiles were then analyzed using the PERL script algorithm.

For the metal binding studies the protein samples or their Cu(I)/Zn(II) complexes were prepared in 20mM ammonium acetate pH 7.5 containing various concentrations of DTT. They were injected into the electrospray ion source of a QSTAR Elite ESI-Q-TOF MS instrument (Applied Biosystems) by a syringe pump at 6 ml min21. ESI-MS spectra were recorded for 5 min in the m/z region from 500 to 3,000 Da with the following instrument parameters: ion spray voltage 5,500 V; source gas 45 l min21; curtain gas 20 l min21; declustering potential 60 V; focusing potential 320 V; detector voltage 2,300 V.

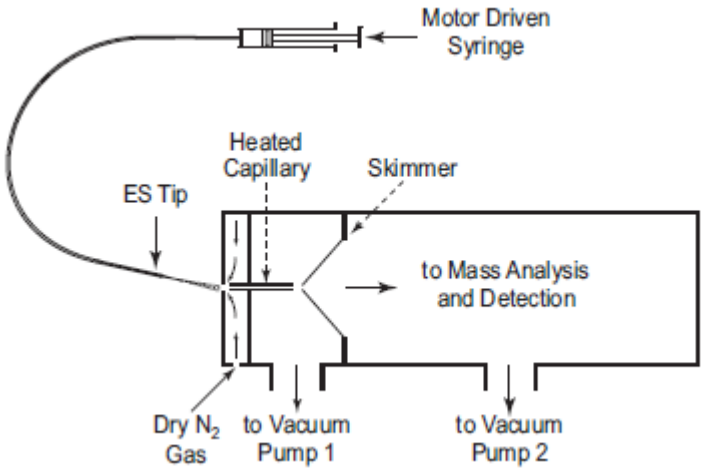

Figure 2.7. Electrospray ion source and interface to mass spectrometer.

Solution containing analyte is supplied to the metal ES spray tip by syringe via a flexible glass capillary. A positive potential is applied to the spray tip (positive ion mode). Positively charged droplets emerge from the spray capillary tip. Solvent evaporation of the charged droplets leads to gas-phase ions. A mixture of ions, small charged droplets and solvent vapor in the ambient gas enters the orifice leading to the nitrogen countercurrent chamber. The weak nitrogen counterflow removes solvent vapor. The ions, driven by an electric potential and pressure difference, enter the lowpressure chamber through the heated capillary. An electric field between the capillary and the skimmer accelerates the ions for a further collision activated ''clean-up'' of the ions.

2.7 NMR SPECTROSCOPY

NMR spectroscopy and X-ray crystallography are the two main techniques that can provide structures of macromolecules at atomic resolution. Both techniques are well established and play already a key role in structural biology as a basis for a detailed understanding of molecular functions. Whereas X-ray crystallography requires single crystals, NMR measurements are carried out in solution under conditions that can be as close as possible to the physiological state. In the NMR experiments, solution conditions such as the temperature, pH and salt concentration can be adjusted so as to closely mimic a given physiological fluid.[24] Or the other way round, the solutions may be changed to quite extreme non physiological conditions, for example, for studies of protein denaturation. Furthermore, in addition to protein structure determination, NMR applications include investigations of

dynamic features of the molecular structures, as well as studies of structural, thermodynamic and kinetic aspects of interactions between proteins and other solution components.[25, 26]

2.7.1 Structure Determination of Proteins with NMR Spectroscopy

NMR spectra are generated by placing a sample in a magnetic field and applying radio-frequency pulses, which perturb the equilibrium nuclear magnetization of those atoms with nuclei of nonzero spin. Transient time domain signals are detected as the system returns to equilibrium. Fourier transformation of the transient signal in to a frequency domain yields a one-dimensional NMR spectrum, which is a series of resonances from the various nuclei at different frequencies, or chemical shifts. The electrons in a molecule surround the nuclei and create a small magnetic field which shields the nuclei slightly from the external field. Therefore, the frequencies of different nuclei vary due to their different chemical environment. This effect is called 'chemical shift'. It is one of the major parameters of NMR spectroscopy since it causes the different positions of the signals in a NMR spectrum. The chemical shift of an atom depends on the electronic environment of its nucleus. The 1H atom is the only atom normally present in proteins that can be observed by NMR. ^{15}N and ^{13}C are used because the most abundant carbon isotope (^{12}C) does not give a NMR signal and the most abundant nitrogen isotope (^{14}N) has undesired NMR properties. In order to get NMR resonances sufficiently sharp for adequate resolution, the molecule must tumble rapidly. The current is around 35kDa but recent advances in both hardware and experimental design promise to allow the study of much larger proteins.[26] Moreover, the protein must be soluble at high concentration (0.2-1 mM, 6-30 mg/ml) and stable for days without aggregation under the experimental conditions. For the NMR measurements the protein is dissolved in 0.25 to 0.5 ml of aqueous buffer that contains about 10 % of D_2O which is necessary for the stabilization of the NMR instrument during the measurement.

NMR spectra of biological macromolecules contain hundreds or even thousands of resonance lines which cannot be resolved in a conventional one-dimensional spectra (1D). With the introduction of additional spectral dimensions these spectra are simplified and some extra information is obtained. The information about protein conformation that is present in NMR spectra arises from the interactions between hydrogen atoms that occur through the covalent bonds (through-bond J couplings) or through space (the nuclear Ovcrhauser, NOE).

Classical example of homonuclear 2D pulse sequences are:

1) 2D COSY: In the COSY (COrrelation SpettroscopY) experiment, magnetization is transferred by scalar coupling. Protons that are more than three chemical bonds apart give no cross signal because the 4J coupling constants are close to 0. Therefore, only signals on protons which are two or three bonds apart are visible in a COSY spectrum (red signals in Figure 2.8a).

2) 2D TOCSY: In the TOCSY (TOtal Correlation SpettroscopY) experiment, magnetization is dispersed over a complete spinsystem of an amino acid by successive scalar coupling. The TOCSY experiment correlates all protons of a spin system. Therefore, not only the red signals are visible (which also appear in a COSY spectrum) but also additional signals (green, shown in Figure 2.8b) which originate from the interaction of all protons of a spin system that are not directly connected via three chemical bonds. Thus a characteristic pattern of signals results for each amino acid from which the amino acid can be identified. However, some amino acids have identical spin systems and therefore identical signal patterns. They are: cysteine, aspartic acid, phenylalanine, histidine, asparagine, tryptophane and tyrosine ('AMX systems') on the one hand and glutamic acid, glutamine and methionine ('AM(PT)X systems') on the other hand.

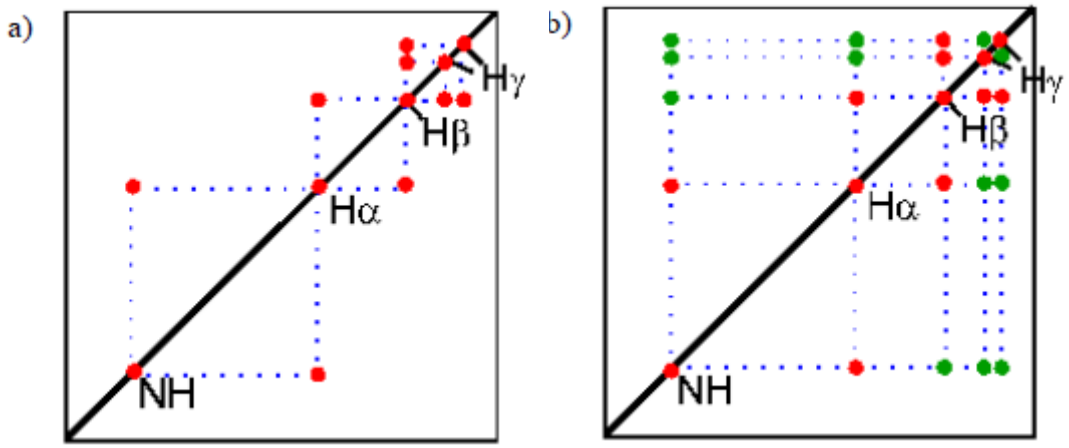

Figure 2.8. General overview a) COSY and b) TOCSY spectra

3) 2D-NOESY: The NOESY experiment uses the dipolar interaction of spins (the nuclear Overhauser effect, NOE) for correlation of protons. The intensity of the NOE is in first approximation propotional to 1/r6, with r being the distance between the protons: The correlation between two protons depends on the distance between them, but normally a signal is only observed if their distance is smaller than 5 Å. The NOESY experiment correlates all protons which are close enough. It also correlates protons which are distant in the amino acid

sequence but close in space due to tertiary structure. This is the most important information for the determination of protein structures.

For unlabelled proteins smaller than 10 kDa the combination of the [^{1}H,^{1}H]-COSY or TOCSY, used for the sequential assignment, with the [^{1}H, ^{1}H]-NOESY spectrum allows the assignment of most proton NMR signals to individual protons.[25,26] For larger proteins extensive signal overlap prevents complete assignments of all ^{1}H signals in proton spectra. This barrier can be overcome with 3D NMR technique and uniformly ^{13}C and ^{15}N labelled proteins. In this way it's possible to further spread out the signals in a third dimension, so that they are distributed in a cube instead of a plane, combining NOESY or TOCSY with a HSQC step.

With sufficient NOE data, a folded conformation can be determined in great detail but only if it is sufficiently stable to be present in a substantial fraction of the molecules. If there is substantial inter conversion of conformations on the NMR time scale all the NMR parameters are averages. The result of NMR structure determination is the set of similar models all of which fit the experimentally determined constraints. A final structure is obtained by averaging the models, and then finding the conformation of minimum energy that lies nearest to this average conformation.

Table 2. Summary of experimental procedures

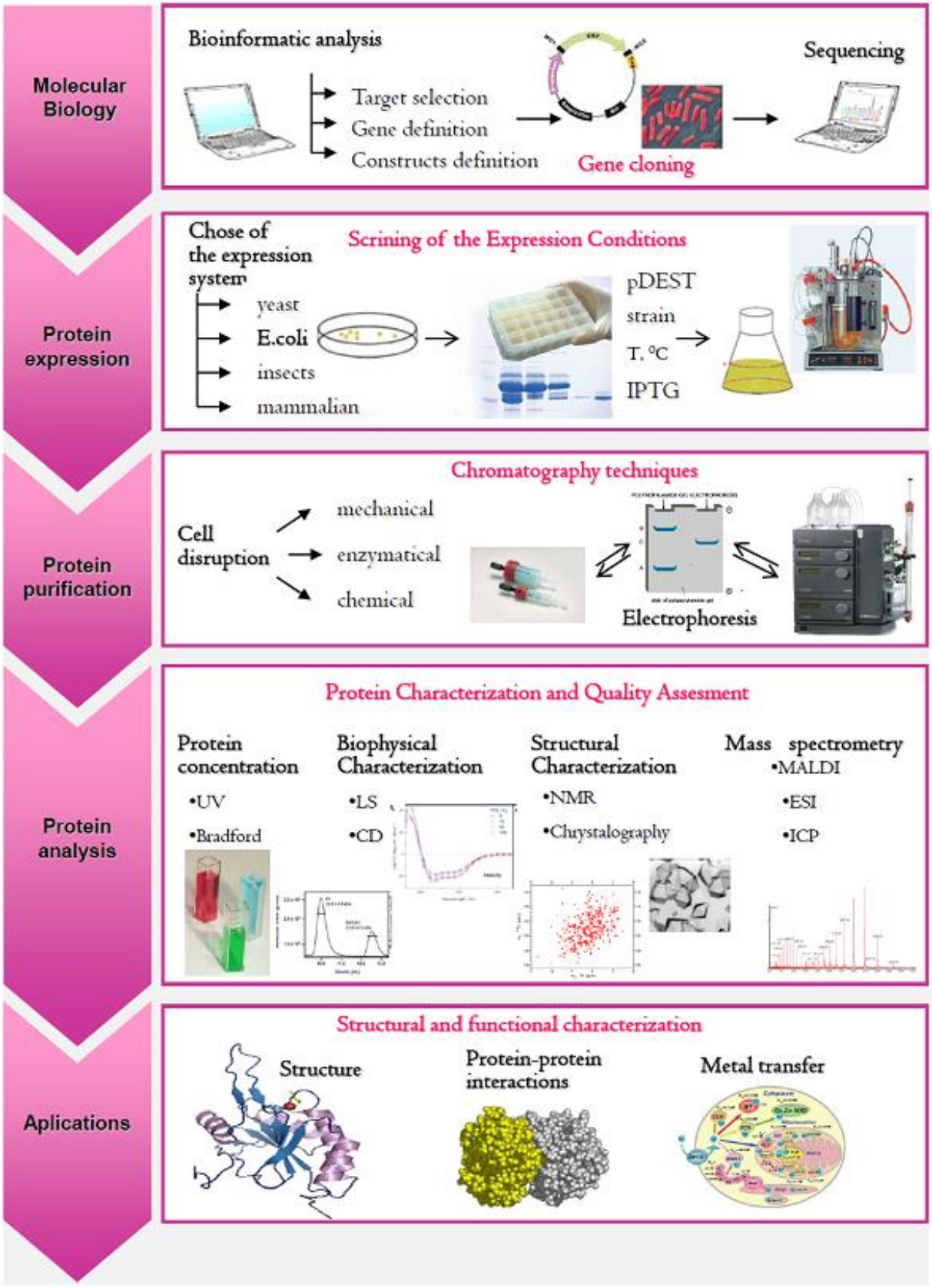

2.8 REFERENCES

1. Emanuelsson, O., Brunak, S., von Heijne, G. & Nielsen, H. Locating proteins in the cell using TargetP, SignalP and related tools. *Nat Protoc* **2**, 953-971 (2007).
2. Zhou, M., Boekhorst, J., Francke, C. & Siezen, R.J. LocateP: genome-scale subcellular-location predictor for bacterial proteins. *BMC Bioinformatics* **9**, 173 (2008).
3. Bendtsen, J.D., Binnewies, T.T., Hallin, P.F. & Ussery, D.W. Genome update: prediction of membrane proteins in prokaryotic genomes. *Microbiology (Reading, Engl.)* **151**, 2119-2121 (2005).
4. Tusnády, G.E. & Simon, I. The HMMTOP transmembrane topology prediction server. *Bioinformatics* **17**, 849-850 (2001).
5. Combet, C., Blanchet, C., Geourjon, C. & Deléage, G. NPS@: network protein sequence analysis. *Trends Biochem. Sci* **25**, 147-150 (2000).
6. Dosztányi, Z., Csizmok, V., Tompa, P. & Simon, I. IUPred: web server for the prediction of intrinsically unstructured regions of proteins based on estimated energy content. *Bioinformatics* **21**, 3433-3434 (2005).
7. Schenk, P.M., Baumann, S., Mattes, R. & Steinbiss, H.H. Improved high-level expression system for eukaryotic genes in Escherichia coli using T7 RNA polymerase and rare ArgtRNAs. *BioTechniques* **19**, 196-198, 200 (1995).
8. Malhotra, A. Tagging for protein expression. *Meth. Enzymol* **463**, 239-258 (2009).
9. Arnau, J., Lauritzen, C., Petersen, G.E. & Pedersen, J. Current strategies for the use of affinity tags and tag removal for the purification of recombinant proteins. *Protein Expression and Purification* **48**, 1-13 (2006).
10. Esposito, D. & Chatterjee, D.K. Enhancement of soluble protein expression through the use of fusion tags. *Current Opinion in Biotechnology* **17**, 353-358 (2006).
11. Schamhart, D.H. & Westerhof, A.C. Strategies for gene cloning. *Urol. Res* **27**, 83-96 (1999).
12. Yokoyama, S. Protein expression systems for structural genomics and proteomics. *Curr Opin Chem Biol* **7**, 39-43 (2003).
13. Shatzman, A.R. Expression systems. *Current Opinion in Biotechnology* **6**, 491-493 (1995).
14. Jana, S. & Deb, J.K. Strategies for efficient production of heterologous proteins in Escherichia coli. *Appl. Microbiol. Biotechnol* **67**, 289-298 (2005).
15. Das, A. Overproduction of proteins in Escherichia coli: vectors, hosts, and strategies. *Meth. Enzymol* **182**, 93-112 (1990).
16. Lesley, S.A. Parallel methods for expression and purification. *Meth. Enzymol* **463**, 767-785 (2009).
17. Hunt, I. From gene to protein: a review of new and enabling technologies for multi-parallel protein expression. *Protein Expression and Purification* **40**, 1-22 (2005).
18. Scopes, R.K. Strategies for protein purification. *Curr Protoc Protein Sci* **Chapter 1**, Unit 1.2 (2001).
19. Linn, S. Strategies and considerations for protein purifications. *Meth. Enzymol* **463**, 9-19 (2009).
20. Kelly, S.M., Jess, T.J. & Price, N.C. How to study proteins by circular dichroism. *Biochim. Biophys. Acta* **1751**, 119-139 (2005).
21. Deléage, G. & Geourjon, C. An interactive graphic program for calculating the secondary structure content of proteins from circular dichroism spectrum. *Comput. Appl. Biosci* **9**, 197-199 (1993).
22. Romanova, E., Annangudi, S. & Sweedler, J. Mass Spectroscopy of Proteins. *Encyclopedia of Neuroscience* 681-687 (2009).
23. Di Marco, V.B. & Bombi, G.G. Electrospray mass spectrometry (ESI-MS) in the study of metal-ligand solution equilibria. *Mass Spectrom Rev* **25**, 347-379 (2006).
24. Wüthrich, K. NMR studies of structure and function of biological macromolecules (Nobel Lecture). *J. Biomol. NMR* **27**, 13-39 (2003).
25. Wider, G. Structure determination of biological macromolecules in solution using nuclear magnetic

resonance spectroscopy. *BioTechniques* **29**, 1278-1282, 1284-1290, 1292 passim (2000).

26. Wüthrich, K. The second decade--into the third millenium. *Nat. Struct. Biol* **5 Suppl**, 492-495 (1998).

3. RESULTS

NOTE: The author of the thesis performed the molecular biological and biochemical part of the all presented projects, performing the cloning of all studied protein constructs, expression and purification of the target proteins. She carried out the protein caracterization using analytical gel filtration, light scattering, circular dichroism and simple NMR experiments. Also she spent some period at the Department of Gene Technology of Tallinn University of Technology performing ESI-MS analysis in order to determining metal binding affinity of studied proteins implicated in cellular copper distribution. Participated in data analysis and interpretation, drafted the manuscripts.

"AFFINITY GRADIENTS DRIVE COPPER TO CELLULAR DESTINATIONS"

Lucia Banci[1], Ivano Bertini[1], Simone Ciofi-Baffoni[1], Tatiana Kozyreva[1], Kairit Zovo[2] and Peep Palumaa[2]

[1] Magnetic Resonance Center CERM and Department of Chemistry, University of Florence, Via Luigi Sacconi 6, 50019, Sesto Fiorentino, Florence, Italy.

[2] Department of Gene Technology, Tallinn University of Technology, Akadeemia tee 15, 12618 Tallinn, Estonia.

Nature. 2010 Jun 3;465(7298):645-8

Vol 465|3 June 2010|doi:10.1038/nature09018 nature

LETTERS

Affinity gradients drive copper to cellular destinations

Lucia Banci[1], Ivano Bertini[1], Simone Ciofi-Baffoni[1], Tatiana Kozyreva[1], Kairit Zovo[2] & Peep Palumaa[2]

Copper is an essential trace element for eukaryotes and most prokaryotes[1]. However, intracellular free copper must be strictly limited because of its toxic side effects. Complex systems for copper trafficking evolved to satisfy cellular requirements while minimizing toxicity[2]. The factors driving the copper transfer between protein partners along cellular copper routes are, however, not fully rationalized. Until now, inconsistent, scattered and incomparable data on the copper-binding affinities of copper proteins have been reported. Here we determine, through a unified electrospray ionization mass spectrometry (ESI-MS)-based strategy, in an environment that mimics the cellular redox milieu, the apparent Cu(I)-binding affinities for a representative set of intracellular copper proteins involved in enzymatic redox catalysis, in copper trafficking to and within various cellular compartments, and in copper storage. The resulting thermodynamic data show that copper is drawn to the enzymes that require it by passing from one copper protein site to another, exploiting gradients of increasing copper-binding affinity. This result complements the finding that fast copper-transfer pathways require metal-mediated protein–protein interactions and therefore protein–protein specific recognition[3]. Together with Cu,Zn-SOD1, metallothioneins have the highest affinity for copper(I), and may play special roles in the regulation of cellular copper distribution; however, for kinetic reasons they cannot demetallate copper enzymes. Our study provides the thermodynamic basis for the kinetic processes that lead to the distribution of cellular copper.

There is currently a consensus that essentially no free copper is available in eukaryotic cells[4], as all copper ions are coordinated to proteins or to ligands of low molecular mass[5] such as reduced glutathione (GSH), the most abundant intracellular copper ligand of low molecular mass in living cells. The cellular distribution of copper among the various proteins and ligands is dictated by thermodynamics in the absence of kinetic barriers, which, however, do exist for copper exchange between certain protein pairs. In eukaryotes, copper enters the cell as Cu(I) through high-affinity plasma membrane copper transporters[6] or low-affinity permeases (Supplementary Fig. 1). Proteins called copper chaperones[7] then bind and transport Cu(I) ions to either cytosolic enzymes or to membrane transporters[8,9] that transfer Cu(I) ions into the organelles for copper enzymes (Supplementary Fig. 1).

The present work investigates, through a unified application of ESI-MS, the copper(I)-binding constants for a set of key cellular copper proteins and small Cu(I)–ligands, as well as the distribution of copper between proteins and between proteins and small ligands. Specifically, we have selected the following: (1) the cytoplasmatic copper chaperones HAH1 and CCS and their partners, namely the soluble cytosolic domains of a Cu(I)–ATPase (Menkes protein) located in the trans-Golgi network membrane[10] and the copper,zinc

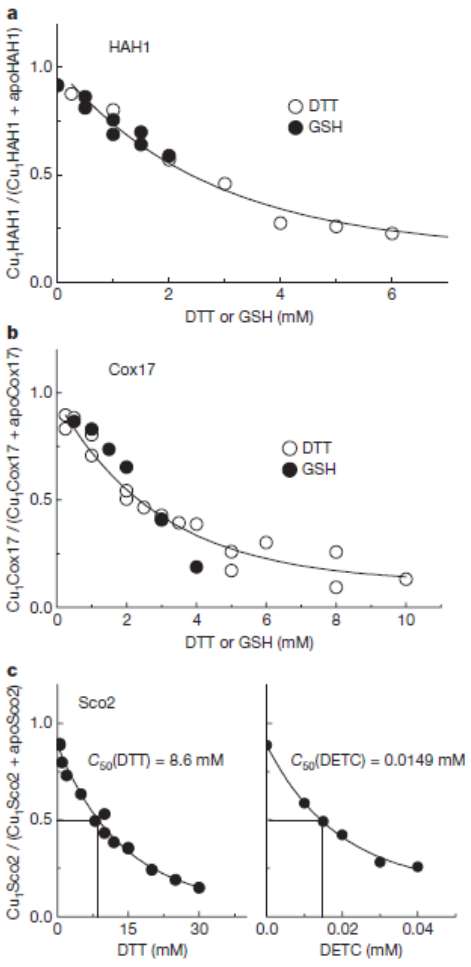

Figure 1 | Determination of the relative Cu(I)-binding affinity of GSH and DETC. **a**, **b**, Fractional content of metallated proteins ($Y = I_{CuProt}/(I_{Prot} + I_{CuProt})$) for HAH1 (**a**) and Cox17 (**b**) at increasing concentrations of DTT (open circles) and GSH (filled circles). **c**, Fractional content of metallated Sco2 ($Y = I_{CuSco2}/(I_{Sco2} + I_{CuSco2})$) at increasing concentrations of DTT (left) and DETC (right). Conditions: proteins 3 μM; 20 mM ammonium acetate, Cu(I)–DTT 5 μM, pH 7.5; $T = 25$ °C. Solid lines, fitting curves.

[1]Magnetic Resonance Center CERM and Department of Chemistry, University of Florence, Via Luigi Sacconi 6, 50019, Sesto Fiorentino, Florence, Italy. [2]Department of Gene Technology, Tallinn University of Technology, Akadeemia tee 15, 12618 Tallinn, Estonia.

superoxide dismutase1 (Cu,Zn-SOD1), respectively (Supplementary Fig. 1); (2) the copper chaperone Cox17 and its protein partners (Sco1/Sco2), all involved in the assembly of the Cu_A site of cytochrome *c* oxidase (CcO) within the mitochondrial intermembrane space[11] (Supplementary Fig. 1); (3) the copper enzyme Cu,Zn-SOD1 and Cu_A domain of CcO, as final recipients of copper ions (Supplementary Fig. 1); (4) metallothionein isoform 2 (MT-2), localized in both cytoplasmic and intermembrane-space compartments[12] (Supplementary Fig. 1).

Our ESI-MS approach, which measures apparent Cu(I)-binding constants in a consistent way for proteins and small ligands with affinity constants differing by several orders of magnitude, relies on the simultaneous monitoring of the variation in the metallated/non-metallated protein ratios at increasing concentrations of a competing Cu(I)-binding ligand, namely dithiothreitol (DTT) or diethyl-dithio-carbamate (DETC). The advantages of this approach are as follows: (1) applicability to a large set of copper proteins with different metal-binding stoichiometries, affinities and binding schemes; (2) the experiments are always performed in the presence of DTT, which creates reducing conditions mimicking the cellular redox environment; (3) DTT forms a stable complex with Cu(I) ions, preventing their oxidation or disproportionation; (4) the apparent Cu(I)-binding affinity of DTT, used as reference to obtain all of the other apparent Cu(I)-binding constants, is known[13] and is such that DTT at millimolar concentrations can effectively compete with most of the Cu(I)-binding proteins at micromolar concentrations; (5) the metal-binding stoichiometry of the various copper-binding molecules simultaneously present in solution can be determined. This approach can be straightforwardly extended to any other metal ion.

The copper-binding affinity of GSH ligand was estimated through four metal-competition experiments performed in parallel between Cu_1HAH1 or Cu_1Cox17 and GSH (Supplementary Fig. 2) or DTT (Supplementary Figs 3a–4a). From these data it results that GSH and DTT have similar apparent Cu(I)-binding constants (Fig. 1A, B and Table 1). Millimolar concentrations of DTT can thus correctly mimic the Cu(I)-binding capacity of GSH, present in the cell at approximately 10 mM concentrations[14]. The metal-binding affinity of DETC was similarly estimated (Fig. 1C and Methods), being about 400 times higher than those of DTT and GSH (Table 1).

The apparent Cu(I)-binding constants of all selected proteins, with the exception of MT-2 and Cu,Zn-SOD1, were determined using DTT

Table 1 | Apparent dissociation constants for Cu(I)-binding proteins and ligands of low-mass*

Protein/ligand	$K_{Cu} \times 10^{15}$ (M)	R^2†
HAH1	16.8 ± 4.8	0.89
$Cox17_{2S\text{-}S}$	17.4 ± 2.3	0.96
Menkes D1	2.5 ± 0.5	0.88
Menkes D2	4.9 ± 1.4	0.73
Menkes D3	104 ± 44	0.82
Menkes D5	13.0 ± 2.9	0.93
Menkes D6	2.6 ± 0.6	0.84
CCS	2.4 ± 0.2	0.96
Sco1	3.1 ± 0.7	0.94
Sco2	3.7 ± 0.5	0.95
Cu_A site of Cox2‡	0.73 ± 0.07 (slow dissociation)	0.86
Cu site of SOD1§	0.23 ± 0.02 (slow dissociation)	0.95
MT-2‖	0.41 ± 0.04 (n = 4.1)	0.97
DTT¶	7,940	
GSH#	9,130 ± 140	0.84
DETC★	13.8 ± 0.2	0.81

* Conditions: 20 mM ammonium acetate pH 7.5, 25 °C. K_{Cu} was calculated by fitting the Cu(I)-binding curves of Cu(I)-binding proteins/ligands to a common hyperbolic equation, corresponding to a simple 1:1 binding equilibrium, or to the Hill equation.
† R^2 describes the quality of the fit. For more details see Methods.
‡ From thermo-stabile bacteria *T. thermophilus*.
§ Calculated from demetallation experiments of Cu,Zn-SOD1 with DETC. For more details see Methods.
‖ Calculated from Cu(I)-competition experiment of Cu_{10}MT-2 with DETC by using the Hill equation (n, Hill coefficient).
¶ Taken from ref. 13.
# Calculated from comparison of the Cu(I)-affinity of GSH with that of DDT.
★ Calculated from the comparison of the Cu(I)-affinity of DETC with that of DDT.

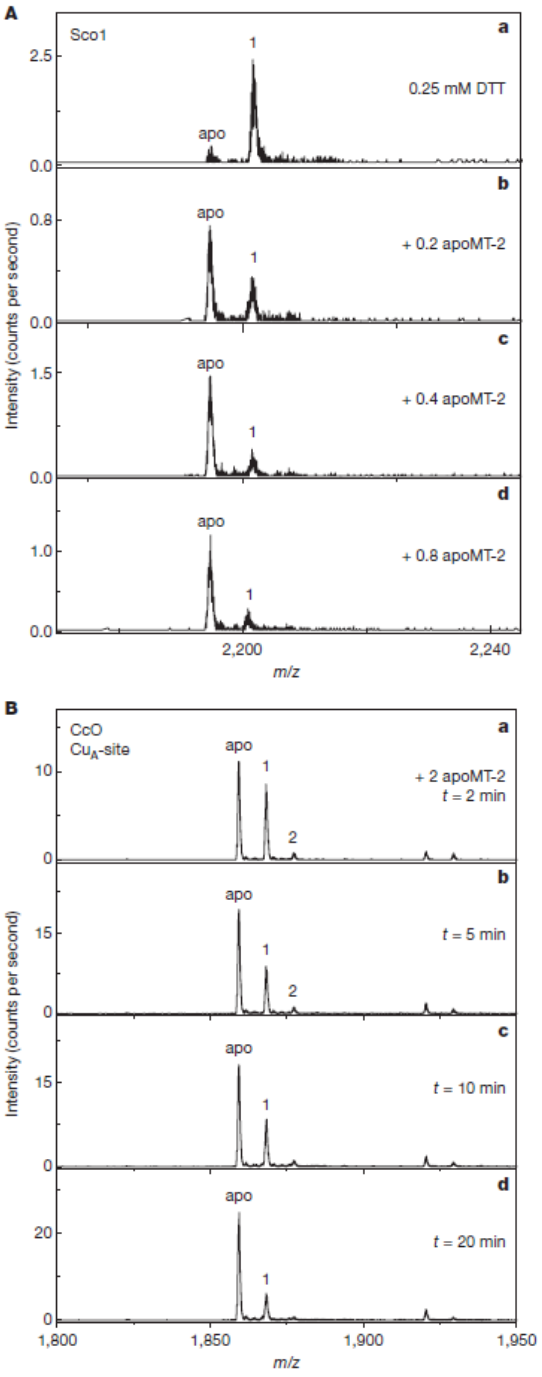

Figure 2 | Demetallation of Cu_1Sco1 and the Cu_A site of CcO by apo-MT-2 as followed by ESI-MS. **A**, ESI-MS spectra of Cu_1Sco1 (2.5 μM) in the absence (**a**) and presence of 0.5 μM (**b**), 1.0 μM (**c**) and 2 μM (**d**) apo-MT-2. **B**, ESI-MS spectra of Cu_2Cox2 (2.5 μM) after addition of apo-MT-2 (2.5 μM), at 2 min (**a**), 5 min (**b**), 10 min (**c**) and 20 min (**d**). The charge state ions +9 (for Sco1) and +10 (for Cox2) are presented and the numbers on the peaks denote the metal stoichiometry of the complex.

as the competing metal-binding ligand and fitting the variation of metallated/non-metallated protein ratios with the concentration of free Cu(I) ions to a single equilibrium (Table 1, Methods and Supplementary Figs 3–13). The Cu(I)-binding constant of MT-2 was determined with the same approach but using DETC and a more complex fitting procedure (Methods). Addition of millimolar DETC to micromolar Cu_{10}MT-2 led to the DETC-concentration-dependent simultaneous formation of the intermediates Cu_6MT-2, Cu_4MT-2 and of apo-MT-2 (Supplementary Fig. 14), the last being the major form of MT-2 at 3 mM DETC, indicating that Cu_{10}MT-2 contains six-metal and four-metal clusters according to the literature[15]. All Cu(I) ions dissociate from both MT-2 thiolate clusters with a positive cooperativity (Supplementary Fig. 14), and an apparent dissociation constant of 0.41 fM was obtained for MT-2 (Table 1 and Methods). DETC was also able to remove copper from 10 μM Cu,Zn-SOD1, with a slow kinetic process (Supplementary Fig. 15 and Methods). An apparent dissociation constant for Cu,Zn-SOD1 of 0.23 fM was estimated from the final equilibrium levels of SOD1 demetallation at different DETC concentrations (Table 1 and Methods). In all the other cases the equilibrium between the apo- and copper-loaded protein forms was reached within 2 min of incubation, namely within the minimal measurement time in ESI-MS, indicating that Cu(I) exchange between these copper proteins and DTT or DETC is faster than minutes. Indeed, these thiol-based chelators can access copper sites in all of these proteins, except in Cu,Zn-SOD1, where copper is barely accessible at the bottom of a 12-Å-deep narrow channel.

The soluble Cox2 domain of CcO from a thermophilic prokaryote was used to determine the copper affinity of apoCu_A site, as eukaryotic Cox2 domains are unstable and unable to bind copper ions (unpublished results from our laboratory and personal communication from D. Winge and B. Ludwig), and a value of 0.73 fM was estimated. To compare this value with that of intact mammalian CcO, the catalytic activity of the rat membrane-bound CcO complex was analysed with respect to its copper content. DETC (2 mM) can quickly inactivate CcO (at micromolar concentration) by approximately 50%, owing to copper removal from the enzyme as shown by inductively coupled plasma mass spectrometry (ICP-MS). This result is consistent with comparable Cu(I)-binding affinities for the mammalian CcO and the isolated prokaryotic Cox2 domain.

When apo-MT-2 is added at sub-stoichiometric or equimolar amounts, it is able to extract Cu(I) ions quickly (within 2 min) from all the investigated proteins (Fig. 2A), except copper enzymes. Copper is not extracted from Cu,Zn-SOD1 with a twofold molar excess of apo-MT-2 within 3 h, as a consequence of the low accessibility of SOD1 copper sites for MT-2, the latter being much larger than DETC. Apo-MT-2 added at twofold molar excess can extract the two Cu(I) ions from the Cu_A site of a prokaryotic Cox2 domain (Fig. 2B), and the metal extraction progressed with a half-life of 3.5 min (Supplementary Fig. 16). The Cu_A site of rat membrane-bound CcO complex is, however, not accessible for apo-MT-2 as up to 20 μM apo-MT-2 cannot inactivate catalytic activity of CcO after incubation of up to 30 min (Supplementary Fig. 17), apparently for kinetic reasons as found for Cu,Zn-SOD1. These results indicate that apo-MT-2 is not able to regulate the metallation state of Cu,Zn-SOD1 and mammalian membrane-bound CcO complex.

Copper chaperones such as HAH1 and Cox17 at micromolar concentrations and GSH at millimolar concentrations have comparable Cu(I)-binding capacities (Table 1), and therefore constitute an exchangeable cellular copper-binding pool. The copper chaperone CCS has seven times higher Cu(I)-binding affinity than Cox17 and HAH1; millimolar concentrations of GSH are therefore unable to compete with CCS for Cu(I) ions. The HAH1 partners are six homologous domains of Menkes protein (Supplementary Fig. 1), each capable of binding one Cu(I) ion through a CXXC metal-binding motif. Domains 1, 2 and 6 of Menkes protein have a copper-binding affinity three to seven times higher than HAH1, whereas domain 5 has only slightly higher affinity and domain 3 much lower affinity than HAH1 (Table 1). This pattern of affinities is consistent with that observed in metal transfer experiments through NMR[16,17]. The mitochondrial Cox17 partners, namely Sco1 and Sco2 (Supplementary Fig. 1), have five times higher Cu(I)-binding affinity than Cox17 (Table 1), so that metal transfer occurs from Cox17 to Sco proteins[18,19]. The partners of both cytoplasmic and mitochondrial chaperones, therefore, have Cu(I)-binding affinities that thermodynamically drive copper transfer from HAH1, Cox17 and CCS metallochaperones (see below) towards their respective partners. GSH at millimolar concentrations is unable to compete with the copper sites of these partner proteins. Cu,Zn-SOD1 has ten times higher Cu(I)-binding affinity than its copper chaperone CCS, so that metal transfer is thermodynamically favoured towards the enzyme as indeed is found even in the presence of stringent copper chelators[20]. The Cu_A site of CcO, as well, has a much higher affinity for Cu(I) ions than Sco1 and Sco2 (Table 1), thus again thermodynamically favouring the transfer of Cu(I) ions from the Sco proteins to the Cu_A site of CcO (Table 1). There is

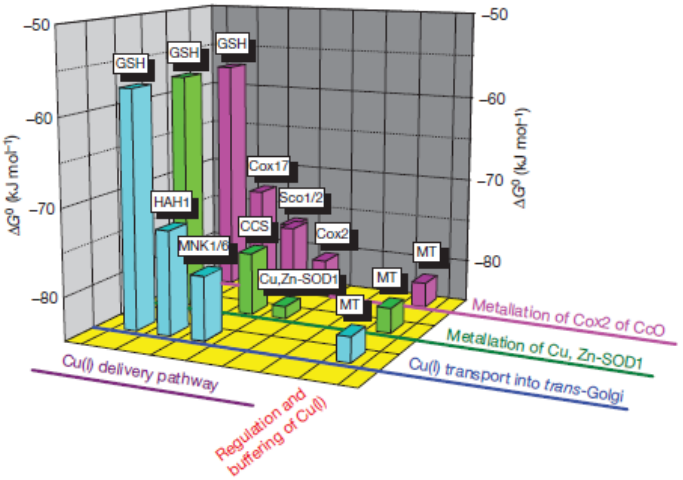

Figure 3 | Free-energy gradients of cellular Cu(I) delivery pathways. Values for ΔG^0 were calculated from the apparent values of K_{Cu} for Cu(I)-binding proteins and GSH (Table 1) by using the relation $\Delta G^0 = -RT \times \ln(K_{Cu})$ (R, gas constant (8.314 J K^{-1} mol^{-1}); T, absolute temperature in kelvins (298 K)). Metallothioneins can participate in buffering of copper(I) and regulation of its distribution.

therefore a distinct Cu(I)-binding hierarchy among Cu(I)-binding proteins, in agreement with the cellular routes for copper delivery, namely from chaperone to intermediate copper transport proteins and finally to enzymes (Fig. 3). Additionally, the fast copper transfer kinetics observed in all copper-handling proteins play a critical functional role because, as already suggested[4], specific protein–protein recognition may favour a certain pathway, overcoming thermodynamic hierarchy directions versus non-target molecules. The cellular compartment, where metallation occurs, can also contribute to prevent the competitive binding of metals to the wrong nascent metalloproteins[21]. The role of metallothioneins is intriguing, as they can act thermodynamically to regulate copper cellular distribution. However, fast copper transfer pathways may overcome the trapping effect of metallothioneins. Copper availability for copper proteins and enzymes therefore depends on a fine balance between the metallothionein expression levels and the kinetic rate constants relative to copper delivery towards final targets along pathways.

Some of the apparent dissociation constant (K_{Cu}) values determined here for the Cu(I)–protein complexes are significantly different from those obtained through the use of varied and disparate approaches, changing by as much as nine orders of magnitude (see, for example, refs 22, 23) for the same protein. These discrepancies show that only a unified methodological approach can provide consistently comparable sets of data, which are necessary to gain a general understanding of the cellular biology of copper.

METHODS SUMMARY

Recombinant protein production. All of the investigated soluble proteins are human with the exception of Cox2, stable and soluble forms of which have so far been isolated or expressed only from a few bacterial sources, namely *Bacillus subtilis*, *Paracoccus denitrificans* and *Thermus thermophilus*[24–26]. The sequence homology between human and bacterial Cox2 proteins in the metal binding site region is approximately 50% and the respective structural models are very superimposable. Recombinant human apo-MT-2, apoCox17 and Cu_2Cox2 domains from *T. thermophilus* were expressed and purified as described previously[26–29]. Recombinant human HAH1, Sco1, Sco2 and the individual domains of human Menkes protein in their apo states were purchased from ProtEra. Human dimeric Cu,Zn-SOD1 was purified from yeast as described previously[30]. Recombinant human CCS has been expressed and purified from *E. coli* as described in Methods. Details of the preparation of mitochondrial fractions from rat liver and measurements of CcO activity are described in Methods.

Determination of dissociation constants for Cu complexes. Apparent dissociation constants for Cu(I) complexes have been determined from their demetallation under the influence of increasing concentrations of competing Cu(I)-binding ligands, namely GSH, DTT or DETC. All details are in Methods.

Full Methods and any associated references are available in the online version of the paper at www.nature.com/nature.

Received 25 August 2009; accepted 17 March 2010.
Published online 12 May 2010.

1. Bertini, I., Cavallaro, G. & McGreevy, K. Cellular copper management – a user's guide. *Coord. Chem. Rev.* **254**, 506–524 (2010).
2. Kim, B. E., Nevitt, T. & Thiele, D. J. Mechanisms for copper acquisition, distribution and regulation. *Nature Chem. Biol.* **4**, 176–185 (2008).
3. Banci, L. *et al.* The Atx1-Ccc2 complex is a metal-mediated protein–protein interaction. *Nature Chem. Biol.* **2**, 367–368 (2006).
4. Rae, T. D., Schmidt, P. J., Pufahl, R. A., Culotta, V. C. & O'Halloran, T. V. Undetectable intracellular free copper: the requirement of a copper chaperone for superoxide dismutase. *Science* **284**, 805–808 (1999).
5. Finney, L. A. & O'Halloran, T. V. Transition metal speciation in the cell: insights from the chemistry of metal ion receptors. *Science* **300**, 931–936 (2003).
6. Nose, Y., Rees, E. M. & Thiele, D. J. Structure of the Ctr1 copper trans'PORE'ter reveals novel architecture. *Trends Biochem. Sci.* **31**, 604–607 (2006).
7. Pufahl, R. A. *et al.* Metal ion chaperone function of the soluble Cu(I) receptor Atx1. *Science* **278**, 853–856 (1997).
8. Huffman, D. L. & O'Halloran, T. V. Function, structure, and mechanism of intracellular copper trafficking proteins. *Annu. Rev. Biochem.* **70**, 677–701 (2001).
9. Linz, R. & Lutsenko, S. Copper-transporting ATPases ATP7A and ATP7B: cousins, not twins. *J. Bioenerg. Biomembr.* **39**, 403–407 (2007).
10. Voskoboinik, I. & Camakaris, J. Menkes copper-translocating P-type ATPase(ATP7A): biochemical and cell biology properties, and role in Menkes disease. *J. Bioenerg. Biomembr.* **34**, 363–371 (2002).
11. Atkinson, A. & Winge, D. R. Metal acquisition and availability in the mitochondria. *Chem. Rev.* **109**, 4708–4721 (2009).
12. Kagi, J. H. R. *Metallothionein.* Birkhäuser Verlag (1993).
13. Krezel, A. *et al.* Coordination of heavy metals by dithiothreitol, a commonly used thiol group protectant. *J. Inorg. Biochem.* **84**, 77–88 (2001).
14. Ostergaard, H., Tachibana, C. & Winther, J. R. Monitoring disulfide bond formation in the eukaryotic cytosol. *J. Cell Biol.* **166**, 337–345 (2004).
15. Nielson, K. B. & Winge, D. R. Preferential binding of copper to the beta domain of metallothionein. *J. Biol. Chem.* **259**, 4941–4946 (1984).
16. Banci, L. *et al.* An NMR study of the interaction between the human copper(I) chaperone and the second and fifth metal-binding domains of the Menkes protein. *FEBS J.* **272**, 865–871 (2005).
17. Banci, L. *et al.* Solution structure and intermolecular interactions of the third metal-binding domain of ATP7A, the Menkes disease protein. *J. Biol. Chem.* **281**, 29141–29147 (2006).
18. Banci, L. *et al.* Human Sco1 functional studies and pathological implications of the P174L mutant. *Proc. Natl Acad. Sci. USA* **104**, 15–20 (2007).
19. Banci, L. *et al.* Mitochondrial copper(I) transfer from Cox17 to Sco1 is coupled to electron transfer. *Proc. Natl Acad. Sci. USA* **105**, 6803–6808 (2008).
20. Rae, T. D., Torres, A. S., Pufahl, R. A. & O'Halloran, T. V. Mechanism of Cu,Zn-superoxide dismutase activation by the human metallochaperone hCCS. *J. Biol. Chem.* **276**, 5166–5176 (2001).
21. Tottey, S. *et al.* Protein-folding location can regulate manganese-binding versus copper- or zinc-binding. *Nature* **455**, 1138–1142 (2008).
22. Yatsunyk, L. A. & Rosenzweig, A. C. Copper(I) binding and transfer by the N-terminus of the Wilson disease protein. *J. Biol. Chem.* **282**, 8622–8631 (2007).
23. Jensen, P. Y., Bonander, N., Moller, L. B. & Farver, O. Cooperative binding of copper(I) to the metal binding domains in Menkes disease protein. *Biochim. Biophys. Acta* **1434**, 103–113 (1999).
24. Lappalainen, P., Aasa, R., Malmström, B. G. & Saraste, M. Soluble Cu_A-binding domain from the *Paracoccus* cytochrome *c* oxidase. *J. Biol. Chem.* **268**, 26416–26421 (1993).
25. Von Wachenfeldt, C., de Vries, S. & Van der Oost, J. The Cu_A site of the caa_3-type oxidase of *Bacillus subtilis* is a mixed-valence binuclear copper center. *FEBS Lett.* **340**, 109–113 (1994).
26. Slutter, C. E. *et al.* Water-soluble, recombinant Cu_A-domain of the cytochrome ba_3 subunit II from *Thermus thermophilus*. *Biochemistry* **35**, 3387–3395 (1996).
27. Eriste, E., Kruusel, K., Palumaa, P., Jörnvall, H. & Sillard, R. Purification of recombinant human apometallothionein-3 and reconstitution with zinc. *Protein Expr. Purif.* **31**, 161–165 (2003).
28. Voronova, A. *et al.* Cox17, a copper chaperone for cytochrome *c* oxidase: expression, purification, and formation of mixed disulphide adducts with thiol reagents. *Protein Expr. Purif.* **53**, 138–144 (2007).
29. Banci, L. *et al.* A structural-dynamical characterization of human Cox17. *J. Biol. Chem.* **283**, 7912–7920 (2008).
30. Hallewell, R. A. *et al.* Genetically engineered polymers of human CuZn superoxide dismutase. *J. Biol. Chem.* **264**, 5260–5268 (1989).

Supplementary Information is linked to the online version of the paper at www.nature.com/nature.

Acknowledgements This work was supported by grants from the Estonian Science Foundation project 7191, the Estonian Ministry of Education and Research (grant SF0140055s08), by the SPINE-II-COMPLEXES contract LSHG-CT-2006-031220, by the FIRB PROTEOMICA MIUR contract RBRN07BMCT and by a World Federation of Scientists scholarship to K.Z. We thank K. Saar for preparative work with rat mitochondrial fractions and for measuring the enzymatic activity of CcO, and C. Massagni for preparing the CCS expression plasmid.

Author Contributions L.B., I.B., S.C.-B., K.Z., P.P. designed the research; K.Z., T.K. and P.P. performed the research. All authors analysed the data and contributed to the writing of the paper.

Author Information Reprints and permissions information is available at www.nature.com/reprints. The authors declare no competing financial interests. Correspondence and requests for materials should be addressed to I.B. (ivanobertini@cerm.unifi.it) or P.P. (peepp@staff.ttu.ee).

doi:10.1038/nature09018 nature

METHODS

Protein expression and purification. All of the expressed proteins are human with the exception of Cox2, stable and soluble forms of which have so far been isolated or expressed only from a few bacterial sources, namely *Bacillus subtilis*, *Paracoccus denitrificans* and *Thermus thermophilus*[24–26]. Recombinant human apo-MT-2, apoCox17 and Cu_2Cox2 domains from *T. thermophilus* were expressed and purified as described previously[26–29]. Human dimeric Cu,Zn-SOD1 was purified from yeast as described previously[30].

The CCS gene was amplified from genomic DNA by PCR, cloned into the Gateway Entry vector pDONR 221 (Invitrogen), and subcloned into the pTH27 Destination vector by a Gateway LR reaction to generate an amino (N)-terminal, His-fused protein. The CCS protein was expressed in *E. coli* BL21(DE3) CodonPlus-RIPL cells (Stratagene), which were grown in Luria-Bertani broth. Protein expression was induced with 0.7 mM isopropyl β-D-thiogalactopyranoside for 16 h. After 1 h, $ZnSO_4$ was added in the culture to a final concentration of 1 mM. Purification was performed by using a HiTrap chelating HP column (Amersham Pharmacia Biosciences) charged with Ni(II). The His tag was then cleaved with AcTEV. The digested protein was concentrated by ultrafiltration and loaded in a 16/60 Superdex 75 chromatographic column (Amersham Biosciences) to separate CCS from the N-terminal His domain. The fractions showing a single component by SDS–polyacrylamide gel electrophoresis were collected, and the protein concentration was measured using the Bradford protein assay.

To investigate the aggregation state of CCS, 0.4–0.1 mM (100 µl) protein samples were run on a Superdex75 HR-10/30 size-exclusion column on an Äkta-FPLC system (GE Healthcare) connected to a multi-angle light scattering analyser (DAWN-EOS, Wyatt Technologies) coupled with quasi-elastic light-scattering detectors. Light scattering and analytical gel filtration data showed that the purified protein is a dimer.

The metal content of CCS was determined by inductively coupled plasma–atomic emission spectrometry. The samples were analysed on a Varian 720-ES supplied with a CETAC 5000AT+ supersonic pulverizer. According to the data collected, a 1:1 zinc/monomeric protein ratio was obtained. Copper ions were only present in a range of 10–20% with respect to monomeric protein concentration.

Reconstitution of proteins with Cu(I) ions. Before metal reconstitution, all purified proteins (with the exception of Cu_2Cox2 and Cu,Zn-SOD1, which are already produced in their metallated states) were reduced by addition of 2 mM DTT and then passed on a Superdex 75 10/300 size exclusion chromatography (SEC) column (GE Healthcare) connected to a Äkta Purifier system (GE Healthcare) by using 20 mM ammonium acetate pH 7.5 as the elution buffer. Also in the case of Cu_2Cox2 and Cu,Zn-SOD1, SEC on a Superdex 75 10/300 column connected to an Äkta Purifier system was performed by using 20 mM ammonium acetate pH 7.5 as the elution buffer.

Apo forms of copper proteins, except for MT-2, were metallated with slight excess of Cu(I)–DTT complex in the presence of DTT. Specifically, by the addition of 5 µM Cu(I)–DTT complex to 3 µM apo-protein samples in 20 mM ammonium acetate, pH 7.5 and containing 0.1–0.25 mM DTT, formation of the monometallic Cu(I)–protein was observed for all proteins, with a small amount of the apo-protein still present as detected by ESI-MS spectra (Supplementary Figs 3–12). Zn_1CCS (5 µM) was reconstituted with 7 µM Cu(I)–DTT, which resulted in formation of Cu_1Zn_1CCS. CCS forms in the electrospray ionization process, in addition to broad peaks of the dimeric state, peaks of the monomeric state. It was possible to resolve the peaks of the metallated/non-metallated CCS monomers, which were thus taken into account in the determination of the Cu(I)-binding affinity of Cu_1Zn_1CCS in metal competition experiments (Supplementary Fig. 13). Addition of 12-fold excess of Cu(I)–DTT in the presence of 10 mM DTT was necessary to produce the fully metallated form of MT-2 (Cu_{10}MT-2, Supplementary Fig. 18), and up to 60 mM DTT did not demetallate Cu_{10}MT-2 present at micromolar concentration (Supplementary Fig. 18). The stock solution of Cu(I)–DTT complex was prepared by dissolving Cu(II)-acetate at 1.3 mM concentration in argon-saturated 20 mM ammonium acetate, pH 7.5, containing 10 mM DTT.

Determination of metal-binding equilibria in the presence of DTT. In a standard experiment, increasing concentrations of DTT were added to the metallated proteins. Samples were then incubated for 2 min, and finally analysed by ESI-MS as described below. In certain experiments, metallated proteins were incubated with increasing concentrations of GSH or DETC and again analysed by ESI-MS. DTT is a non-ionic compound and thus has only a slight influence on the ionization efficiency of proteins in the ESI-MS process, enabling detection of protein peaks even when DTT is present at 60 mM concentration. Unlike DTT, GSH is an ionic compound and substantially suppresses peak intensities in ESI-MS spectra already at low millimolar concentrations. Protein ion peaks almost disappear in the presence of 2–4 mM GSH, and many intensive disturbing peaks appear from GSH in the observed spectral region (Supplementary Fig. 2). Therefore, GSH is less suitable for ESI-MS-based metal-competition experiments than DTT because it cannot be used at high millimolar concentrations. As DETC forms a covalent adduct with Sco2, only apo and Cu_1Sco2 species were taken into account in the determination of the apparent Cu(I)-binding constant of DETC.

ESI-MS measurements. Samples (3 or 5 µM) of proteins or their Cu(I) complexes in 20 mM ammonium acetate pH 7.5 containing various concentrations of DTT, GSH or DETC were injected into the electrospray ion source of a QSTAR Elite ESI-Q-TOF MS instrument (Applied Biosystems) by a syringe pump at 6 µl min^{-1}. ESI-MS spectra were recorded for 5 min in the m/z region from 500 to 3,000 Da with the following instrument parameters: ion spray voltage 5,500 V; source gas 45 l min^{-1}; curtain gas 20 l min^{-1}; declustering potential 60 V; focusing potential 320 V; detector voltage 2,300 V. Because of the original setting of the aerosol current over the orifice hole and retrograde curtain gas flow in the ESI chamber of the QSTAR Elite Q-TOF MS/MS instrument, DTT did not contaminate or block the orifice hole during experiments at high DTT concentrations.

Determination of dissociation constants for Cu(I)–ligand complexes. The copper-binding affinities of GSH and DETC ligands were indirectly estimated by comparing their ability to extract Cu(I) ions from selected Cu(I) proteins with that of DTT, whose conditional Cu(I)-binding affinity is available[13]. In particular, the metal-binding affinity of DETC was estimated by comparing its ability to extract Cu(I) ions from Cu_1Sco2 with that of DTT. Experiments performed in parallel with DTT and DETC showed that DETC competes effectively with Sco2 for Cu(I) ions and that DETC and DTT extract 50% of the Cu(I) ions from Cu_1Sco2 at concentrations of 14.9 µM and 8.6 mM, respectively (Fig. 1c), thus determining an apparent dissociation constant for Cu(I)DETC complex of $(1.38 \pm 0.02) \times 10^{-14}$ M (Table 1).

Extraction of Cu(I) from Cu,Zn-SOD1. In the reference experiment, a 10 µM sample of Cu,Zn-SOD1 (concentration is calculated for SOD1 monomers and equals to the concentration of metal-binding sites) in 20 mM ammonium acetate pH 7.5, 1 mM DTT was run on a Superdex 75 10/300 SEC column connected to an Äkta Purifier system by using degassed 20 mM ammonium acetate pH 7.5 as the elution buffer. The peak corresponding to dimeric Cu,Zn-SOD1 was collected, diluted four times with ultrapure 2% HNO_3 (Sigma) and analysed for copper content by ICP-MS on a Thermo X Series 2 ICP-MS instrument (Thermo Scientific). Next, 10 µM samples of Cu,Zn-SOD1 in 20 mM ammonium acetate pH 7.5, 1 mM DTT, were incubated with different concentrations of DETC (0.25, 0.5 and 1.0 mM) and aliquots from the incubation mixture were injected into SEC column after 30, 90 and 180 min of incubation. SOD1 peaks were collected and analysed for copper content as described above. The kinetic data of copper extraction from Cu,Zn-SOD1 at different DETC concentrations are presented in Supplementary Fig. 15. Fitting of these kinetic data to the equation of exponential decay yielded half-lives and equilibrium levels of SOD1 demetallation at different DETC concentrations. Cu(I) extraction from Cu,Zn-SOD1 by DETC was very slow and occurred with half-lives of 132, 72 and 54 min at 0.25, 0.5 and 1.0 mM DETC, respectively. That the rate of Cu,Zn-SOD1 demetallation depends on concentration of DETC indicates that metal extraction from SOD occurs through a ligand exchange process and not over free Cu(I) ions. In the latter case the rate limiting step would be the dissociation of Cu(I) from Cu,Zn-SOD1, which depends on conformational dynamics of protein and does not depend on concentration of metal chelator. Using the conditional dissociation constant for Cu(I)–DETC complex, which is equal to 13.8 fM (Table 1), concentrations of free Cu(I) ions in different incubation mixtures at equilibrium were determined and these values were used for calculation of the dissociation constant for Cu,Zn-SOD1. K_{Cu} values obtained at different DETC concentrations were in good agreement and an average value of $K_{Cu} = 0.23 \pm 0.02$ fM was obtained.

By using the approach described above, an attempt was made to extract Cu(I) ions from Cu,Zn-SOD1 by apo-MT-2; however, up to 180 min incubation of Cu,Zn-SOD1 (10 µM) with apo-MT-2 (20 µM) did not affect the copper content of Cu,Zn-SOD1 (Supplementary Fig. 15).

Calculation of dissociation constants for Cu(I)–protein complexes. Apparent values of K_{Cu} for the Cu_1–protein complexes were calculated according to the following simplified reaction scheme, already introduced in previous studies[18,31–33]:

$$\text{Cu(I)} - \text{protein} \xleftrightarrow{K_{Cu}} \text{protein} + \text{Cu(I)} \quad (1)$$

$$\text{Cu(I)} - \text{DTT} \xleftrightarrow{K_D} \text{DTT} + \text{Cu(I)} \quad (2)$$

where K_D is the conditional dissociation constant for the Cu(I)–DTT complex, which at pH = 7.4, $I = 0.1$, $T = 25°$ C, is equal to 7.94×10^{-12} M (ref. 13). K_{Cu} was calculated in two steps. First, the concentrations of free Cu(I) ions in the presence

doi:10.1038/nature09018 nature

of various concentrations of DTT were calculated by using the K_D value of the Cu(I)–DTT complex. Second, the fractional content of Cu_1-protein species (Y), calculated from the intensities (I) of apo-protein and $Cu(I)_1$–protein peaks in ESI-MS spectra ($Y = I_{Cu1\text{–protein}}/(I_{protein} + I_{Cu1\text{–protein}})$), was correlated with the concentration of free Cu(I) ions in the sample. In the case of titration of Cu_2Cox2 with DTT, we calculated from ESI-MS spectra the fractional occupancy of the two Cu(I)-binding sites ($Y = (2I_{Cu2Cox2} + I_{CuCox2})/2(I_{Cox2} + I_{Cu1Cox2} + I_{Cu2Cox2})$) and correlated this parameter with the concentration of free Cu(I) ions in the sample. Binding curves for all proteins, presented in Supplementary Figs 3b–13b, were nonlinearly fitted with a common hyperbolic equation, corresponding to a simple 1:1 binding equilibrium with the program Origin 6.1 (OriginLab Corporation). In all cases, a good fit was obtained and, therefore, there was no need to use more complicated binding schemes. The obtained apparent dissociation constants for Cu_1–protein and Cu_n–protein complexes, K_{Cu}, are in all cases equal to the concentration of free Cu(I) ions at 50% loading of the protein with Cu(I) ions; as such, these constants are comparable among different proteins. The Cu-binding affinity of MT-2 was determined from titration results of Cu_{10}MT-2 with DETC by correlating the fractional occupancy of Cu(I)-binding sites in MT-2 with the concentration of free Cu(I) ions. The fractional occupancy of Cu(I)-binding sites in MT-2 (Y) was calculated from ESI-MS spectra (considering that there are ten Cu(I)-binding sites in MT-2) by using the following equation:

$$Y = \sum_{0}^{10} nI_{Cu_nMT-2}/10 \times \sum_{0}^{10} I_{Cu_nMT-2} \quad (3)$$

where $I_{Cu_nMT\text{-}2}$ denotes the intensity of the Cu_nMT-2 peak in the ESI-MS spectra. The fractional occupancy of Cu(I)-binding sites in MT-2 was correlated with the concentration of free Cu(I) ions in the sample calculated using the apparent dissociation constant for DETC ($K_{Cu} = 13.8$ fM), determined in the current study. The obtained binding curve for MT-2, presented in Supplementary Fig. 14b, is sigmoidal and could not be fitted with a simple 1:1 binding equilibrium. The sigmoidal binding curve was fitted nonlinearly with the Hill equation (equation (4)) and linearly to the linear version of the Hill equation with the program Origin 6.1 (OriginLab Corporation).

$$Y = \frac{[Cu(I)]^n}{K_{Cu}^n + [Cu(I)]^n} \quad (4)$$

The nonlinear and linear fitting presented in Supplementary Fig. 14b yielded K_{Cu} values of 0.41 ± 0.02 and 0.40 ± 0.04 fM, and n values of 4.1 ± 0.7 and 3.3 ± 0.4, respectively. K_{Cu} is equal to the concentration of free Cu(I) ions at half saturation of MT-2 with Cu(I) ions, reflecting the apparent average affinity of MT-2 towards Cu(I) ions. A Hill coefficient larger than 1 indicates that positive cooperativity exists in the binding of Cu(I) ions to MT-2. Indeed, there are most probably two metal–thiolate clusters in Cu_{10}MT-2, composed of 4 and 6 Cu(I) ions (Supplementary Fig. 14a); however, both of them dissociate cooperatively in a very narrow region of free Cu(I) ions, which indicates that their apparent dissociation constants are very close and averaged to $K_{Cu} = 0.41 \pm 0.02$ fM. It should be noted that in Cu(I)-binding studies of metallothioneins, we used the thiol reagent DTT in the reaction medium, which is different from many earlier Cu(I)-titration studies of metallothioneins performed under anaerobic conditions with Cu(I)-acetonitrile complex, and where no cooperativity was observed[34].

The half-life of the metal extraction process in Cu_2Cox2 was determined by fitting of the experimental ESI-MS data in Supplementary Fig. 16 to a common first-order kinetics curve by using the Origin 6.1 program (OriginLab Corporation).

Preparation of mitochondrial fractions from rat liver and CcO assay. Mitochondrial fractions were prepared as previously described[35]. Briefly, rat liver was disrupted with scissors and suspended in isolation medium (300 mM sucrose, 10 mM HEPES and 0.2 mM EDTA, pH 7.2). Tissue was homogenized in a glass–Teflon homogenizer and incubated for 15 min with 2 mM trypsin. After incubation, trypsin inhibitor was added and homogenization was repeated. The homogenate was centrifuged at 1,250*g* for 10 min. The supernatant was centrifuged at 6,300*g* for 10 min to isolate mitochondria and the pellet was washed afterwards three times with isolation medium described above. Finally, the mitochondria pellet was suspended in 1.5 ml isolation medium and divided into 50-µl aliquots. The mitochondrial membrane was disrupted with Triton X-100 and the suspension was used for the CcO activity assay.

CcO activity towards reduced cytochrome *c* was performed by monitoring the decrease in absorbance at 550 nm due to reduced cytochrome *c*[36] on a Shimadzu UV-2401 PC spectrophotometer. Cytochrome *c* (Sigma) was reduced with 5 mM DTT and purified by SEC on a Superdex 75 column (elution with 50 mM HEPES buffer, pH 7.3) connected to an Äkta Purifier system. The reaction mixture contained 3 µM reduced cytochrome *c*, 1 µl of mitochondria suspension in 300 µl of 50 mM HEPES buffer, pH 7.3. Addition of sodium azide inhibited oxidation of cytochrome *c* with an inhibition constant of 69 ± 9 M, which is consistent with the literature[37], thus confirming the presence of active CcO in mitochondrial fractions. The effect of apo-MT-2 on activity of CcO was studied by adding different concentrations of apo-MT-2 to the mitochondrial fractions in the cuvette. After 2–30 min of incubation with apo-MT-2, 3 µM of reduced cytochrome *c* was added to the reaction mixture and the CcO activity was measured. Metal extraction experiments were performed with 2 mM DETC, which was added to the rat CcO fractions in 50 mM HEPES pH 7.3, 5 mM DTT and, after various incubation times, 50-µl aliquots were applied to 1 ml G25 desalting column, eluted with 50 mM HEPES buffer, pH 7.4. High molecular mass fractions were collected and analysed for CcO activity in the presence of 3 µM reduced cytochrome *c* and for copper content by ICP-MS (Agilent ICP-MS 7500a, Agilent Technologies). Results were compared with a control experiment, performed with CcO without addition of DETC. After incubation for 5 min with DETC, a 43% decrease in enzymatic activity and a 55% decrease in copper content were observed in the high molecular mass fraction containing CcO; no further decrease in enzymatic activity or copper content was observed for up to 60 min of incubation.

31. Krezel, A. & Maret, W. Thionein/metallothionein control Zn(II) availability and the activity of enzymes. *J. Biol. Inorg. Chem.* **13**, 401–409 (2008).
32. Hitomi, Y., Outten, C. E. & O'Halloran, T. V. Extreme zinc-binding thermodynamics of the metal sensor/regulator protein, ZntR. *J. Am. Chem. Soc.* **123**, 8614–8615 (2001).
33. Palumaa, P., Kangur, L., Voronova, A. & Sillard, R. Metal-binding mechanism of Cox17, a copper chaperone for cytochrome *c* oxidase. *Biochem. J.* **382**, 307–314 (2004).
34. Presta, A., Green, A. R., Zelazowski, A. & Stillman, M. J. Copper binding to rabbit liver metallothionein. Formation of a continuum of copper(I)-thiolate stoichiometric species. *Eur. J. Biochem.* **227**, 226–240 (1995).
35. Saks, V. A., Kupriyanov, V. V., Elizarova, G. V. & Jacobus, W. E. Studies of energy transport in heart cells. The importance of creatine kinase localization for the coupling of mitochondrial phosphorylcreatine production to oxidative phosphorylation. *J. Biol. Chem.* **255**, 755–763 (1980).
36. Leavesley, H. B., Prabhakaran, K., Borowitz, J. L. & Isom, G. E. Interaction of cyanide and nitric oxide with cytochrome *c* oxidase: implications for acute cyanide toxicity. *Toxicol. Sci.* **101**, 101–111 (2008).
37. Yonetani, T. & Ray, G. S. Kinetics of the aerobic oxidation of ferrocytochrome *c* by cytochrome *c* oxidase. *J. Biol. Chem.* **240**, 3392–3398 (1965).

SUPPLEMENTARY INFORMATION

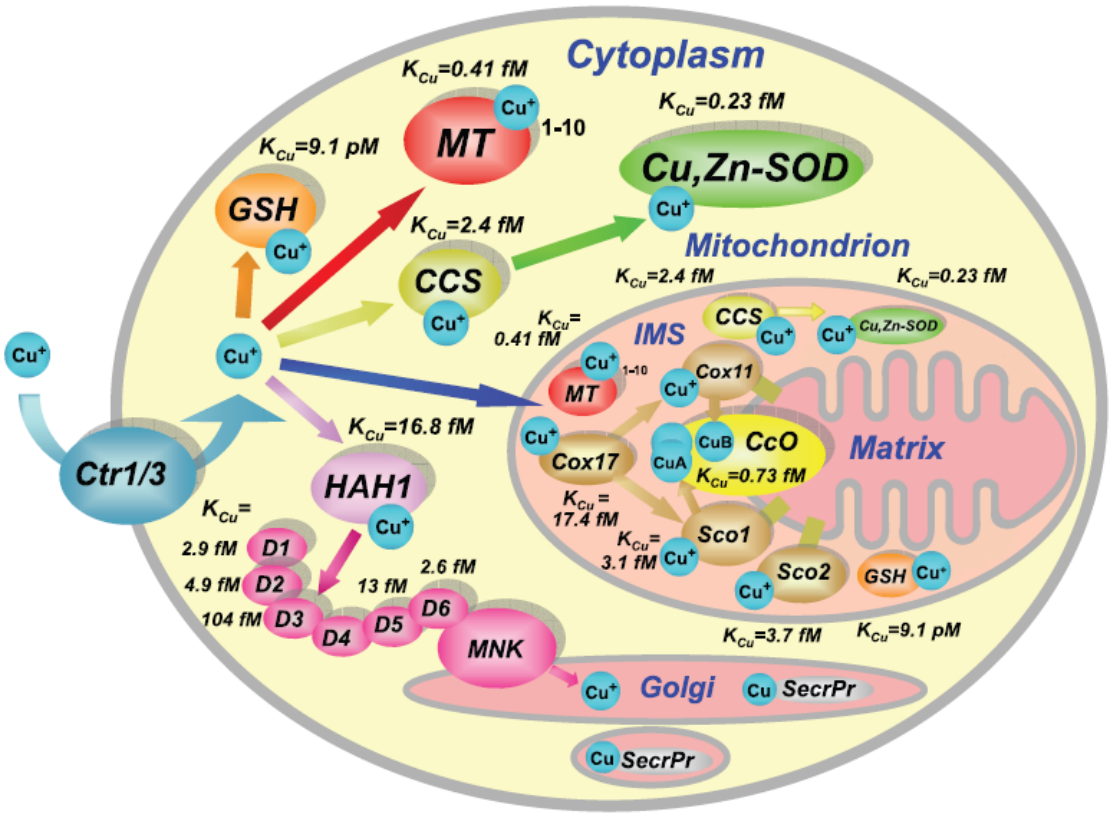

Figure S1. Cu(I)-binding proteins/ligands and copper trafficking pathways in an eukaryotic cell. Blue spheres - Cu ions; Ctr1/3 - copper influx transporters; CCS - copper chaperone for Cu,Zn-SOD1; HAH1 - copper chaperone for the Menkes protein (MNK); D1-D6 - Cu(I)-binding domains of MNK; MT - metallothionein; GSH - glutathione; Cox11, Cox17, Sco1, Sco2 - copper chaperones and co-chaperones of cytochrome *c* oxidase; CcO - cytochrome *c* oxidase. According to current knowledge, the copper ions are delivered from Cox17 to Sco1 and/or Sco2, and to Cox11 co-chaperones, which metallate the binuclear Cu_A site and the Cu_B site of CcO, respectively. SecPr - secreted copper proteins such as ceruloplasmin, lysyl oxidase, tyrosinase, and dopamine β-hydroxylase. Apparent Cu(I)-binding dissociation constants (K_{Cu}) measured in this work for Cu(I)-binding proteins and GSH are also reported.

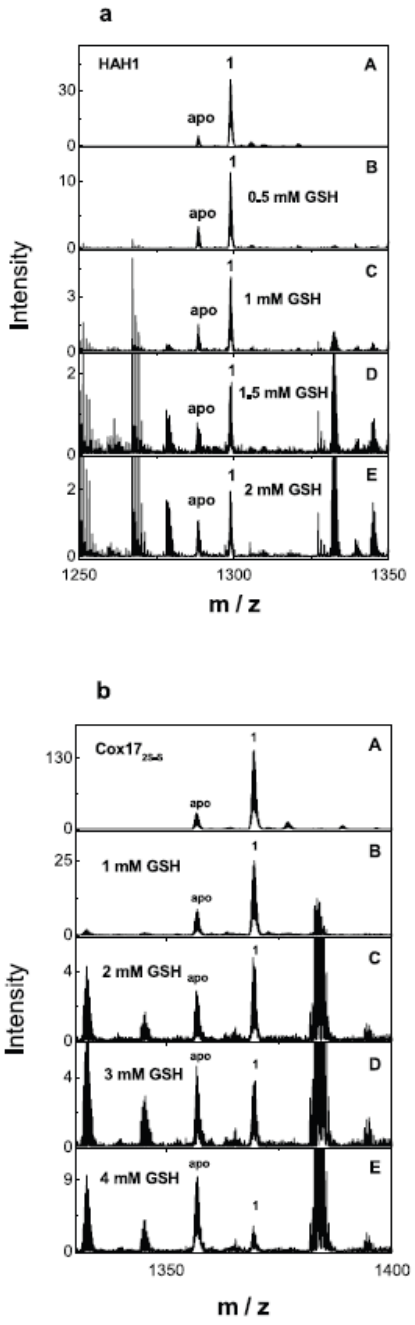

Figure S2. Influence of GSH on the metallation level of HAH1 and Cox17.
a - ESI-MS spectra of Cu_1HAH1 in the presence of 0.25 - 2 mM GSH; **b** - ESI-MS spectra of Cu_1Cox17_{2S-S} in the presence of 0.25 - 4 mM GSH. Conditions: HAH1 or $Cox17_{2S-S}$ 3 μM; 20 mM ammonium acetate, Cu(I)DTT 5 μM, pH 7.5; T = 25ºC. Ions with a charge state +5 ions are shown; numbers on the peaks denote the metal stoichiometry of the complex. Nonlabelled peaks originate from the GSH sample.

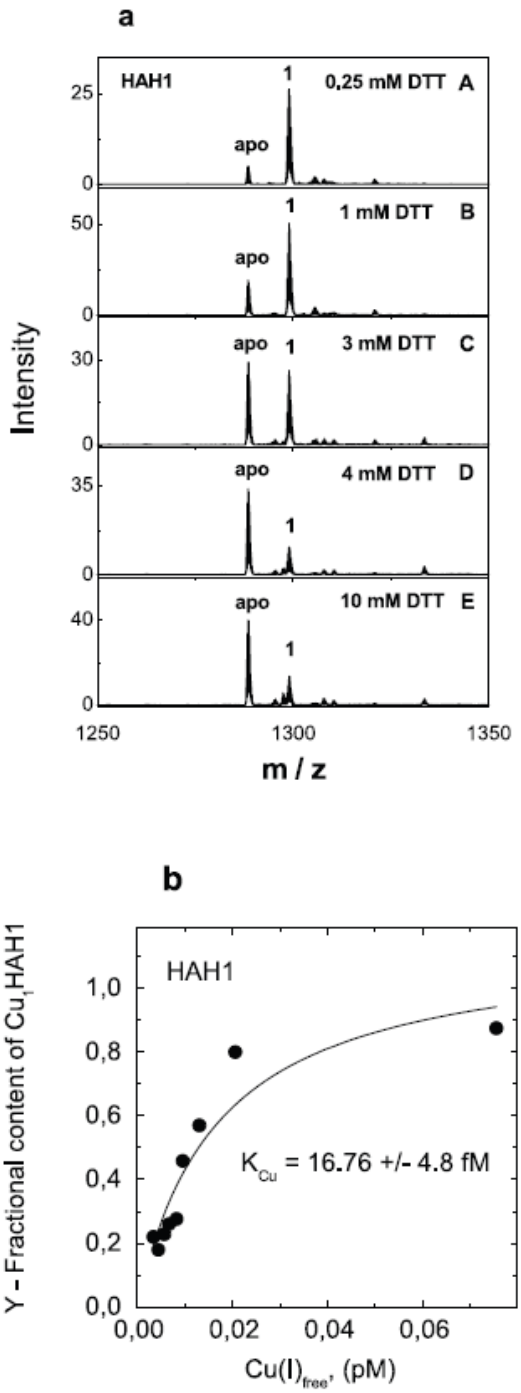

Figure S3. Determination of the apparent dissociation constant for Cu_1HAH1.
a - ESI-MS spectra of Cu_1HAH1 in the presence of 0.25 - 10 mM DTT. Conditions: HAH1 3 µM; 20 mM ammonium acetate, Cu(I)DTT 5 µM, pH 7.5; T = 25ºC. Ions with a charge state +5 are shown; numbers on the peaks denote the metal stoichiometry of the complex. **b -** Dependence of the fractional content of Cu_1HAH1 ($Y = I_{CuHAH1} / (I_{HAH1} + I_{CuHAH1})$) from the concentration of free Cu(I) ions in the metal competition experiment. Solid line shows the fitting curve with $K_{Cu} = 16.76 \times 10^{-15}$ M.

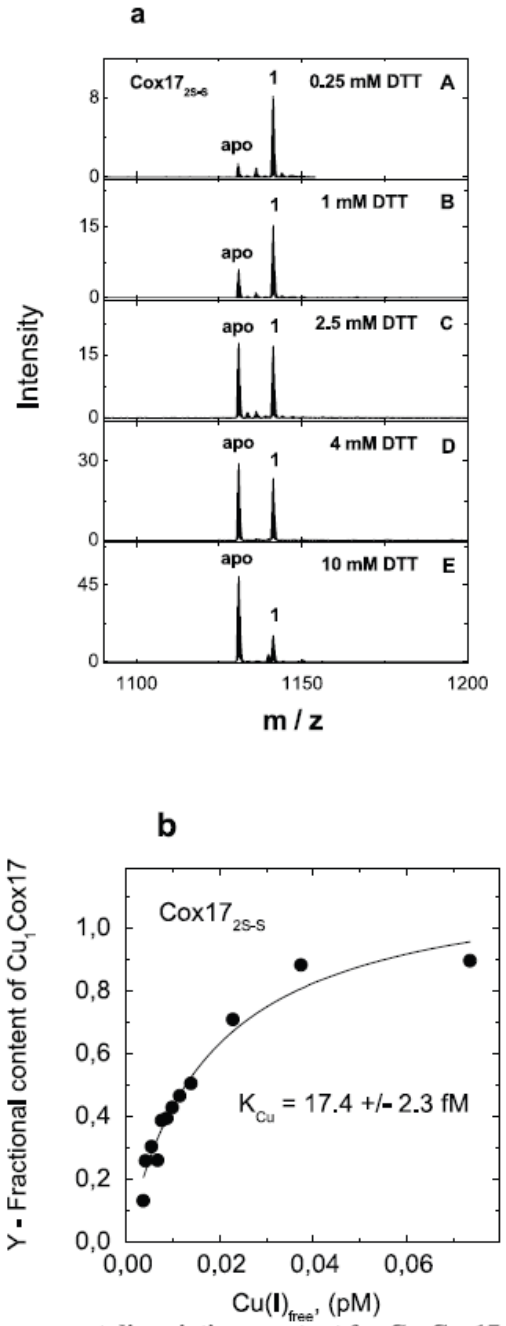

Figure S4. Determination of the apparent dissociation constant for Cu_1Cox17_{2S-S}.
a - ESI-MS spectra of Cu_1Cox17_{2S-S} in the presence of 0.25 - 10 mM DTT. Conditions: $Cox17_{2S-S}$ 3 μM; 20 mM ammonium acetate, Cu(I)DTT 5 μM, pH 7.5; T = 25°C. Ions with a charge state +5 are shown; numbers on the peaks denote the metal stoichiometry of the complex. **b -** Dependence of the fractional content of Cu_1HAH1 ($Y = I_{CuCox17} / (I_{Cox17} + I_{CuCox17})$) from the concentration of free Cu(I) ions in the metal competition experiment. Solid line shows the fitting curve with $K_{Cu} = 17.4 \times 10^{-15}$ M.

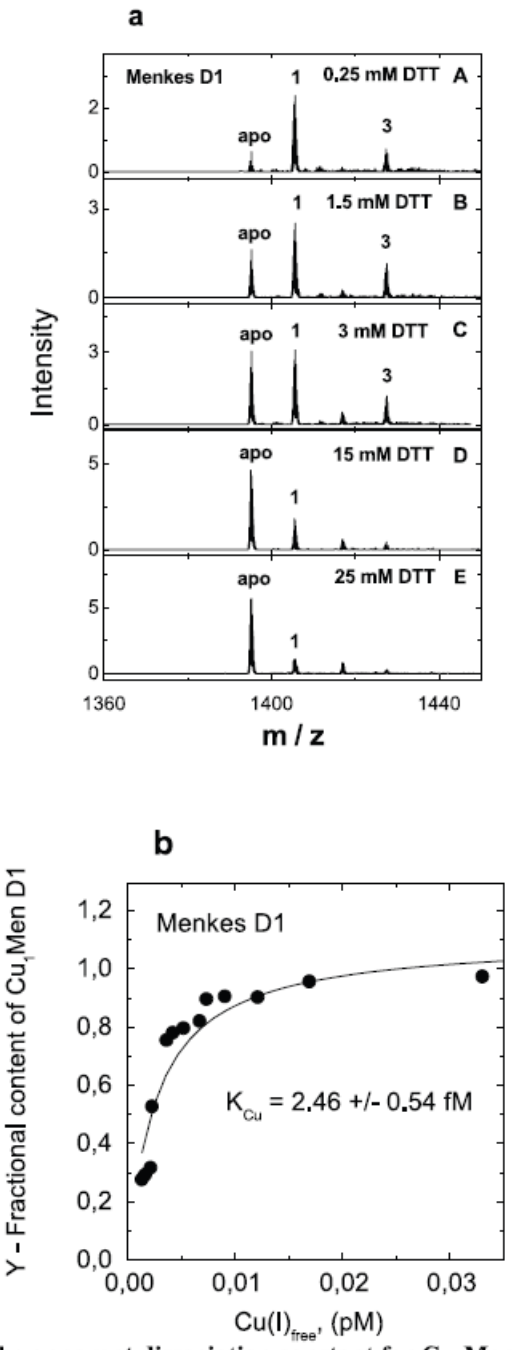

Figure S5. Determination of the apparent dissociation constant for Cu_1Menkes D1.
a - ESI-MS spectra of Cu_1Menkes D1 in the presence of 0.25 - 25 mM DTT. Conditions: Menkes D1 3 μM; 20 mM ammonium acetate, Cu(I)DTT 5 μM, pH 7.5; T = 25ºC. Ions with a charge state +5 and +6 are shown; numbers on the peaks denote the metal stoichiometry of the complex. **b -** Dependence of the fractional content of Cu_1Menkes D1 ($Y = I_{CuMenkes\ D1} / (I_{Menkes\ D1} + I_{CuMenkes\ D1})$) from the concentration of free Cu(I) ions in the metal competition experiment. Solid line shows the fitting curve with $K_{Cu} = 2.46 \pm 0.54$ M.

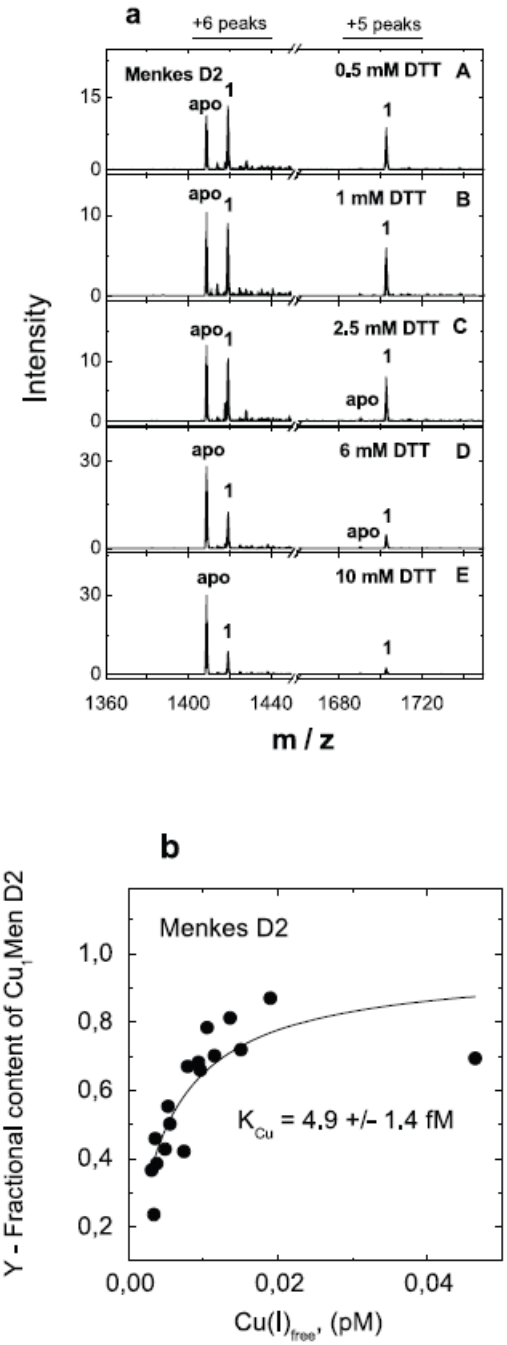

Figure S6. Determination of the apparent dissociation constant for Cu_1Menkes D2.
a - ESI-MS spectra of Cu_1Menkes D2 in the presence of 0.25 - 10 mM DTT. Conditions: Menkes D2 3 μM; 20 mM ammonium acetate, Cu(I)DTT 5 μM, pH 7.5; T = 25ºC. Ions with a charge state +5 and +6 are shown; numbers on the peaks denote the metal stoichiometry of the complex. **b -** Dependence of the fractional content of Cu_1Menkes D2 ($Y = I_{CuMenkes\ D2} / (I_{Menkes\ D2} + I_{CuMenkes\ D2})$) from the concentration of free Cu(I) ions in the metal competition experiment. Solid line shows the fitting curve with $K_{Cu} = 4.90 \times 10^{-15}$ M.

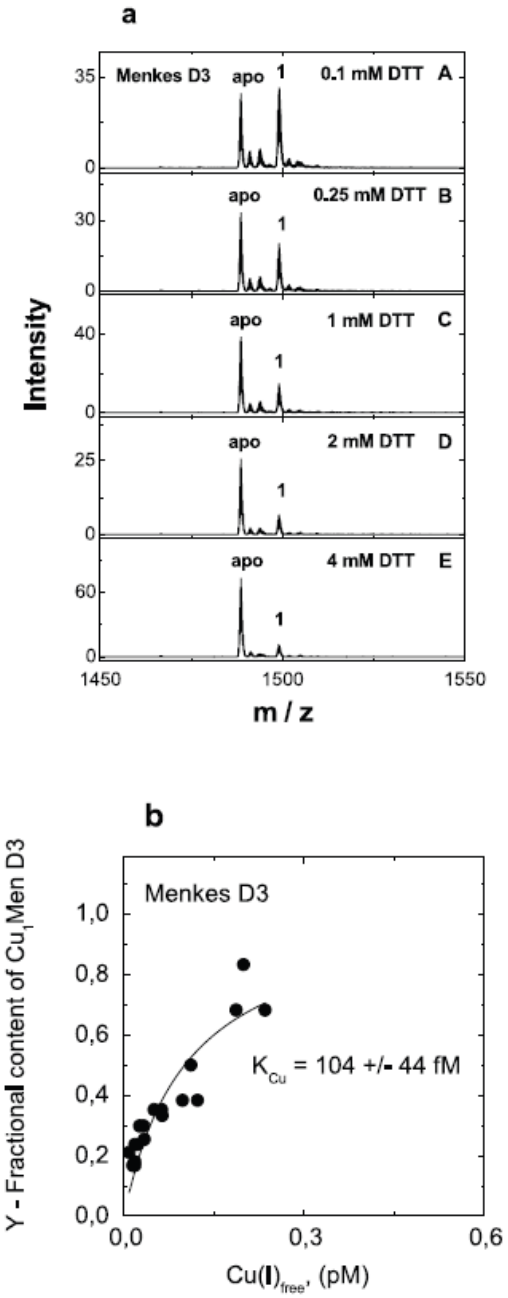

Figure S7. Determination of the apparent dissociation constant for Cu_1Menkes D3.
a - ESI-MS spectra of Cu_1Menkes D3 in the presence of 0.25 - 4 mM DTT. Conditions: Menkes D3 3 µM; 20 mM ammonium acetate, Cu(I)DTT 5 µM, pH 7.5; T = 25ºC. Ions with a charge state +5 are shown; numbers on the peaks denote the metal stoichiometry of the complex. **b -** Dependence of the fractional content of Cu_1Menkes D3 ($Y = I_{CuMenkes\ D3} / (I_{Menkes\ D3} + I_{CuMenkes\ D3})$) from the concentration of free Cu(I) ions in the metal competition experiment. Solid line shows the fitting curve with $K_{Cu} = 104 \times 10^{-15}$ M.

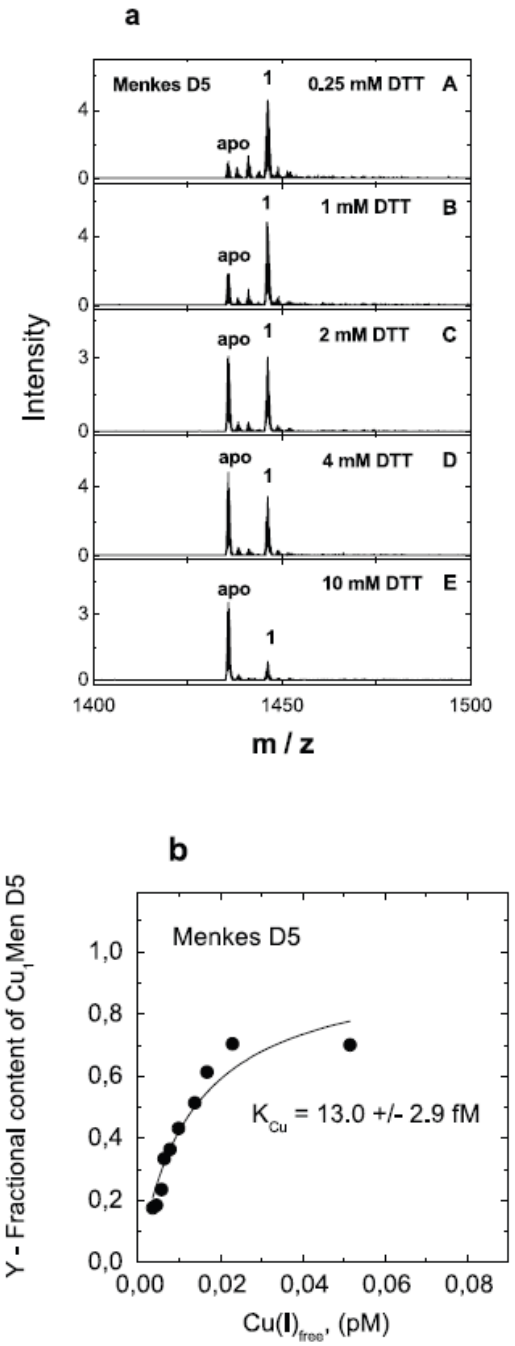

Figure S8. Determination of the apparent dissociation constant for Cu_IMenkes D5.
a - ESI-MS spectra of Cu_IMenkes D5 in the presence of 0.25 - 10 mM DTT. Conditions: Cu_IMenkes D5 3 μM; 20 mM ammonium acetate, Cu(I)DTT 5 μM, pH 7.5; T = 25ºC. Ions with a charge state +5 are shown; numbers on the peaks denote the metal stoichiometry of the complex. **b -** Dependence of the fractional content of Cu_IMenkes D5 ($Y = I_{CuMenkes\ D5} / (I_{Menkes\ D5} + I_{CuMenkes\ D5})$) from the concentration of free Cu(I) ions in the metal competition experiment. Solid line shows the fitting curve with $K_{Cu} = 13.0 \times 10^{-15}$ M.

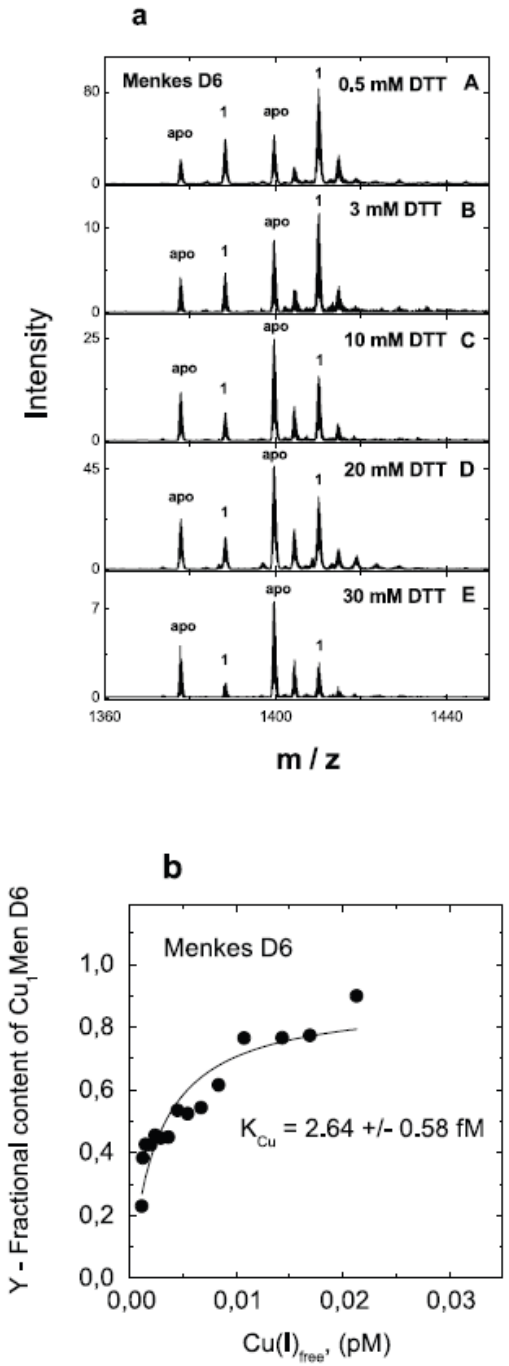

Figure S9. Determination of the apparent dissociation constant for Cu_1Menkes D6.
a - ESI-MS spectra of Cu_1Menkes D6 in the presence of 0.25 - 30 mM DTT. Conditions: Menkes D6 3 µM; 20 mM ammonium acetate, Cu(I)DTT 5 µM, pH 7.5; T = 25ºC. Ions with a charge state +5 are shown; numbers on the peaks denote the metal stoichiometry of the complex. **b -** Dependence of the fractional content of Cu_1Menkes D6 ($Y = I_{CuMenkes\ D6} / (I_{Menkes\ D6} + I_{CuMenkes\ D6})$) from the concentration of free Cu(I) ions in the metal competition experiment. Solid line shows the fitting curve with $K_{Cu} = 2.64 \times 10^{-15}$ M.

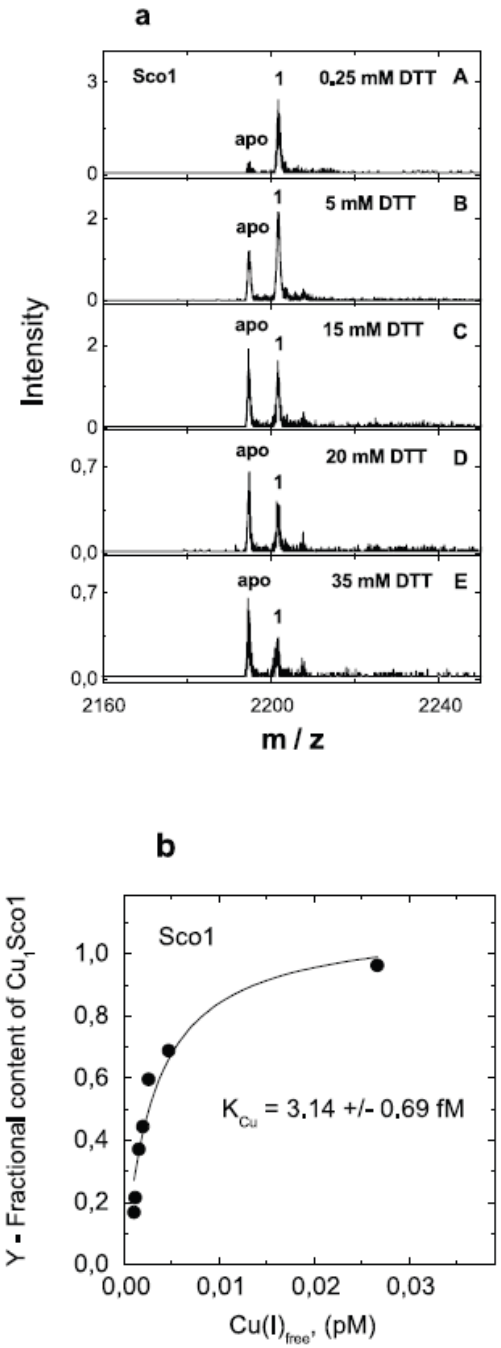

Figure S10. Determination of the apparent dissociation constant for Cu_1Sco1.
a - ESI-MS spectra of Cu_1Sco1 in the presence of 0.25 - 35 mM DTT. Conditions: Sco1 3 μM; 20 mM ammonium acetate, Cu(I)DTT 5 μM, pH 7.5; T = 25ºC. Ions with a charge state +5 are shown; numbers on the peaks denote the metal stoichiometry of the complex. **b** - Dependence of the fractional content of Cu_1Sco1 ($Y = I_{CuSco1} / (I_{Sco1} + I_{CuSco1})$) from the concentration of free Cu(I) ions in the metal competition experiment. Solid line shows the fitting curve with $K_{Cu} = 3.14 \times 10^{-15}$ M.

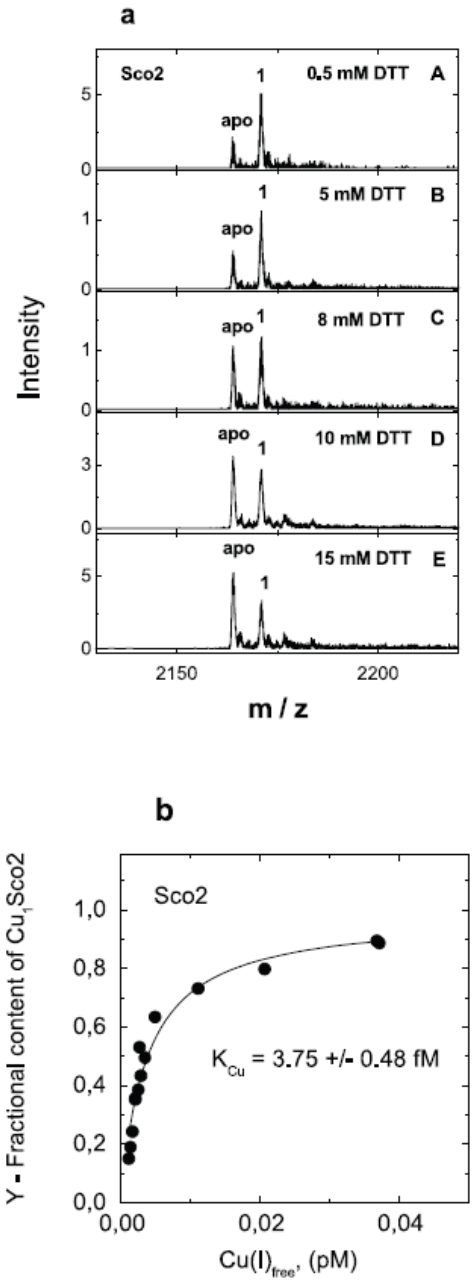

Figure S11. Determination of the apparent dissociation constant for Cu_1Sco2.
a - ESI-MS spectra of Cu_1Sco2 in the presence of 0.25 - 25 mM DTT. Conditions: Sco2 3 μM; 20 mM ammonium acetate, Cu (I)DTT 5 μM, pH 7.5; T = 25ºC. Ions with a charge state +5 are shown; numbers on the peaks denote the metal stoichiometry of the complex. **b -** Dependence of the fractional content of Cu_1Sco2 ($Y = I_{CuSco2} / (I_{Sco2} + I_{CuSco2})$) from the concentration of free Cu (I) ions in the metal competition experiment. Solid line shows the fitting curve with $K_{Cu} = 3.75 \times 10^{-15}$ M.

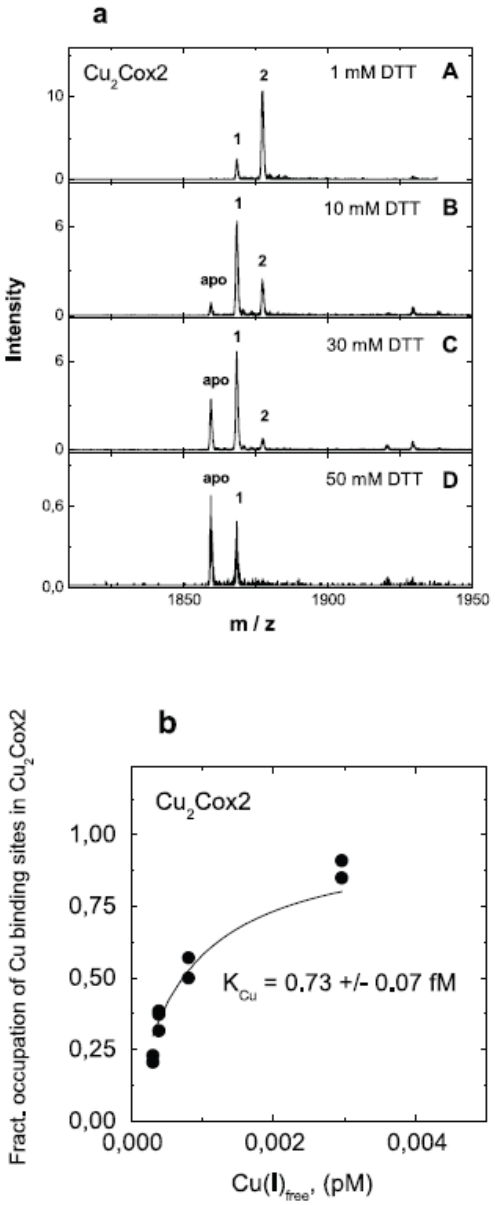

Figure S12. Determination of the apparent dissociation constant for Cu_2Cox2.
a - ESI-MS spectra of Cu_2Cox2 in the presence of 0.25 - 50 mM DTT. Conditions: Cox2 3 μM; 20 mM ammonium acetate, Cu(I)DTT 5 μM, pH 7.5; T = 25°C. Ions with a charge state +9 are shown; numbers on the peaks denote the metal stoichiometry of the complex. **b** - Fractional occupancy of Cu-binding sites in Cox2 ($Y = 2I_{Cu2Cox2} + I_{CuCox2} / 2(I_{Cox2} + I_{Cu1Cox2} + I_{Cu2Cox2})$) at different concentrations of free Cu(I) ions in the metal competition experiment. Solid line shows the fitting curve with $K_{Cu} = 0.73 \times 10^{-15}$ M.

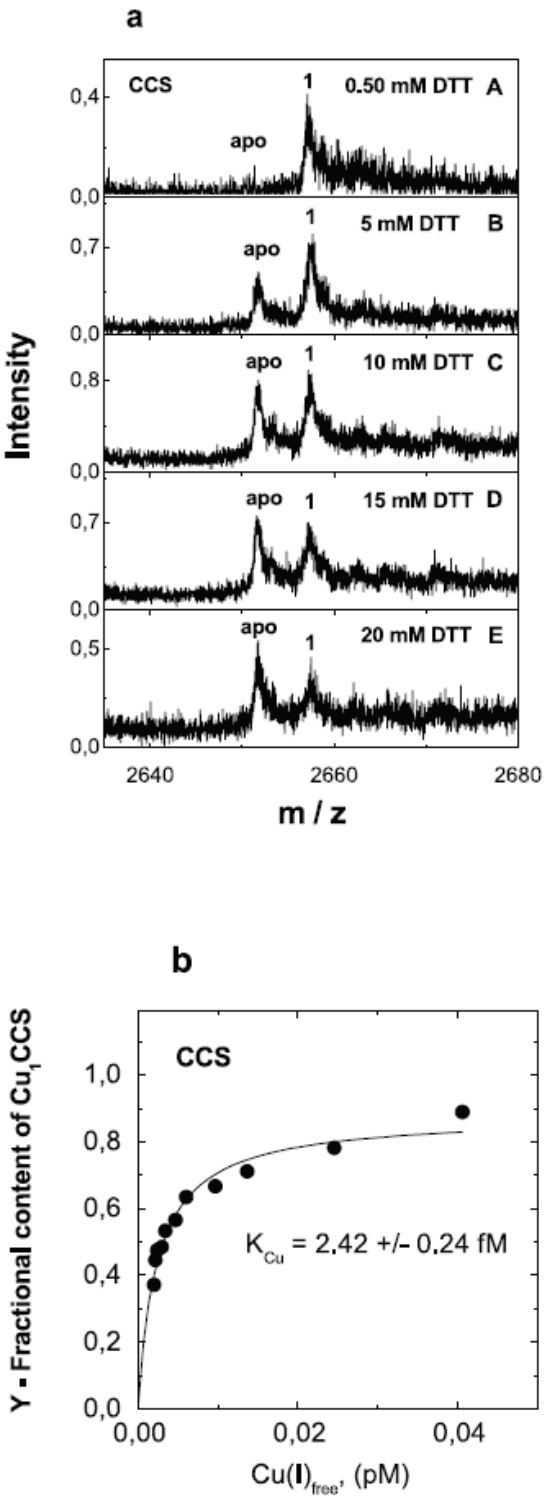

Figure S13. Determination of the apparent dissociation constant for Cu_1CCS1.
a – ESI-MS spectra of Cu_1CCS1 in the presence of 0.5-20 mM DTT. Conditions: CCS1 5 μM; 20 mM ammonium acetate, Cu(I)DTT 7 μM, pH 7.5; T = 25°C. Ions with a charge state +9 are shown; numbers on the peaks denote the metal stoichiometry of the complex. **b** - Dependence of the fractional content of Cu_1CCS1 ($Y = I_{Cu_1CCS1} / (I_{CCS1} + I_{Cu_1CCS1})$) from the concentration of free Cu(I) ions in the metal competition experiment. Solid line shows the fitting curve with $K_{Cu} = 2.42 \times 10^{-15}$ M.

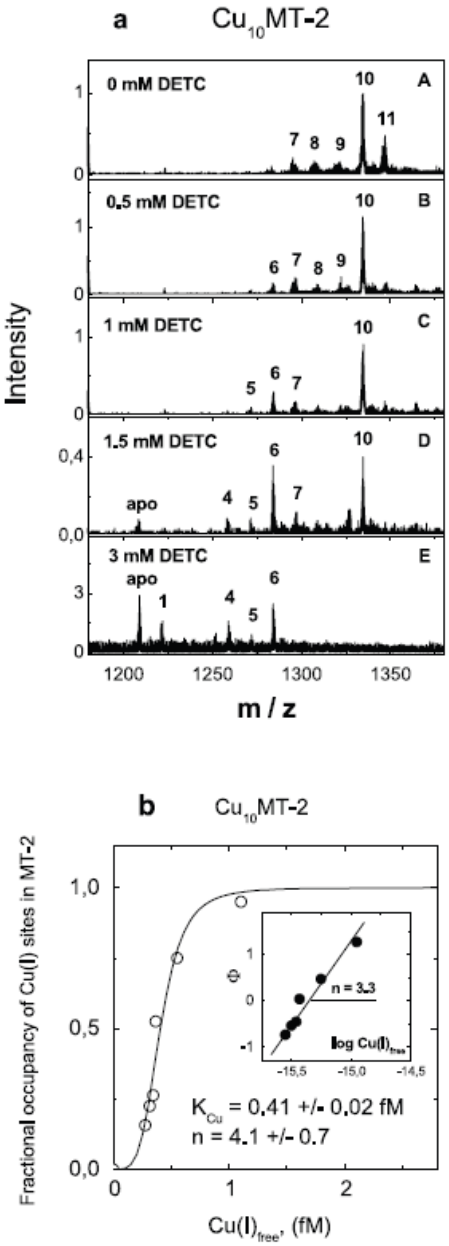

Figure S14. Determination of the apparent dissociation constant for Cu_nMT-2 in metal competition experiments with DETC. **a** - ESI-MS spectra of Cu_nMT-2 in the presence of 0 - 3 mM DETC. Conditions: MT-2 3.3 μM; 20 mM ammonium acetate, Cu(I)DTT 40 μM, DTT 10 mM, pH 7.5; T = 25ºC. Ions with a charge state +5 are shown; numbers on the peaks denote the metal stoichiometry of the complex. **b** - Fractional occupancy of Cu(I)-binding sites in MT-2 ($Y = (\Sigma\, n \times I_{CunMT\text{-}2} / 10 \times \Sigma\, I_{CunMT\text{-}2})$) (n=0-10) at different concentrations of free Cu(I) ions in a metal competition experiment. The solid line shows the fitting curve with sigmoidal Hill equation $K_{Cu} = 0.41 \times 10^{-15}$ M, n=4.1 (see Materials and Methods section). The inset shows the same results in Hill coordinates [$\Phi = Y/(1-Y)$], the solid line presents the linear fit of the data.

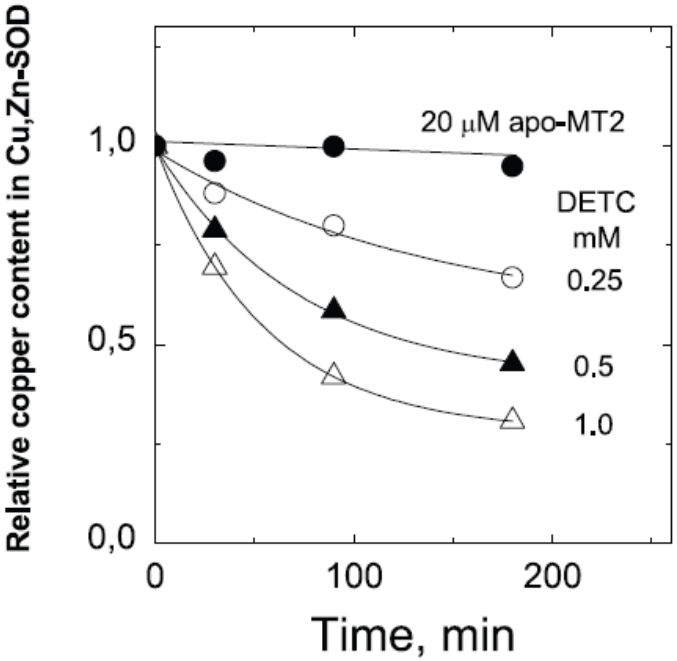

Figure S15. Kinetics of copper extraction from Cu,Zn-SOD1. Conditions: Cu,Zn-SOD1 10 μM; 20 mM ammonium acetate pH 7.5, 1 mM DTT, T = 25ºC. Copper extraction from Cu,Zn-SOD1 was perfomed by adding 0.25 mM (-○-), 0.5 mM (-▲-), 1.0 mM (-Δ-) DETC and 20 μM apo-MT-2 (-●-).

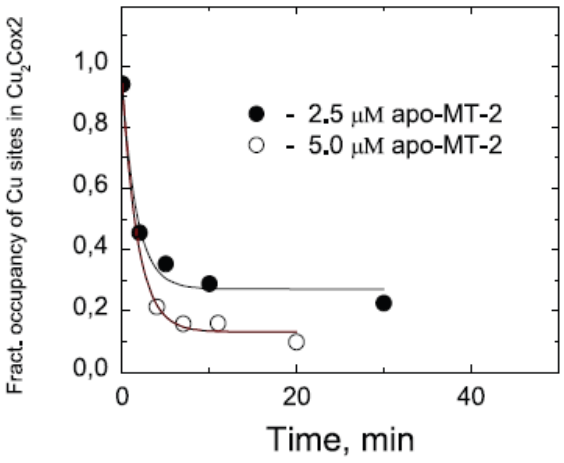

Figure S16. Kinetics of demetallation of Cu_2Cox2 by apoMT-2.
Conditions: Cox2 3 μM; 20 mM ammonium acetate, Cu(I)DTT 5 μM, pH 7.5; T = 25ºC.

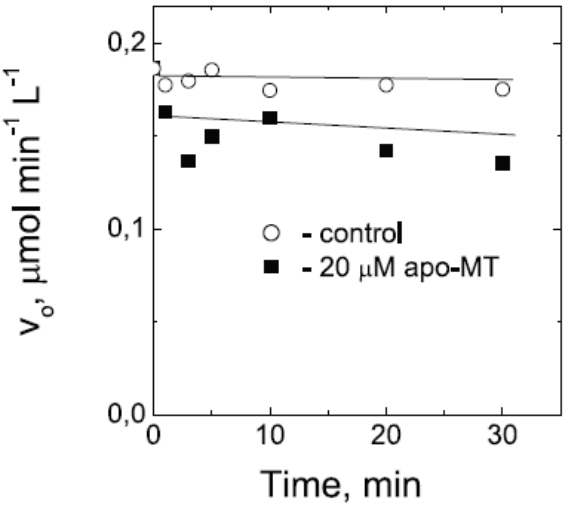

Figure S17. Influence of apo-MT-2 on the activity of rat cytochrome c oxidase.
Reaction conditions: ○ - no apo-MT-2; ■ - 20 mM apo-MT-2 in medium containing disrupted mitochondrial fractions in 50 mM Hepes buffer pH 7.3, 25°C. After specified incubation time the reaction was initiated by addition of 3 μM reduced cytochrome c (ε_{550} = 2.84 x 10^5 $M^{-1}cm^{-1}$) and initial velocity of substrate oxidation was measured spectrophotometrically by decrease of optical density at 550 nm.

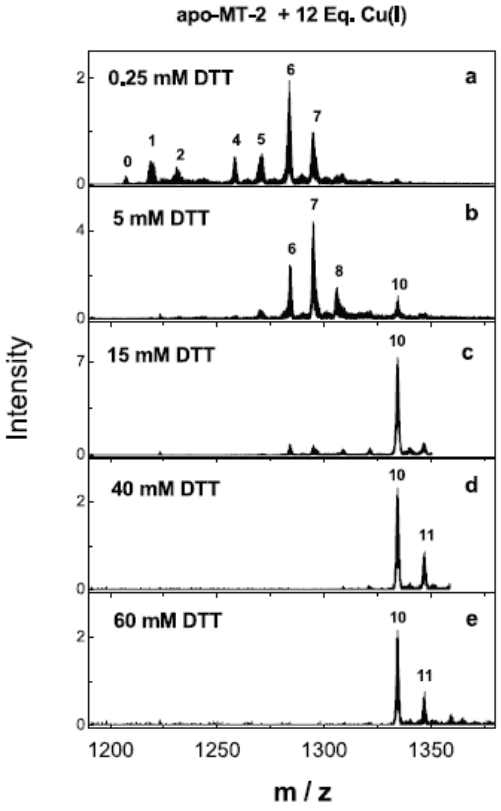

Figure S18. Influence of DTT on metallation level of Cu_nMT-2 followed by ESI-MS.
Conditions: apoMT-2 3.3 μM; 20 mM ammonium acetate, 40 μM Cu(I)DTT, pH 7.5, T = 25°C. (a) 0.25 mM DTT; (b) 5 mM DTT; (c) 15 mM DTT; (d) 40 mM DTT, (e) 60 mM DTT. Ions with a charge state +5 are shown; numbers on the peaks denote the metal stoichiometry of the complex.

"HCCS-SOD1 INTERACTIONS: IMPLICATIONS FOR THE METAL TRANSFER PROCESS"

Lucia Banci[1], Ivano Bertini[1], Francesca Cantini[1], Tatiana Kozyreva[1], Chiara Massagni[1], Kairit Zovo[2] and Peep Palumaa[2]

[1] Magnetic Resonance Center CERM and Department of Chemistry, University of Florence, Via Luigi Sacconi 6, 50019, Sesto Fiorentino, Florence, Italy.

[2] Department of Gene Technology, Tallinn University of Technology, Akadeemia tee 15, 12618 Tallinn, Estonia.

In preparation

INTRODUCTION

SOD1 is a well known cuproenzyme implicated in the efficient catalityc detoxification of reactive superoxide anion, a normal product of cellular respiration, to molecular oxygen and hydrogen peroxide [$2O^-_2 + 2H^+ \rightarrow H_2O_2 + O_2$].[131] In mammalians SOD1 is ubiquitously expressed in all tissues and whithin cells it is basically localized in the cytosol, although small amounts are found also in the nucleous, peroxisomes and IMS of mitochondria.[132,133,134,135,136] Most structurally characterized forms of eukaryotic SOD1 are remarkably stable homodimer, retaining enzymatic activity at elevated temperatures and in the presence of denaturating agents.[137,138] Each subunit of the mature protein folds as an eight-stranded Greek-key β-barrel with, one Zn and one Cu ion. The highly conserved disulfide bridge between Cys57 and Cys146 confers stability to the protein fold and plays an important role in orientation of the molecule for the superoxide anion uptake.[139,140] At micromolar concentrations the apoSOD1 homodimer dissociates into free monomers upon reduction of the Cys57-Cys146 disulphide bond.[138,141,142] The disulfide breakage results indeed in an enhanced confomrational flexibility of the zinc coordinating loop IV which leads to a weakening of the interactions across the dimer interface.[143] Upon metals binding, the disulphide-depleted protein restores its ability to dimerize.[141,142,138] In the active protein the Cu(II) ion is coordinated by four histidines (His46, 48, 63 and 120), forming a distorted square plane, and interacts with a water molecule. One of the histidines, His 63, is also a ligand of the Zn^{2+} ion which completes its coordination sphere with three other amino acid residues (His71, His80, and Asp83) in a distorted tetrahedral arrangement. Binding of the Zn^{2+} ion is not essential for the dismutation reaction, but confers high protein stability to SOD1.[144] The copper ion is in the catalytic center.

While copper and zinc incorporation into the apo-SOD1 polypeptide can be achieved *in vitro* by addition of the corresponding metal salts[145], the process is more complex in the cell. The copper chaperone for superoxide dismutase, CCS, was proposed to be implicated in the copper delivery to SOD in 1997 by the group of Culotta, observing the effect on yeast mutants lacking the copper chaperone for superoxide dismutase.[146] CCS proteins have been identified in various species including humans, rodents, insects, and plants. While CCS is 15- to 30-fold and 5-fold less abundant than SOD1 in mammalian [147] and yeast cells[148] respectively, the cellular distribution and expression of CCS appear to parallel those of SOD1. It has also been found that post-translational modifications of apo-SOD1 by CCS requires

oxygen.[149] In vitro experiments have shown that CCS can activate apo-SOD1 under aerobic conditions but not in the absence of oxygen.[149]

hCCS is a dimeric protein where each monomer is constituted by three distinct polypeptide domains. The N-terminal domain 1 (~8kDa) harbours the MXCXXC metal binding motif typical for the Atx-like family metallochaperones, but it is not essential for the SOD1 activation under normal conditions and only seems necessary for copper aquiring under extreme copper limit conditions.[150] Domain 2 exhibits 47% sequence identity and adopts a similar tertiary fold with it's target enzyme SOD1. It has been postulated that this domain plays a critical role in target recognition prior copper transfer.[151,150,152] While no metal binding sites are present in yeast CCS Domain II, all of the SOD1 zinc binding ligands are conserved in the human protein. In fact, an equimolar amount of zinc ion is bound in human CCS Domain II when overexpressed in *E. Coli.*[153] Zinc binding is essential to human CCS function possibly because it contributes to protein stabilization.[154] Three of the four histidine residues present in the SOD1 copper binding site are also conserved in Domain II of human CCS, with the fourth histidine replaced by an aspartate. The copper ion is not bound at this site, and SOD1 activation by CCS is still observed after mutations of these His residues to Ala.[150] Domain 3 is a short polypeptide tail (30-40 aminoacids) with disordered secondary structure, that was proposed to be essential to the CCS function.[150] It is sufficient alone to bind Cu^{+} ions. However, extensive EXAFS experiments have recently led to the proposal that human CCS can form two distinct clusters with different stoichiometry: a polynuclear Cu_4S_6 cluster involving extra Cys residues from Domain II and a dinuclear Cu_2S_4 cluster when these extra Cys residues are unavailable.[155,156,157,158] Futhermore the experiments with the tomato CCS support the fact of the simultaneous involvement of both domains in Cu binding.[159] But the copper coordination in the full length hCCS protein still remains controversial.

The mechanism of SOD1 activation as a main subject has been tackled in the numerous reviews.[138,160,161,162] Given the similarity of SOD1 and CCS dimer interfaces, a monomeric CCS molecule has been proposed to interact with a monomeric SOD1 molecule through its SOD1-like Domain II, thus mimicking SOD1 dimerization. Based on the high dimer stability of either SOD1 (K_d, 1×10^{-10} M^{-1})[163] or CCS (K_d, 3.0×10^{-6} M^{-1} in yeast) the hetero-tetramer model, in which both proteins do not need to dissociate into monomers, has been proposed.[164] However, the heterodimerization model supported by crystalografical data has endured lately upon the heterotetramer model.[165] According to the first model, the initial step of SOD1 activation is the incorporation of Zn^{2+} ion into the disulfide-reduced protein,

since it is expected, that this could prevent the aggregation of the immature apo protein and future re-reduction of the disulfide bridge.[143] Zn^{2+} ion would thus serve a structural role in organizing the monomeric SOD1 polypeptide to a state suitable for reaction with Cu-CCS[144,143]

Futher, the reduced E,ZnSOD1SH forms the heterodimeric complex with CCS, as far as reduced disulfide favours the monomeric state of the protein.[144] Complex formation in the presence of oxigen permit copper transfer and intermolecular disulfide linkage between two proteins.[144] The subsequent conformational changes induce isomerisation of the intermolecular disulfide into intramolecular disulfide within SOD1 molecule and promote the dissociation of the docked complex to the separate proteins.

This work contributes to the understanding of the molecular mechanism of target recognition and copper transfer process between the hCCS and it's physiological patner protein SOD1 in order to shed some light on the post-translational mechanism of the SOD1 activation process assisted by it's coppper chaperone proten. To elucidate this mechanism we executed NMR titrations of apo- and E,ZnSOD1 with the disulphide bond oxidized and reduced, with hCCS protein and investigated the thermodynamical and kinetical basis of copper transfer from hCCS to SOD1 by ESI-MS spectrometry.

To avoid interference effect arising from Cys6 and Cys 111 in this study we used the thermostable mutant of hSOD1AS (C6A, C111S), which is structurally and functionally equivalent to the wild type protein.[166,167,168]

EXPERIMENTAL PROCEDURES

Protein expression and purification-The hCCS gene was amplified by PCR, cloned into the Gateway pDONR 221 Entry vector (Invitrogen), and subcloned into the pTH27 Destination vector by a Gateway LR reaction to generate an N-terminal, His fused protein.The truncated forms of hCCS: D1; D1,2; D2; D2,3 were cloned using a pENTR/TEV/D-TOPO version of Gateway technology. They were expressed as MBP-D1; GB1-D2; Trx-D1,2; GB1-D2,3 fusions. The hCCS were expressed in *Escherichia coli* BL21(DE3) Codon Plus RIPL cells (Stratagene), BL21(DE3)C41 pRosetta (Stratagen) and Origami pLysS (Novagen) for the full length protein and truncated constructs of the protein respectively. The cells were grown in LB (for mass experiments) and isotopically labeled minimal media [$(^{15}NH_4)_2SO_4$ and/or $^{13}C_6H_{12}O_6$] (for NMR experiments). Protein expression was induced with 0.7 mM isopropyl β-D-thiogalactopyranoside for 16 h. $ZnSO_4$ was added in the culture to a final

concentration of 1 mM. Purification was performed by using a HiTrap chelating HP column (Amersham Pharmacia Biosciences) charged with Ni(II). The His tag was cleaved with AcTEV. The digested protein was concentrated by ultrafiltration and loaded in a 16/60 Superdex 75 chromatographic column (Amersham Biosciences) to separate CCS from the N-terminal His domain. The fractions showing a single component by SDS/PAGE were collected, and the protein concentration was measured using the Bradford protein assay. To investigate the aggregation state of CCS, 0.4-1.0 mM (100 μL) protein samples were run on a Superdex 75 HR-10/30 size-exclusion column on an Äkta-FPLC system (GE Healthcare, Giles, United Kingdom) connected to a multiangle light scattering analyzer (DAWN-EOS, Wyatt Technologies, Santa Barbara, CA) coupled with quasi-elastic lightscattering detectors. The metal content was determined by inductively coupled plasma MS. The samples were analyzed with ICP-AES Varian 720-ES supplied with a CETAC 5000AT+ supersonic pulverizer.

Human asSOD1 (hasSOD1) was expressed in the *Escherichia coli* TOPP1 (Stratagene) cells. The enzymes were secreted, after induction with 0.5 mM isopropyl β-D-thiogalactopyranoside, for 16h. Cells were ruptured by osmotic shock and the protein purified to homogeneity by anion-exchange chromatography on DEAE-Sepharose CL-6R (Amersham Pharmacia Biosciences). The apo-protein was obtained by dialysis against 10 mM EDTA in 50 mM sodium acetate pH 3.8. The chelating agent was removed by extensive dialysis against 100 mM NaCl in the same buffer and then against acetate buffer alone, gradually increasing the pH from 3.8 to 5.5. The metalated derivatives of the protein were obtained through addition of a CoCl solution. Metal uptake was followed spectrophotoinetrically with subsequnt remetalation of the protein by addition of a stoichioinetric amount of ZnSO4 or/and [Cu(I)(CH3CN)4]PF6 solution. The reduction of disulfide bridge and preparation of fully reduced proteins apo-hasSOD1SH-SH and E,Zn-hasSOD1SH-SH was accomplished by addition of 200mM dithiothreitol under a nitrogen atmosphere in an anaerobic chamber. The NMR samples of the E,Zn-hasSOD1SH-SH were in 100 mM sodium phosphate buffer, pH 6, 90% H2O/10% D2O. The final protein concentration ranges between 0,3 and 1 mM. 0,5 ml of sample was loaded into high quality NMR tubes that were capped with latex serum caps in the glovebox.

Interaction of hCCS with copper- hCCS full length and truncated forms D1, D2,3 were reduced with 2 mM DTT, which was then removed in an anaerobic chamber through PD-10

desalting column. Titrations of reduced proteins with copper were performed by additions of Cu(I), added as $Cu(I)(CH_3CN)_4$ PF_6 up to a metal:protein ratio of 2:1.

Reconstitution of CCS proteins with Cu(I) ions forESI-MS. Prior to metal reconstitution, all hCCS proteins were reduced by addition of 2 mM DTT and purified by SEC on a Superdex 75 10/300 column (GE Healthcare, Giles, United Kingdom) connected to a Äkta Purifier system (GE Healthcare, Giles, United Kingdom) by using 20 mM ammonium acetate pH 7.5 as the elution buffer. Apo forms of copper proteins, were reconstituted with slight excess of Cu(I)-DTT complex in the presence of excess DTT. Specifically, by the addition of 15 μM Cu(I)DTT complex to 10 μM apo-protein samples in 20 mM ammonium acetate, pH 7.5 and containing 0.25 mM DTT, formation of the monometallic Cu(I)-protein form was observed for all proteins, with a small amount of the apo-protein form still present as detected by ESI-MS spectra. CCS exposed in ESI-MS in addition to broad peaks of dimers also monomer peaks, which were formed in electrospray ionization process. It was possible to resolve peaks of metallated CCS monomers, which were taken into account in determination of Cu(I)-binding affinity of Cu1Zn1CCS in metal competition experiments. The Cu(I)DTT complex was prepared by dissolving Cu(II)acetate at 1.3 mM concentration in argon-saturated 20 mM ammonium acetate, pH 7.5, containing 10 mM DTT.

Determination of metal-binding equilibria in the presence of DTT. In a standard experiment, increasing concentrations of DTT were added to the metallated proteins. Samples were then incubated for 2 min, and finally analysed by ESI-MS as described below. DTT is a nonionic compound and thus has only a slight influence on the ionization efficiency of proteins in the ESI-MS process, enabling detection of protein peaks even when DTT is present at 50mM concentration.

ESI-MS measurements. 10 μM samples of proteins or their Cu(I) complexes in 20mM ammonium acetate pH 7.5 containing various concentrations of DTT were injected into the electrospray ion source of a QSTAR Elite ESI-Q-TOF MS instrument (Applied Biosystems, Foster City, USA) by a syringe pump at 7 μl/min and ESI-MS spectra were recorded during for 5 min in the m/z region from 500-5000 Da with the following instrument parameters: ion spray voltage 5500 V; source gas 55L/min; curtain gas 20 L/min; declustering potential 60V; focusing potential 320 V; detector voltage 2550V. Thanks to the original settting of the aerosol current over the orifice hole and retrograde curtain gas flow in the ESI chamber of the QSTAR Elite QTOF MS/MS instrument, DTT did not contaminate or block the orifice hole

during experiments at high DTT concentrations. Determination of dissociation constants for Cu(I)-ligand complexes.

Calculation of dissociation constants for Cu-protein complexes. Apparent dissociation constants (K_{Cu}) for the Cu1-protein complexes were determined using DTT as a competing metal-binding ligand and calculated according to the following simplified reaction scheme, already introduced in previous studies[169,170]:

$$Cu_1Protein \xleftrightarrow{K_{Cu}} Protein + Cu^+$$

$$Cu_1DTT \xleftrightarrow{K_D} DTT + Cu^+$$

where K_D is the conditional dissociation constant for the Cu(I)-DTT complex, which at pH = 7.4, I = 0.1, T = 25° C is equal to 7.94×10-12 M 16. K_{Cu} was calculated in two steps: first, the concentrations of free Cu(I) ions in the presence of various concentrations of DTT were calculated by using the K_D value for the Cu(I)-DTT complex. Secondly, the fractional content of Cu1-protein species (Y), calculated from the intensities of apoprotein and Cu(I)1-protein peaks in ESI-MS spectra ($Y = I_{Cu1\text{-}protein} / (I_{Protein} + I_{Cu1\text{-}protein})$), was correlated with the concentration of free Cu(I) ions in the sample, were non-linearly fitted with a common hyperbolic equation, corresponding to a simple 1:1 binding equilibrium with the program "Origin 6.1" (OriginLab Corporation, USA). In all cases, a good fit was obtained and, therefore, there is no need to use more complicated binding schemes. The obtained apparent dissociation constants for Cu1Protein and Cu_nProtein complexes, K_{Cu}, are in all cases equal to the concentration of free Cu(I) ions at 50% loading of the protein with Cu(I) ions and as such these constants are comparable among different proteins. In all reactions the equilibrium between the apo- and copper-loaded forms of the hCCS proteins was reached within the minimal mesurement time of the ESI-MS spectrometer, order minutes.

*Calculation of dissociation constants for Zn-protein complexe*s- The hCCS D1 was reconstituted with the slight excess of Zn(II) in the presence of DDT as a competing metal-binding ligand and mainly the peaks of ZnD1 were observed in ESI-MS spectra. The increase of the DTT concentration resulted in decrease of the Zn-bound D1 peak and increase of the apo-protein form, indicating that millimolar concentration of DTT competes with protein for binding of Zn(II) ions. The dissociation constant for Zn(II)-DTT complex used in calculations is equal $1{,}25*10^{-7}$M (pH 7,5; T=25^0C, I=0,1). The calculations were performed according to the scheme discribed above for the Cu-protein complexes.

NMR experiments- NMR spectra were acquired using Bruker Avance 900, 800, 700, 600 and 500 spectrometers operating at proton nominal frequencies of 899.20, 800.13, 700.13, 600.13, and 500.13 MHz, respectively. All used triple-resonance (TXI 5-mm) probes were equipped with pulsed-field gradients along the z-axis. The 900, 800, 700 and 500 MHz spectrometers were equipped with a triple-resonance cryoprobe. All 2D and 3D spectra were collected at 298K and 310K forhCCS proteins, processed using the TOPSPIN software package.

hCCS - asSOD1 interactions- Titrations of asSOD1 with hCCS proteins were performed as follow: solutions at different concentrations of reduced or oxidized, unlabelled or ^{15}N labeled E,E-asSOD1 or E,Zn-asSOD1, obtained as described above, were prepared in 100mM phosphate and 100mM NaCl buffer at pH 6. Similarly, solutions at different concentrations of unlabeled or ^{15}N labeled reduced hCCS (full length or truncated form) were prepared in the same buffer as described previously. Additions of aliquots from the solution of reduced, unlabelled hCCS to the solution of reduced (or oxidized) ^{15}N labeled E,E-asSOD1 (or E,ZnSOD1) were performed and ^{1}H-^{15}N-HSQC spectra acquired at 298K for each addition. The other titration was performed by additions of aliquots from the solution of unlabelled E,E-asSOD1 (or E,ZnSOD1) to the solution of ^{15}N labeled reduced hCCS and ^{1}H-^{15}N-HSQC spectra acquired at 310K for each addition.

RESULTS AND DISCUSSION

Protein expression

In addition to the full length hCCS we have produced various constructs of the hCCS and characterized them in terms of their metal binding ability, thermodynamics of their metallation as well as their behavior in metal transfer to hSOD1. Thus domain 1, domain 2, domain1,2 and domain 2,3 (here after D1; D2; D1,2; D2,3) have been expressed in *E.coli* to a yield of about 10mg/L in minimum medium. In the analytical gel filtration and light scattering the aggregation state of the both copper bound and copper depleted form of the full length protein appears to be a dimer. The final pure protein was isolated with one equivalent of zinc per monomeric protein. Copper ions were only present in a range of 10-20% with respect to monomeric protein concentration. The isolated D2, D1,2 and D2,3 proteins in the MALDI spectrum represented apparent molecular massses of 33,1; 54,7; 41,8kDa corresponding to the

expected values of the dimeric species and they also contained 1eq of Zn per monomer. The D1 monomeric polypeptide showed the molecular mass of 9,3kDa.

The D1 and D2 are well folded proteins as monitored by the dispersion of the amide signals. The full length hCCS and the D2,3 construct show, together with well dispersed amide signals, also a number of signals clustered in the typical spectral region of unstructured proteins. The latter peaks mainly correspond to the D3 domain which is a short polypeptide without any tendency to form a secondary structure. Moreover the D1 and D2 are structurally independent each other, as their ^{15}N HSQC spectra.

Metal binding properties of hCCS

When the various constructs are titrated with Cu(I) ion, different behavior have been observed. Addition of Cu(I) to the D1 construct leads to the formation of the copper bound derivative. When this process is followed by NMR through ^{15}N HSQC spectra on ^{15}N labelled D1, two sets of signals arising from the apo and Cu(I)-bound forms of D1 are observed, indicating that the metallated form exchanged with the free one at rates slower than the resonance frequency differences between the two forms. Similar behaviour was also observed when ^{15}N labelled D1 sample was titrated with a Zn(II) ion. Changes of chemical shifts upon Zn(II) addition were observed for the same residues as for the copper one, indicating that D1 is able to bind either Cu(I) or Zn(II) (Figure 1).

Apparent affinity constant of hCCS D1 for Cu(I) and Zn(II), determined through ESI-MS according to scheme discribed in "Methods" are 40±0,23fM and 0,47±0,06nM respectively (Figure 2, 3). The observed affinity constant for Zn(II) ion suggests that metalation of D1, might occur in the cellular conditions. And as a biological implication of this process D1 of hCCS could be involved in Zn(II) transfer to SOD1.

When D2,3 of hCCS construct was titrated with Cu(I) a variation of the chemical shifts of some signals was observed in the ^{15}N HSQC spectra. Only one set of NH signals was always present within the titration steps, whose chemical shift changed upon addition of increasing amounts of Cu(I), indicating that the Cu(I)-bound form and the apo- form exchanged with the faster rate respect to the resonance frequency differences of the two species. Moreover a substantial number of signals also became broad beyond detection by increasing Cu(I) amount. The behaviour of the full length hCCS is more complex as it is the sum of the behaviour of the two individual D1 and D2,3 constructs. Indeed, while the signals of the apo

D1 disappear and those of the Cu(I)-bound form appear, the signals of the D2,3 show changes in chemical shift with increasing amount of copper ions.

hCCS and SOD1 interactions. Metal transfer

Consistently with its copper chaperone function, Cu(I)-bound hCCS is able to transfer Cu(I) to hSOD1 either to apo or to the E,Zn form and either with the oxidized or reduced disulfide bond, even if the behaviour and process is different in the latter two cases. The ability of entire hCCS and the different copper-loaded constructs of hCCS to transfer Cu(I) to hSOD1 have been studied through NMR and ESI-MS spectroscopy. First, the interaction between SOD1 and the Cu(I) loaded full length hCCS protein was investigated by adding the latter to ^{15}N-enriched SOD1 (E,E and E,Zn form). In both cases we observed the transfer of Cu(I) ion from the hCCS protein to hSOD1 and the appearance of NH signals of a Cu(I)-bound hSOD1 in the case of E-ESOD(S-S) and of the Cu-ZnSOD1 species in the case of E-ZnSOD(S-S) (Figure 4). Both spectra were superimposable, with those obtained after metallation of corrisponding species E-ESOD1(S-S) and E-ZnSOD1(S-S) with $Cu(CH3CN)_4^+$. ESI-MS spectrometry allowed us to observe partial transfer of the Cu(I) ion from the full length hCCS, to E-ESOD1(S-S) protein within 2 minutes, but not to the EZnSOD1 (S-S) species. It is important to note that the timescale of the performed NMR experiments and the ESI-MS experiments is much different. No protein-protein complex formation was detected in both titrations through NMR and ESI-MS spectroscopy.

In contrast no metal transfer from the Cu(I)-bound D1 to the ^{15}N labelled-E,ZnSOD1(S-S) was observed and only partial transfer to the E,ESOD1(S-S) in the presence of a large excess of Cu(I) loaded hCCS D1, as showed in the ^{1}H spectra (Figure 5). When similar experiments was performed by ESI-MS after 1h of incubation we could detect less than 40% of Cu(I)-bound form of SOD1 S-S, in case of E,ESOD1(S-S) used as initial reactant and again we didn't observe Cu(I) transfer from Cu(I)-bound D1 to the E,ZnSOD1(S-S) species. The same results were obtained with a double domain construct containing Cu(I)-bound domain 1 and 2 of hCCS (Cu(I)-D1,2).

Since CCS D1 is unable to efficiently metallate E,ESOD1(S-S) at variance with what observed with the full-length protein, we tested if the D2,3 of hCCS construct alone is capable to metalate hSOD1 or whether the concomitant presence of all the three domains of hCCS are required for this process. Thus, the titration experiments, followed by ESI-MS were performed adding the Cu(I)-bound form of a D2,3 of hCCS construct (Cu(I)-D2,3) to either

E,ESOD1 (S-S) or E,ZnSOD1 (S-S) proteins. The formation of the copper bound form of SOD1 was not observed within 1h but the appearence of two new twin-peaks were detected in both titrations. The deconvolution of these peaks in the E,ESOD1 (S-S) titration yields molecular masses of 36,856Da and 36,920Da and in the E,ZnSOD1 (S-S) titration molecular masses of 36914Da and 36983Da. These molecular masses correspond to the heterodimer SOD1/D2,3 and SOD1/CuD2,3 complexes, respectively. (Figure 6) Similar peaks were detected also when Cu(I)-D2,3 was added to the reduced E-ESOD1(SH-SH) or E-ZnSOD1(SH-SH) forms. Specifically, in the latter cases the twin-peaks have much higher intensity with respect to the SOD1(S-S)/Cu(I)-D2,3 mixtures, indicating that these complexes are highly populated only when the disulfide bond is reduced. Similar results were found when the Cu(I)- D1,2 or D2 constructs were added to the reduced forms of both E,ESOD1 and E,ZnSOD1 proteins. Indeed, peaks corresponding to the molecular mass of an heterodimer complex (43370Da corresponding to E,ESOD/CuD1,2; 43436Da-E,ZnSOD/CuD1,2; 32486Da and 32549Da for E,ESOD1/D2 and E,ZnSOD1/D2 respectively) were detected in the ESI-MS spectra. When the disulfide bond of SOD1 is present, no protein-protein complexes have been observed. These results are in agreement with the proposed role for D2 of hCCS in the target recognition and complex formation and suggest the necessity of hSOD1 disulfide reduction for the efficient complex formation. The interactions between hCCS and the reduced forms of SOD1 was also investigated through NMR spectroscopy, by analyzing the perturbations caused in the $^{1}H–^{15}N$ HSQC spectra of ^{15}N-labeled E,ESOD1(SH-SH) upon addition of unlabelled Cu(I)-D2,3. The intensity of the amide signals decreases in the ^{1}H-^{15}N TROSY-HSQC spectra and concomitantly amide signals from a possible intermediate species are detected at the end of the titration. This behaviour is in agreement with the formation of protein-protein complexes, observed in the ESI-MS experiments. Moreover, after 4 hours the signals of a metallated SOD1 species were present in the ^{1}H-^{15}N TROSY-HSQC spectrum of the Cu(I)-D2,3/^{15}N E,ESOD1(SH-SH) reaction mixture. The chemical shifts of the latter signals are different from those observed when a Cu(I)-bound form of SOD1 is obtained after titration of either E,ESOD1(SH-SH) or E,ESOD1(S-S) with $Cu(CH3CN)_4^+$ complex.

Taking together both NMR and ESI-MS data we could conclude that, the Cu(I) transfer to either E,ESOD1 or E,ZnSOD1 with the disulfide bond already formed, is efficient only in the presence of the full length Cu(I)-hCCS. The Cu(I)-bound forms of the D1, D1,2, D2,3 of hCCS constructs are indeed not able to fully metallate hSOD1 protein. Moreover the present

data indicate that the complex formation between Cu(I)-bound hCCS and SOD1 proteins depends on the reduction state of the latter protein. The heterodimeric complex is preferentially formed only when the disulfide bond is reduced. Since size-exclusion chromatography shows that reduction of the disulfide bond shifts the monomer–dimer equilibrium towards monomer in both E,ESOD1 and E,ZnSOD1, thus the heterodimer formation with Cu(I)-CCS is more probable for SOD1 with the disulfide bond reduced, than with the oxidized one, given that the latter undergoes self-association to form a dimer. Moreover, the incubation of the E,ZnSOD1(SH-SH) with full-length Cu(I)-CCS produces an initial mass peak corresponding to the heterodimeric complex in the ESI-MS which converts within 1h to a Cu(I)-Zn(II) loaded dimer SOD1 form at the end of the reaction (Figure 7). These data suggest, that hCCS protein can participate in the disulfide bond formation in it's physiological partner SOD1. While hCCS has been defined as one of metallochaperone proteins, it's assistance to SOD1 folding through the disulfide formation suggesting the functional role as a real "chaperone" protein. The different behavior of the SOD1 species in different redox state towards metal transfer has to rely on kinetic ground, which might arise from the occurrence or absence of specific protein-protein interactions.

hCCS as a Zn chaperone

To address the possible role of the hCCS in Zn(II) transfer to SOD1 NMR titrations of ^{15}N labelled oxidized disulfide bond E,ESOD1(S-S) with ^{15}N labelled Zn(II)-bound D1 was performed. The ^{1}H-^{15}N HSQC spectrum of the mixture showed the formation of the E,ZnSOD1 species and the appearance of amide signals of the apo D1 (Figure 8) indicating that Zn ion is transferred in the correct binding site of SOD1 protein. The ^{1}H-^{15}N HSQC spectrum of the mixture is superimposable with the one of the E,ZnSOD1 protein. Once E,ESOD1:Zn(II)-bound D1 ratio reaches 1:2 the Zn,ZnSOD1 species was observed. These data were also confirmed through the ESI-MS experiments. On the mass spectra we could clearly detect decreasing of the Zn(II)-bound D1 peak intensity and increasing of the intensity of the apoD1 peak together with the formation of the metallated E,ZnSOD1 form. Taken together these data suggest that D1 of hCCS protein can transfer Zn(II) metal ion to E,ESOD1 protein *in vitro*. Therefore, if the E,ESOD1 form initially metallated by Cu(I)CCS full length protein was subsequently mixed with 1 equivalent of Zn(II)-D1 we observed the formation of the Cu,ZnSOD1 species indicating that Zn-bound D1 is able to transfer Zn(II) to a hSOD1 species already containing a Cu(I) ion. The present data show that the affinity of D1 construct is sufficient that the Zn(II) binding to this domain might occur in the cellular conditions.

Despite the importance of the Zn ion for SOD1 biogenesis, few information is available about the acquisition of this metal ion by SOD1 in the cells. In fact, no zinc chaperone has been identified up to now. Taking into account the ability of hCCS to bind Zn(II) in the Atx-like D1 and to transfer it to the E,ESOD1 protein we could speculate about the possible role of hCCS in the Zn transfer to SOD1 *in vivo.*

REFERENCES

1. McCord, J.M. & Fridovich, I. Superoxide dismutase. An enzymic function for erythrocuprein (hemocuprein). *J. Biol. Chem* **244**, 6049-6055 (1969).
2. Kobayashi, T. et al. Ultrastructural localization of superoxide dismutase in human skin. *Acta Derm. Venereol* **73**, 41-45 (1993).
3. Crapo, J.D., Oury, T., Rabouille, C., Slot, J.W. & Chang, L.Y. Copper,zinc superoxide dismutase is primarily a cytosolic protein in human cells. *Proc. Natl. Acad. Sci. U.S.A* **89**, 10405-10409 (1992).
4. Lindenau, J., Noack, H., Possel, H., Asayama, K. & Wolf, G. Cellular distribution of superoxide dismutases in the rat CNS. *Glia* **29**, 25-34 (2000).
5. Field, L.S., Furukawa, Y., O'Halloran, T.V. & Culotta, V.C. Factors controlling the uptake of yeast copper/zinc superoxide dismutase into mitochondria. *J. Biol. Chem* **278**, 28052-28059 (2003).
6. Sturtz, L.A., Diekert, K., Jensen, L.T., Lill, R. & Culotta, V.C. A fraction of yeast Cu,Zn-superoxide dismutase and its metallochaperone, CCS, localize to the intermembrane space of mitochondria. A physiological role for SOD1 in guarding against mitochondrial oxidative damage. *J. Biol. Chem* **276**, 38084-38089 (2001).
7. Forman, H.J. & Fridovich, I. On the stability of bovine superoxide dismutase. The effects of metals. *J. Biol. Chem* **248**, 2645-2649 (1973).
8. Furukawa, Y. & O'Halloran, T.V. Posttranslational modifications in Cu,Zn-superoxide dismutase and mutations associated with amyotrophic lateral sclerosis. *Antioxid. Redox Signal* **8**, 847-867 (2006).
9. Beyer, W.F., Fridovich, I., Mullenbach, G.T. & Hallewell, R. Examination of the role of arginine-143 in the human copper and zinc superoxide dismutase by site-specific mutagenesis. *J. Biol. Chem* **262**, 11182-11187 (1987).
10. Fisher, C.L., Cabelli, D.E., Tainer, J.A., Hallewell, R.A. & Getzoff, E.D. The role of arginine 143 in the electrostatics and mechanism of Cu,Zn superoxide dismutase: computational and experimental evaluation by mutational analysis. *Proteins* **19**, 24-34 (1994).
11. Lindberg, M.J., Normark, J., Holmgren, A. & Oliveberg, M. Folding of human superoxide dismutase: disulfide reduction prevents dimerization and produces marginally stable monomers. *Proc. Natl. Acad. Sci. U.S.A* **101**, 15893-15898 (2004).
12. Arnesano, F. et al. The unusually stable quaternary structure of human Cu,Zn-superoxide dismutase 1 is controlled by both metal occupancy and disulfide status. *J. Biol. Chem* **279**, 47998-48003 (2004).
13. Hörnberg, A., Logan, D.T., Marklund, S.L. & Oliveberg, M. The coupling between disulphide status, metallation and dimer interface strength in Cu/Zn superoxide dismutase. *J. Mol. Biol* **365**, 333-342 (2007).
14. Furukawa, Y., Torres, A.S. & O'Halloran, T.V. Oxygen-induced maturation of SOD1: a key role for disulfide formation by the copper chaperone CCS. *EMBO J* **23**, 2872-2881 (2004).
15. Bertini, I., Manganl, S. & Viezzoli, M.S. Structure and Properties of Copper-Zinc Superoxide Dismutases. **45**, 127-250 (1998).
16. Culotta, V.C. et al. The copper chaperone for superoxide dismutase. *J. Biol. Chem* **272**, 23469-23472 (1997).
17. Rothstein, J.D. et al. The copper chaperone CCS is abundant in neurons and astrocytes in human and rodent brain. *J. Neurochem* **72**, 422-429 (1999).
18. Rae, T.D., Schmidt, P.J., Pufahl, R.A., Culotta, V.C. & O'Halloran, T.V. Undetectable intracellular free copper: the requirement of a copper chaperone for superoxide dismutase.

Science **284**, 805-808 (1999).
19. Brown, N.M., Torres, A.S., Doan, P.E. & O'Halloran, T.V. Oxygen and the copper chaperone CCS regulate posttranslational activation of Cu,Zn superoxide dismutase. *Proc. Natl. Acad. Sci. U.S.A* **101**, 5518-5523 (2004).
20. Schmidt, P.J. et al. Multiple protein domains contribute to the action of the copper chaperone for superoxide dismutase. *J. Biol. Chem* **274**, 23719-23725 (1999).
21. Lamb, A.L. et al. Crystal structure of the copper chaperone for superoxide dismutase. *Nat. Struct. Biol* **6**, 724-729 (1999).
22. Lamb, A.L., Wernimont, A.K., Pufahl, R.A., O'Halloran, T.V. & Rosenzweig, A.C. Crystal structure of the second domain of the human copper chaperone for superoxide dismutase. *Biochemistry* **39**, 1589-1595 (2000).
23. Rae, T.D., Torres, A.S., Pufahl, R.A. & O'Halloran, T.V. Mechanism of Cu,Zn-superoxide dismutase activation by the human metallochaperone hCCS. *J. Biol. Chem* **276**, 5166-5176 (2001).
24. Endo, T., Fujii, T., Sato, K., Taniguchi, N. & Fujii, J. A pivotal role of Zn-binding residues in the function of the copper chaperone for SOD1. *Biochem. Biophys. Res. Commun* **276**, 999-1004 (2000).
25. Barry, A.N. & Blackburn, N.J. A Selenocysteine Variant of the Human Copper Chaperone for Superoxide Dismutase. A Se-XAS Probe of Cluster Composition at the Domain 3−Domain 3 Dimer Interface†. *Biochemistry* **47**, 4916-4928 (2008).
26. Stasser, J.P., Siluvai, G.S., Barry, A.N. & Blackburn, N.J. A multinuclear copper(I) cluster forms the dimerization interface in copper-loaded human copper chaperone for superoxide dismutase. *Biochemistry* **46**, 11845-11856 (2007).
27. Stasser, J.P., Eisses, J.F., Barry, A.N., Kaplan, J.H. & Blackburn, N.J. Cysteine-to-Serine Mutants of the Human Copper Chaperone for Superoxide Dismutase Reveal a Copper Cluster at a Domain III Dimer Interface†. *Biochemistry* **44**, 3143-3152 (2005).
28. Eisses, J.F., Stasser, J.P., Ralle, M., Kaplan, J.H. & Blackburn, N.J. Domains I and III of the human copper chaperone for superoxide dismutase interact via a cysteine-bridged Dicopper(I) cluster. *Biochemistry* **39**, 7337-7342 (2000).
29. Zhu, H. et al. Cobalt(2+) binding to human and tomato copper chaperone for superoxide dismutase: implications for the metal ion transfer mechanism. *Biochemistry* **39**, 5413-5421 (2000).
30. Rosenzweig, A.C. & O'Halloran, T.V. Structure and chemistry of the copper chaperone proteins. *Curr Opin Chem Biol* **4**, 140-147 (2000).
31. Culotta, V.C., Yang, M. & O'Halloran, T.V. Activation of superoxide dismutases: putting the metal to the pedal. *Biochim. Biophys. Acta* **1763**, 747-758 (2006).
32. Banci, L., Bertini, I., Cantini, F. & Ciofi-Baffoni, S. Cellular copper distribution: a mechanistic systems biology approach. *Cell. Mol. Life Sci* **67**, 2563-2589 (2010).
33. Khare, S.D., Caplow, M. & Dokholyan, N.V. The rate and equilibrium constants for a multistep reaction sequence for the aggregation of superoxide dismutase in amyotrophic lateral sclerosis. *Proc. Natl. Acad. Sci. U.S.A* **101**, 15094-15099 (2004).
34. Hall, L.T. et al. X-ray crystallographic and analytical ultracentrifugation analyses of truncated and full-length yeast copper chaperones for SOD (LYS7): a dimer-dimer model of LYS7-SOD association and copper delivery. *Biochemistry* **39**, 3611-3623 (2000).
35. Lamb, A.L., Torres, A.S., O'Halloran, T.V. & Rosenzweig, A.C. Heterodimeric structure of superoxide dismutase in complex with its metallochaperone. *Nat. Struct. Biol* **8**, 751-755 (2001).
36. Hallewell, R.A. et al. Thermostabilization of recombinant human and bovine CuZn superoxide dismutases by replacement of free cysteines. *Biochem. Biophys. Res. Commun* **181**, 474-480 (1991).

37. Lepock, J.R., Frey, H.E. & Hallewell, R.A. Contribution of conformational stability and reversibility of unfolding to the increased thermostability of human and bovine superoxide dismutase mutated at free cysteines. *J. Biol. Chem* **265**, 21612-21618 (1990).
38. Parge, H.E., Hallewell, R.A. & Tainer, J.A. Atomic structures of wild-type and thermostable mutant recombinant human Cu,Zn superoxide dismutase. *Proc. Natl. Acad. Sci. U.S.A* **89**, 6109-6113 (1992).
39. Palumaa, P., Kangur, L., Voronova, A. & Sillard, R. Metal-binding mechanism of Cox17, a copper chaperone for cytochrome c oxidase. *Biochem. J* **382**, 307-314 (2004).
40. Banci, L. et al. Affinity gradients drive copper to cellular destinations. *Nature* **465**, 645-648 (2010).
41. Rakhit, R. et al. Oxidation-induced misfolding and aggregation of superoxide dismutase and its implications for amyotrophic lateral sclerosis. *J. Biol. Chem* **277**, 47551-47556 (2002).

FIGURES

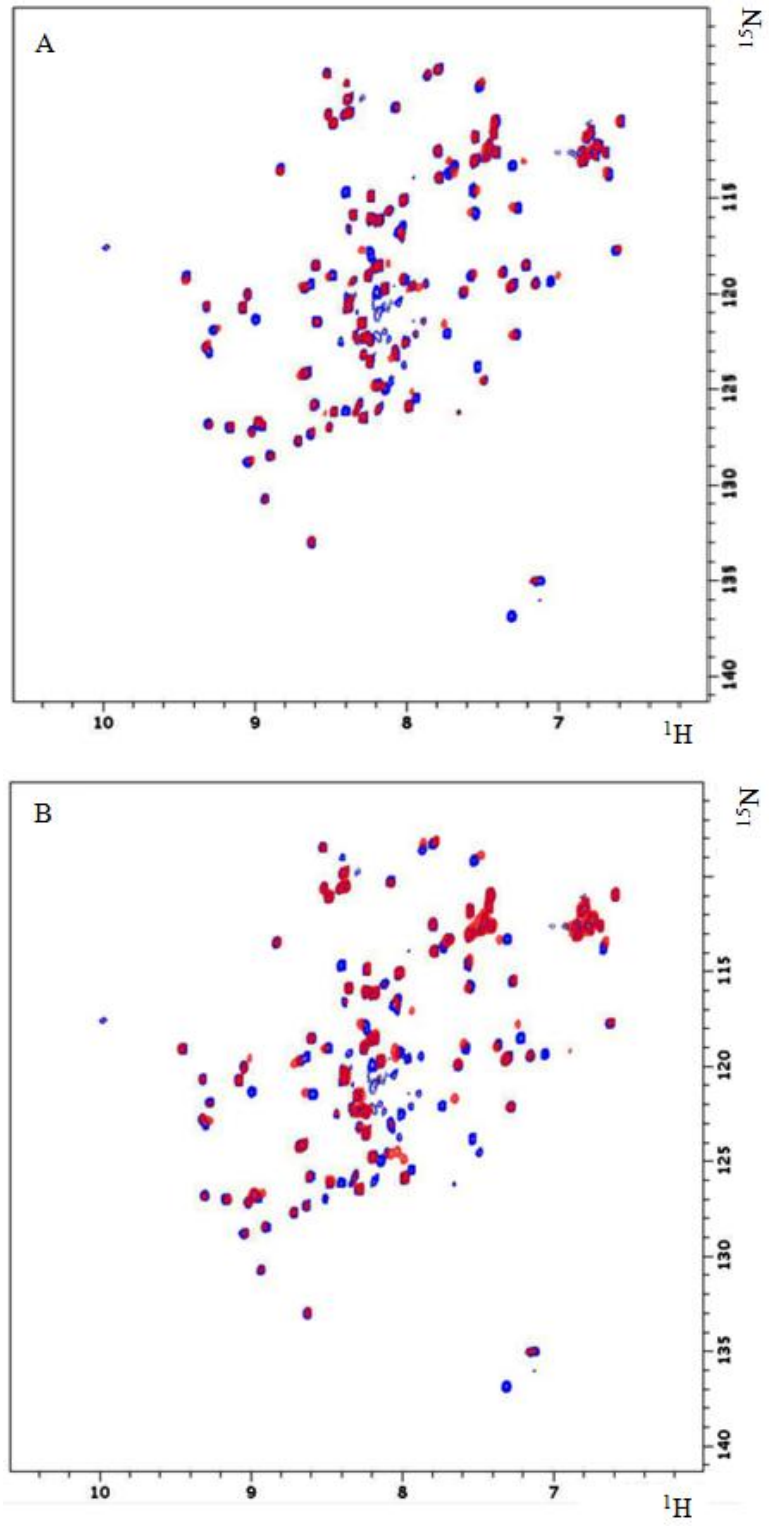

Figure 1. Superimposition of the ^{1}H-^{15}N HSQC spectra

A) apoD1hCCS (in blue) and Zn(II)D1hCCS (in red) B) apoD1hCCS (in blue) and Cu(I)D1hCCS (in red)

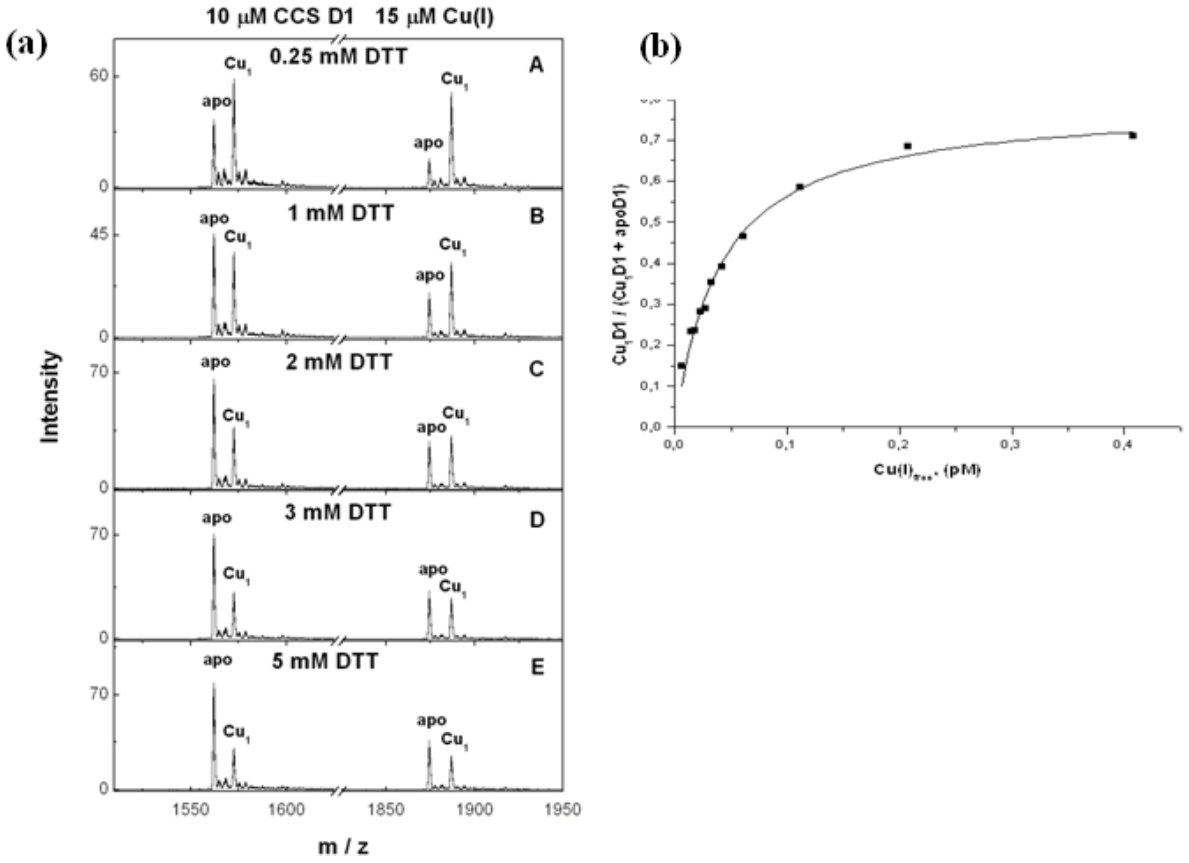

Figure 2. Determination of the apparent dissociation constant for Cu_1D1

(a) - ESI-MS spctra of Cu_1D1 in the presence of 0,5 – 25mMDTT. (b) - Dependence of the fractional content of Cu_1D1 ($Y= I_{CuD1} / (I_{D1} + I_{CuD1})$) from the concentration of free Cu(I) ions in the metal competition experiment. Solid line shows the fitting curve with K_{cu} = 40±0,23fM

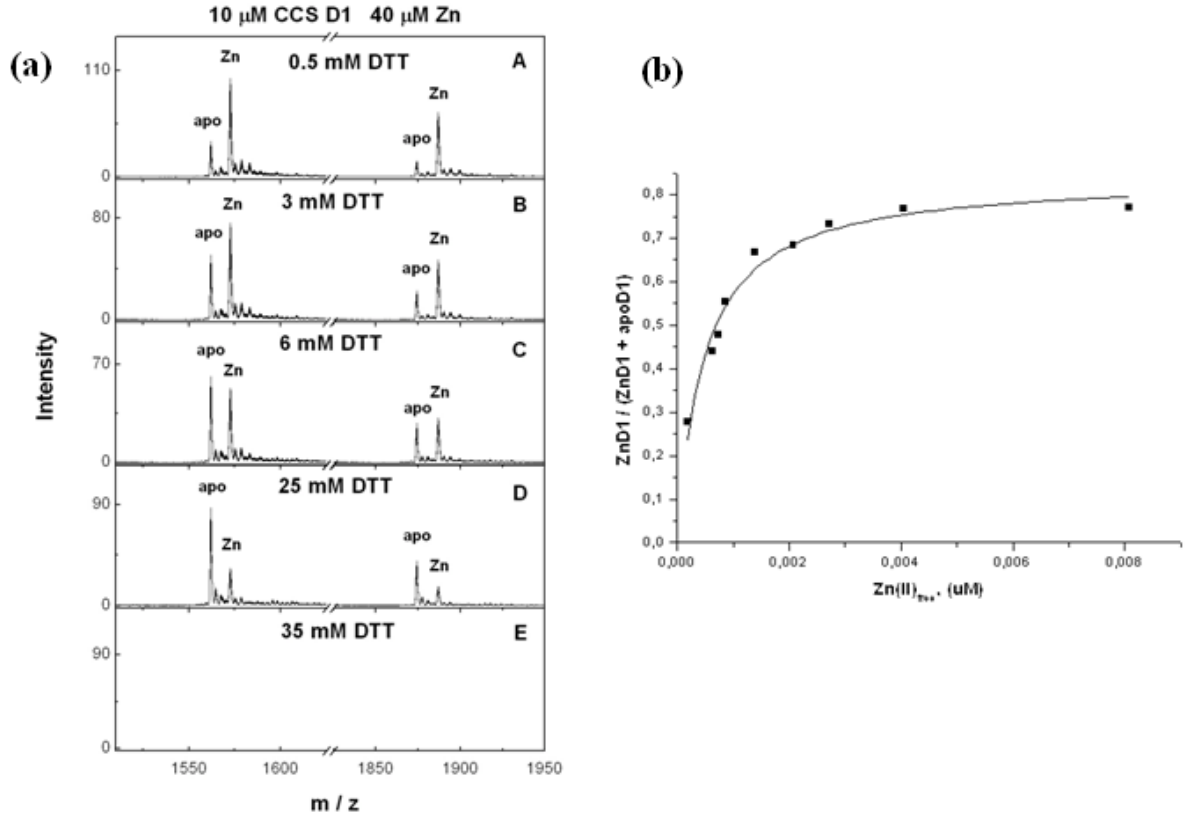

Figure 3. Determination of the apparent dissociation constant for Zn_2D1

(a) - ESI-MS spctra of Zn_2D1 in the presence of 0,5 – 25mMDTT. (b) - Dependence of the fractional content of Zn_2D1 ($Y= I_{ZnD1} / (I_{D1} + I_{ZnD1})$) from the concentration of free Zn(II) ions in the metal competition experiment. Solid line shows the fitting curve with K_{zn} = 0,47± 0,06nM

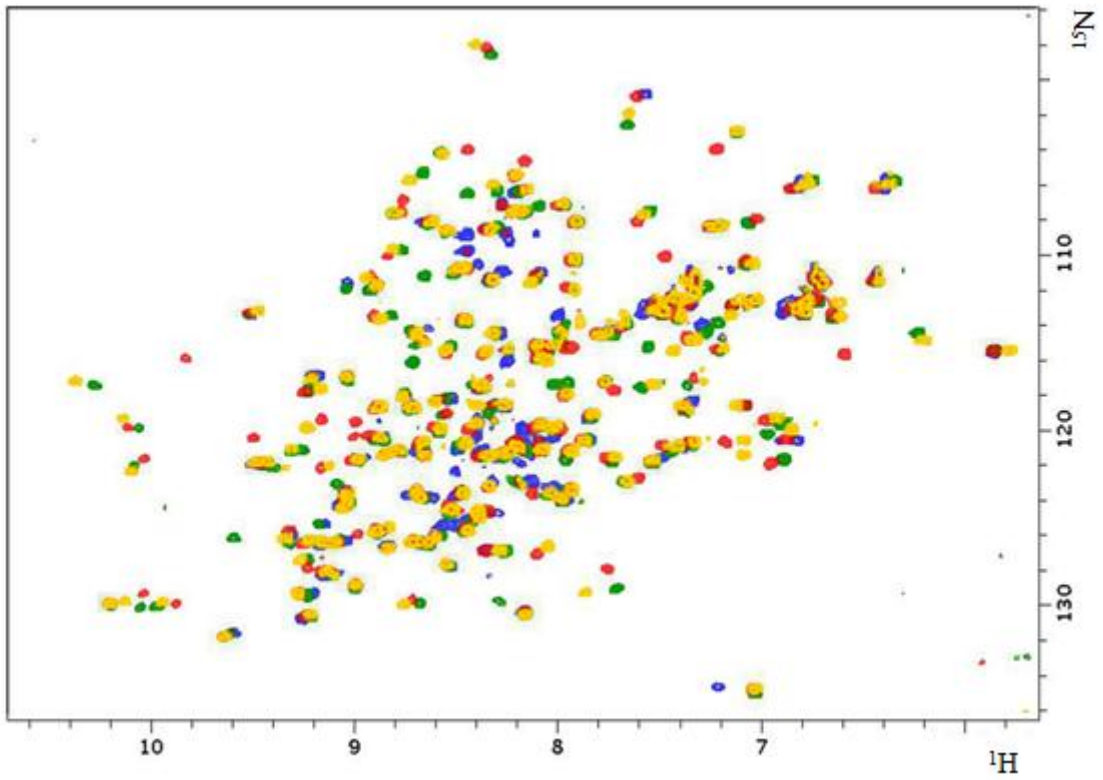

Figure 4. Overview of the ^{1}H-^{15}N HSQC spectra of the titration Cu(I)hCCS full length with SOD1(S-S) proteins.

In blue ^{15}N E-ESOD1(S-S); in red ^{15}N E-ESOD1(S-S) + Cu(I)CCS full lengh unlabeled; in green ^{15}N E-ZnSOD1(S-S); in yellow ^{15}N E-ZnSOD1(S-S) + Cu(I)CCS full lengh unlabeled

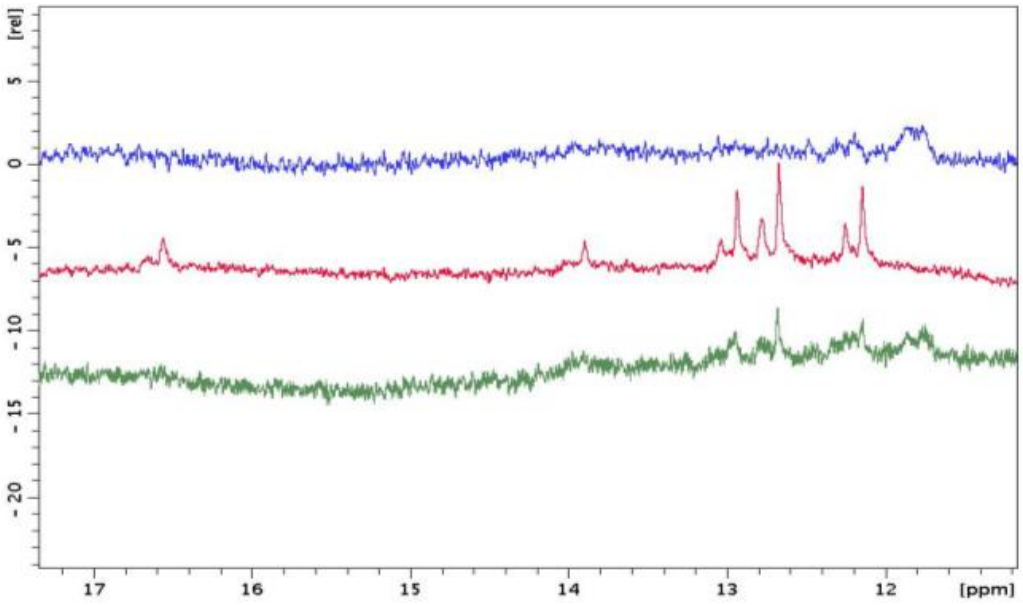

Figure 5. Overview of the 1D spectra of the titration Cu(I)hCCS proteins with SOD1(S-S) proteins.

In blue ^{15}N E-ESOD1(S-S); in red ^{15}N E-ESOD1(S-S) + Cu(I)CCS full lengh unlabeled; in green ^{15}N E-ESOD1(S-S) + ^{15}N CuD1CCS

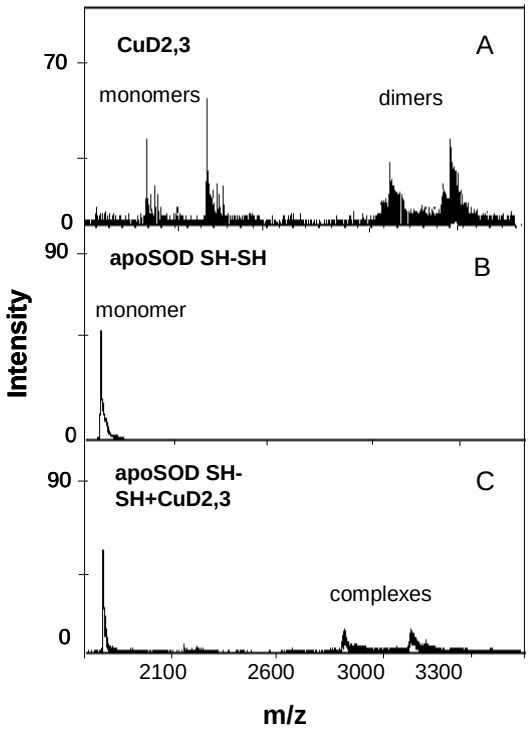

Figure 6. Superimposition of the ESI-MS spectra

A Spectrum of the CuD2,3hCCS The first 2 groups of signals in the left part of the spectrum corresponding to the monomeric state of the protein while the othere two in the right one belong to the dimer species **B** Spectrum of the E,ESOD1 SH-SH. The protein is mostly in the monomeric state.**C** Spectrum of the reaction mixture between CuD2,3hCCS and E,ESOD1SH-SH. Complex formation

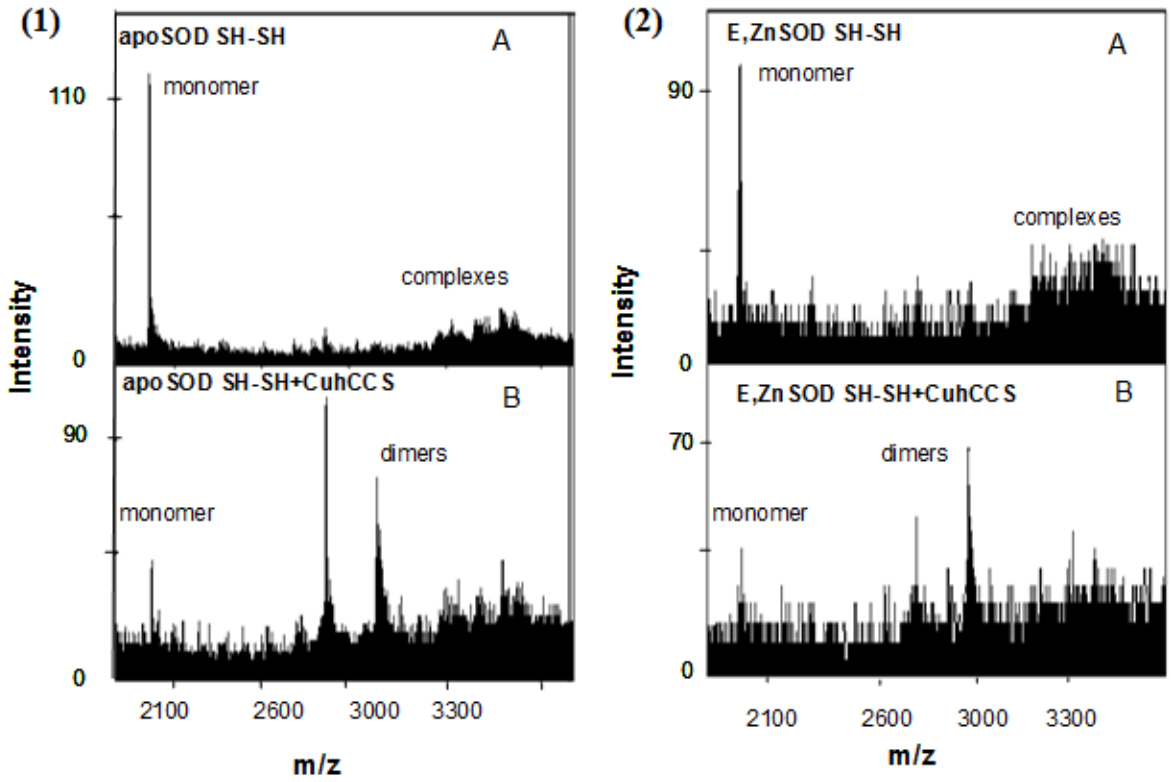

Figure 7. Superimposition of the ESI-MS spectra of the reaction mixtures:

(1) - E,ZnSOD1 SH-SH and Cu-hCCS ful length (2) - E,ESOD1 SH-SH and Cu-hCCS ful length A. Reaction mixture uppon mixing, B.the same reaction mixture after 1h at RT

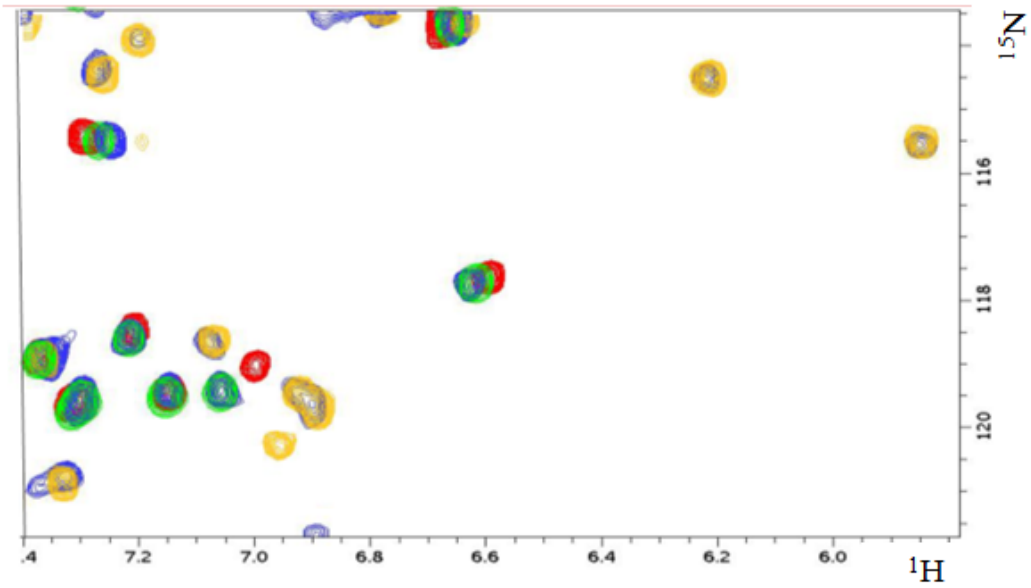

Figure 8. Overview of the ^{1}H-^{15}N HSQC spectra of the titration Zn(II)D1hCCS with SOD1(S-S) proteins.

In red ^{15}N ZnD1CCS; in blue ^{15}N ZnD1CCS + ^{15}N E-ESOD1(S-S); in green ^{15}N apoD1CCS; in yellow ^{15}N E-ZnSOD1(S-S)

"SCO PROTEINS ARE INVOLVED IN ELECTRON TRANSFER PROCESSES"

Lucia Banci[1,2], Ivano Bertini[1,2], Simone Ciofi-Baffoni[1,2], Tatiana Kozyreva[1], Mirko Mori[1,2], and Shenlin Wang[1]

[1] Magnetic Resonance Center CERM and Department of Chemistry, University of Florence, Via Luigi Sacconi 6, 50019, Sesto Fiorentino, Florence, Italy.

[2] Department of Chemistry, University of Florence, Via della Lastruccia 3, 50019 Sesto Fiorentino, Florence, Italy.

In press, JBIC

Published online 23 December 2010 - DOI 10.1007/s00775-010-0735-x

J Biol Inorg Chem
DOI 10.1007/s00775-010-0735-x

ORIGINAL PAPER

Sco proteins are involved in electron transfer processes

Lucia Banci · Ivano Bertini · Simone Ciofi-Baffoni · Tatiana Kozyreva · Mirko Mori · Shenlin Wang

Received: 12 August 2010 / Accepted: 9 November 2010

Abstract Sco proteins are widespread in eukaryotic and in many prokaryotic organisms. They have a thioredoxin-like fold and bind a single copper(I) or copper(II) ion through a CXXXC motif and a conserved His ligand, with both tight and weak affinities. They have been implicated in the assembly of the Cu_A site of cytochrome *c* oxidase as copper chaperones and/or thioredoxins. In this work we have structurally characterized a Sco domain which is naturally fused with a typical electron transfer molecule, i.e., cytochrome *c*, in *Pseudomonas putida*. The thioredoxin-like Sco domain does not bind copper(II), binds copper(I) with weak affinity without involving the conserved His, and has redox properties consisting of a thioredoxin activity and of the ability of reducing copper(II) to copper(I), and iron(III) to iron(II) of the cytochrome *c* domain. These findings indicate that the His ligand coordination is the discriminating factor for introducing a metallochaperone function in a thioredoxin-like fold, typically responsible for electron transfer processes. A comparative structural analysis of the Sco domain from *P. putida* versus eukaryotic Sco proteins revealed structural determinants affecting the formation of a tight-affinity versus a weak-affinity copper binding site in Sco proteins.

Keywords Electron transfer · Metallochaperones · Cytochrome · Nuclear magnetic resonance · Structure–function relationship

The atomic coordinates and the structural restraints of *Pseudomonas putida* cytochrome *c* have been deposited in the RCSB Protein Data Bank (ID 2L4D). The resonance assignments have been deposited in the Biological Magnetic Resonance Data Bank (code 17236).

An Interactive 3D Complement page in Proteopedia is available at: http://proteopedia.org/wiki/index.php/Journal:JBIC:6.

Electronic supplementary material The online version of this article (doi:10.1007/s00775-010-0735-x) contains supplementary material, which is available to authorized users.

L. Banci · I. Bertini (✉) · S. Ciofi-Baffoni · T. Kozyreva · M. Mori · S. Wang
Magnetic Resonance Center CERM,
University of Florence, Via Luigi Sacconi 6,
50019 Sesto Fiorentino, Florence, Italy
e-mail: ivanobertini@cerm.unifi.it

L. Banci · I. Bertini · S. Ciofi-Baffoni · M. Mori
Department of Chemistry,
University of Florence,
Via della Lastruccia 3, 50019 Sesto Fiorentino,
Florence, Italy

Abbreviations

A_{650}	Absorbance at 650 nm
AMS	4-Acetamido-4′-maleimidylstilbene-2,2′-disulfonic acid
BCS	Bathocuproinedisulfonic acid
CcO	Cytochrome *c* oxidase
c-di-GMP	Bis(3′–5′)-cyclic dimeric guanosine monophosphate
DTT	Dithiothreitol
EDTA	Ethylenediaminetetraacetic acid
GSH	Reduced glutathione
hSco1	Human Sco1
hSco2	Human Sco2
HSQC	Heteronuclear single quantum coherence
LB	Luria–Bertani
NOE	Nuclear Overhauser effect
NOESY	Nuclear Overhauser effect spectroscopy
PAS	Per-Arnt-Sim

Published online: 23 December 2010

OD_{600}	Optical density at 600 nm
PAGE	Polyacrylamide gel electrophoresis
SDS	Sodium dodecyl sulfate

Introduction

Sco is a family of proteins ubiquitous to all kingdoms of life. Ortholog and paralog genome browsing has shown that more than one representative of this class is often present in bacterial and eukaryotic genomes [1, 2]. The 3D structures of Sco homologs from human, yeast, *Thermus thermophilus*, and *Bacillus subtilis* have been determined [3–9], showing a thioredoxin-like fold capable of binding Cu(I) and Cu(II) ions with a wide range of reported affinities (K_d values from micromolar to femtomolar) [10–12]. Sco proteins are implicated in the maturation of cytochrome *c* oxidase (CcO), being essential for the assembly of the Cu_A center, a binuclear copper binding site located in the Cox2 subunit of CcO [13–16]. Specifically, it appears that the molecular function of Sco proteins is related to copper delivery to the Cu_A site [17] and/or thiol disulfide oxidoreductase activity toward Cox2 [9] or other homologs of the Sco family involved in the Cu_A assembly [18]. In addition to the implication of the role of Scos in Cu_A maturation, the thiol disulfide oxidoreductase activity has been proposed to play a role in signaling pathways. For example, in the photosynthetic prokaryote *Rhodobacter sphaeroides* the Sco homolog may be central to the regulation of the photosynthetic regulatory response system which involves the two-component signaling proteins PrrA and PrrB [19]. A signaling role for mitochondrial Sco proteins in the maintenance of cellular copper homeostasis has also been postulated, although the route of signal transduction has not been defined [20]. Consistent with their possible multiple functional properties, extensive analysis of completely sequenced prokaryotic genomes revealed that 18% of them contain Sco proteins but not Cu_A-containing proteins or vice versa [1]. Furthermore, in several cases, multiple Sco-encoding genes occur even if only a single potential Sco target, i.e., the Cox2 subunit, is encoded in the genome [1]. Overall, all literature data indicate that there may be quite a variety of functions of Sco proteins which may be linked to the specific mechanism of action and physiological role of Sco proteins. In this frame, specific sequence variations that occurred during evolution can result in fine structural changes influencing the reduction potential of the metal binding Cys residues and the metal binding affinity.

This work contributes to the understanding of the molecular function of the Sco proteins. A possible role of Sco proteins in delivery of copper to CcO was proposed in 1996 by Glerum et al. [21, 22], observing the effect on yeast mutants lacking the mitochondrial copper chaperone Cox17. In that system, overexpression of yeast Sco1 in the presence of high copper concentrations was able to rescue the respiratory deficiency. Yeast strains lacking Sco1 are also respiratory-deficient, and excess copper and/or overexpression of Cox17 cannot compensate the Sco1-associated CcO deficiency. The absolute requirement of Sco1 in activation of CcO in yeast indicates that Sco1 functions downstream from Cox17 in the delivery of copper to CcO. Indeed, in vitro, eukaryotic Sco1 can receive copper from the copper chaperone Cox17 [23, 24]. The Sco protein family is characterized by the presence of a conserved CXXXC motif involved in copper, zinc, or nickel binding [17, 25]. Accordingly, structures of the highly homologous human paralogs [human Sco1 (hSco1) and human Sco2 (hSco2)] show that the copper binding site comprises two Cys residues from the CXXXC motif and an additional conserved His residue, which is positioned in sequence far from the CXXXC motif in a long loop [4, 5]. In addition, Scos have a fold similar to that of the thioredoxin family, thus suggesting a possible role of Sco proteins also as a thiol disulfide oxidoreductase. The two Cys residues have been proposed to be the active-site residues in the thiol disulfide oxidoreductase function. The conserved His residue plays a role in the copper chaperone versus thioredoxin function since when in human thioredoxin a His residue is introduced in place of a conserved *cis*-Pro located in the loop featuring the conserved His in Sco proteins, copper binding is observed [26]. The thioredoxin property of Scos has also been supported by the X-ray structures of the oxidized apo form from *B. subtilis* Sco1 and of the oxidized form of a nickel-bound hSco1 having a disulfide bond in the CXXXC motif [4, 8]. Moreover, overexpression of wild-type hSco2, or knockdown of hSco2, in human cells alters the ratio of oxidized to reduced Cys residues in hSco1, suggesting that hSco2 acts as a thiol disulfide oxidoreductase toward hSco1 during Cox2 maturation [18]. Further evidence of the thioredoxin function of Scos comes from a recent investigation of the molecular mechanism of Cu_A assembly in *T. thermophilus* [9]. In this system a new periplasmic protein (PCu_AC) has been identified; it is able to selectively insert two Cu(I) ions into Cox2 of CcO. Sco1 is unable to receive copper ions from PCu_AC and to deliver them to Cox2, but works as a thioredoxin maintaining the Cys copper ligands of the Cu_A site in the reduced state. All these results strongly suggests that Sco proteins may exhibit more than one function, including copper transfer and/or redox activities.

Starting from our previous bioinformatic analysis of Sco proteins encoded in prokaryotic genomes [1], we focused on the genome of *Pseudomonas putida* KT2440, which contains six Sco-like sequences in different genomic

contexts: two *Sco* genes are genetically related to the maturation of caa_3-type CcO, one is close to a protein involved in Cu(I) binding [27], one is fused to a cytochrome *c*, and the last two are adjacent to each other and close to putative cytochrome *c* and multicopper oxidase proteins. The protein named pp3183 was chosen here as a target since it is formed by a Sco domain fused to a well-known electron transfer protein, cytochrome *c*, this system being potentially involved in electron transfer processes. The solution structures of both cytochrome *c* and Sco domains, separately expressed (pp-Sco and pp-Cyt *c*, hereafter), were determined and the electron transfer reaction between them was investigated by means of their measured redox potentials. Copper binding and thioredoxin properties of the Sco domain were also investigated to gain functional insight into this protein.

Materials and methods

Protein expression and purification

The soluble domain of the *pp_3183* gene was amplified by PCR from the genome DNA (ATCC® number 47054D-5™), cloned into the Gateway Entry vector pENTR/TEV/D-TOPO (Invitrogen), and subcloned into the pDEST-His-periMBP destination vector by Gateway LR reaction to generate an N-terminal, His-periMBP fused protein. The protein was expressed in *Escherichia coli* BL21(DE3)C41 harboring pEC86 plasmid cells, encoding for the *ccm* genes necessary for the attachment of the biosynthesized heme *c* into the pp-Cyt *c* domain [28]. Cells were grown in 1 L of rich Luria–Bertani (LB) medium at 310 K shaken at 140 rpm. Upon reaching a cell optical density at 600 nm (OD_{600}) of 0.5, the cells were pelleted by a 10-min centrifugation at 5,000*g*. The cells were then washed using an M9 salt solution, excluding all nitrogen and carbon sources. The cell pellet was resuspended in isotopically labeled minimal medium [$(^{15}NH_4)_2SO_4$ and/or $^{13}C_6H_{12}O_6$] with 0.2 mM δ-aminolevulinic acid, which generates the biosynthesis of heme from the hosts. Protein expression was induced at OD_{600} of 0.7 by addition of isopropyl β-D-thiogalactopyranoside to a concentration of 0.7 mM for 16 h. The temperature was decreased to 298 K for the protein expression. After cell rupture by sonication, purification was performed by using a HiTrap chelating HP column (Amersham Pharmacia Biosciences) charged with Ni(II). The His-periMBP tag was cleaved with AcTEV. The digested protein was concentrated by ultrafiltration and charged in a second HiTrap chelating HP column, followed by a 16/60 Superdex 75 chromatographic column (Amersham Biosciences) to separate the protein from the N-terminal His-periMBP tag. The fractions showing a single component by sodium dodecyl sulfate (SDS) polyacrylamide gel electrophoresis (PAGE) were collected. At the end of the purification procedure, concentrated fractions were polished from the MBP traces with an amylose resin column. The protein concentration was measured using the absorbance at 280 nm and the Bradford protein assay. The pp-Sco domain was amplified by PCR from the pDEST-His-periMBP plasmid containing the soluble domain of the *pp_3183* gene, cloned into the Gateway Entry vector pENTR/TEV/D-TOPO (Invitrogen), and subcloned into the pDEST-His-MBP destination vector by Gateway LR reaction to generate an N-terminal, His-MBP fused protein. The protein was expressed in *E. coli* BL21(DE3)C41 cells, which were grown in LB medium or M9 minimal medium [$(^{15}NH_4)_2SO_4$ and/or $^{13}C_6H_{12}O_6$] for the production of unlabeled and labeled samples, respectively. To increase the yield of the protein, fermentation in a fermentor (Infors, Bottmingen, Switzerland) with 1.5 L of the medium was performed. The conditions were maintained as follows: 55% oxygen, stirring at 400 rpm, 310 K during the cell growth and 298 K for the protein expression, pH 7.0. Protein expression was induced with 0.7 mM isopropyl β-D-thiogalactopyranoside for 16 h. Purification was performed by using a HiTrap chelating HP column (Amersham Pharmacia Biosciences) charged with zinc(II). The His-MBP tag was cleaved with AcTEV. The digested protein was concentrated by ultrafiltration and loaded on a second HiTrap chelating HP column followed by a 16/60 Superdex 75 chromatographic column (Amersham Biosciences) to separate pp-Sco protein from the N-terminal His-MBP domain. The fractions showing a single component by SDS-PAGE were collected, and the protein concentration was measured using the Bradford protein assay. To prevent disulfide formation, which might occur because of the presence of two Cys residues in the CXXXC motif, the protein samples were kept in anaerobic conditions and reduced by addition of 5 mM dithiothreitol (DTT).

The pp-Cyt *c* domain was amplified by PCR from the pDEST-His-periMBP plasmid containing the soluble domain of the *pp_3183* gene, cloned into the Gateway Entry vector pENTR/TEV/D-TOPO (Invitrogen), and subcloned into the pDEST-His-peri MBP destination vector by Gateway LR reaction to generate an N-terminal, His-periMBP fused protein. The recombinant protein was expressed in *E. coli* BL21(DE3)C41 cells, harboring the pEC86 plasmid [28]. The cells were grown in LB or M9 media [$(^{15}NH_4)_2SO_4$ and/or $^{13}C_6H_{12}O_6$] for the production of unlabeled or labeled samples, respectively. The purification procedure for pp-Cyt *c* was performed as described above for the full-length construct.

NMR experiments

NMR experiments (Table S1) to obtain the resonance assignment and structure determination were performed on 0.8 mM ^{13}C,^{15}N-labeled and ^{15}N-labeled oxidized pp-Cyt *c* samples and on 0.5 mM ^{13}C,^{15}N-labeled and ^{15}N-labeled pp-Sco samples in 200 mM phosphate and 1 mM ethylenediaminetetraacetic acid (EDTA) buffer at pH 7.0. All 2D and 3D spectra were collected at 300 and 308 K for pp-Cyt *c* and pp-Sco, respectively, processed using the TOPSPIN software package, and analyzed using CARA [29]. The ^{1}H–^{15}N and ^{1}H–^{13}C heteronuclear single quantum coherence (HSQC) spectra of both pp-Cyt *c* and pp-Sco show well-dispersed resonances, indicating that the proteins are essentially folded. The assignment of ^{1}H, ^{13}C, and ^{15}N resonances of pp-Cyt *c* is as follows: 90.2, 76.5 and 89.0%, respectively. The presence of a paramagnetic metal ion, Fe(III), affects NMR signals and the ^{1}H spectrum exhibits several upfield- and downfield-shifted signals experiencing different linewidths (Fig. S1). For pp-Sco, 167 out of an excepted 172 backbone HN resonances were assigned. The amide resonances are missing for residues Ala48, Ala80, Gly94, Trp95, and Gly158. Triple resonance spectra allowed the assignment of 85.3% of backbone resonances (Table S2).

Structure calculation of pp-Cyt *c*

The proton–proton distance restraints obtained from 2D nuclear Overhauser effect spectroscopy (NOESY), 3D ^{13}C-resolved NOESY, and 3D ^{15}N-resolved NOESY were used, together with 100 φ and ψ dihedral angle constraints obtained from the chemical shift index analysis [30], to calculate the structure with the CYANA program [31]. In addition, 22 hydrogen bonds derived from HNCO long-range experiments [32] were used in the structure calculations. The heme, the axial ligands, and the two Cys residues covalently linked to the heme moiety were treated as previously reported [33–36]. The 20 conformers with the lowest residual target function values were subjected to restrained energy minimization in explicit solvent water with the AMBER 10 program [37]. Structure quality was evaluated using the validation programs PSVS [38] and WHATIF [39]. The results of this statistical analysis are reported in Table S3.

Experimentally validated homology model of pp-Sco

A structural model of the pp-Sco domain was generated using the I-TASSER server [40], which combines the methods of threading, ab initio modeling, and structural refinement to build reliable models. Protein structures 2B7K (crystal structure of yeast Sco1 [7]), 1ON4 (solution structure of *B. subtilis* Sco1 [8]) and 2HRN (solution structure of Cu(I) P174L hSco1 [24]) were chosen by I-TASSER as the templates in the modeling. The calculated structural model was validated on the basis of the experimental data obtained from TALOS+ [41] and 2D/3D NOESY experiments. Specifically, the chemical shifts of Hα, C$'$, Cα, and Cβ atoms indicate the same secondary structure elements as found in the model, and proton–proton distance constraints derived from the analysis of 2D/3D NOESY experiments identified 200 unambiguous nuclear Overhauser effect (NOE) distances, 60 of which corresponded to long-range distances, which are in agreement with the tertiary structural organization of the model.

Relaxation data

^{15}N R_1, R_2, and steady-state heteronuclear NOE measurements [42, 43] were performed at 11.7 T (500 MHz) or 16.4 T (700 MHz), at 308 or 300 K, using standard pulse sequences on pp-Cyt *c* and pp-Sco. The pp-Cyt *c* sample (0.8 mM protein concentration) was oxidized, whereas the pp-Sco sample (0.5 mM protein concentration) was reduced. R_2 values were measured using a refocusing delay of 450 µs. In all experiments the water resonance was suppressed with a "water flip-back" scheme. Relaxation rates R_1 and R_2 were determined by fitting the cross-peak intensities measured as a function of the delay within the pulse sequence to a single-exponential decay. Three additional R_1 and R_2 points at short delays were acquired to estimate the experimental error (mean R_1 and R_2 error values ranging from 5 to 6%). The heteronuclear NOE values were obtained from the ratio of the peak intensity for ^{1}H-saturated and unsaturated spectra (the signal-to-noise ratio in the $^{15}N\{^{1}H\}$ NOE spectra is 20). For each protein the experimental relaxation rates were used to estimate the correlation time for molecule reorientation τ_m, excluding those residues having an exchange contribution to the R_2 value, identified following a protocol reported in [44], or exhibiting large-amplitude internal motions, as monitored by low NOE values. The reorientation tumbling rate was also estimated using the available structures with the "shell modeling" approach implemented in HYDRONMR [45]. The calculation was performed by using a viscosity of water at 298 or 308 K of 8.9×10^{-4} or 7.1×10^{-4} N s m^{-2}, respectively. Tensor 2.0 was used to carry out the analysis of internal motion using the Lipari–Szabo approach [46].

Redox potential measurements

The redox potential of pp-Cyt *c* was determined following a standard spectrophotometric procedure [47], which measures the absorbance at 550 nm as a function of different oxidized to reduced ratios. The redox potential of

pp-Sco was determined following a protocol previously described for thioredoxins based on the measurement of fluorescence between 300 and 500 nm at different reduced glutathione (GSH) to oxidized glutathione ratios [48].

Interaction of pp-Sco with copper

pp-Sco was reduced using an excess of 5 mM DTT, which was then removed in an anaerobic chamber through two passages in a PD-10 desalting column. Full reduction of Cys residues was tested through 4-acetamido-4′-maleimidylstilbene-2,2′-disulfonic acid (AMS) SDS-PAGE analysis and confirmed by comparing the $^{1}H–^{15}N$ HSQC spectrum of the sample with the spectra of fully oxidized and fully reduced pp-Sco obtained by addition of 2 mM H_2O_2 or of 5 mM DTT, respectively, in the same experimental conditions.

Titrations of reduced pp-Sco (0.1–0.2 mM) with copper were anaerobically performed by addition of Cu(I) as $Cu(I)(CH_3CN)_4PF_6$, or of Cu(II) as $CuSO_4$, up to a metal-to-protein ratio of 3:1. In the first case, the Cu(I) metal excess was removed by dialysis and the bound metal content was estimated through the reaction of Cu(I) with bathocuproinedisulfonic acid (BCS), as the complex $Cu(I)(BCS)_2$ has a characteristic absorbance at 482 nm ($\varepsilon = 12.5\ mM^{-1}\ cm^{-1}$). The presence of Cu(I) ions in the Cu(II)/Sco mixture was checked through the addition of BCS. To identify whether the His ring is involved in the Cu(I) metal coordination, a $^{1}H–^{15}N$ HSQC experiment tailored to measure the ^{2}J NH couplings was performed using an INEPT delay of 22 ms. A titration of reduced pp-Sco (0.1 mM) with copper was performed by addition of Cu(I) as $Cu(I)(CH_3CN)_4PF_6$ in the presence of stoichiometric GSH up to a metal-to-protein ratio of 1:1.

pp-Sco/pp-Cyt *c* interaction

Additions of aliquots of a 0.8 mM solution of oxidized, unlabeled pp-Cyt *c* to a 0.3 mM solution of reduced, ^{15}N-labeled pp-Sco were followed through $^{1}H–^{15}N$ HSQC spectra acquired at 308 K. Similarly, a 0.1 mM solution of ^{15}N-labeled oxidized pp-Cyt *c* was titrated with 0.8 mM solution of reduced, unlabeled pp-Sco and $^{1}H–^{15}N$ HSQC spectra were acquired at 308 K. Reduction of pp-Cyt *c* upon addition of reduced pp-Sco was also followed through UV–vis spectra. Oxidation of Cys residues in pp-Sco was tested through not reducing AMS SDS-PAGE analysis.

Turbidimetric assay of insulin disulfide reduction

The pp-Sco-catalyzed reduction of insulin disulfides was monitored using the method of Holmgren [49]. The assay mixture was prepared in cuvettes by addition of 0.17 mM insulin and 5 µM pp-Sco in 0.1 M potassium phosphate, 2 mM EDTA (pH 7.0) buffer in a final volume of 600 µL. The reaction was started by addition of DTT (0.5 mM). *E. coli* thioredoxin (5 µM) was used as a positive control, and the sample with only DTT was tested as a negative control. The contents of the cuvettes were thoroughly mixed and the cuvettes were placed in the spectrophotometer to turbidimetrically follow the precipitation of reduced insulin chains at 650 nm for up to 80 min. The time for the start of precipitation, defined as an increase of 0.02 of the absorbance at 650 nm (A_{650}) over a stable baseline recording, was determined. In the assay the lag time is a consequence of the time needed to accumulate a sufficient quantity of precipitated insulin chains as a result of the reduction of insulin molecules by the protein investigated. The rate of precipitation at 650 nm, defined as the maximal increase $\Delta A_{650}\ min^{-1}$ in the interval between 0 and 1.0, was calculated. The rate calculated for the positive control thioredoxin in this experiment (0.076 $\Delta A_{650}\ min^{-1}$) is comparable with that obtained by Holmgren [49].

Results

Bioinformatic analysis and protein expression

A previous bioinformatic analysis of Sco proteins encoded in prokaryotic genomes pointed at various roles for this protein family [1]. Starting from that analysis, we focused on Sco proteins which can be potentially involved in electron transfer processes. In this regard, the genome of *P. putida* contains a protein, named pp3183, where a typical electron transfer protein, i.e., cytochrome *c*, is fused to a Sco-like domain. In the *P. putida* genome, upstream of pp3183 there is a protein containing both a diguanylate cyclase GGDEF and a phosphodiesterase EAL domain. The cyclase and phosphodiesterase are enzymes involved in bacterial signal transduction and regulation upon a vast array of extracellular signals, with both enzymes controlling cellular bis(3′–5′)-cyclic dimeric guanosine monophosphate (c-di-GMP) levels [50]. c-di-GMP is a soluble molecule that stimulates the biosynthesis of adhesins and exopolysaccharide cell surface components and inhibits various forms of bacterial motility. Moreover, c-di-GMP controls the virulence of animal and plant pathogens, progression through the cell cycle, antibiotic production, and other cellular functions [51]. Therefore, the gene association between Sco and cytochrome *c* domains in pp3183 suggests that it may be fundamental for electron-transfer-mediated signaling pathways. On the other hand, pp3183 has, as a downstream gene, a putative multicopper oxidase, thus potentially suggesting its participation in a

copper chaperone function. From this analysis it emerges that pp3183 is a good target molecule to address the electron transfer versus copper chaperone properties of Sco proteins.

A hydropathy analysis indicates that pp3183 protein contains a single N-terminal transmembrane-spanning helix, suggesting that it is a membrane-bound protein with both Sco and cytochrome *c* domains sequentially oriented toward the periplasm. Multiple sequence alignment of the cytochrome *c* domain of pp3183 and bacterial/eukaryotic cytochrome *c* shows that the typical CXXCH heme-binding pattern is conserved as well as a high sequence similarity (cytochrome *c* domain of pp3183 vs. cytochromes *c* from *Rhodothermus marinus* and human approximately 50%). In contrast, multiple sequence alignment performed for the Sco domain of pp3183 with those Sco sequences (from *B. subtilis*, *T. thermophilus*, yeast, and human, Fig. S2) whose functional and structural properties were more deeply investigated, shows a global low sequence similarity (approximately 14%). However, the CXXXC metal binding motif is conserved along all these sequences. The third His ligand is replaced by Leu131 in the pp3183 sequence, but a His residue is only four residues upstream of Leu131 (Fig. S2).

A soluble form of pp3183 protein without the N-terminal transmembrane segment was expressed in *E. coli* cells. This protein construct shows a rapid tendency to degrade (about 3 days) to the single cytochrome *c* and Sco-like domains (Fig. 1a) as well as to aggregate at concentrations higher than 0.5 mM. From the matrix-assisted laser desorption/ionization mass spectrometry analysis (Fig. 1b) of the degraded protein mixture we identified the sequence of the two isolated domains. On this basis and from the analysis of the secondary structure prediction of the pp3183 sequence, two constructs corresponding to the cytochrome *c* and Sco-like domains (Fig. S3) were produced. The interdomain interaction in the full-length construct was analyzed by comparing the isolated versus the full-length construct $^{1}H–^{15}N$ HSQC spectra and by measuring backbone longitudinal relaxation rates (carefully verifying, through SDS gel, that no protein degradation occurred during NMR data acquisition): (1) no significant chemical shift variations (backbone combined chemical shift mean variation, $\langle\Delta\delta_{HN}\rangle = [(\Delta\delta_{HN})^2 + (\Delta\delta_N/6.51)^2]^{0.5}$, of 0.034 and 0.026 ppm for Sco and cytochrome *c* domains, respectively) were observed; (2) the R_1 mean value of the cytochrome *c* domain in the full-length construct ($1.13 \pm 0.15\ s^{-1}$) compares with that of the single pp-Cyt *c* domain ($1.39 \pm 0.15\ s^{-1}$), indicating that in the full-length construct it acts as an independent domain. Therefore, both chemical shifts and relaxation NMR data indicate that the two domains do not show a domain–domain interaction surface and that they are moving independently in solution. Consistently, the high instability of the two-domain construct toward degradation indicates that the linker (approximately 15 amino acids) is solvent-exposed and thus accessible to proteolytic enzymes. These features indicate that there are essentially no steric effects between the two domains and therefore they do not play a role in the functional properties. On this basis, the structural, redox, and metal binding properties of the isolated proteins were analyzed and then the interaction between them was investigated.

Structural characterization of pp-Cyt *c*

The reorientational correlation time ($\tau_c = 7.22 \pm 0.87$ ns), as estimated from the R_2/R_1 ratio, indicates that the cytochrome *c* domain behaves in solution as a monomer. The solution structure of pp-Cyt *c* (Fig. 2a), obtained using

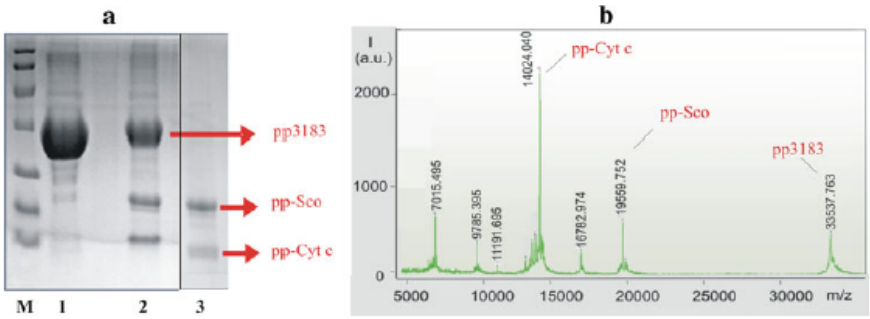

Fig. 1 Degradation of pp3183 construct. **a** Sodium dodecyl sulfate polyacrylamide gel electrophoresis (SDS-PAGE) analysis of pp3183 construct kept at room temperature for 1 week showing degradation after about 3 days to form the cytochrome *c* and Sco1-like domains. The analysis was performed after purification (*1*), 3 days (*2*), and 1 week (*3*). **b** Matrix-assisted laser desorption/ionization mass spectrometry analysis of the degraded protein mixture after 3 days. The analysis shows the molecular mass of a protein at 33,537.8 Da corresponding to the calculated molecular mass of pp3183 (33,549.5 Da). Additionally, two other peaks at 19,560 and 14,024 Da corresponding to the molecular masses of pp-Sco and pp-Cyt *c* domains are shown

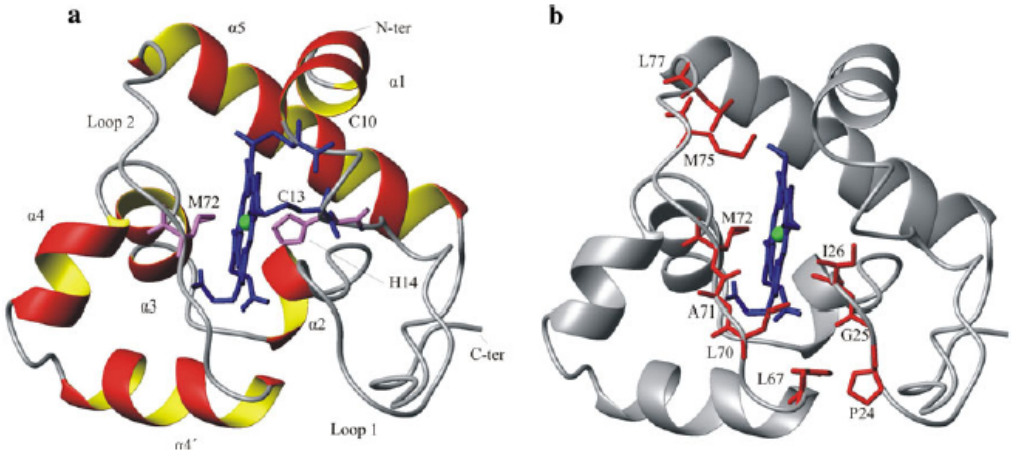

Fig. 2 Solution structure of pp-Cyt *c*. **a** The mean structure is shown with the heme (in *blue*) and the axial iron ligands His14 and Met72 (in *magenta*). Cys10 and Cys13 covalently linking the heme to the polypeptide chain are shown in *blue*. Fe(III) is depicted as a *green sphere*. **b** Hydrophobic heme environment of pp-Cyt *c*. Hydrophobic residues with side chain heavy atoms are shown in *red*

distance and angle NMR-derived constraints (see "Materials and methods" for details), shows the presence of six α-helices including residues 3–9, 33–36, 41–45, 49–54, 58–67, and 79–95. The protein has an unstructured segment at the C-terminus (residues 96–106) and a disordered region between Asn18 and Ile26. R_1 and R_2 relaxation rates as well as $^{15}N\{^1H\}$ NOE values are essentially homogeneous along the sequence (Fig. S4, average values of 1.39 ± 0.15, 11.1 ± 2.0, and 0.70 ± 0.24 s^{-1}, respectively), with the exception of the afore-mentioned unstructured/disordered regions, which show a low R_2/R_1 ratio and low $^{15}N\{^1H\}$ NOE values, indicating backbone motions on the nanosecond to picosecond timescale.

The minimal requirement for the cytochrome *c* fold is the presence of the three structural elements found in all the cytochrome *c* structures, i.e., the N- and C-terminal α-helices (helix α1 and helix α5, respectively, in mitochondrial cytochromes), as well as a long helix (helix α3, in mitochondrial cytochromes) preceding a short helix and the loop containing the second axial ligand to the heme iron, which is nearly always a Met [52]. These structural elements are all present in pp-Cyt *c*. Interestingly, pp-Cyt *c* has an additional α-helix (helix α4′, 58–66) inserted between helix α4 and loop 2 that shields the lower part of the heme from solvent. The heme group, with essentially the same orientation as in other cytochromes *c*, is covalently attached to the protein by two thioether bonds with the side chains of Cys10 and Cys13, which are located in loop 1. The heme iron is coordinated by the axial ligands His14 in loop 1 and Met72 in loop 2. The heme group is located in a hydrophobic pocket and is almost completely shielded from the solvent (only 6% of its surface is solvent-accessible, Fig. 2b).

A search for structurally related proteins in the Protein Data Bank performed through the DALI Web server identified only one structure with a *Z* score above 10 (19% identity, 30% similarity), i.e., that of cytochrome *c* from *R. marinus* (3CP5 [53]). The backbone root mean square deviation between the latter structure and the mean minimized structure of pp-Cyt *c* is 3.4 Å (calculated on the fragments 1–17 and 27–95). pp-Cyt *c* shares a very similar fold with 3CP5, with the exception of a longer N-terminal region comprising an additional α-helix in cytochrome *c* from *R. marinus*. Interestingly, helix α4′, which is present in both cytochrome *c* structures, has been defined as characteristic of a subfamily of bacterial cytochrome *c* [53]. This structural region is often occupied by variable α-helical or β-sheet motifs which are distinctly placed in the respective amino acid sequences, supporting divergent evolution of *c*-type cytochromes, with several independent DNA deletion and insertion events.

Structural characterization of pp-Sco

Heteronuclear R_1 relaxation data (Fig. S4, average value 1.21 ± 0.14 s^{-1}) indicate that the protein reorients in solution as a monomer. Indeed, the value of 1.21 ± 0.14 s^{-1} compares well with the values for homologous proteins from different organisms with a similar fold in a monomeric state (hSco1, 1.38 ± 0.11 s^{-1} [4]; *B. subtilis* Sco1, 1.40 ± 0.06 s^{-1} [3]) and with the value expected for a monomeric pp-Sco (1.39 ± 0.05 s^{-1} at the same magnetic field and temperature as obtained from the HYDRONMR program [45]). Light scattering data obtained for pp-Sco at room temperature also confirm that the protein behaves in solution as a monomer. The R_2 mean value of pp-Sco

(23.4 ± 3.51 s^{-1}, Fig. S4) is, however, much higher than expected for a monomeric state (17.5 ± 0.64 s^{-1} at the same magnetic field and temperature as obtained from the HYDRONMR program for a monomeric protein state). As already found for hSco2 protein [5], which shows the presence of conformational fluctuations occurring along the whole amino acid sequence on a microsecond to millisecond timescale, the high R_2 values of pp-Sco are affected by an exchange contribution and indicate the occurrence of remarkable backbone motions. A model-free analysis was performed to substantiate the presence of microsecond to millisecond slow dynamics. We found that essentially all residues are affected by an exchange contribution to the transverse relaxation rate (mean R_{ex} value of 5.33 s^{-1}). This result is in agreement with what is expected on the basis of the global increase of the experimental R_2 values with respect to the predicted R_2 value of 17.5 ± 0.64 s^{-1} obtained for a rigid molecule.

The ^{1}H–^{15}N HSQC spectrum shows a large chemical shift dispersion, indicating a well-folded protein (Fig. S5). Also the average $^{15}N\{^{1}H\}$ NOE value (0.70 ± 0.17) is indicative of a well-folded protein. The variability of the $^{15}N\{^{1}H\}$ NOE among the various residues (Fig. S4) is larger than that typically observed for a rigid protein, indicating the presence of conformational flexibility. However, no negative heteronuclear NOEs were observed, with the exception of two residues at the C-terminus. This behavior, at variance with what is observed for highly mobile proteins, is in agreement with the above-discussed dynamic properties of pp-Sco [54].

Backbone chemical shift analysis indicated a secondary structure element arrangement typical of the Sco protein fold (34% α-helices and 15% β-strands). However, the 2D/3D NOESY spectra of pp-Sco have much fewer NOE cross-peaks than expected for a protein with a similar size (Fig. S5). The above-mentioned conformational exchange processes can justify the strong reduction in the number of NOE cross-peaks. Therefore, the resulting picture is that of a protein that has reasonably well defined secondary structural elements, but with a tertiary structure that is fluxional among different conformational arrangements. This behavior prevented us from obtaining a high-resolution structure of pp-Sco. A homology model approach was then pursued using the I-TASSER server [40], which combines the methods of threading, ab initio modeling, and structural refinement. The model obtained is in agreement with the folding topology derived from chemical shift analysis of pp-Sco. Sixty long-range NOEs connecting all secondary structure elements were also identified to validate the overall fold arrangement. The pp-Sco structure contains four α-helices and seven β-strands organized in a thioredoxin fold (Fig. 3a). The CXXXC metal-binding motif and the third ligand, His127, in loop 8 are close in space (Fig. 3a), suggesting the presence of the copper binding site common to eukaryotic Scos. Therefore, to address the metal binding properties of pp-Sco, we performed NMR titrations with both Cu(I) and Cu(II) ions.

Interaction with copper ions

An NMR titration was performed in anaerobic conditions on a reduced pp-Sco sample by addition of up to stoichiometric amounts of Cu(I) ions. The chemical shift changes, observed on the ^{1}H–^{15}N HSQC maps, show that Cys residues of the CXXXC metal-binding motif as well as surrounding residues were affected by metal additions. To monitor the metal binding effect on the putative His127 ligand, ^{2}J NH coupling-based ^{1}H–^{15}N HSQC experiments (Fig. S6) were performed during the titration. The chemical shift patterns of all His residues do not change upon metal addition, indicating that His127 is not involved in metal coordination. When pp-Sco was treated with an excess of 2–3 equiv of Cu(I), only 60% of copper was found to be bound to the protein, indicating the presence of a weak-affinity copper binding site. Indeed, working at a protein concentration of 0.1–0.2 mM, a tight-affinity site implicates that only 1 equiv of copper is necessary to fully charge the metal binding site. A titration of pp-Sco with Cu(I) up to 1 equiv in the presence of 1 equiv of GSH showed no chemical shift perturbation, indicating a Cu(I) affinity weaker than that of Cu(I) for GSH. Therefore, we conclude that the lack of His127 coordination in pp-Sco prevents the formation of a tight-affinity site, such as that found in hSco1 and hSco2 which typically involve the conserved His in metal coordination.

Previous works showed that Sco proteins are usually able to bind Cu(II) ions [11, 17]. By addition of 1 equiv of Cu(II) under anaerobic conditions to reduced apo pp-Sco, no evidence of the formation of Cu(II)–Sco species was observed in the UV–vis spectra [typically Cu(II)–Sco proteins have two bands at 360 and 470 nm], suggesting its inability to bind Cu(II) ion. The ^{1}H–^{15}N HSQC spectrum of the Cu(II)/pp-Sco solution showed the presence of the Cys-oxidized state of pp-Sco (Fig. 4a). The presence of a disulfide bond in pp-Sco was also confirmed by AMS SDS-gel analysis (Fig. 4b). The formation of Cu(I) ions, as a result of the redox reaction, was demonstrated through use of BCS, whose Cu(I) complex shows a characteristic absorbance at 483 nm. Taken together these data indicate that pp-Sco does not stably bind Cu(II) ion and is implicated in Cu(II) reduction in vitro.

Redox properties of pp-Sco

Several studies have pointed out that Sco proteins can act as thiol disulfide oxidoreductases [9, 18, 19]. They all share

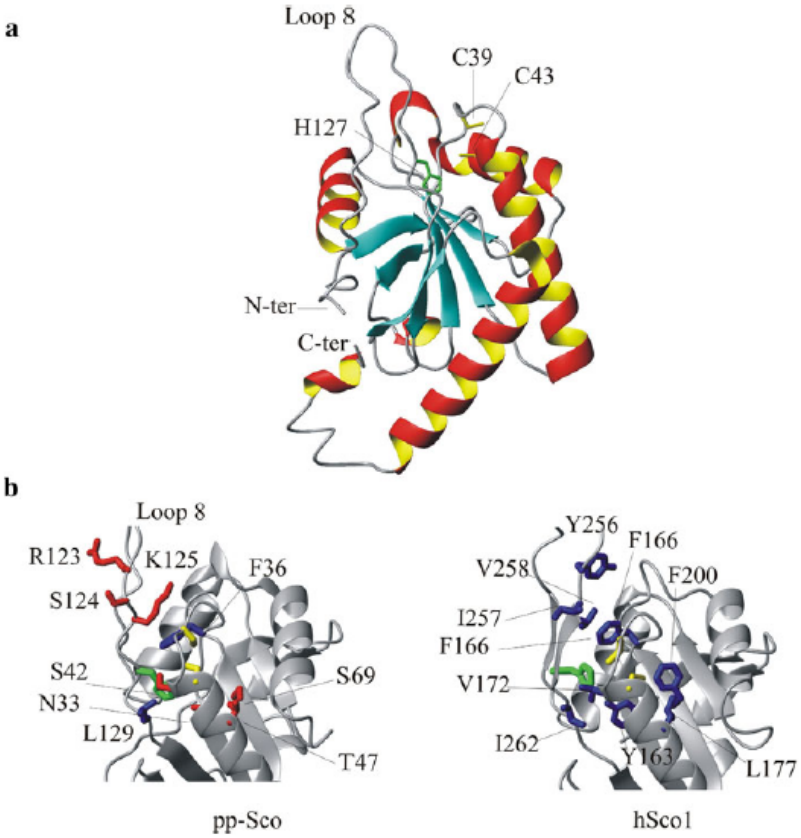

Fig. 3 Structural model of pp-Sco. **a** The overall fold (four α-helices and seven β-strands) is the same as found for homologous eukaryotic and bacterial Sco proteins organized in a thioredoxin fold. **b** The hydrophilic residues of pp-Sco close to the metal binding region replaced by hydrophobic residues in the eukaryotic Scos (i.e., human Sco1, in *blue*) are shown in *red*. In **a** and **b** the Cys residues belonging to the metal binding CXXXC motif and the putative third His ligand in loop 8 are shown in *yellow* and *green*, respectively

a thiol disulfide oxidoreductase fold but thioredoxin activity has been documented only for the Sco homolog from *R. sphaeroides* [19]. We investigated pp-Sco thioredoxin activity following the enhanced reduction of insulin in the presence of DTT. Figure 5 shows that *E. coli* thioredoxin can enhance the reduction of insulin, compared with control samples (DTT alone). When pp-Sco was reacted with insulin, reduction was about sixfold slower compared with thioredoxin, and there was a longer lag time (36 min). However, these data show that although not as kinetically effective as thioredoxin, pp-Sco is able to mediate the reduction of insulin disulfide bonds and its thioredoxin activity is about 2 times higher than that of the Sco homolog from *R. sphaeroides* [19]. Then, we investigated the electron transfer process between pp-Sco and pp-Cyt *c*. Specifically, on the basis of standard redox potential measurements of pp-Cyt *c* and pp-Sco domains (+0.260 ± 0.020 and −0.250 ± 0.022 mV, respectively), we may hypothesize there is an electron transfer reaction between oxidized Fe(III) pp-Cyt *c* and reduced pp-Sco with an electron transfer direction similar to that observed in the insulin reduction, Fe(III) thus being reduced to Fe(II) and the Cys residues of the CXXXC motif forming a disulfide bond. To probe this reaction, titrations of reduced pp-Sco with oxidized pp-Cyt *c* under anaerobic conditions were performed and followed by NMR spectroscopy (see "Materials and methods" for details). Addition of a stoichiometric amount (2:1) of pp-Cyt *c* to pp-Sco was able to completely oxidize the latter protein upon reduction of iron in pp-Cyt *c*, as shown by the final NMR spectra (Fig. 6a, b). This result was confirmed by the UV–vis spectrum of the final mixture, which shows characteristic absorbances at 416, 521, and 550 nm due to the presence of reduced pp-Cyt *c* (Fig. 6c). NMR data also show that the oxidized and reduced states of the ^{15}N-detected protein interconvert slowly (more than milliseconds) on the NMR timescale, and that no accumulation of the pp-Cyt *c*/pp-Sco complex occurs in solution, and therefore a highly transient protein–protein interaction is predicted to be at the basis of the observed electron transfer process.

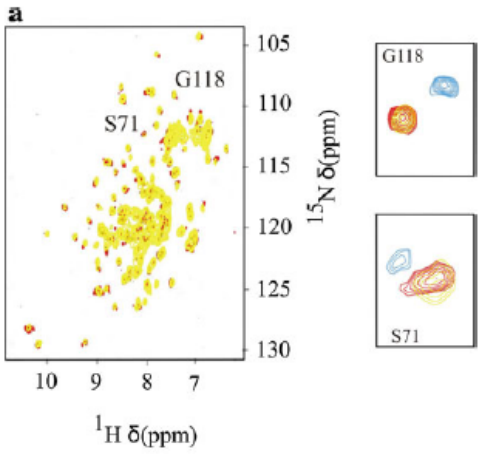

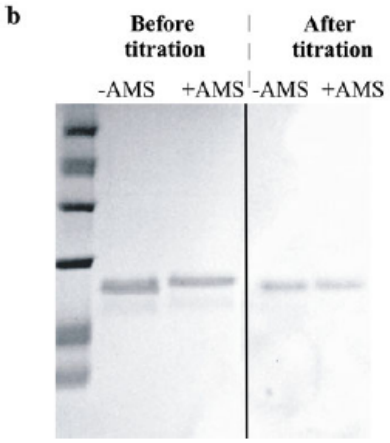

Fig. 4 Interaction of pp-Sco with Cu(II) ions. **a** The presence of the Cys-oxidized state of pp-Sco was revealed by the comparison of ^{1}H–^{15}N heteronuclear single quantum coherence (HSQC) spectra of the Cu(II)/pp-Sco mixture (*red*) and the oxidized sample (*yellow*). Zoom regions showing selected residues (Gly118 and Ser71) which monitor the redox state of pp-Sco are shown in *yellow*, *blue*, and *red* for oxidized sample, reduced sample, and Cu(II)/pp-Sco mixture, respectively. **b** The change of the redox state of pp-Sco from the reduced to the oxidized state was verified through not reducing 4-acetamido-4′-maleimidylstilbene-2,2′-disulfonic acid (*AMS*) SDS-PAGE analysis, which was performed before and after titration of reduced pp-Sco with 1 equiv of Cu(II). After Cu(II) addition, no band shift was observed in the presence or absence of AMS, indicating the resulting oxidized state of the pp-Sco protein

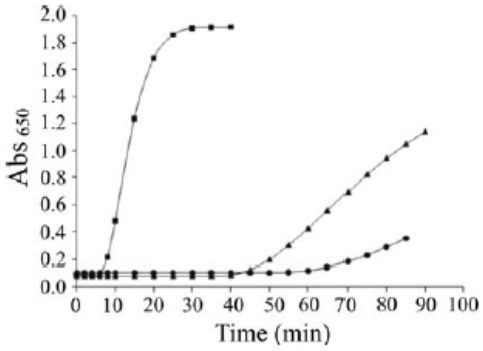

Fig. 5 Insulin reductase activity of pp-Sco. pp-Sco (5 μM, *triangles*) activity was compared with *Escherichia coli* thioredoxin activity (5 μM, *squares*), and dithiothreitol activity (0.5 mM, *circles*). The precipitation of insulin was monitored at 650 nm for 90 min

Discussion

The Cu_A center is contained within subunit II in the CcO subfamily of heme–copper oxidases. Cu_A receives electrons from reduced cytochrome *c* and passes them onto a low-spin heme center (i.e., cytochrome *a*) present in subunit I of CcO. Sco proteins have been implicated as an accessory factor in the assembly of CcO. Evidence from studies in yeast, *B. subtilis*, and *T. thermophilus* supports a specific role of Scos in the assembly of the Cu_A center of CcO [9, 13–16]. Several different molecular views have been proposed for the Sco's role in Cu_A assembly. Sco has been proposed to be a copper-delivery agent that specifically brings copper to apo subunit II of CcO [17]. The discovery that Sco is a member of the thioredoxin family has rekindled interest in a possible redox role for Sco in the Cu_A assembly [55]. The Cu_A site includes two copper ions bridged by two thiol side chains from two close-by Cys residues. The two Cys residues need to be in a reduced state because formation of a disulfide bond would preclude incorporation of copper into the Cu_A site. Therefore, the thiol oxidoreductase function of the Sco protein can be relevant for the Cu_A site formation. This mechanism has been demonstrated to be operative in the assembly of the Cu_A site of *T. thermophilus* ba_3 oxidase [9]. The thiol disulfide oxidoreductase activity has been also suggested to act with other homologs of the Sco family involved in the eukaryotic Cu_A assembly [18]. Another possibility, functionally unrelated to Cu_A assembly, is that the Cys-redox properties of Sco proteins serve in a more general role as a redox signaling molecule [6, 20].

In this work, we have focused on a Sco protein derived from *P. putida*, which is naturally fused with a typical redox transfer molecule, i.e., cytochrome *c*, to better understand the possible functional roles of the Sco proteins and structural determinants at the basis of the Sco function. We found that the pp-Sco domain is involved in electron transfer processes. The redox properties of pp-Sco include (1) thioredoxin activity or (2) reduction of Cu(II) to Cu(I) or (3) reduction of Fe(III) to Fe(II) in the pp-Cyt *c* protein. In particular, we have shown that pp-Sco is able to transfer electrons to pp-Cyt *c* and therefore to reduce Fe(III) to Fe(II). The Cu(II)–Cu(I)/Cys disulfide redox reactivity was also observed for *B. subtilis* Sco1 when the third His ligand

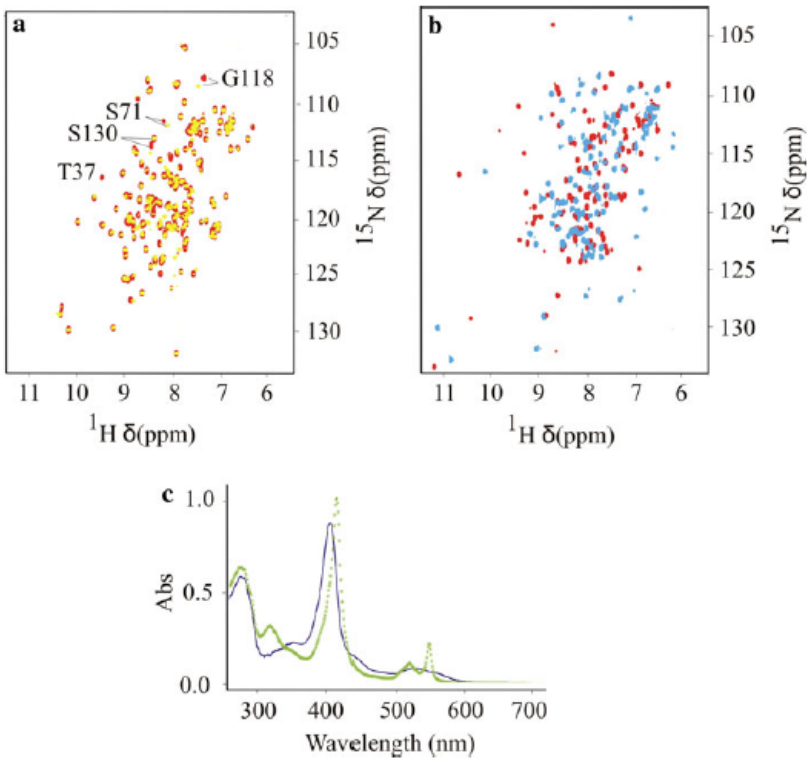

Fig. 6 pp-Sco/pp-Cyt *c* interaction. **a** Comparison of ^{1}H–^{15}N HSQC spectra before (*red*) and after (*yellow*) the addition of 2 equiv of oxidized unlabeled pp-Cyt *c* to a solution of reduced ^{15}N-labeled pp-Sco. **b** Comparison of ^{1}H–^{15}N HSQC before (*red*) and after (*blue*) the addition of 2 equiv of pp-Sco to a solution of oxidized ^{15}N-labeled pp-Cyt *c*. **c** UV–vis spectra of pp-Cyt *c* at the end of the titration (*green dots*). The characteristic absorbances at 416, 521, and 550 nm due to the reduced form of pp-Cyt *c* were observed. The UV–vis spectrum of oxidized pp-Cyt *c* is also shown (*blue line*)

was mutated [56] and in Sco from *R. sphaeroides* [19]. The peculiar redox properties found in pp-Sco are combined with copper binding properties different from those typically present in eukaryotic and the up to now investigated bacterial Sco proteins. The latter proteins always involve two Cys residues and one His residue in the copper ion coordination [12, 57, 58], suggesting a metallochaperone function for Cu(I) or Cu(II) ions. Differently, pp-Sco is able to bind Cu(I), but through the CXXXC motif only, i.e., without His ligand participation, thus resulting in a weak-affinity copper binding site and the inability to coordinate the Cu(II) ion. The affinity for Cu(I) is weaker than that of the copper ligand glutathione, so we can predict that the periplasmic concentration of glutathione [59] can remove copper ion from the weak-affinity metal binding site of pp-Sco. These results suggest that pp-Sco does not function as a Cu(II) chaperone nor, most likely, as a Cu(I) chaperone. They also indicate that the His ligand coordination is the discriminating factor for introducing the metallochaperone function in Sco proteins. This points out a relation between the coordination of the His ligand and the functional properties of the CXXXC motif, which can be either a copper chaperone or thioredoxin, or both. The functional relevance of the His location in a thioredoxin fold is also supported by the finding that when in human thioredoxin a His residue is introduced in place of a conserved *cis*-Pro located in the loop featuring the conserved His in Sco proteins, copper binding is observed [26].

In eukaryotic Scos the His residue takes a single conformation bound to the Cu(I) ion [4, 5]. In contrast, extended X-ray absorption fine structure data on the Cu(I) form of *B. subtilis* ScoI suggested that Cu(I) coordination is described by an equilibrium between two equally populated His-on and His-off states [25, 56]. This different structural-dynamic property may determine the weaker Cu(I) binding affinity usually observed for the bacterial Scos, i.e., from *B. subtilis* and *R. sphaeroides*, with respect to the eukaryotic ones [10, 12, 19]. Since all the bacterial Scos investigated up to now have a His ligand in the surroundings of the CXXXC motif, it can be argued that the residues affecting the second coordination sphere of the Cu(I) ion are mainly responsible for the structural-dynamic variability of bacterial Scos versus mitochondrial Scos. These second-sphere interactions would thus influence metal binding affinity determining His coordination. To identify these interactions, we compared the crystal structures of human and yeast apo Scos with the crystal structure of pp-Sco, specifically analyzing the metal binding region surrounding the CXXXC motif and the His-ligand loop. We found that in the proximity of the CXXXC motif and the His ligand, eukaryotic Scos have a hydrophobic network which is absent in pp-Sco. Indeed, Asn33, Ser42,

Thr47, and Ser69, close to the CXXXC motif, and Arg123, Ser124, and Lys125, in the His-ligand loop, of pp-Sco, are replaced by hydrophobic aromatic and aliphatic residues in eukaryotic Scos (Fig. 3b). The interactions between the latter hydrophobic residues can be essential, in the metallated state of eukaryotic Scos, to stabilize the two protein regions containing the metal ligands which are located far apart from each other in the apo form, and to determine the appropriate coordination geometry. Both aspects contribute to form a tight-affinity copper binding site. On the other hand, the lack of these interactions in pp-Sco does not allow appropriate ligand orientation and structural stability of the two distant metal- ligand-containing regions, thus determining the inability of pp-Sco to firmly bind either Cu(II) or Cu(I) ions. The conformational plasticity observed for the metal-ligand-containing region of pp-Sco is also present in another well-characterized bacterial Sco protein. Indeed, the crystal structure of apo *B. subtilis* Sco1 showed that, in two crystallographically independent molecules, the His copper ligand is oriented either close to or far from the Cys ligands and that both loops containing the copper ligands exhibit conformational disorder in the structure [8]. This behavior indicates that the copper ligands sample different conformations and that crystallization freezes the lowest-energy ones. This is also in agreement with NMR solution data of the same protein showing that both loops display large conformational motions [3]. Therefore, we propose a model where the conserved His ranges between conformations suitable or not suitable to coordinate Cu(I) ion as a consequence of the presence or lack of hydrophobic interactions in the surrounding metal binding region. These structural properties establish the molecular grounds to address the divergent function of the Sco protein family.

Our results therefore identify a Sco protein with redox activities but without relevant copper binding abilities. This suggests that the pp-Sco domain of the pp3183 protein is involved in functional processes which are alternatives to a metallochaperone function. One of the *pp_3183* neighboring genes codifies for a protein containing GGDEF and EAL domains able to regulate the concentration of c-di-GMP, which is a key player in the selection between the motile planktonic and sedentary biofilm-associated bacterial "lifestyles." GGDEF and EAL domains are often associated with sensor PAS (Per-Arnt-Sim) domains [60], which work as sensors for the perception of changes in oxygen concentration, light intensity, voltage, and redox potential [61]. In particular, a class of bacterial signal transduction proteins possesses a soluble N-terminal cytochrome *c* PAS domain (sensor domain) in the periplasm and the C-terminal GGDEF and EAL domains (transduction domains) in the cytoplasm [62]. Both pp-Cyt *c* and pp-Sco domains are predicted to be periplasmic. Thus, in analogy with the functional role found for the periplasmic cytochrome *c*-containing PAS domains, pp-Cyt *c* and pp-Sco could work as sensor domains perceiving changes in periplasmic redox potential crucial to be transmitted to the cytoplasm for activating cellular responses. Similarly, cytoplasmatic electron transfer processes have been found in flavin-binding PAS domains which work as a sensor in signal transduction through changes in the redox state of its flavin adenine dinucleotide prosthetic group [63].

In conclusion, we have characterized a Sco protein implicated in electron transfer processes and not in copper binding. The inability of the His residue to be coordinated to the copper ion prevents the formation of a tight-affinity metal binding site. This finding suggests that during evolution, specific amino acid variations occurred in the surroundings of the CXXXC catalytic site in a thioredoxin-like fold to acquire copper binding affinities at different levels from bacteria to eukaryotes. The redox properties found in the pp-Sco domain and the genome context analysis of pp3183 protein contribute to describing an appealing view on the possible functional processes involving the Sco protein family, above all related to cellular signaling pathways.

Acknowledgments This work was supported by the European Commission ("From Receptor to Gene: Structures of Complexes from Signaling Pathways Linking Immunology, Neurobiology and Cancer," SPINE2-COMPLEXES contract LSHG-CT-2006-031220). Italian FIRB PROTEOMICA MIUR contract RBRN07BMCT and PRIN 2007 contract 2007M5MWM9 are also acknowledged for financing.

References

1. Banci L, Bertini I, Cavallaro G, Rosato A (2007) J Proteome Res 6:1568–1579
2. Arnesano F, Banci L, Bertini I, Martinelli M (2005) J Proteome Res 4:63–70
3. Balatri E, Banci L, Bertini I, Cantini F, Ciofi-Baffoni S (2003) Structure 11:1431–1443
4. Banci L, Bertini I, Calderone V, Ciofi-Baffoni S, Mangani S, Martinelli M, Palumaa P, Wang S (2006) Proc Natl Acad Sci USA 103:8595–8600
5. Banci L, Bertini I, Ciofi-Baffoni S, Gerothanassis IP, Leontari I, Martinelli M, Wang S (2007) Structure 15:1132–1140
6. Williams JC, Sue C, Banting GS, Yang H, Glerum DM, Hendrickson WA, Schon EA (2005) J Biol Chem 280:15202–15211
7. Abajian C, Rosenzweig AC (2006) J Biol Inorg Chem 11:459–466
8. Ye Q, Imriskova-Sosova I, Hill BC, Jia Z (2005) Biochemistry 44:2934–2942
9. Abriata LA, Banci L, Bertini I, Ciofi-Baffoni S, Gkazonis P, Spyroulias GA, Vila AJ, Wang S (2008) Nat Chem Biol 4:599–601
10. Banci L, Bertini I, Ciofi-Baffoni S, Kozyreva T, Zovo K, Palumaa P (2010) Nature 465:645–648

11. Imriskova-Sosova I, Andrews D, Yam K, Davidson D, Yachnin Y, Hill BC (2005) Biochemistry 44:16949–16956
12. Davidson DE, Hill BC (2009) Biochim Biophys Acta 1794:275–281
13. Mattatall NR, Jazairi J, Hill BC (2000) J Biol Chem 275:28802–28809
14. Lode A, Kuschel M, Paret C, Rodel G (2000) FEBS Lett 485:19–24
15. Schulze M, Rodel G (1988) Mol Gen Genet 211:492–498
16. Rigby K, Cobine PA, Khalimonchuk O, Winge DR (2008) J Biol Chem 283:15015–15022
17. Horng YC, Leary SC, Cobine PA, Young FB, George GN, Shoubridge EA, Winge DR (2005) J Biol Chem 280:34113–34122
18. Leary SC, Sasarman F, Nishimura T, Shoubridge EA (2009) Hum Mol Genet 18:2230–2240
19. Badrick AC, Hamilton AJ, Bernhardt PV, Jones CE, Kappler U, Jennings MP, McEwan AG (2007) FEBS Lett 581:4663–4667
20. Leary SC, Cobine PA, Kaufman BA, Guercin GH, Mattman A, Palaty J, Lockitch G, Winge DR, Rustin P, Horvath R, Shoubridge EA (2007) Cell Metab 5:9–20
21. Glerum DM, Shtanko A, Tzagoloff A (1996) J Biol Chem 271:14504–14509
22. Glerum DM, Shtanko A, Tzagoloff A (1996) J Biol Chem 271:20531–20535
23. Horng YC, Cobine PA, Maxfield AB, Carr HS, Winge DR (2004) J Biol Chem 279:35334–35340
24. Banci L, Bertini I, Ciofi-Baffoni S, Leontari I, Martinelli M, Palumaa P, Sillard R, Wang S (2007) Proc Natl Acad Sci USA 104:15–20
25. Andruzzi L, Nakano M, Nilges MJ, Blackburn NJ (2005) J Am Chem Soc 127:16548–16558
26. Su D, Berndt C, Fomenko DE, Holmgren A, Gladyshev VN (2007) Biochemistry 46:6903–6910
27. Banci L, Bertini I, Ciofi-Baffoni S, Katsari E, Katsaros N, Kubicek K, Mangani S (2005) Proc Natl Acad Sci USA 102:3994–3999
28. Arslan E, Schulz H, Zufferey R, Kuenzler P, Thoeny-Meyer L (1998) Biochem Biophys Res Commun 251:744–747
29. Keller RLJ (2004) The computer aided resonance assignment tutorial. CANTINA, Goldau
30. Wishart DS, Sykes BD (1994) J Biomol NMR 4:171–180
31. Guntert P (2004) Methods Mol Biol 278:353–378
32. Cornilescu G, Hu J-S, Bax A (1999) J Am Chem Soc 121:2949–2950
33. Baistrocchi P, Banci L, Bertini I, Turano P, Bren KL, Gray HB (1996) Biochemistry 35:13788–13796
34. Banci L, Bertini I, Bren KL, Gray HB, Sompornpisut P, Turano P (1995) Biochemistry 34:11385–11398
35. Banci L, Bertini I, Quacquarini G, Walter O, Diaz A, Hervás M, De la Rosa MA (1996) J Biol Inorg Chem 1:330–340
36. Banci L, Bertini I, Bren KL, Gray HB, Sompornpisut P, Turano P (1997) Biochemistry 36:8992–9001
37. Case DA, Darden TA, Cheatham TE, Simmerling CL, Wang J, Duke RE, Luo R, Merz KM, Wang B, Pearlman DA, Crowley M, Brozell S, Tsui V, Gohlke H, Mongan J, Hornak V, Cui G, Beroza P, Schafmeister CE, Caldwell JW, Ross WS, Kollman PA (2008) AMBER 10. University of California, San Francisco
38. Bhattacharya A, Tejero R, Montelione GT (2007) Proteins 66:778–795
39. Vriend G (1990) J Mol Graph 8:52–56
40. Zhang Y (2008) BMC Bioinformatics 9:40
41. Shen Y, Delaglio F, Cornilescu G, Bax A (2009) J Biomol NMR 44:213–223
42. Kay LE, Nicholson LK, Delaglio F, Bax A, Torchia DA (1992) J Magn Reson 97:359–375
43. Grzesiek S, Bax A (1993) J Am Chem Soc 115:12593–12594
44. Tjandra N, Feller SE, Pastor RW, Bax A (1995) J Am Chem Soc 117:12562–12566
45. Garcia de la Torre JG, Huertas ML, Carrasco B (2000) J Magn Reson 147:138–146
46. Dosset P, Hus JC, Blackledge M, Marion D (2000) J Biomol NMR 16:23–28
47. Craig DB, Nichols ER (2006) J Chem Educ 83:1325–1326
48. Haugstetter J, Blicher T, Ellgaar L (2005) J Biol Chem 280:8371–8380
49. Holmgren A (1979) J Biol Chem 254:9627–9632
50. Hengge R (2009) Nat Rev Microbiol 7:263–273
51. Schirmer T, Jenal U (2009) Nat Rev Microbiol 7:724–735
52. Bertini I, Cavallaro G, Rosato A (2006) Chem Rev 106:90–115
53. Stelter M, Melo AM, Pereira MM, Gomes CM, Hreggvidsson GO, Hjorleifsdottir S, Saraiva LM, Teixeira M, Archer M (2008) Biochemistry 47:11953–11963
54. Yao J, Chung J, Eliezer D, Wright PE, Dyson HJ (2001) Biochemistry 40:3561–3571
55. Winge DR (2003) Structure 11:1313–1314
56. Siluvai GS, Nakano MM, Mayfield M, Nilges MJ, Blackburn NJ (2009) Biochemistry 48:12133–12144
57. Cawthorn TW, Poulsen BE, Davidson DE, Andrews D, Hill BC (2009) Biochemistry 48:4448–4454
58. Saenkham P, Vattanaviboon P, Mongkolsuk S (2009) FEMS Microbiol Lett 293:122–129
59. Messens J, Collet JF, Van Belle K, Brosens E, Loris R, Wyns L (2007) J Biol Chem 282:31302–31307
60. Taylor BL, Zhulin IB (1999) Microbiol Mol Biol Rev 63:479–506
61. Gilles-Gonzalez MA, Gonzalez G (2004) J Appl Physiol 96:774–783
62. Londer YY, Dementieva IS, D'Ausilio CC, Pokkuluri PR, Schiffer M (2006) FEMS Microbiol Lett 258:173–181
63. Qi Y, Rao F, Luo Z, Liang ZX (2009) Biochemistry 48:10275–10285

SUPPLEMENTARY MATERIAL

SCO PROTEINS ARE INVOLVED IN ELECTRON TRANSFER PROCESSES

Lucia Banci[1,2], Ivano Bertini[1,2], Simone Ciofi-Baffoni[1,2], Tatiana Kozyreva[1], Mirko Mori[1,2], and Shenlin Wang[1]

[1]Magnetic Resonance Center CERM, University of Florence, Via Luigi Sacconi 6, 50019, Sesto Fiorentino, Florence, Italy.

[2]Department of Chemistry, University of Florence, Via della Lastruccia 3, 50019 Sesto Fiorentino, Florence, Italy.

Table S1. NMR experiments performed on pp-Cyt c and pp-Sco for spectral assignment and structural and dynamic characterization.

Experiments	Dimension of acquired data (nucleus)			Spectral width (ppm)			NS[a]
	t_1	t_2	t_3	F_1	F_2	F_3	
[^{1}H-^{1}H]-NOESY[b]	1024 (^{1}H)	2048 (^{1}H)		16	16		128
^{1}H-^{15}N-HSQC[d]	256 (^{15}N)	1024 (^{1}H)		40	16		8
^{1}H-^{13}C-HSQC[d]	256 (^{13}C)	1024 (^{1}H)		80	20		8
CBCANH[c]	112 (^{13}C)	48 (^{15}N)	1024 (^{1}H)	80	36	14	32
CBCA(CO)NH[c]	106 (^{13}C)	48 (^{15}N)	1024 (^{1}H)	80	36	14	32
HNCO[d]	88 (^{13}C)	48 (^{15}N)	2048 (^{1}H)	20	36	14	8
HNCA[d]	112 (^{13}C)	48 (^{15}N)	2048 (^{1}H)	40	36	14	16
HN(CO)CA[d]	128 (^{13}C)	48 (^{15}N)	2048 (^{1}H)	40	36	14	16
HN(CA)CO[d]	128 (^{13}C)	48 (^{15}N)	2048 (^{1}H)	40	36	14	16
(h)CCH-TOCSY[d]	208 (^{13}C)	50(^{13}C)	1024 (^{1}H)	78	78	14	16
^{13}C-edited [^{1}H-^{1}H]-NOESY[e]	200 (^{1}H)	50 (^{13}C)	1024 (^{1}H)	78	14	14	32
^{15}N-edited [^{1}H-^{1}H]-NOESY[e]	148 (^{1}H)	44 (^{15}N)	1024 (^{1}H)	13	35	12	32
^{15}N R_1[e,f]	128 (^{15}N)	1024 (^{1}H)		40	16		16
^{15}N R_2[c,f]	128 (^{15}N)	1024 (^{1}H)		40	16		16
steady-state heteronuclear NOEs[e,f]	128 (^{15}N)	1024 (^{1}H)		40	16		16

[a] number of acquired scans. NMR spectra were acquired using Bruker Avance 900[b], 800[c], 700[d], 600[e] and 500[f] spectrometers operating at proton nominal frequencies of 899.20, 800.13, 700.13, 600.13, and 500.13 MHz, respectively. All used triple-resonance (TXI 5-mm) probes were equipped with pulsed-field gradients along the z-axis. The 900, 800, 700 and 500 MHz spectrometers were equipped with a triple-resonance cryoprobe.

Table S2. ^{1}H, ^{15}N and ^{13}C resonance assignments (ppm) for pp-Sco at 308 K.

Residue	N	HN	C	CA	HA	CB	HB	CD
G1	105.600	7.730	175.984	44.212	3.859			
A2	119.448	7.620	178.741	52.575	4.296	15.491		
S3	114.613	7.890	172.612	63.353	4.023	65.443	4.430	
Y4	124.720	8.250	172.468	52.878		39.058		
F5	115.523	8.650		53.971				
N7	115.718	7.840	173.162	52.526		31.461		
I8	126.614	8.830						
L10	122.782	8.990	172.030	50.523	4.824	45.989	1.501	25.507
							1.289	
L11	119.953	8.890	174.616	50.115	5.480	43.323	1.429	24.160
							1.225	
T12	109.151	8.450	175.518	57.286	5.467	70.258	3.870	19.013
Q13	116.542	8.390	171.000	55.587	4.109	24.324	1.986	31.133
							1.917	
D14	117.332	7.700	173.724	51.496	4.958	38.350	2.639	
							2.562	
G15	109.240	8.490	170.856	42.985	4.162			
					3.396			
E16	118.958	7.130	178.166	52.820	4.258	27.669	2.046	33.470
							1.919	
K17	119.257	7.830	176.696	56.508	4.050	29.462	1.950	22.351
							1.931	
V18	120.060	7.950	175.460	62.311	3.610	36.282	1.551	15.079
								11.453
H19	117.347	7.930	173.158	53.050	3.779	26.547	3.217	
							2.970	
F20	122.406	8.110		58.055	4.236	35.266	3.085	
							2.991	
F21	121.132	9.240	173.011	54.184	4.223	37.540	2.984	
							2.818	
D22	119.698	7.900	173.601	54.102				
D23	119.218	8.060	177.686	51.775	4.524	38.346	2.642	
							2.562	
L24	119.751	7.990	172.865	54.014	4.158	39.324	1.667	24.403
I25	114.856	8.040	177.101	57.619				
K26	119.753	8.050		53.900				
D27	118.261	6.890	173.141	49.388	4.870	38.495	2.650	
							2.565	
K28	115.638	7.400	175.863	56.419	4.099	27.220	1.923	
V29	119.852	7.780	174.137	64.529	3.255	28.245	2.198	20.797
							1.580	18.936
V30	119.198	8.530	171.892	57.242				
A31	125.181	9.010	173.878	48.100	5.255	18.234		

Residue	N	HN	C	CA	HA	CB	HB	CD
I32	117.972	8.950	171.032	52.532	4.472	38.935		23.961
								22.651
N33	121.405	8.610	174.546	52.620	4.903	36.178	2.733	
							2.650	
F34	120.363	8.260	172.353	53.879	4.279	33.547	2.357	
							2.223	
I35	122.108	7.710	173.389	59.542	4.096	34.569		
F36	117.278	8.660	173.964	55.122	4.536	35.903	3.069	
							2.917	
T37	116.658	9.450	174.252	60.847	4.163	68.527		
G38	109.933	8.720	172.094	42.865				
C39	116.860	7.770	172.899	57.624		28.728		
S40	118.453	8.910	172.333	53.611				
D41	122.314	8.260	176.927	52.135				
S42	116.511	8.120	174.299	58.977		60.585		
C43	122.501	8.410		56.158				
V45	121.140	8.550	171.057	55.255				
E46	120.627	8.070	173.101	47.547		20.065		
T47	120.658	9.460		57.425	4.115	67.293		
R49	120.802	7.870	174.827	57.252	4.370	29.279	2.393	
L50	119.149	7.950	173.360	56.619	4.019			
R51	122.725	7.930	173.545	53.720	4.102	30.123	1.749	26.280
							1.666	
Q52	120.769	8.020	175.931	56.186	3.733	26.561	2.038	
							1.917	
V53	118.778	8.640	176.439	57.768		29.022		
Q54	118.558	8.240	175.915	56.619	4.084	26.745	2.044	33.812
							1.936	
K55	116.751	7.880	173.231	54.963	4.136	31.259	1.788	21.877
							1.681	
I56	122.886	7.880	173.216	58.335		35.605		
L57	125.358	8.330	176.287	53.108		41.015		
G58	108.742	7.910		44.570	3.911			
					3.786			
D59	116.203	8.520	172.827	56.734				
R60	120.648	8.620	177.015	55.928	4.278			
V61	120.921	7.760	173.504	60.730	4.108	26.875	2.223	19.380
								18.988
G62	114.505	8.760	169.360	42.517	4.280	31.000		
					3.940			
K63	121.903	7.690	172.180	54.777	4.554		1.786	22.153
							1.684	
D64	113.335	8.380	172.640	50.570	4.496	38.828	2.463	
I65	121.581	7.120	170.741	57.984	4.048	39.864		
F66	126.358	8.640	169.609	55.065	4.341	39.655	2.759	
L67	121.126	7.170	172.333	50.145	3.914	38.834		

Residue	N	HN	C	CA	HA	CB	HB	CD
Y68	120.377	8.910	178.022	52.935	4.843	39.509	2.864	
S69	118.733	8.270	176.842	56.683	3.986	61.925		
I70	116.052	8.090	170.198	59.655	3.864	36.555		
S71	111.740	8.158	167.435	54.080		63.002		
I72	125.083	8.830	177.248	57.137	5.583			
D73	121.456	8.790		48.438	5.240	39.077	2.319	
Y74	117.010	7.810	174.137	57.648	4.198	34.922	3.109	
							3.007	
N76	113.326	7.280	172.374	51.036	4.627	35.834	2.915	
D77	121.999	8.200	173.897	52.054				
T78	116.157	7.960		56.640	4.017	60.795	4.375	
T81	119.579	7.910	173.590	62.334	4.480	69.982		
L82	119.878	8.060	175.632	54.753	3.741	40.747		24.388
K83	120.507	8.600	176.180	56.679	4.043	29.583	1.944	22.374
R84	119.178	7.650	175.777	56.331	4.096	27.317	2.031	24.790
							1.908	
Y85	122.591	7.740	173.935	59.082	3.983	35.174	3.123	
							2.739	
A86	119.706	8.410	177.447	52.180	3.794	14.769		
E87	116.587	8.030	176.786	55.969	3.946	27.028	2.077	33.795
							1.924	
K88	120.744	8.090	175.734	56.292	4.036	29.274	1.947	22.399
F89	112.887	7.420	172.698	54.719	4.544	35.950		
G90	108.243	7.350	172.094	44.623	3.907			
					3.777			
I91	121.112	7.780	173.964	60.732	3.926			
G92	116.451	8.160		41.878	3.926			
					3.751			
T96	117.206	8.520	174.446	55.792				
L97	118.109	8.780	172.986	51.266	4.523	41.712		
L98	118.994	8.450	172.640	50.908	5.397	41.350	1.613	26.227
							1.425	
T99	114.267	8.790	168.820	56.043	4.019	60.597	3.502	22.311
G100	108.592	8.160	169.101	42.198	3.940			
E101	121.319	9.280		51.496	4.501			
D103	116.195	9.030	176.071	54.662	4.347	37.318	2.632	
							2.579	
D104	120.672	7.040	175.154	54.559	4.426	37.740	2.627	
							2.589	
I105	120.745	7.940	175.461	60.596	3.879	34.421	2.019	25.777
								14.146
E106	120.627	8.250	175.863	57.045	3.997	25.820	2.094	32.947
							1.975	
Q107	118.094	7.640	173.216	52.676	4.465	29.375	2.089	
							1.969	
L108	126.842	8.890	169.676	48.100		38.828		
				5				

Residue	N	HN	C	CA	HA	CB	HB	CD
R109	118.384	8.500	172.899	54.086		28.123		
R110	123.801	7.700	174.425	54.745				
S111	118.574	8.370	170.636	55.546	4.539	61.390	3.924	
							3.779	
L112	125.989	8.030	176.266	52.245	4.463	39.648	1.593	24.096
							1.498	
G113	104.051	7.000	169.302	42.690	4.284			
					4.106			
L114	124.761	7.550	172.090	49.885				
W115	123.237	8.990	172.612	59.732				
I116	115.177	8.270	174.301	58.868		36.296		
D117	117.285	8.070		55.228	3.806	38.755	2.952	
							2.595	
G118	108.508	7.270	173.532	42.633	3.778			
L119	125.749	7.760	171.691	54.950				
E120	123.116	7.850	172.151	52.717		27.777		
N121	124.213	8.450	173.216	53.108	4.283	31.346	2.420	
							2.321	
G122	113.575	8.410		44.554	3.912			
					3.785			
R123	120.707	8.590	172.842	53.251		30.770		
S124	118.362	9.640	170.191	52.360	4.892	60.124	3.883	
							3.783	
K125	123.489	8.190	172.151	53.223	4.457	28.238		
D126	117.571	7.960	173.728	52.950	4.380	37.562	2.813	
							2.651	
H127	115.377	7.440	173.826	55.986	4.321	28.698		
N128	119.293	9.180	173.590	54.374	4.495	35.950	2.787	
							2.731	
L129	120.731	7.120	173.360	54.002		62.140		
S130	113.920	8.440	170.396	56.561	4.363	41.631	3.843	
L131	123.588	8.360	172.468	52.014	4.938	38.828	1.608	23.750
I132	125.229	8.930	172.201	57.261	4.179	39.842		
					3.985			
I133	120.382	8.940	171.716	55.744				
G134	108.417	8.520	167.489	43.726				
N135	114.505	7.540	172.525	47.698		37.447		
Q136	122.695	8.560	176.050	56.734	4.069	26.396	2.031	31.129
							1.918	
A137	117.112	7.910	176.756	51.971	4.114	16.036		
T138	104.091	6.970	173.590	58.137	4.348	66.455	4.286	18.828
G139	110.237	7.750	170.918	43.726	4.169			
					3.992			
R140	120.848	7.050	175.756	52.456	4.373	28.218	1.806	24.284
							1.722	

Residue	N	HN	C	CA	HA	CB	HB	CD
W141	123.354	8.220	175.720	54.835		35.490	3.076	
							2.918	
M142	120.955	8.820	175.835	56.546	4.075	28.583	2.031	31.141
							1.911	
K143	117.581	7.610	176.497	56.299	4.032	29.776	1.941	22.342
A144	121.438	8.150	175.432	55.640		16.257		
S145	118.535	8.680		57.828	4.362	67.236	4.224	
							4.112	
F147	113.877	7.620	172.782	54.429	4.491	37.332	2.974	
							2.810	
E148	118.900	7.740	174.961	53.892	4.239	27.470	2.038	34.549
							1.860	
S149	121.488	9.030		59.819	4.377			
Y151	115.352	7.400	175.642	59.094	3.978	35.999	3.127	
							2.745	
I152	121.288	7.160	175.921	60.526	3.873	34.322	2.020	25.797
								14.168
L153	119.940	7.710	175.806	55.440	4.167	39.404	1.641	24.391
							1.451	
A154	118.444	8.400	176.612	52.705	3.788	15.575		
D155	119.295	7.600	175.950	54.777	4.345	37.365	2.633	
							2.576	
R156	118.980	8.100	169.158	51.756	4.503	29.761	1.817	24.110
L157	119.161	8.110		54.709	4.098	40.677	1.551	24.369
N159	120.559	7.700	173.389	52.450	4.473	29.327	2.566	
							2.503	
S160	115.080	8.030	171.086	55.927	4.015	60.700	3.510	
L161	120.365	7.410	175.115	55.338	3.772	38.872	1.695	23.905
							1.397	
H162	111.450	7.820	173.820	53.511	4.347	38.828	3.121	
N163	113.400	6.420	174.597	52.319	4.506	36.641	2.738	
							2.644	
W164	114.115	6.640	172.266	57.367	4.377	35.375	2.997	
K165	120.321	7.290	171.086	55.835	3.946	33.845	2.414	25.767
							2.161	
Q166	120.377	9.980	172.583	53.856	4.293	27.777	2.046	33.602
							1.877	
A167	124.887	7.960	173.043	52.432	4.131	15.634		
S168	119.664	8.720	175.753	59.945	4.320		4.231	
							4.114	
A169	129.341	8.530		51.324	3.969	16.496		
M170	118.937	7.670	174.971	54.033	4.266	36.649		
S171	121.482	9.060		59.824				
N172	114.278	6.800	172.151	50.553	5.013		3.002	
							2.850	

Residue	N	HN	C	CA	HA	CB	HB	CD
D173	120.235	8.170	173.406	51.898	5.094	38.253	2.560	
							2.453	
Y174	119.866	7.930	172.957	55.295	4.500	35.605	3.066	
							2.916	
A175	124.455	7.990	174.655	49.942	4.241	16.381		
Q176	118.516	8.000	172.583	52.705	4.279	26.741	2.051	31.090
							1.929	
A177	126.342	8.160		47.985	4.537	15.233		
Q179	120.440	8.380	172.324	53.044	4.324	29.146	2.285	30.087
							2.184	
I180	122.574	8.270	172.120	51.947		38.399		
R181	119.797	8.120	171.221	55.387				
S182	118.526	7.180		51.615	4.076			

Table S3. Statistical analysis of the energy-minimized family of 20 conformers of pp-Cyt *c*

	pp-Cyt *c* (20 conformers)
r.m.s. violations per meaningful distance constraints (Å)[a]	
Intra-residue (418)	0.0110 ± 0.0009
Sequential (238)	0.0134 ± 0.0024
Medium range (241)	0.0125 ± 0.0026
Long range (147)	0.0103 ± 0.0030
Total (1044)	0.0120 ± 0.0009
r.m.s. violations per meaningful angle constraints (°)[a]	
Phi (100)	4.48 ± 1.01
Psi (100)	1.48 ± 1.48
Average number of constraints per residue (1266[b])	12
Average number of violations per conformer	
Phi	6.75 ± 1.67
Psi	1.45 ± 1.07
NOE violations larger than 0.3 Å	0.000 ± 0.00
NOE violations between 0.1 and 0.3 Å	5.25 ± 1.97
Average r.m.s.d. to the mean (Å)[c]	
Backbone	0.8
Heavy	1.4
Structural analysis[d]	
% of residues in most favourable regions	85.5
% of residues in allowed regions	13.2
% of residues in generously allowed regions	0.5
% of residues in disallowed regions	0.8
G-factor	-0.25
WHAT IF structure Z-scores[e]	

1st generation packing quality	-2.760
2st generation packing quality	-1.952
Ramachandran plot appearance	-2.066
χ_1/χ_2 rotamer normality	-1.305
Backbone conformation	-1.118
WHAT IF RMS Z-scores[e]	
Bond lengths	0.657
Bond angles	1.192
Omega angle restraints	1.552
Side chain planarity	1.113
Improper dihedral distribution	1.019
Inside/Outside distribution	1.008

[a] The number of meaningful constraints for each class is reported in parenthesis.

[b] Total number of NOE (1044), H-bond (22), angle constraints (200).

[c] The RMSD to the mean structure is reported considering the segments 1-17 and 27-95.

[d] As it results from the Ramachandran plot analysis. The statistic analysis is reported considering the segments 1-17 and 27-95.

[e] A Z-score is defined as the deviation from the average value for this indicator observed in a database of high-resolution crystal structures, expressed in units of the standard deviation of this database-derived average. Typically, Z-scores below a value of -3 are considered poor, those below -4 are considered bad. The statistic analysis is reported considering the segments 1-17 and 27-95.

Figure S1. The paramagnetic ^{1}H NMR spectrum of pp-Cyt *c* with the assignment of the paramagnetically shifted signals.

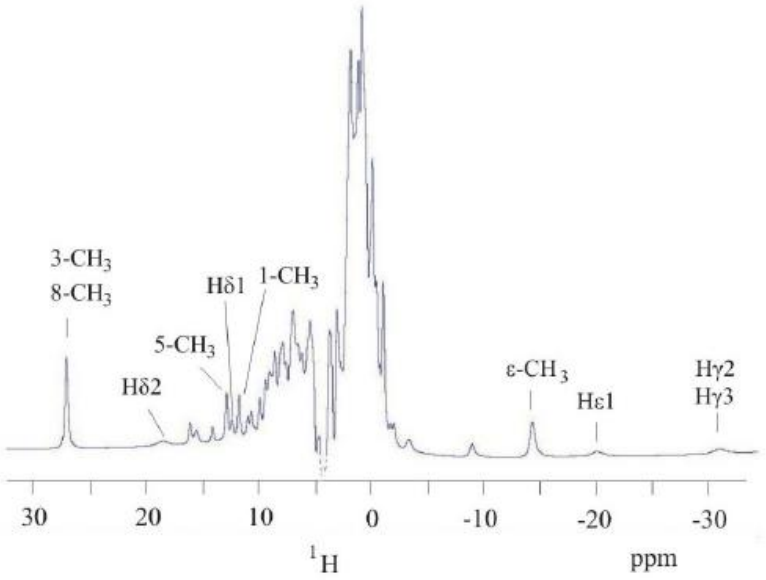

Figure S2. Alignment of Sco from *P. putida* (pp-Sco) with Sco proteins from yeast (ySco1), human (hSco1), *T. Thermophilus* (tSco) and *B. subtilis* (*Bs*Sco1). Conserved active site cysteines and histidines are in bold and highlighted in grey.

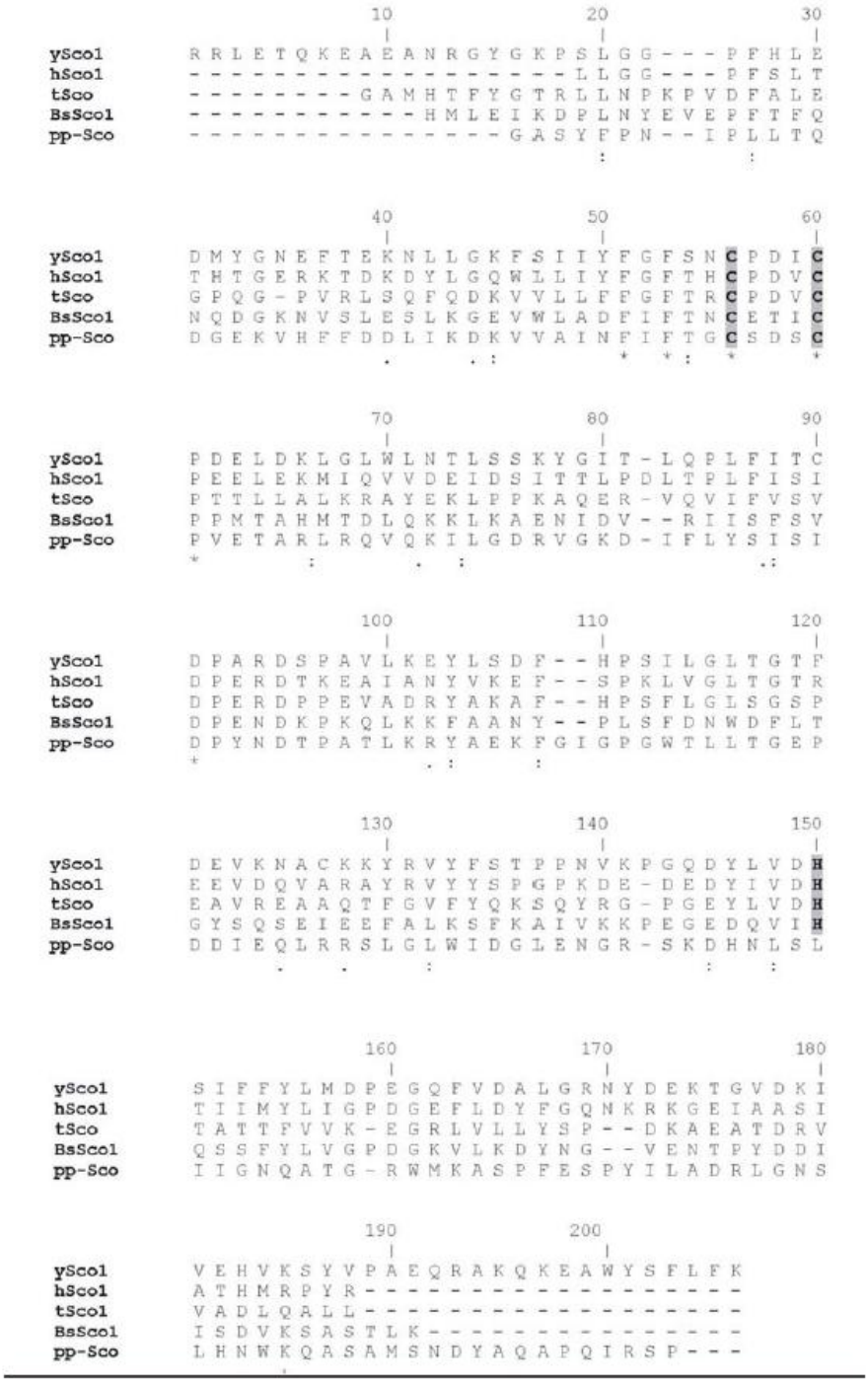

Figure S3. Amino acid sequences of the cloned constructs: the full-length pp3183 construct and the two constructs pp-Sco (in bold) and pp-Cyt *c* (in italic).

pp-3183 GSFTM**GASYFPNIPLLTQDGEKVHFFDDLIKDKVVAINFIFTGCSDSCPVETARLRQVQKILGDRVGKDIFLYSI**
SIDPYNDTPATLKRYAEKFGIGPGWTLLTGEPDDIEQLRRSLGLWIDGLENGRSKDHNLSLIIGNQATGRWMKAS
PFESPYILADRLGNSLHNWKQASAMSNDYAQAPQIRSP*SSGEQIFRTRCSSCHTVGNTEPGQPGIGPDLLGVTRQ*
RDANWLVRWLKVPDQMLAEKDPLAMLLFEQYNRLAMPNMRLGDAEVSALISYLEEETARLQTPVTNRGIP

pp-Sco GSFTM**GASYFPNIPLLTQDGEKVHFFDDLIKDKVVAINFIFTGCSDSCPVETARLRQVQKILGDRVGKDIFLYSI**
SIDPYNDTPATLKRYAEKFGIGPGWTLLTGEPDDIEQLRRSLGLWIDGLENGRSKDHNLSLIIGNQATGRWMKAS
PFESPYILADRLGNSLHNWKQASAMSNDYAQAPQIRSP

pp-Cyt *c* GSFTM*SGEQIFRTRCSSCHTVGNTEPGQPGIGPDLLGVTRQRDANWLVRWLKVPDQMLAEKDPLAMLLFEQYNRL*
AMPNMRLGDAEVSALISYLEEETARLQTPVTNRGIP

Figure S4. ^{15}N Relaxation parameters R_1, R_2, and heteronuclear $^{15}N\{^1H\}$ NOE versus residue number for both pp-Sco and pp-Cyt *c*.

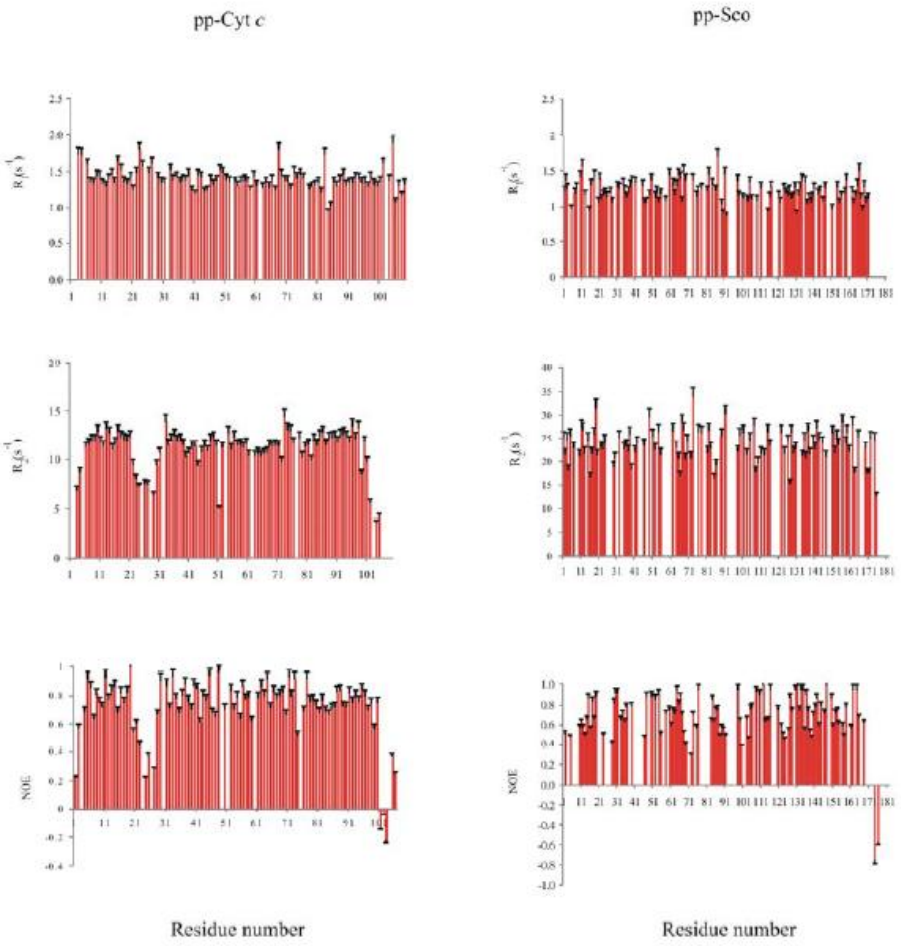

Figure S5. (A) ^{1}H-^{15}N HSQC spectrum recorded on reduced pp-Sco at 308K; (B) H^{N} region of 2D NOESY spectrum recorded on reduced pp-Sco at 308K.

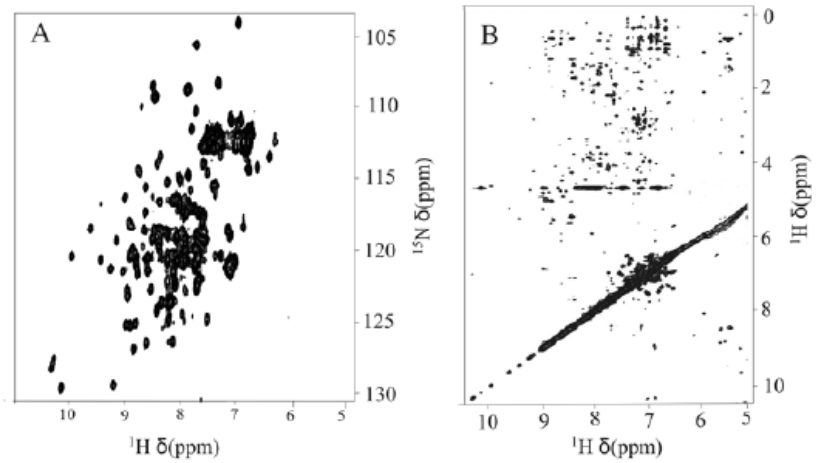

Figure S6. ^{1}H-^{15}N HSQC spectrum optimized for the detection of ^{2}J NH of His rings, recorded on pp-Sco before (in red) and after (in blue) the addition of stoichiometric amounts of Cu(I).

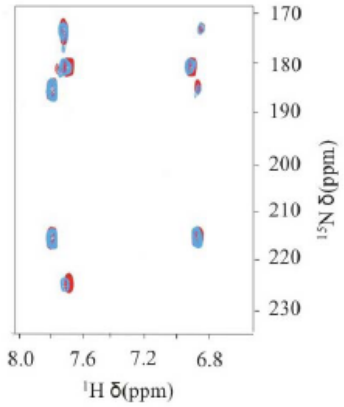

16

4. GENERAL DISCUSSION

Copper is absolutely required for aerobic life, but paradoxically, is highly toxic. Within the living cell, complex systems for copper trafficking evolved to satisfy cellular requirements while minimizing toxicity.[1] It has been rationalized by assuming that Cu, like other redox-active metals, is sequestered in nonreactive forms as it is transported into cells and moves through cellular compartments. However, the agents of such trafficking and the mechanisms of delivery of Cu to it's final destinations have, until recently, remained largely unknown. Our knowledge of this area has increased substantially during the last decade with the identification of copper chaperone family proteins.[2,3,4] They are involved in at least three high-affinity pathways, active in conditions of low Cu concentration, and some of them can be entirely bypassed when there are high concentrations of Cu salts in the medium. Until now only inconsistent, non-comparable data on the copper affinities of proteins involved in copper trafficking pathways have been reported. In order to elucidate the factors driving the copper ion between the protein partners along the cellular copper routes, using ESI-MS spectrometry we measured the apparent Cu(I)-binding affinities for a representative set of proteins involved in enzymatic redox catalysis, in copper transfer pathways and storage of surplus copper. In this study we provided the thermodynamic basis for the kinetic processes that leads to the distribution of cellular copper. The resulting picture shows that the copper is drawn to the copper enzymes according to the gradients of increasing copper affinity among the copper-handling proteins.[5]

Cu-Zn superoxide dismutase (SOD1) is a well characterized cytosolic scavenger of oxygen free radicals that requires copper and zinc binding to potentiate its enzymatic activity. Many FALS-associated mutations of Cu,ZnSOD1 are now recognized to cause the death of motor neuron cells through a toxic gain-of-function of the enzyme.[6] There are several theories for the nature of this new function, but many lines of evidence support the possibility that adventitious reactions catalyzed by the copper ion cofactor are central to the progression of the disease. Copper chaperone for SOD1 (hCCS) prevents copper ions from binding to intracellular copper scavengers and provides the SOD1 enzyme with the necessary copper co-factor.[3] Given the reasonable viability of cells that lack SOD1 entirely, a disruption in the process that supplies the ALS mutant enzymes with copper ions could stand as a uniquely promising approach to intervention in the destructive effects of the disease. The knowledge of the function and chemical mechanism of the hCCS/SOD1 system could provide a strong foundation to evaluate potential drugs that can control the activity of SOD1 *in vivo*.

Our understanding of the mechanism of hCCS metallochaperone action begins with the determination of metal binding capacities of it's constituent domains. In our work we tried to determine the native metal stoichiometry of hCCS for both copper and zinc ions as well as the metal-ligand environment. The significant part of the project was dedicated to the measuring the metal binding affinity of hCCS relative to it's partner SOD1 in the metal transfer step of the activation mechanism. The SOD1 has a Cu(I)-binding affinity 3 times higer than its copper chaperone, so that the metal transfer is thermodynamically favored towards the SOD1 enzyme. The other branch of this research concerns the elucidation of the metal transfer mechanism between hCCS and SOD1. We were studying the role of protein-protein interactions in the activity of hCCS and its target protein SOD1. Analytical gel filtration, light scattering, NMR and ESI-MS spectroscopy are among the techniques that was used to analyze these interactions. The data support the fact, that the Cu(I) transfer to either E,ESOD1 or E,ZnSOD1, is efficient only in the presence of the full length Cu(I)-hCCS. The Cu(I)-bound forms of independent domains of hCCS are indeed not able to fully metallate hSOD1 protein. The heterodimeric complex between two proteins is preferentially formed only when the disulfide bond of SOD1 protein is reduced. Moreover hCCS protein can assist to SOD1 folding through the disulfide bond formation, playing role as a real "chaperone" protein. Taking into account the ability of hCCS to bind Zn(II) in it's Atx-like D1 and to transfer it to the SOD1 protein *in vitro* we could speculate about the possible role of hCCS in the Zn transfer to SOD1 *in vivo*. But more detailed studies in the physilogical conditions still should be performed to get the clear picture of the entire process of the SOD1 activation by it's copper chaperone hCCS.

Cytochrome c oxidase (CcO), the last enzyme of the respiratory chain, is a member of a superfamily of heme-copper-containing terminal oxidases that are present in all aerobic organisms. Sco proteins have been implicated as an accessory factors in the assembly of this integral membrane enzyme. Sco has been proposed to be a copper delivery agent that specifically brings copper to COX 2 subunit of cytochrome *c* oxidase.[7] Alternatively, the discovery that Sco is a member of the thioredoxin family has rekindled interest in a possible redox role for this protein in Cu_A assembly.[8] Presumably, the two cysteines within the Cu_A site are in a reduced state because the disulfide formation would preclude the copper incorporation into this site. Sco could then function as a thiol oxidoreductase specific for the Cu_A site as it has been demonstrated in the assembly of the Cu_A site in *T. Thermophilus*.[9] Also the Cys-redox properties of Sco proteins could serve in a more general role as a redox

signaling. In our work, we have focused on a recombinant, soluble form of a Sco protein from *P. putida*, which is naturally fused with a typical redox transfer molecule cytochrome *c*, in order to gain hints on the proposed redox functional role of Sco protein family. To address this question, the solution structures of both cyt c and Sco domains, separately expressed, were determined and the electron transfer reaction between them was investigated in accordance to their measured redox potentials. Copper binding and thioredoxin properties of the Sco domain were also investigated to characterize this class of the proteins in order to understand the evolution link between thioredoxins and copper chaperones. The observed copper binding properties of pp-Sco was different from those typically present in eukaryotic and the up to now investigated bacterial Sco proteins.[10,11] These latter always involve two cysteines and one histidine in the copper ion coordination, suggesting a metallochaperone function for Cu(I) or Cu(II) ions. Differently, pp-Sco is able to bind Cu(I), but through the CXXXC motif only, i.e. without His ligand participation, thus determining a weak-affinity copper-binding site and the inability to coordinate the Cu(II) ion. These facts indicate that the His ligand coordination is the discriminating factor for introducing the metallochaperone function in Sco proteins. But we found that pp-Sco domain is involved in electron transfer processes. Moreover, pp-Sco has a thioredoxin fold with no relevant copper binding properties, suggesting that the inability of the His ligand to coordinate the copper ion in pp-Sco plays the crucial role to determine functional properties diverging from the metallochaperone function. The redox properties of pp-Sco include indeed i) thioredoxin activity or ii) reduction of copper(II) to copper(I) or iii) reduction of iron(III) to iron(II) in pp-Cyt *c* protein partner. In particular, we have shown that pp-Sco is able to transfer electrons to pp-Cyt *c* and therefore to reduce Fe(III) to Fe(II). This is the first example of a Sco protein implicated in electron transfer processes and not in copper-chaperoning function. The most probably, during evolution, specific amino acid variations occurred in the surrounding of the CXXXC catalytic site in a thioredoxin-like fold to acquire copper binding affinities at different levels from bacteria to eukaryotes.

A class of bacterial signal transduction proteins possesses a soluble N-terminal cyt *c* PAS domain (sensor domain) in the periplasm and the C-terminal GGDEF and EAL domains (transduction domains) in the cytoplasm.[12] In analogy with the functional role found for periplasmic, signal sensor cyt c-containing PAS domains, pp-Cyt c and pp-Sco domains of pp3183 could indeed perceive changes in redox potential crucial to be transmitted to the cytoplasm for activating cellular responses. The neighbouring pp3182 protein contains a large

predicted periplasmic segment which could be the partner domain of pp3183 to transmit the signal toward the cytosolic C-terminal GGDEF and EAL domains. However, the subsequent studies at cellular level are necessary to attribute a possible functional meaning of the observed redox activity.

4.1 REFERENCES

1. Kim, B., Nevitt, T. & Thiele, D.J. Mechanisms for copper acquisition, distribution and regulation. *Nat. Chem. Biol* **4**, 176-185 (2008).
2. Pufahl, R.A. et al. Metal ion chaperone function of the soluble Cu(I) receptor Atx1. *Science* **278**, 853-856 (1997).
3. Culotta, V.C. et al. The copper chaperone for superoxide dismutase. *J. Biol. Chem* **272**, 23469-23472 (1997).
4. Valentine, J.S. & Gralla, E.B. Delivering copper inside yeast and human cells. *Science* **278**, 817-818 (1997).
5. Banci, L. et al. Affinity gradients drive copper to cellular destinations. *Nature* **465**, 645-648 (2010).
6. Banci, L. et al. SOD1 and amyotrophic lateral sclerosis: mutations and oligomerization. *PLoS ONE* **3**, e1677 (2008).
7. Rigby, K., Cobine, P.A., Khalimonchuk, O. & Winge, D.R. Mapping the functional interaction of Sco1 and Cox2 in cytochrome oxidase biogenesis. *J. Biol. Chem* **283**, 15015-15022 (2008).
8. Winge, D.R. Let's Sco1, Oxidase! Let's Sco! *Structure* **11**, 1313-1314 (2003).
9. Abriata, L.A. et al. Mechanism of Cu(A) assembly. *Nat. Chem. Biol* **4**, 599-601 (2008).
10. Davidson, D.E. & Hill, B.C. Stability of oxidized, reduced and copper bound forms of Bacillus subtilis Sco. *Biochim. Biophys. Acta* **1794**, 275-281 (2009).
11. Cawthorn, T.R., Poulsen, B.E., Davidson, D.E., Andrews, D. & Hill, B.C. Probing the kinetics and thermodynamics of copper(II) binding to Bacillus subtilis Sco, a protein involved in the assembly of the Cu(A) center of cytochrome c oxidase. *Biochemistry* **48**, 4448-4454 (2009).
12. Londer, Y.Y., Dementieva, I.S., D'Ausilio, C.A., Pokkuluri, P.R. & Schiffer, M. Characterization of a c-type heme-containing PAS sensor domain from Geobacter sulfurreducens representing a novel family of periplasmic sensors in Geobacteraceae and other bacteria. *FEMS Microbiol. Lett* **258**, 173-181 (2006).